PACIFIC EARTHQUAKE ENGINEERING
RESEARCH CENTER

NGA-West2 Ground Motion Prediction Equations for Vertical Ground Motions

PEER 2013/24
SEPTEMBER 2013

NGA-West2 Ground Motion Prediction Equations for Vertical Ground Motions

PEER Report 2013/24
Pacific Earthquake Engineering Research Center
Headquarters at the University of California, Berkeley

September 2013

ABSTRACT

This report documents the development of the NGA-West2 empirical ground-motion prediction equations (GMPEs) for ground-motion intensity measures derived from recordings of the vertical component of ground motion. The extensive and expanded PEER NGA-West2 ground-motion database recorded from shallow crustal earthquakes in active tectonic domains was used to develop GMPEs for the vertical component of peak ground acceleration (PGA), peak ground velocity (PGV), and 5%-damped elastic pseudo-absolute acceleration response spectral ordinates (PSA) at periods ranging from 0.01 to 3 sec (the NGA-West2 consensus period range for vertical component).

Other research products and findings of the NGA-West2 project, including the development of a comprehensive database of ground motion recorded worldwide and development of GMPEs for horizontal components, have been published in a series of reports by the Pacific Earthquake Engineering Research Center (PEER). The focus of this report is on vertical ground motion. Since the NGA-West2 database and numerous NGA-West2 PEER reports have already been published and can be referenced, the consensus of the NGA-West2 GMPE developers was that for vertical ground motion a single PEER report with independent chapters authored by different NGA-West2 GMPE developers would be published. Each chapter of this report explains the details of a specific GMPE for vertical component developed by a specific ground-motion model developer team.

ACKNOWLEDGMENTS

This study was sponsored by the Pacific Earthquake Engineering Research Center (PEER) and funded by the California Earthquake Authority, California Department of Transportation, and the Pacific Gas & Electric Company. Any opinions, findings, and conclusions or recommendations expressed in this material are those of the authors and do not necessarily reflect those of the sponsoring agencies.

We greatly benefitted from constructive interactions among the NGA researchers, including (in alphabetical order by last name): Linda Al Atik, Tim Ancheta, Jack Baker, Annemarie Baltay, Bob Darragh, Steve Day, Jennifer Donahue, Rob Graves, Nick Gregor, Tom Hanks, Tadahiro Kishida, Albert Kottke, Sanaz Rezaeian, Badie Rowshandel, Shrey Shahi, Tom Shantz, Paul Spudich, Jennie Watson-Lamprey, and Katie Wooddell. We thank Claire Johnson for her skillful editing of the report.

CONTENTS

1. Introduction

The PEER Next Generation of Ground Motion Attenuation Phase 2 Project (the "PEER NGA-West2 Project") is a multidisciplinary research initiative coordinated by the Pacific Earthquake Engineering Research Center (PEER) to extend the original NGA Project, now called the NGA-West1 Project, to develop ground-motion models for shallow crustal earthquakes in active tectonic regions. An overview of the PEER NGA-West2 Project components, process, and products is presented in Bozorgnia et al. [2012]. Various NGA-West2 research products, including the NGA-West2 database, five ground-motion prediction equations (GMPEs) for horizontal ground motion, and results of numerous supporting research projects have been recently published as a series of PEER reports [PEER 2013]. A sub-project in NGA-West2 is the development of GMPEs for vertical ground motion, which is the focus of this report.

Similar to the case of horizontal ground motion, we have posted the "flatfile" of vertical ground motion at the PEER web site [PEER Vertical Flatfile 2013]. The flatfile includes extensive metadata [Ancheta, et al. 2013], peak ground-motion values, and 5%-damped elastic pseudo-absolute response-spectral acceleration (PSA) at 111 oscillator periods.

Each GMPE developer team, based on their selection criteria, selected a subset of the vertical ground-motion data to develop their GMPEs for the vertical component.

To meet the needs of the earthquake engineering community, all of the NGA-West2 *vertical* models were required to be applicable to the following conditions:

1. they should include the ground-motion intensity measures PGA, PGV, and 5%-damped elastic pseudo-absolute response-spectral acceleration (PSA) for a minimum set of periods ranging from 0–3 sec;
2. they should be valid for shallow crustal earthquakes with strike-slip, reverse, and normal mechanisms in active tectonic regions;
3. they should be valid for moment magnitudes ranging from 3.0 to: 8.5 for strike-slip faults, 8.0 for reverse faults, and 7.5 for normal faults;
4. they should be valid for distances ranging from 0 to 200 (preferably 300 if possible) km; and
5. they should incorporate the time-averaged shear-wave velocity in the top 30 m of the site (V_{S30}) as a site parameter, although no specific range of V_{S30} values was specified.

If a GMPE developer team chose different ranges of such parameters, they needed to explain the reasoning for their choice.

After internal discussions, the consensus of the NGA-West2 researchers was that the behavior of vertical ground motion beyond a period of 3 sec is complicated and needs further investigation; thus, the maximum required period for NGA-West2 vertical GMPEs was established at 3 sec. Considering that most structural components and systems are stiff vertically and have short vertical periods, the new vertical GMPEs can be used for most structures. For structural systems with vertical periods longer than 3 sec we recommend a special case study to quantify vertical component and its effects.

The NGA-West2 group also concluded that more detailed and validated simulations to develop nonlinear site response in the vertical direction will be needed in the future. For example, the degree of soil nonlinearity is correlated with the P-wave velocity profile and the depth to the water table. Thus, use of simulation-based model(s) for vertical nonlinear soil response will be carried out in a future task.

Ground-motion simulation results for the amplification of vertical motion in deep basins were also found to need more investigations; thus, the NGA-West2 consensus was to avoid an explicit modeling of deep basin effects until the simulations are further advanced.

This report documents the development of the NGA-West2 GMPEs for vertical component. Each chapter of this report explains details of a specific GMPE for vertical ground motion developed by a specific ground motion model developer team.

REFERENCES

Ancheta T.D., Darragh R., Stewart J.P., Seyhan E., Silva W.J., Chiou B.S.-J., Wooddell K.E., Graves R.W, Kottke A.R., Boore D.M., Kishida T., Donahue J.L. (2013). PEER NGA-West2 database, *Report PEER 2013/03*, Pacific Earthquake Engineering Research Center, University of California, Berkeley, CA.

Bozorgnia Y., Abrahamson N.A., Campbell K.W., Rowshandel B., Shantz T. (2012). NGA-West2: A comprehensive research program to update ground motion predictions equations for shallow crustal earthquakes in active tectonic regions, *Proceedings, 15th World Conference on Earthquake Engineering*, Paper No. 2572, Lisbon, Portugal.

PEER (2013). PEER reports on NGA-West2 products and findings, http://peer.berkeley.edu/publications/peer_reports_complete.html

PEER Vertical Flatfile (2013). http://peer.berkeley.edu/ngawest2/databases/

2. GKAS13: Ground Motion Prediction Equation for the Vertical Ground Motion Component

ZEYNEP GÜLERCE[1]

RONNIE KAMAI[2]

NORMAN A. ABRAHAMSON[3]

WALTER J. SILVA[4]

2.1 INTRODUCTION

Vertical ground motions are often considered in the seismic design of critical structures such as nuclear power plants and dams. Recent studies suggest that the effect of the vertical component ground motion can also be significant for the seismic response of ordinary highway bridges for sites located within about 15 km of major faults [Kunnath et al. 2008; Gülerce and Abrahamson 2010]. The vertical design spectra may be developed in a probabilistic seismic hazard assessment (PSHA) by computing the hazard for the vertical ground motions using vertical ground motion prediction equations (GMPEs) or by using a V/H ratio model to scale the horizontal spectrum that was developed using the results of horizontal component PSHA.

Although a large number of researchers have developed GMPEs for the horizontal ground motion component, vertical component equations have not been included except for a few cases: Abrahamson and Silva [1997], Campbell [1997], Sadigh et al. [1997], Ambraseys and Douglas [2003], Bozorgnia and Campbell [2004], and Ambraseys et al. [2005]. The PEER NGA-W1 models [Abrahamson and Silva, 2008; Boore and Atkinson, 2008; Campbell and Bozorgnia, 2008; Chiou and Youngs 2008; Idriss 2008] provided improved horizontal GMPEs that include recent large magnitude earthquakes, but the GMPEs for the vertical components of the NGA-W1 models were not developed.

[1] Middle East Technical University, Turkey
[2] Ben Gurion University of the Negev, Israel
[3] Pacific Gas & Electric, Co, San Francisco, California
[4] Pacific Engineering and Analysis, El Cerrito, California

We derived empirical models for peak ground acceleration and 5% damped spectral acceleration of the vertical component using the subset of the PEER NGA-W2 database [Ancheta et al. 2013] selected by Abrahamson et al. [2013] horizontal GMPE (ASK13). Although the NGA-W2 database represents a large increase in the data set as compared to the 2008 NGA database [Chiou et al. 2008], the large magnitude (M>7) and short distance (R < 15 km) range is still only sparsely sampled. To develop a GMPE that extrapolates to large magnitudes and short distances in a reasonable manner, we rely on seismological and geotechnical models for constraining the extrapolation. Therefore, our approach to the development of our GMPE is not traditional curve fitting (e.g., using the minimum number of parameters needed to explain the observations), but, rather, it is a model building exercise that uses analytical results from seismological and geotechnical models to constrain the extrapolation outside the range well represented in the empirical data. Therefore, we used the analytical modeling of finite-fault effects to constrain the hanging wall (HW) effects [Donahue and Abrahamson 2013]. The functional form of the proposed vertical GMPE is consistent with the functional form used for the horizontal component model, except that the model described here does not include nonlinear site amplification and soil depth effects.

2.1.1 Dataset Selection

The ASK13 ground motion model is based on a subset of the NGA-W2 database described by Ancheta et al. [2013]. The general approach used by Abrahamson et al. [2013] for selecting the subset of data for use in the regression analysis was to include all earthquakes, including aftershocks (Class 2 events as defined by Wooddell and Abrahamson [2013]) in active crustal regions (ACR) under the assumption that the median ground motions from earthquakes in ACRs at distances less than about 80 km are similar around the world. At distances greater than 80 km, differences in crustal structure can have significant effects on the ground motion leading to a change in the attenuation at large distances (e.g., Q term). A summary of the criteria used in ASK13 for excluding earthquakes and recordings is given in Abrahamson et al. [2013]. The same dataset selected by ASK13 for the horizontal component is used for this study, with small changes listed below:

- Remove recordings for which the vertical component is missing, or not processed
- Remove recordings for which the vertical component is identified as questionable in the flatfile (see Chapter 1).

Our final dataset includes 15,597 recordings from 326 earthquakes, compared to 15,750 recordings from 326 earthquakes in ASK13. Out of the additional 153 recordings that were removed from the vertical dataset, 98 were removed due to the spectral quality flag and the rest were missing the vertical spectral acceleration values. The response spectral values for the selected recordings are only used in the regression analysis for spectral frequencies greater than 1.25 times the high-pass corner frequency used in the record processing, as defined in the NGA-West2 database. This requirement produces a data set that varies as a function of period. The period dependence of the number of earthquakes and number of recordings used in the regression analysis is shown in Figure 2.1.

The significant drop in the number of recordings between 2–3 seconds indicates that the long-period predictions from this model are not well constrained by the empirical data. The magnitude-distance distributions for peak ground acceleration (PGA) and spectral acceleration at T = 3 sec are shown in Figure 2.2(a) and 2.2(b), respectively.

2.1.2 Model Parameters

The independent parameters used in the regression analysis are the same as the source, distance, and site parameters used by ASK13. Currently, the parameter representing the ground motion level on rock (spectral acceleration at the period of interest for V_{S30}=1180 m/sec) is not used because the nonlinear site response effects are not yet incorporated.

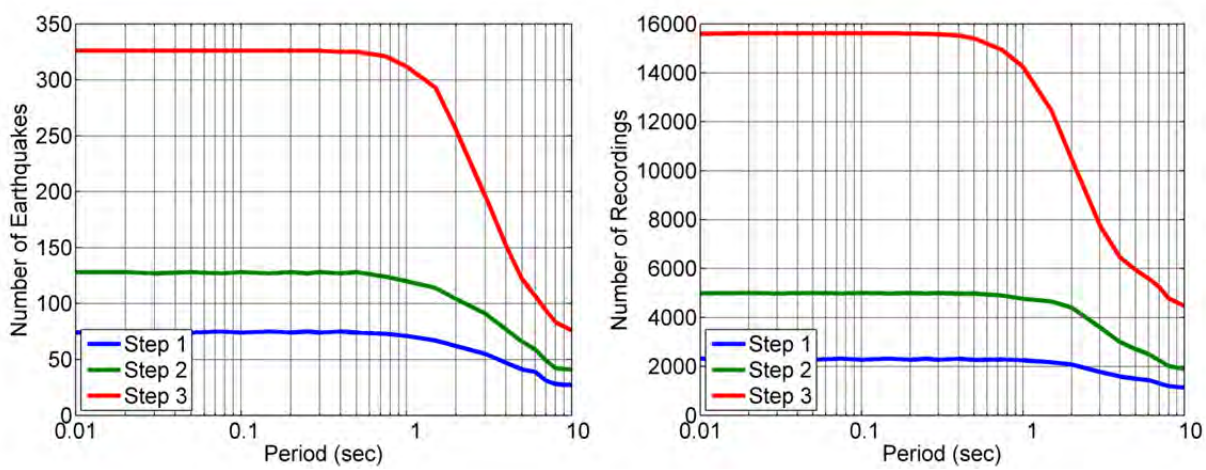

Figure 2.1 Number of earthquakes and number of recordings in the selected subset by period.

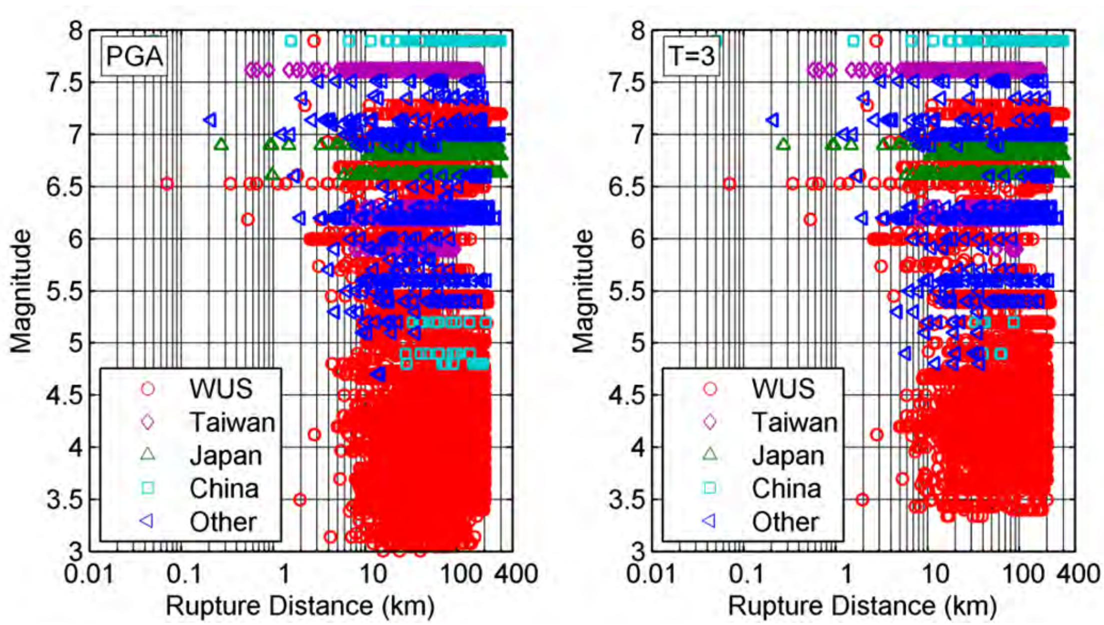

Figure 2.2 Magnitude-distance distributions for the final subset.

2.2 FUNCTIONAL FORM OF THE MODEL

Preliminary analysis of the vertical flatfile pointed at several features of the shallow site response in the linear range (low shaking intensity): (a) on average, the V_{S30} scaling of vertical component is weaker than the horizontal component, (b) there are significant regional differences, and (c) the vertical V_{S30} scaling doesn't fit well with a constant slope for all regions. These features can be seen in Figure 2.3, which presents residuals of a basic model fit to the data without site effects. The basic regression is performed for each region separately (California – CA, Japan – JP, Taiwan – TW, and China – CN), and is limited to a distance of 80 km and PGA≤0.1*g* (to avoid nonlinear effects). On average, Figure 2.3 shows that the V_{S30} scaling of CA data tends to curve downwards at low V_{S30} values, while the TW V_{S30} scaling is generally linear (constant slope with respect to V_{S30}). The JP V_{S30} scaling at short periods is flat, meaning that shallow site response for vertical ground motions does not correlate well with V_{S30}. This trend in the JP V_{S30} scaling at short periods is not seen for data at larger distances (80–400 km). Given this inconsistency, the regional differences in the V_{S30} scaling is uncertain, and we have not incorporated regional V_{S30} scaling in the current model. The CN V_{S30} range is more limited, so it is difficult to draw general conclusions, but it does not seem to fit with either of the other regions.

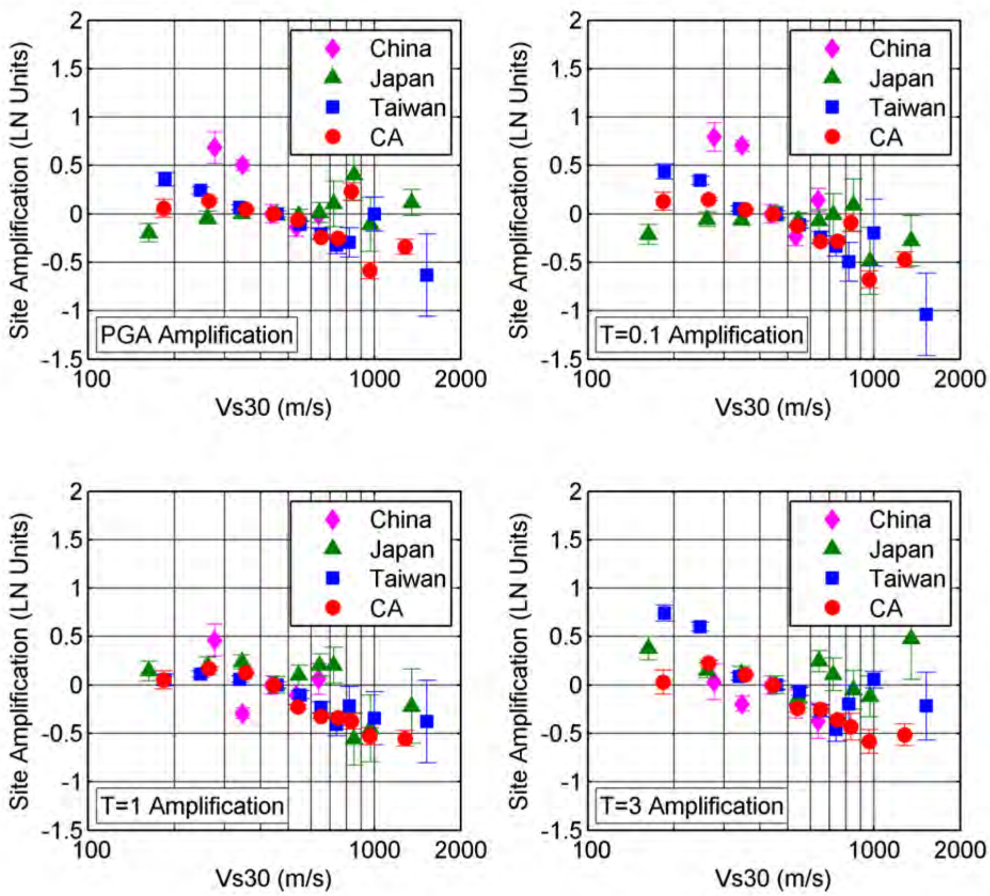

Figure 2.3 Non-parametric evaluation of the Vs30 scaling for four different regions.

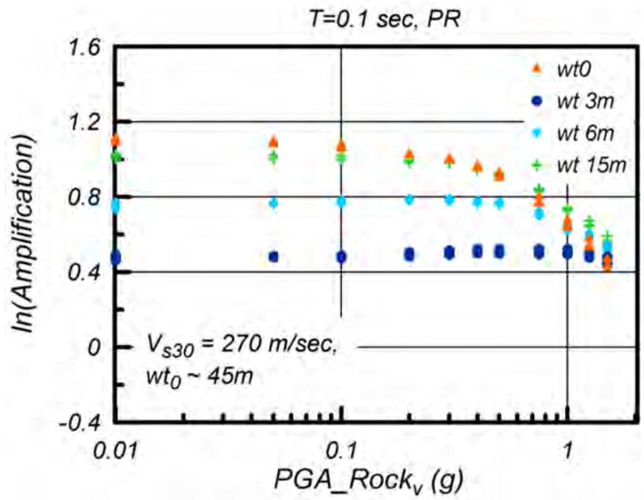

Figure 2.4 **1D site response simulation results for a profile with V_{s30} = 270 m/sec but four different corresponding V_p profiles (represented by depth to water table).**

In addition to the challenges in defining the linear range of the shallow site response, nonlinear response of vertical ground motions are still poorly understood. For example, 1D equivalent linear site response simulations show that the degree of nonlinearity is strongly correlated with the P-wave velocity profile and the depth to the water table, due to the propagation of compressional waves through the profile. Figure 2.4 presents an example of simulation results for a profile with V_{S30} = 270 m/sec, at T = 0.1 sec, using the Peninsular Range material properties. It can be seen that as the water table becomes shallower, the degree of nonlinearity is significantly reduced. In order to incorporate the simulations into our GMPE, it is required to first evaluate what the average water table is for the empirical data and that was beyond the scope of the current project.

Finally, the Z_1 (depth to V_s=1000 m/sec) scaling is strongly correlated with the V_{S30} scaling and a separate Z_1 component has not been incorporated in this version of our model. As can be seen by the slope of the residuals in Figure 2.24(c), Z_1 scaling should be considered at periods of about T = 1 sec and longer. The Z_1 scaling will be addressed in future developments of the model.

Due to the current limitations in our understanding of shallow and deep site response of vertical ground motions, the functional form of the model is consistent with the functional form used by ASK13, with the following exceptions:

- Nonlinear site response is not included
- Depth to bedrock is not included.

These aspects will be addressed in future studies and will be incorporated into future developments of a vertical GMPE.

The model for the median ground motion is given by:

$$lnSa(g) = f_1(M, R_{rup}) + F_{RV} f_7(M) + F_N f_8(M) + F_{AS} f_{11}(CR_{jb}) + f_5(V_{s30}) + F_{HW} f_4(R_{jb}, R_{rup}, R_x, R_{y0}, W, dip, Z_{TOR}, M) + f_6(Z_{TOR}) + Regional(R_{rup}) \tag{2.1}$$

The base form of the magnitude and distance dependence for strike-slip earthquakes is similar to Abrahamson and Silva [2008] horizontal model (AS08), with additional breaks in the magnitude scaling for small magnitudes:

$$f_1 = \begin{cases} a_1 + a_5(M - M_1) + a_8(8.5 - M)^2 + [a_2 + a_3(M - M_1)]\ln(R) + a_{17} R_{rup} & for\ M > M_1 \\ a_1 + a_4(M - M_1) + a_8(8.5 - M)^2 + [a_2 + a_3(M - M_1)]\ln(R) + a_{17} R_{rup} & for\ M_2 \le M < M_1 \\ a_1 + a_4(M_2 - M_1) + a_8(8.5 - M_2)^2 + a_6(M - M_2) & \\ \quad +[a_2 + a_3(M_2 - M_1)]\ln(R) + a_{17} R_{rup} & for\ M < M_2 \end{cases} \tag{2.2}$$

where

$$R = \sqrt{R_{rup}^2 + c_4^2} \tag{2.3}$$

Based on preliminary regression results, the breaks in the magnitude scaling in Equation (2.2) are set at $M_1 = 6.75$ and $M_2 = 5.0$.

A preliminary evaluation of the SOF factor for the horizontal component showed that the difference between ground motions for different faulting style was not seen for the large set of small magnitude data from California. Therefore, a magnitude dependent SOF factor was used for both RV (f_7) and NML (f_8) earthquakes in which the full scaling is only applied for magnitudes greater than 5 and is tapered to zero effect for magnitude 4 or smaller. The same functional form is adopted for the vertical GMPE as shown below in Equations (2.4) and (2.5):

$$f_7(M) = \begin{cases} a_{11} & for\ M > 5.0 \\ a_{11}(M - 4) & for\ 4 \le M \le 5 \\ 0 & for\ M < 4.0 \end{cases} \tag{2.4}$$

$$f_8(M) = \begin{cases} a_{12} & for\ M > 5.0 \\ a_{12}(M - 4) & for\ 4 \le M \le 5 \\ 0 & for\ M < 4.0 \end{cases} \tag{2.5}$$

Nonlinear site effects are not incorporated into the model; therefore, we assumed linear vertical amplification for the vertical component as given in Equation (2.6):

$$f_5(V_{S30}^*) = (a_{10}) ln\left(\frac{V_{S30}^*}{V_{Lin}}\right) \tag{2.6}$$

where

$$V_{S30}^* = \begin{cases} V_{s30} & for\ \ V_{s30} < V_1 \\ V_1 & for\ \ V_{s30} \ge V_1 \end{cases} \tag{2.7}$$

To constrain the V_1 term, non-parametric models of the V_{S30} scaling that were used by ASK13 is adopted for the vertical component:

$$V_1 = \begin{cases} 1500 & for\ T \le 0.5sec \\ \exp(-0.35\ln\left(\frac{T}{0.5}\right) + \ln(1500)) & for\ 0.5sec > T > 3sec \\ 800 & for\ T \ge 3sec \end{cases} \quad (2.8)$$

Donahue and Abrahamson [2013] used results from finite-fault simulations to constrain the dependence of the HW effects on magnitude, dip, and distance (over the rupture). Based on these results, the HW model used in ASK13 includes five tapers to produce a smoothly varying HW effect as a function of the dip, magnitude, location over the rupture, depth, and distance off of the ends of the rupture. Preliminary analysis indicated that the same model is applicable to the vertical ground motion component with minor changes as given below:

$$f_4\left(R_{jb}, R_{rup}, R_x, R_{y0}, dip, Z_{tor}, M\right) = a_{13} T_1(dip) T_2(M) T_3(R_x, W, dip) T_4(Z_{tor}) T_5(R_x, R_{y0}) \quad (2.9)$$

where

$$T_1(dip) = \begin{cases} (90 - dip)/45 & for\ dip > 30 \\ 60/45 & for\ dip < 30 \end{cases} \quad (2.10)$$

$$T_2(M) = \begin{cases} 1 + \mathrm{a}_{2\mathrm{HW}}(M - 6.5) & for\ M \ge 6.5 \\ 1 + \mathrm{a}_{2\mathrm{HW}}(M - 6.5) - (1 - \mathrm{a}_{2\mathrm{HW}})(M - 6.5)^2 & for\ 5.5 < M < 6.5 \\ 0 & for\ M \le 5.5 \end{cases} \quad (2.11)$$

$$T_3(R_x) = \begin{cases} h_1 + h_2(R_x/R_1) + h_3(R_x/R_1)^2 & for\ R_x < R_1 \\ 1 - \left(\frac{R_x - R_1}{R_2 - R_1}\right) & for\ R_1 \le R_x \le R_2 \\ 0 & for\ R_x > R_2 \end{cases} \quad (2.12)$$

$$T_4(Z_{TOR}) = \begin{cases} 1 - \frac{Z_{TOR}^2}{100} & for\ Z_{TOR} \le 10\ km \\ 0 & for\ Z_{TOR} \ge 10\ km \end{cases} \quad (2.13)$$

$$T_5(R_x, R_{y0}) = \begin{cases} 1 & for\ R_{y0} < R_{y1} \\ 1 - \frac{R_{y0} - R_{y1}}{5} & for\ R_{y0} - R_{y1} < 5 \\ 0 & for\ R_{y0} - R_{y1} \ge 5 \end{cases} \quad (2.14a)$$

where $R_1 = W cos(dip)$, $R_2 = 4R_1$, $R_{y1} = R_x \tan(20)$, $h_1 = 0.25$, $h_2 = 1.5$ and $h_3 = -0.75$.

If the R_{y0} distance metric is not available, the T_5 taper can be replaced using the following model:

$$T_5(R_{jb}) = \begin{cases} 1 & for\ R_{jb} = 0 \\ 1 - \frac{R_{jb}}{30} & for\ R_{jb} < 30 \\ 0 & for\ R_{jb} \ge 30 \end{cases} \quad (2.14b)$$

Based on preliminary evaluations, we adopted the same depth scaling as that of the ASK13 horizontal model:

$$f_6(Z_{TOR}) = \begin{cases} a_{15}\frac{Z_{TOR}}{20} & for\ Z_{TOR} < 20\ km \\ a_{15} & for\ Z_{TOR} \geq 20\ km \end{cases} \tag{2.15}$$

Previous studies, such as AS08, have found that the median short-period ground motions from aftershocks are smaller than the median ground motions from mainshocks. The definition for aftershocks has been modified in the NGA-West2 project using the definition of Class 1 and Class 2 events as described in Wooddell and Abrahamson [2013]. According to this new terminology, we define Class 2 events as those events that have a CR_{jb} < 15 km and that fall within the Gardner and Knopoff [1974] time window. Following the hypothesis that the stress drops are lower for earthquakes that re-rupture the Class 1 mainshock rupture plane, the ground motions from Class 2 events are scaled using the following expression:

$$f_{11}(CR_{jb}) = \begin{cases} a_{14} & for\ CR_{jb} \leq 5 \\ a_{14}\left[1 - \frac{CR_{jb}-5}{10}\right] & for\ 5 < CR_{jb} < 15 \\ 0 & for\ CR_{jb} \geq 15 \end{cases} \tag{2.16}$$

We allowed for regionalization of the Q term for the data from Taiwan, Japan, and China. In all cases, the additional coefficient is added to the base model (all other regions, dominated by California), which is used as a reference. For all three regions, we allow for a difference in the large distance (linear R) terms, such that the linear R coefficients a_{25} for Taiwan, a_{28} for China, and a_{29} for Japan, are added to the base model coefficient, a_{17}. The regionalization is given by:

$$Regional(R_{rup}) = F_{TW}(a_{25}R_{rup}) + F_{CN}(a_{28}R_{rup}) + F_{JP}(a_{29}R_{rup}) \tag{2.17}$$

where F_{TW} equals 1.0 for Taiwan and 0 for all other regions, F_{CN} equals 1.0 for China and 0 for all other regions, and F_{JP} equals 1.0 for Japan and 0 for all other regions.

2.3 REGRESSION ANALYSIS

The random-effects model was used for the regression analysis following the procedure described by Abrahamson and Youngs [1992]. The regression is performed in a number of steps, starting with a more limited data set and then proceeding to the full range, including M>3.0, R_{rup}<300 km. Table 2.1 lists the parameters that were regressed in each step and those which were smoothed and fixed following each step.

To arrive at a smooth model, the coefficients were smoothed in a series of steps (Table 2.1). Smoothing might be performed for a number of reasons, including: (1) to assure a smooth spectra, and (2) to constrain the model to a more physical behavior where the data is sparse. In the first run, fictitious depth term (c_4) is smoothed. The c_4 term is constrained to a constant value as shown in Figure 2.5 to prevent the large changes in the spectra as the model is extrapolated to very short distances.

In the second run, the magnitude dependent geometrical spreading term (a_3) and the linear magnitude scaling terms for large (a_5) and moderate (a_4) events were constrained while the quadratic magnitude term (a_8) is set to zero. As Figure 2.7 implies, the data would lead to oversaturation if allowed. We constrained the a_5 term to imply full saturation. In these steps, only moderate-to-large magnitude earthquakes recorded within 80 km for all regions (50 km for Japan) were included in regression to define the basic magnitude scaling.

In Run 3, the quadratic magnitude scaling term (a_8) is smoothed at first (Figure 2.8). In this step, we expanded the dataset to earthquakes with magnitudes 4.5 and larger. We constrained the quadratic magnitude term by considering the effect on the spectral displacement values. In the AS08 model, the spectral displacement was constrained after the regression to reach a constant value at long periods. In ASK13 model and the current model, an individual constant displacement constraint is not applied, but the regression led to reasonably constant displacement spectra without the additional constraint as shown in Figure 2.9(a) and (b).

Table 2.1 Estimated and constrained parameters at each step of regression.

Step	Data Set	Estimated Parameters	Parameters Smoothed after run
1	M>5.5, R_{rup}< 50 km for Japan, R_{rup}< 80 km for others	*a*1, *a*2, *a*3, *a*4, *a*5, *a*10, *a*11, *a*12, *a*13, *a*14, *a*15, c4	*c*4 (ficticious depth)
2a	M>5.5, R_{rup}< 50 km for Japan, R_{rup}< 80 km for others	*a*1, *a*2, *a*3, *a*4, *a*5, *a*10, *a*11, *a*12, *a*13, *a*14, *a*15	*a*3 (mag dep GS)
2b	M>5.5, R_{rup}< 50 km for Japan, R_{rup}< 80 km for others	*a*1, *a*2, *a*4, *a*5, *a*10, *a*11, *a*12, *a*13, *a*14, *a*15	*a*5 (linear mag, M>7.75)
2c	M>5.5, R_{rup}< 50 km for Japan, R_{rup}< 80 km for others	*a*1, *a*2, *a*4, *a*10, *a*11, *a*12, *a*13, *a*14, *a*15	*a*4 (linear mag, M5-M6.75)
3a	M>4.5, R_{rup}< 50 km for Japan, R_{rup}< 80 km for others	*a*1, *a*2, a6, a8, *a*10, *a*11, *a*12, *a*13, *a*14, *a*15	*a*8 (quadratic magnitude)
3b	M>4.5, R_{rup}< 50 km for Japan, R_{rup}< 80 km for others	*a*1, *a*2, *a*6, *a*10, *a*11, *a*12, *a*13, *a*14, *a*15	*a*13 (HW)
3c	M>4.5, R_{rup}< 50 km for Japan, R_{rup}< 80 km for others	*a*1, *a*2, a6, *a*10, *a*11, *a*12, *a*14, *a*15	*a*14 (eqk class)
3d	M>4.5, R_{rup}< 50 km for Japan, R_{rup}< 80 km for others	*a*1, *a*2, a6, *a*10, *a*11, *a*12, *a*15	a15 (Z_{TOR})
3e	M>4.5, R_{rup}< 50 km for Japan, R_{rup}< 80 km for others	*a*1, *a*2, a6, *a*10, *a*11, *a*12,	*a*11 (RV SOF) *a*12 (NML SOF)
3f	M>4.5, R_{rup}< 50 km for Japan, R_{rup}< 80 km for others	*a*1, *a*2, a6, *a*10	*a*10 (linear site response)
4a	M>4.5, R_{rup}< 50 km for Japan, R_{rup}< 300 km for CA, R_{rup}< 80 km for others	*a*1, *a*2, a6, *a*17	*a*17 (linear R)
4b	M>4.5, R_{rup}< 50 km for Japan, R_{rup}< 300 km for CA, R_{rup}< 80 km for others	*a*1, *a*2, a6	*a*2 (GS)
4c	M>3.0, R_{rup}< 50 km for Japan, R_{rup}< 300 km for CA, R_{rup}< 80 km for others	*a*1, *a*6	*a*6 (small mag linear)
5a	M>3.0, R_{rup}< 300 km for CA, Japan, China, and Taiwan. R_{rup}< 80 km for others	*a*1, *a*25, *a*28, *a*29	*a*25, *a*28, *a*29 (regional Q terms)
5b	M>3.0, R_{rup}< 300 km for CA, Japan, China, and Taiwan. R_{rup}< 80 km for others	*a*1	*a*1 (constant) *s*1-*s*4 (standard dev)

Next, smoothing of the parameters a_{13}, a_{14}, a_{15}, a_{11}, a_{12}, and a_{10} (shown in Figures 2.10 to 2.14) were performed to assure that the final model spectra will be smooth across the application range, including where it is extrapolated outside of the range well constrained by the data.

In step 4, smoothing of the long distance scaling parameter (a_{17}) (see Figure 2.15) was performed by expanding the dataset to the ground motions that are recorded within 300 km for California. The a_{17} term is constrained to be negative across all periods to assure that the ground motion will continue to attenuate at long distances and not curve upwards, as some of the regressed coefficients suggest. The same dataset is used to constrain the geometrical spreading term (a_2) (Figure 2.16), but the dataset is expanded to smaller events (M>3) in order to fix the linear magnitude scaling term for small magnitude events (Figure 2.17).

In step 5, the data from the other three well-recorded regions (China, Japan, and Taiwan) are extended to a distance of 300 km and a regional term for the anelastic attenuation is given to each of the four long-distance regions (Figure 2.18). Finally, the constant (a_1) and standard deviation terms are smoothed (Figure 2.19).

The values of the smoothed coefficients for the median ground motion are listed in Tables 2.2 and 2.3.

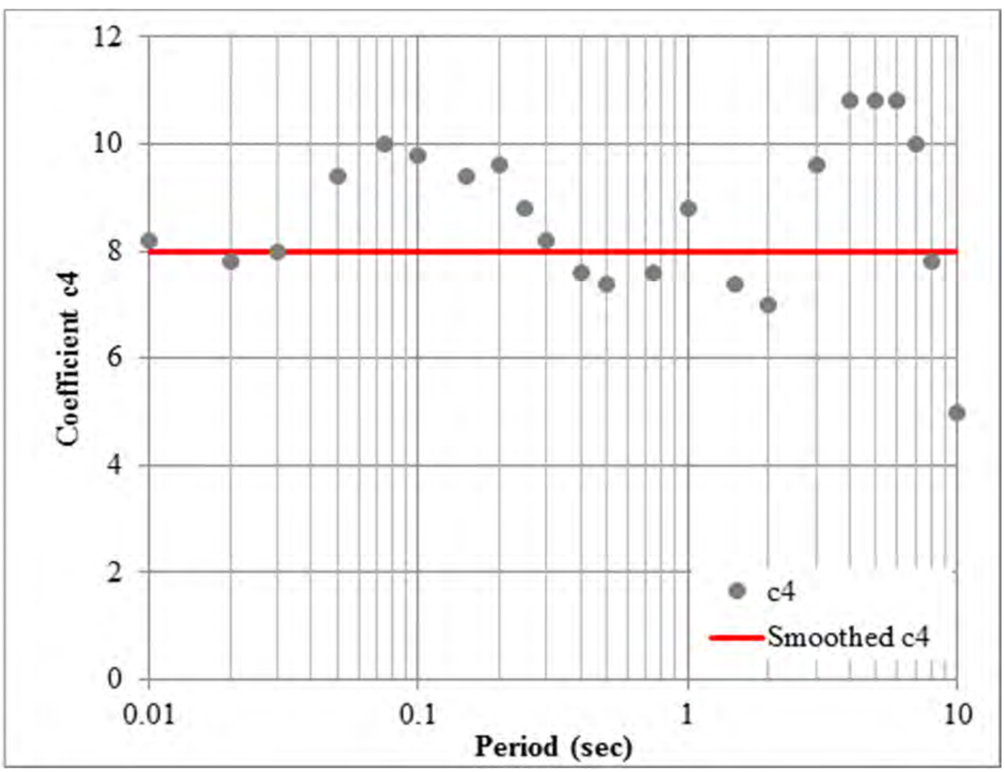

Figure 2.5 Smoothing of the fictitious depth term.

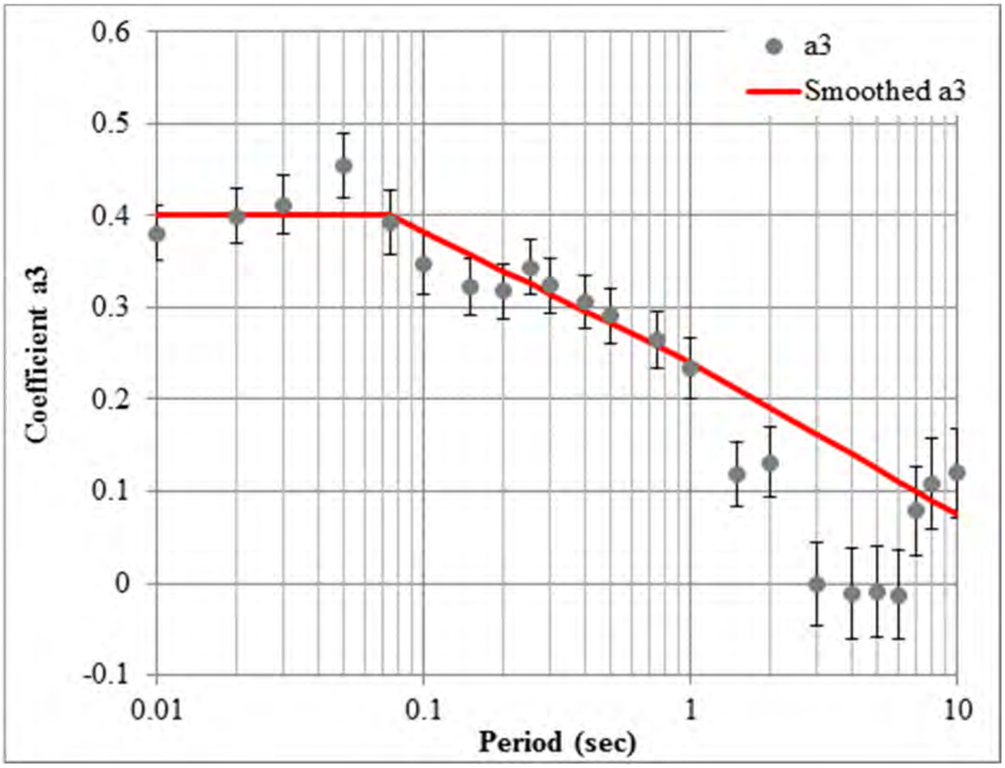

Figure 2.6 Smoothing of magnitude dependent geometrical spreading term.

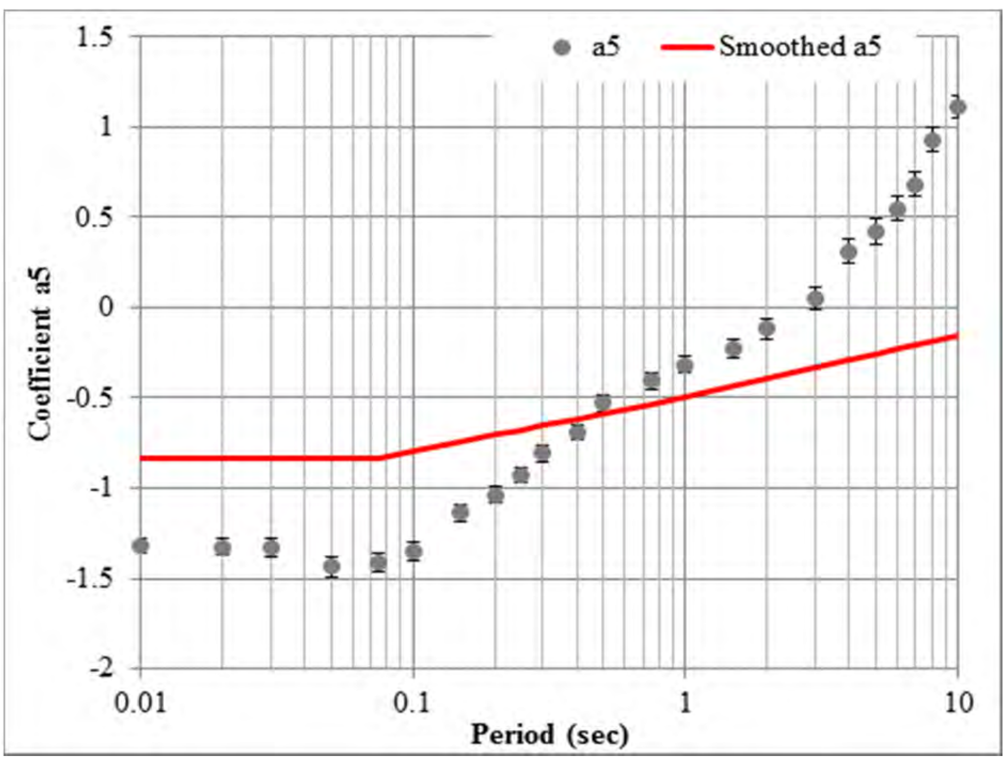

Figure 2.7 Smoothing of the linear magnitude term for large magnitude events.

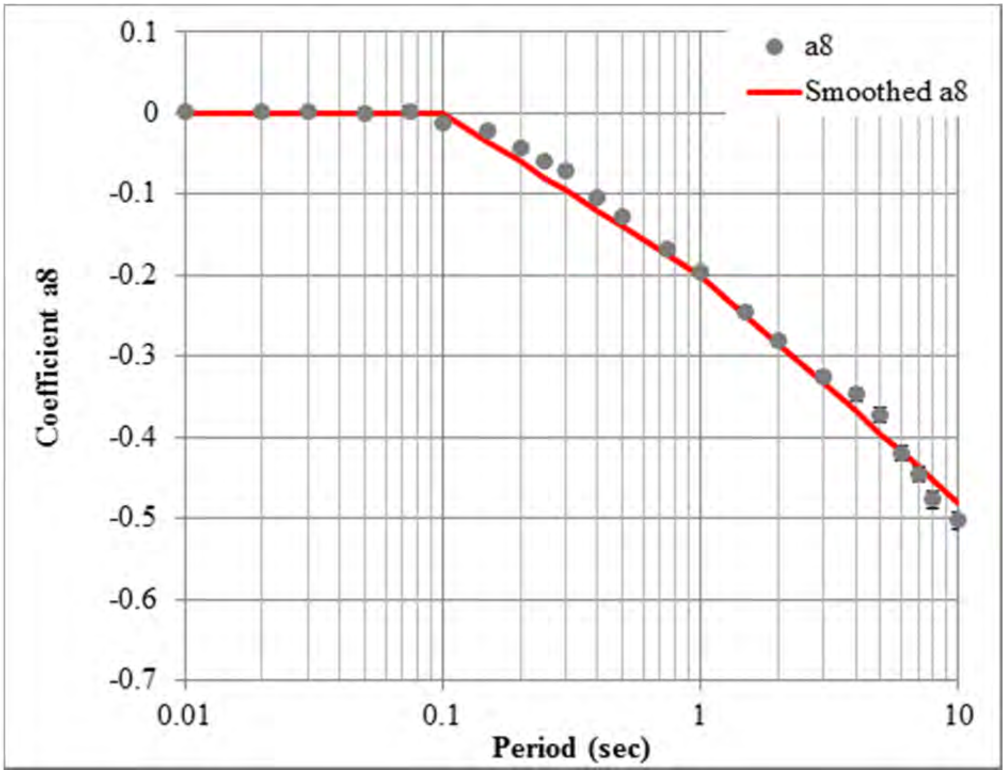

Figure 2.8 Smoothing of the quadratic magnitude coefficient.

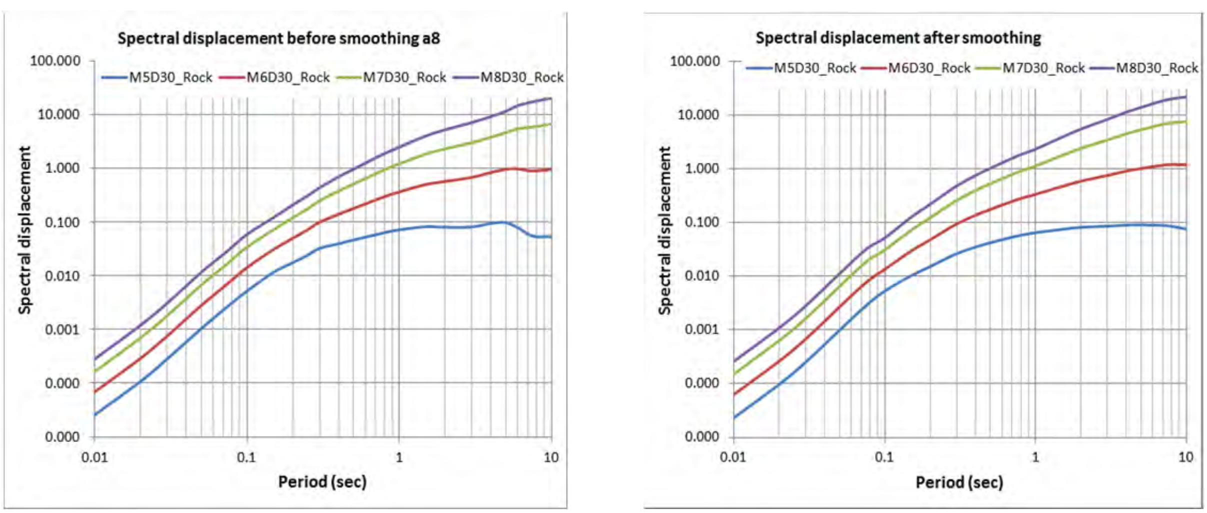

Figure 2.9 Spectral displacements for M5-M8 strike slip earthquakes at 30 km distance for V_{s30} = 1180 m/sec: (a) before smoothing a_8 and after smoothing.

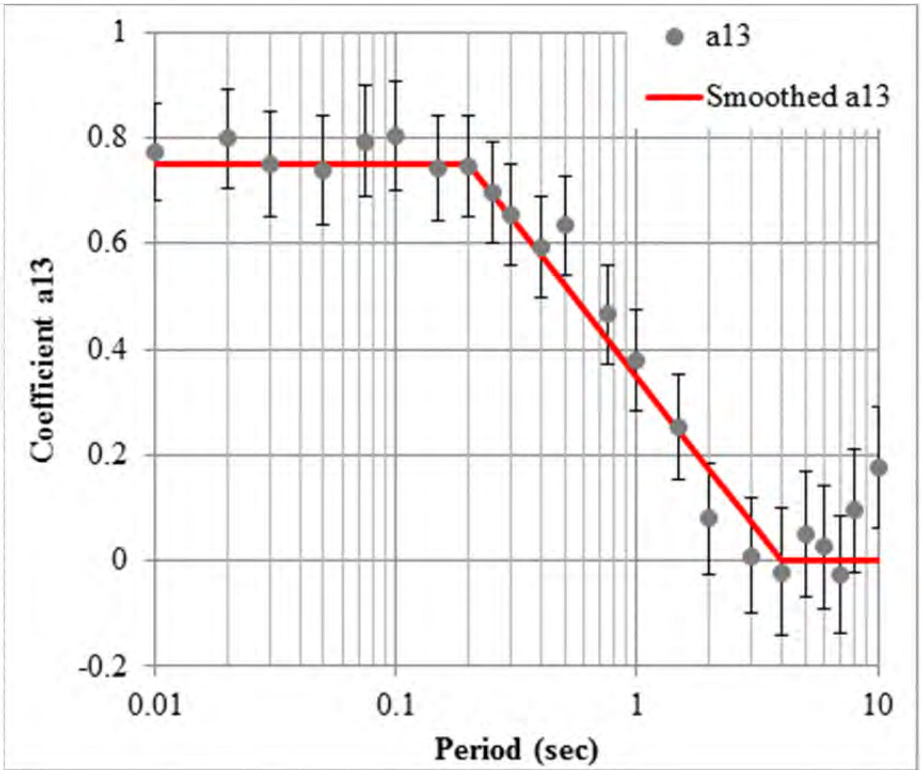

Figure 2.10 Smoothing of the hanging-wall term.

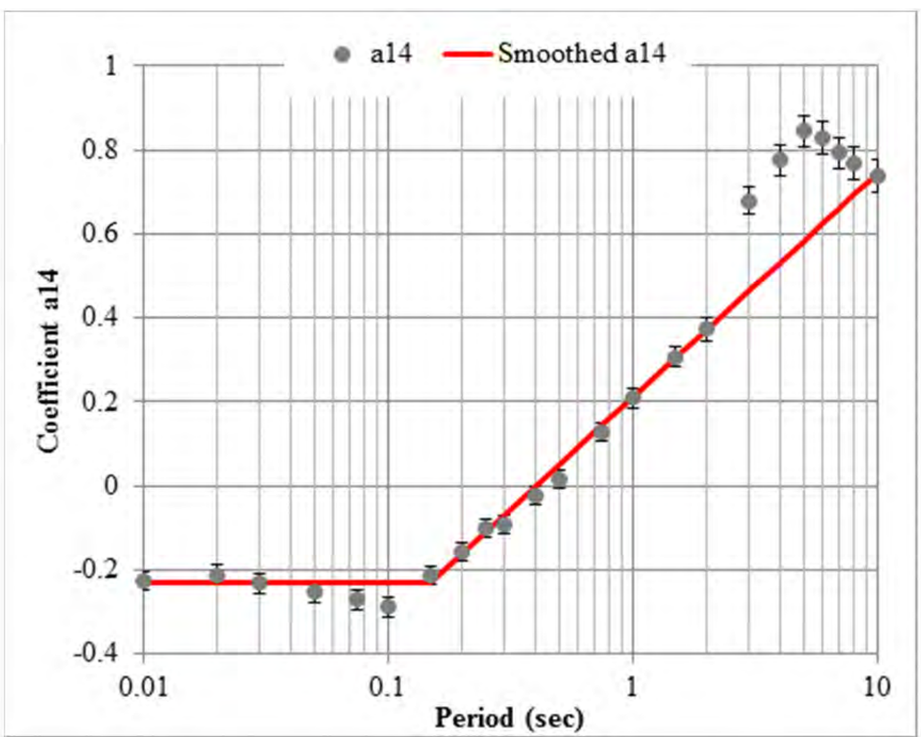

Figure 2.11 Smoothing of the earthquake class coefficients.

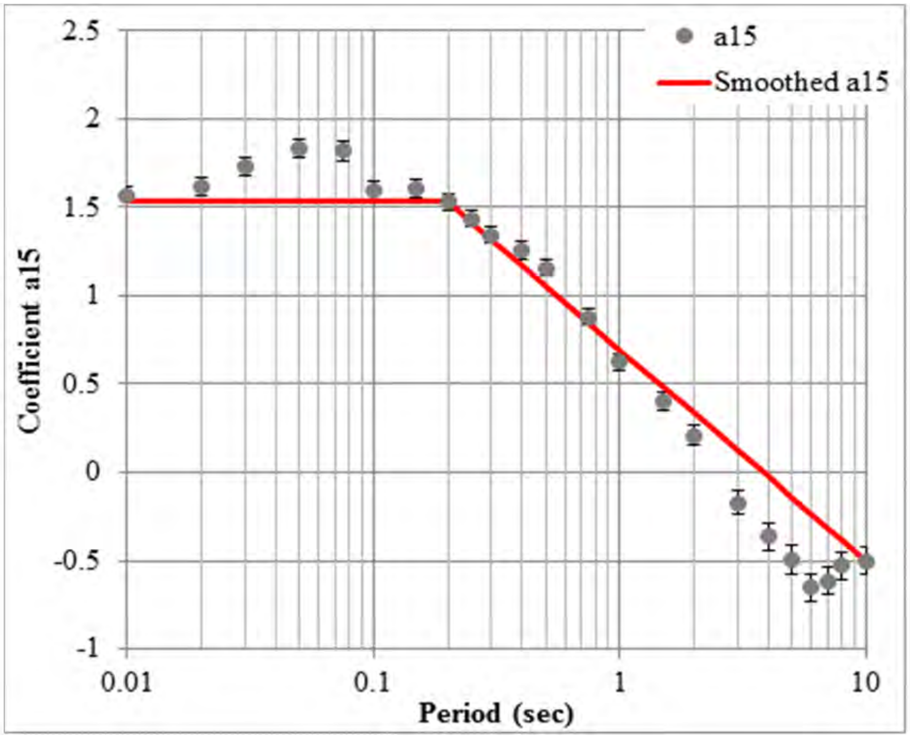

Figure 2.12 Smoothing of the Z_{TOR} coefficients.

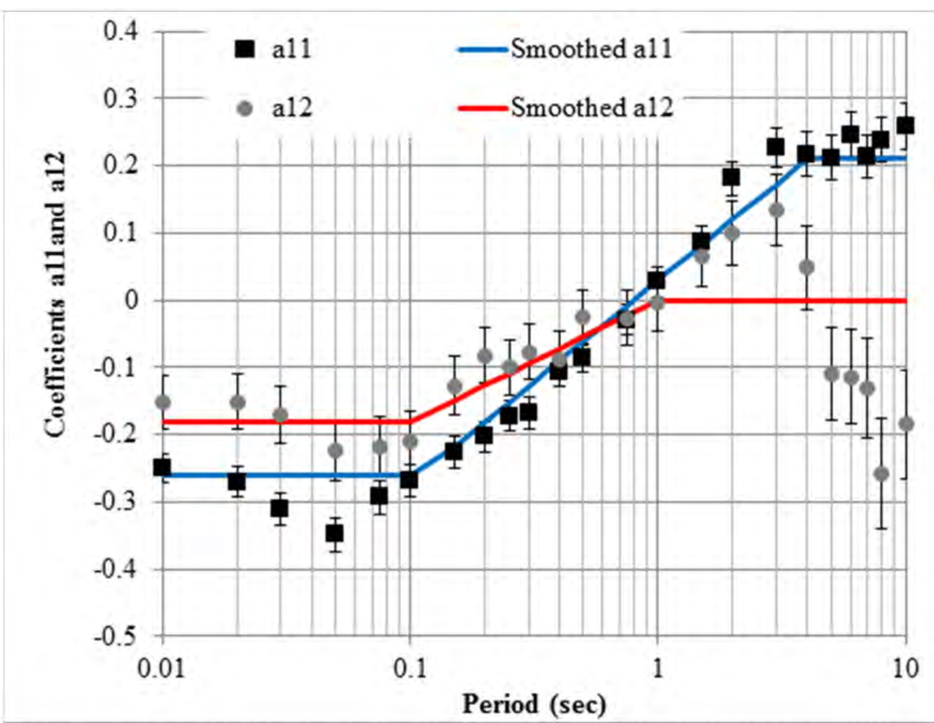

Figure 2.13 Smoothing of the SOF coefficients.

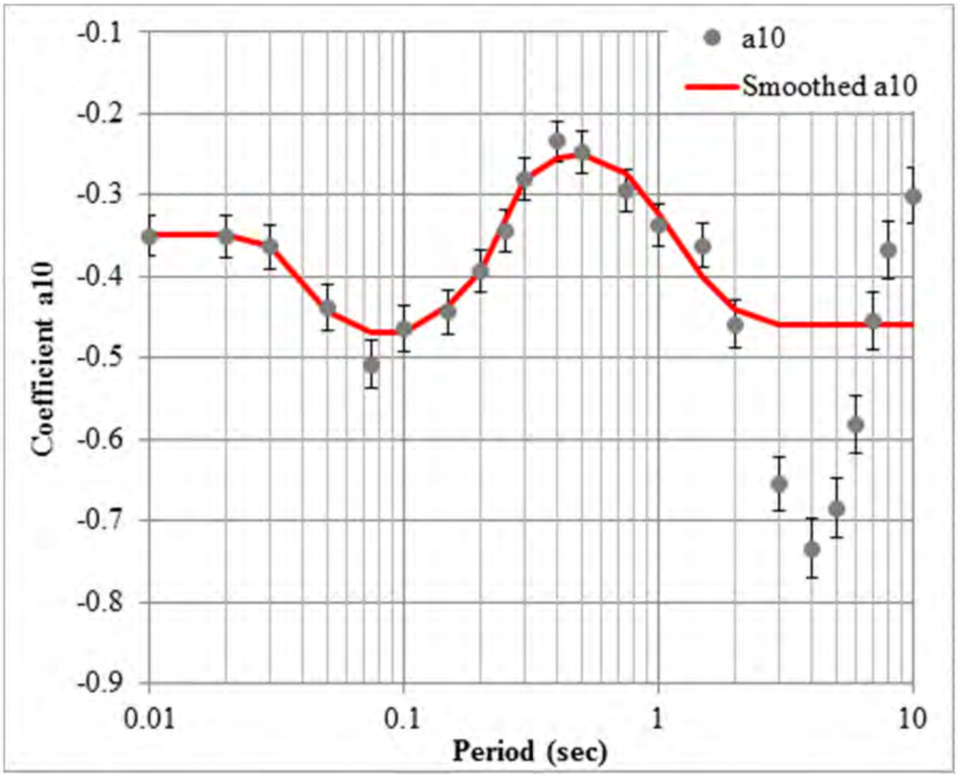

Figure 2.14 Smoothing of the regional V_{S30} scaling for the linear range.

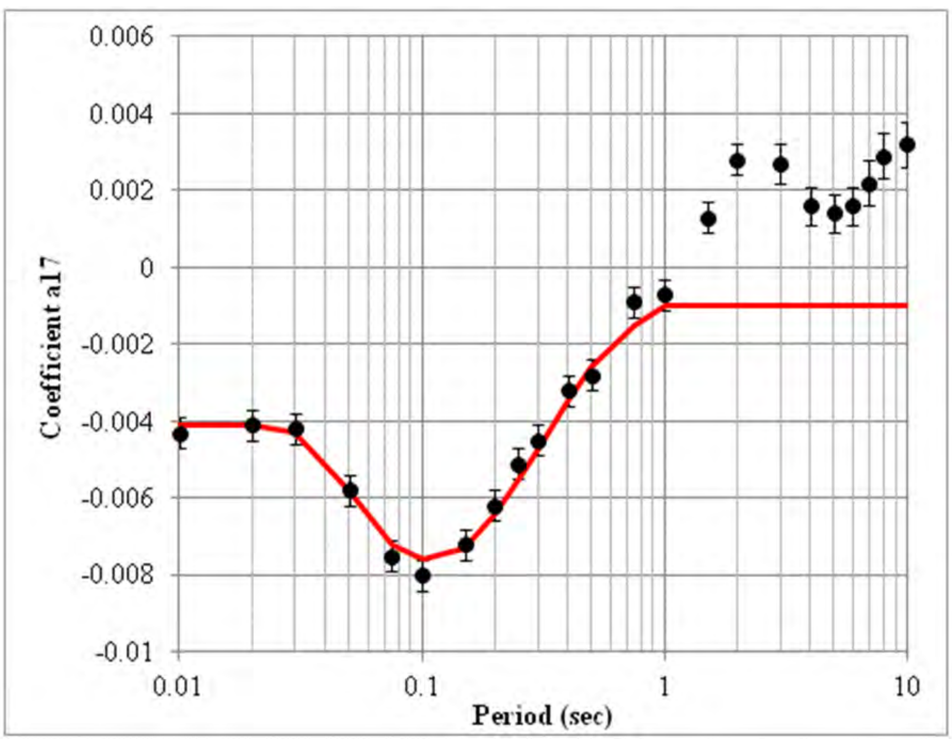

Figure 2.15 Smoothing of the long distance attenuation coefficients.

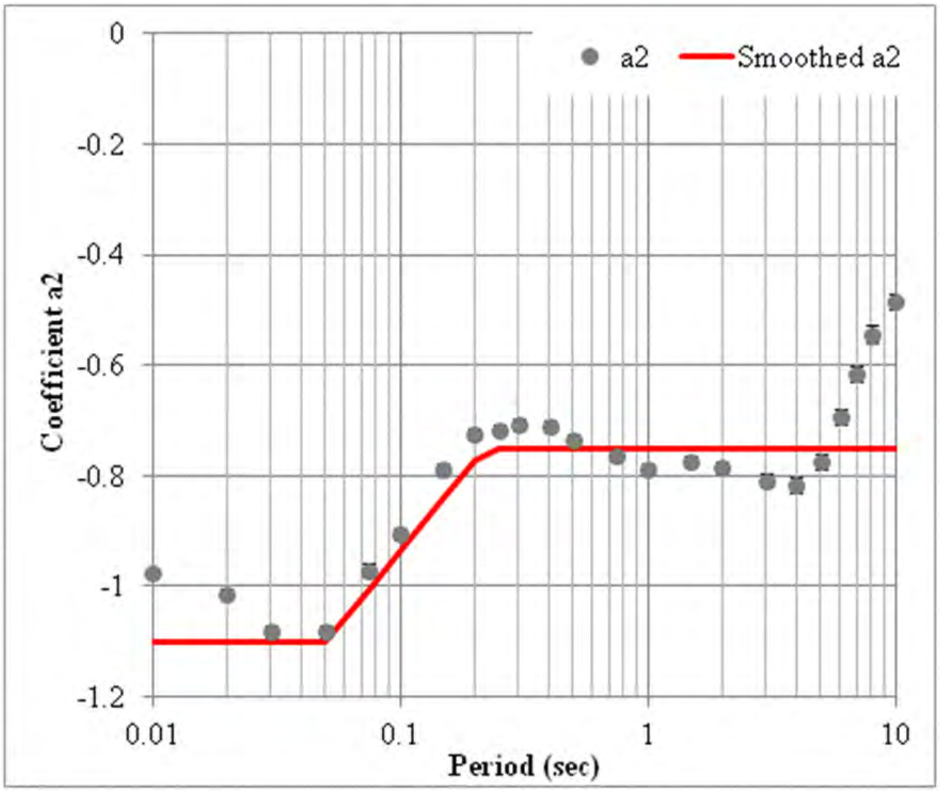

Figure 2.16 Smoothing of the geometrical spreading term.

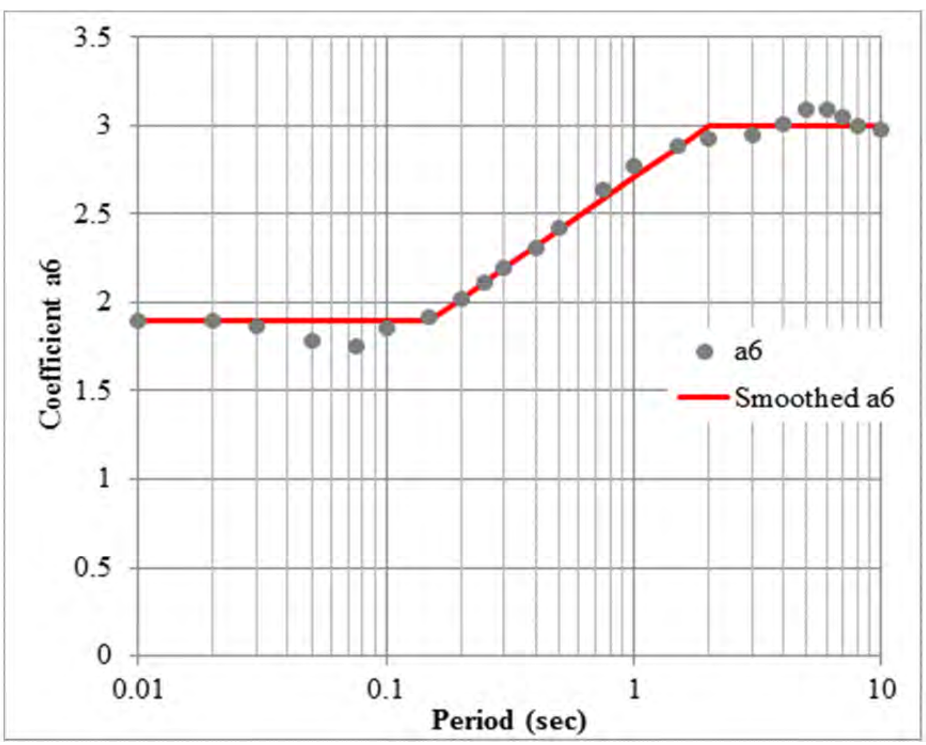

Figure 2.17 Smoothing of the linear magnitude term for small magnitude events.

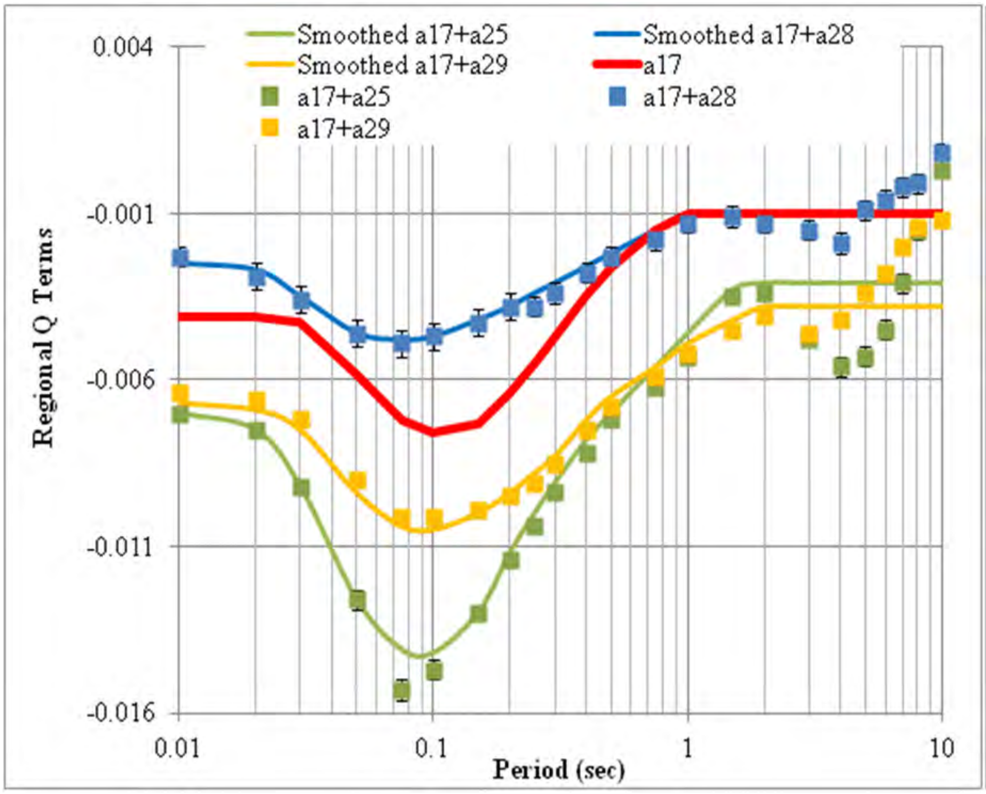

Figure 2.18 Smoothing of the large distance scaling different regions.

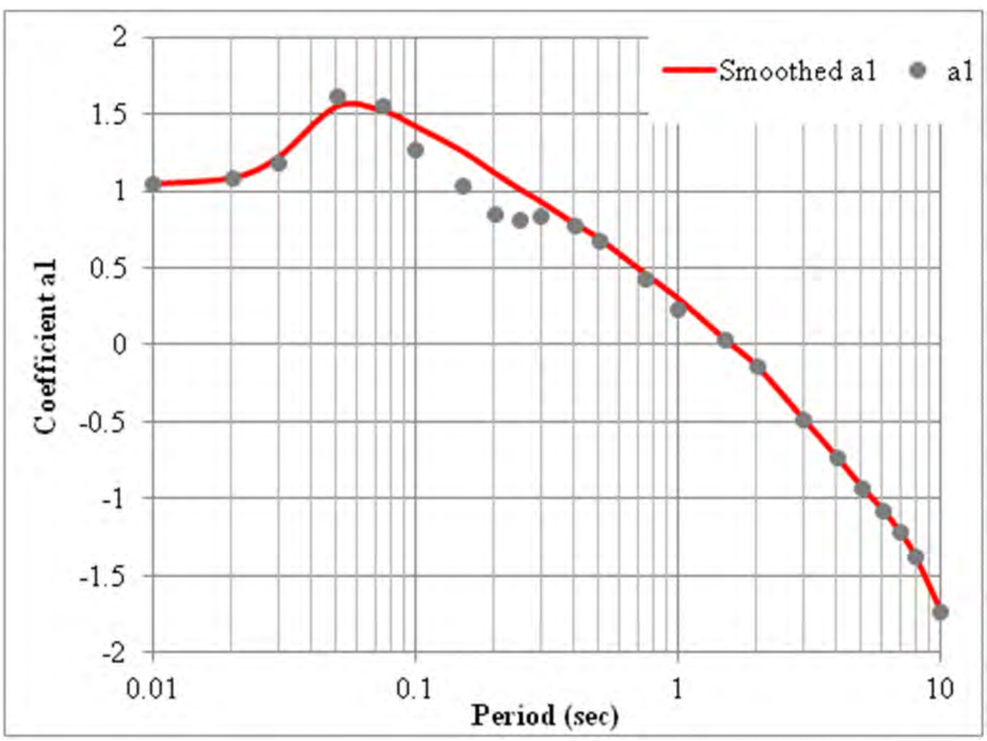

Figure 2.19 Smoothing of the constant term.

Table 2.2(a) Coefficients for the median ground motion.

Parameter	V_{LIN}	c_4	a_1	a_2	a_3	a_4	a_5	a_6
PGA	660	8	1.025	-1.100	0.400	-0.380	-0.832	1.900
T=0.010	660	8	1.045	-1.100	0.400	-0.380	-0.832	1.900
T =0.020	680	8	1.085	-1.100	0.400	-0.380	-0.832	1.900
T =0.030	770	8	1.220	-1.100	0.400	-0.380	-0.832	1.900
T =0.050	800	8	1.550	-1.100	0.400	-0.380	-0.832	1.900
T =0.075	800	8	1.520	-1.004	0.400	-0.380	-0.832	1.900
T =0.100	800	8	1.420	-0.936	0.382	-0.380	-0.795	1.900
T =0.150	740	8	1.260	-0.841	0.357	-0.380	-0.743	1.900
T =0.200	590	8	1.117	-0.773	0.339	-0.380	-0.706	2.022
T =0.250	495	8	1.010	-0.750	0.326	-0.380	-0.677	2.117
T =0.300	430	8	0.930	-0.750	0.314	-0.380	-0.654	2.194
T =0.400	360	8	0.790	-0.750	0.297	-0.380	-0.617	2.317
T =0.500	340	8	0.690	-0.750	0.283	-0.380	-0.588	2.411
T =0.750	330	8	0.460	-0.750	0.258	-0.380	-0.536	2.584
T =1.000	330	8	0.300	-0.750	0.240	-0.380	-0.499	2.706
T =1.500	330	8	0.038	-0.750	0.211	-0.380	-0.438	2.878
T =2.000	330	8	-0.142	-0.750	0.190	-0.380	-0.395	3.000
T =3.000	330	8	-0.482	-0.750	0.161	-0.380	-0.335	3.000

Table 2.2(b) Coefficients for the median ground motion.

Parameter	a_8	a_{10}	a_{11}	a_{12}	a_{13}	a_{14}	a_{15}	a_{17}
PGA	0.000	-0.350	-0.260	-0.180	0.750	-0.230	1.530	-0.004
T=0.010	0.000	-0.420	-0.260	-0.180	0.750	-0.230	1.530	-0.004
T=0.020	0.000	-0.420	-0.260	-0.180	0.750	-0.230	1.530	-0.004
T=0.030	0.000	-0.420	-0.260	-0.180	0.750	-0.230	1.530	-0.004
T=0.050	0.000	-0.420	-0.260	-0.180	0.750	-0.230	1.530	-0.006
T =0.075	0.000	-0.448	-0.260	-0.180	0.750	-0.230	1.530	-0.007
T =0.100	0.000	-0.469	-0.260	-0.180	0.750	-0.230	1.530	-0.008
T =0.150	-0.035	-0.497	-0.217	-0.148	0.750	-0.230	1.530	-0.007
T =0.200	-0.060	-0.517	-0.180	-0.126	0.750	-0.163	1.530	-0.006
T =0.250	-0.080	-0.533	-0.151	-0.108	0.694	-0.112	1.414	-0.006
T =0.300	-0.095	-0.546	-0.127	-0.094	0.649	-0.069	1.320	-0.005
T =0.400	-0.120	-0.566	-0.090	-0.072	0.577	-0.003	1.170	-0.004
T =0.500	-0.140	-0.582	-0.061	-0.054	0.521	0.049	1.055	-0.003
T =0.750	-0.175	-0.610	-0.008	-0.023	0.419	0.143	0.844	-0.002
T =1.000	-0.200	-0.690	0.030	0.000	0.347	0.210	0.695	-0.001
T =1.500	-0.249	-0.780	0.082	0.000	0.246	0.304	0.484	-0.001
T =2.000	-0.284	-0.810	0.120	0.000	0.174	0.371	0.335	-0.001
T =3.000	-0.334	-0.761	0.173	0.000	0.072	0.465	0.125	-0.001

Table 2.3 Coefficients for the median ground motion for other regions.

Parameter	a_{25}	a_{28}	a_{29}
PGA	-0.0029	0.0016	-0.0026
T=0.010	-0.0029	0.0016	-0.0026
T=0.020	-0.0034	0.0014	-0.0028
T=0.030	-0.0049	0.0008	-0.0032
T =0.050	-0.0068	0.0012	-0.0036
T =0.075	-0.0069	0.0024	-0.0032
T =0.100	-0.0066	0.0029	-0.0029
T =0.150	-0.0057	0.0031	-0.0027
T =0.200	-0.0048	0.0026	-0.003
T =0.250	-0.0045	0.0021	-0.0033
T =0.300	-0.0044	0.0016	-0.0036
T =0.400	-0.0043	0.0009	-0.0037
T =0.500	-0.0044	0.0004	-0.0039
T =0.750	-0.0041	0	-0.0041
T =1.000	-0.0036	0	-0.0039
T =1.500	-0.0023	0	-0.0032
T =2.000	-0.0021	0	-0.0028
T =3.000	-0.0021	0	-0.0028

2.4 RESIDUALS

In this section, residuals from the regression analysis are shown as functions of all the main independent parameters to allow an evaluation of the model. The residuals are shown for PGA and spectral periods of 0.1 and 1.0 sec.

2.4.1 Inter-event Residuals

The inter-event residuals are plotted as functions of magnitude, depth-to-top of rupture, and rake in Figures 2.20(a) through 2.20(c) for PGA and spectral periods of 0.1and 1.0 sec, respectively. The open circles represent the Western U.S (WUS) data while the open squares represent all other regions. For all periods, there is not a strong magnitude or rake dependence. For Z_{TOR}, there is no trend up to 15 km but the average residual beyond 15 km is slightly negative. Given the sparse data at that range (only nine events) we consider the model scaling of Z_{TOR} to be acceptable, but note that it is poorly constrained for Z_{TOR} > 15 km.

2.4.2 Intra-event Residuals

The base model is evaluated through the distance dependence of the intra-event residuals by magnitude bins for WUS data in Figures 2.21(a) through 2.21(c). The magnitude bins 3, 4, 5, 6, and 7 correspond to magnitude ranges of: 3≤M<3.5, 3.5≤M<4.5, 4.5≤M<5.5, 5.5≤M<6.5 and 6.5≤M<8, respectively. There are no apparent trends in the residuals up to a distance of about 100 km. At longer distances, the magnitude-bin 6 data is slightly under-predicted. The magnitude-bin 7 data is fit by the model out to distance of 200 km for all periods and only slightly over-predicted for longer distances.

The linear site response model is evaluated through the V_{S30} dependence of the intra-event residuals, shown in Figures 2.22(a) through 2.22(c) for WUS, Japan, and all other regions separately. Overall, the WUS data shows no trend in the residuals as a function of V_{S30}. There are two WUS recordings with V_{S30} = 2000 m/sec that are high for all spectral periods. This could be related to lower kappa, which is not accounted for in this model. The Japanese at T = 1 sec is under-predicted at low V_{S30} and over-predicted at high V_{S30}, indicating that this data has a weaker V_{S30} scaling than our average model. As discussed above, while we recognize the need to regionalize the V_{S30} scaling, this version of the model does not account for a regionalized V_{S30} scaling at this time.

The effect of nonlinear site response is evaluated through the Sa_{1180} dependence of the intra-event residuals for soil sites, shown in Figures 2.23(a) through 2.23(c) for sites with 180<V_{s30}<360 m/sec only, for WUS, Japan, and all other regions separately. For the WUS residuals there is no observed trend despite not including nonlinear effects in the model, indicating that the current data in the NGA-West2 database does not include much nonlinearity. The Japanese data, however, is over-predicted at strong shaking intensity, indicating that the Japanese data does have some nonlinear effects that are currently not accounted for by the model.

Finally, the $Z_{1.0}$ scaling is evaluated by examining the residuals for four different V_{s30} bins in Figure 2.24(a) through 2.24(c). The intra-event residuals are plotted as a function of $Z_{1.0.}$ There are no trends for PGA and T = 0.1 sec, but at T = 1.0 sec, the data is under-predicted as $Z_{1.0}$ increases, indicating that there is some basin amplification that is currently not accounted for by the model at longer periods.

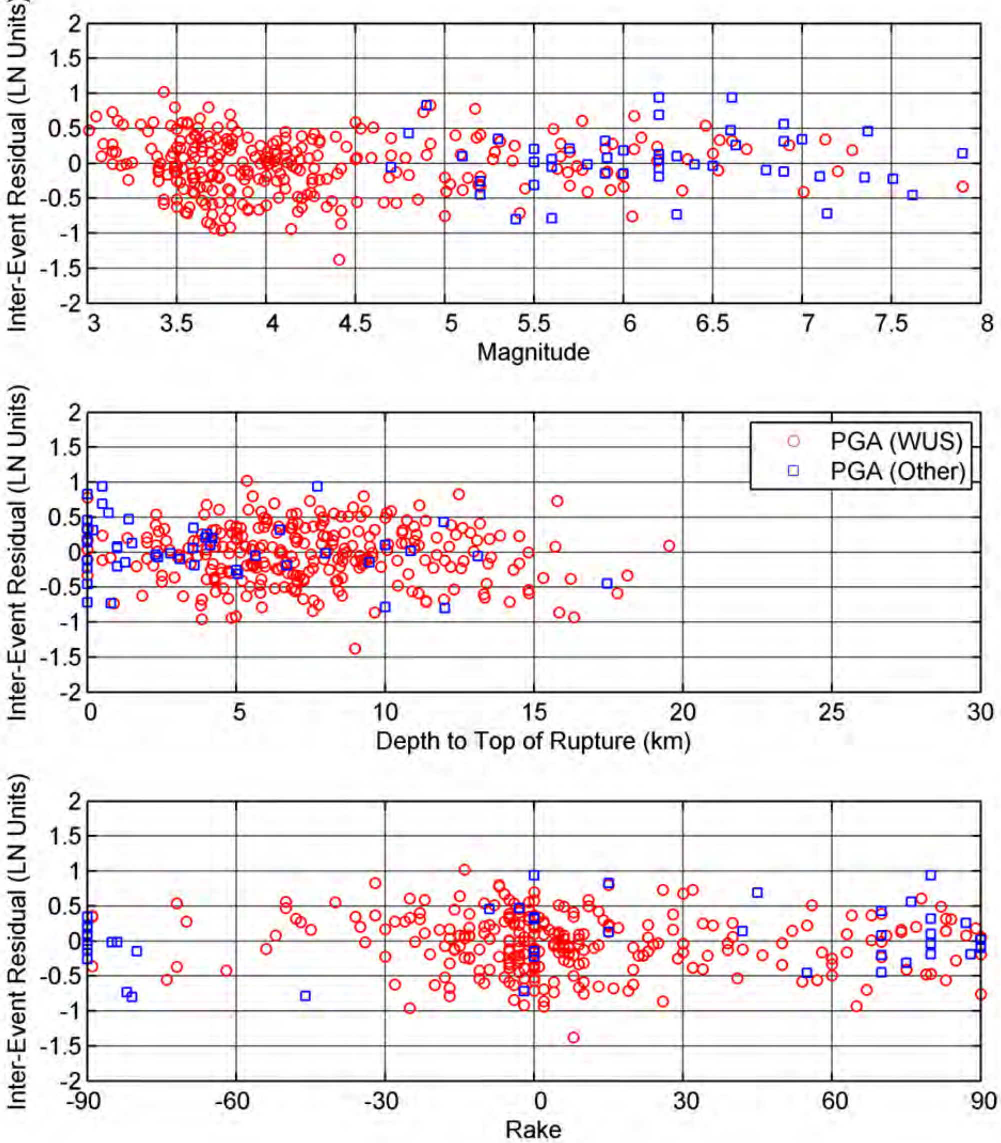

Figure 2.20(a) Event terms for PGA.

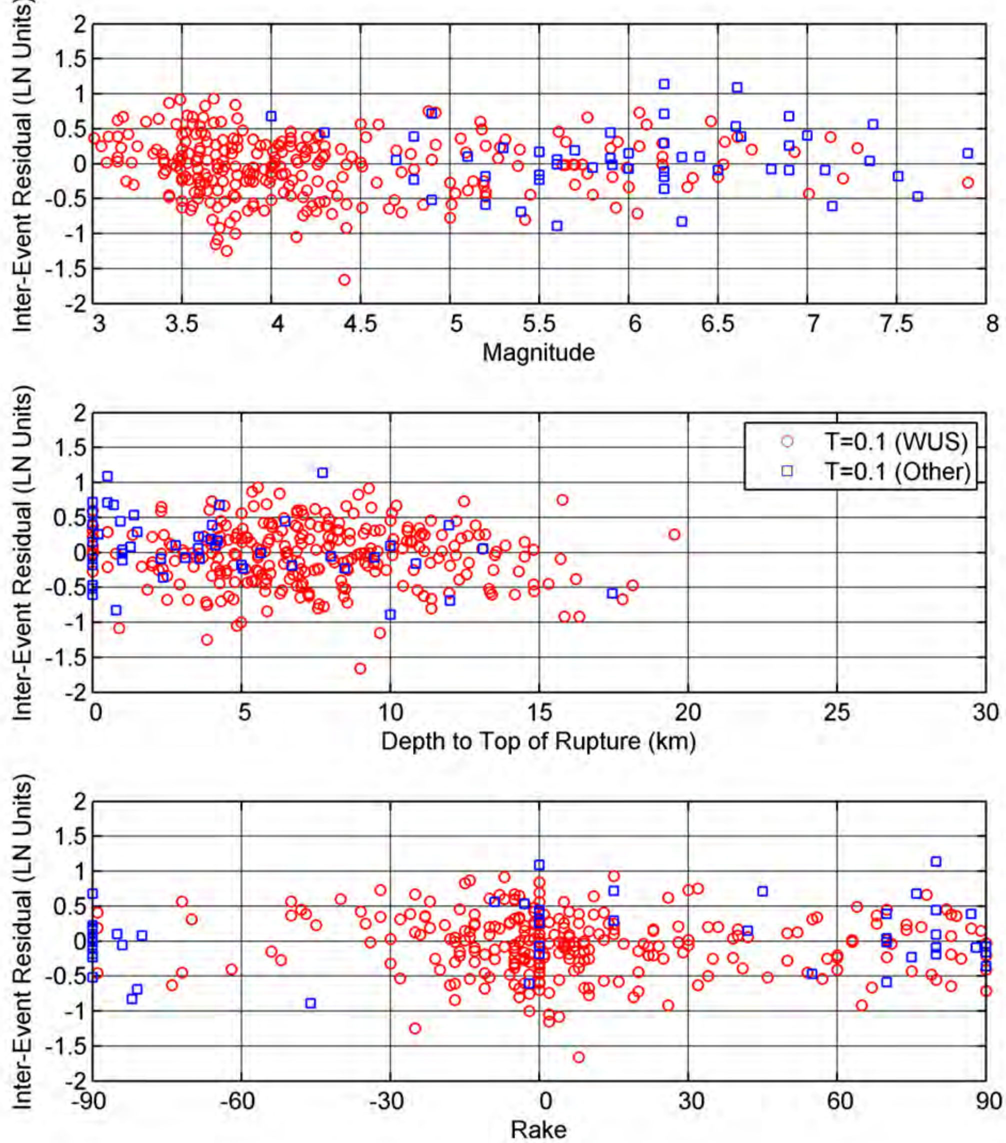

Figure 2.20(b) **Event terms for *T* = 0.1 sec.**

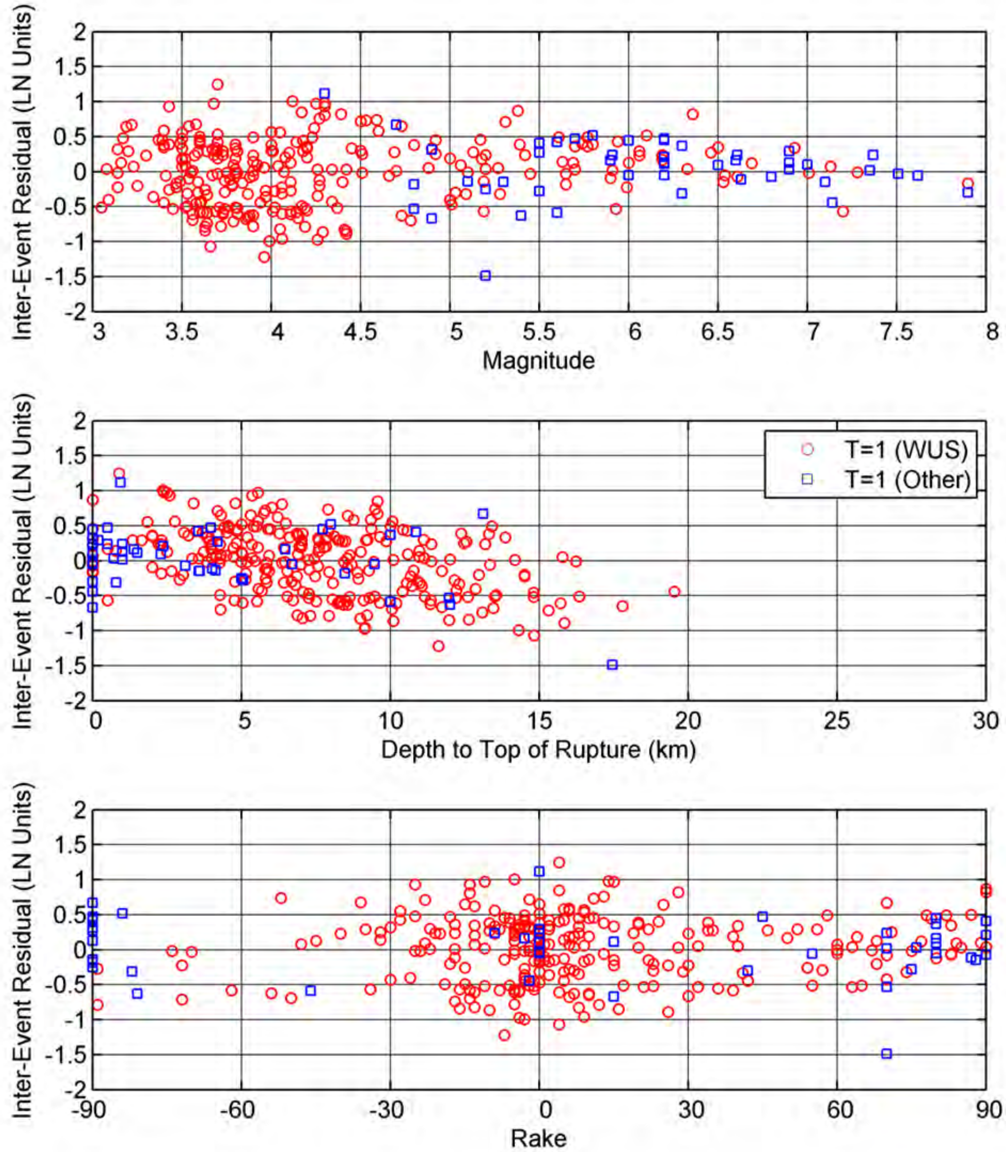

Figure 2.20(c) **Event terms for *T* = 1.0 sec.**

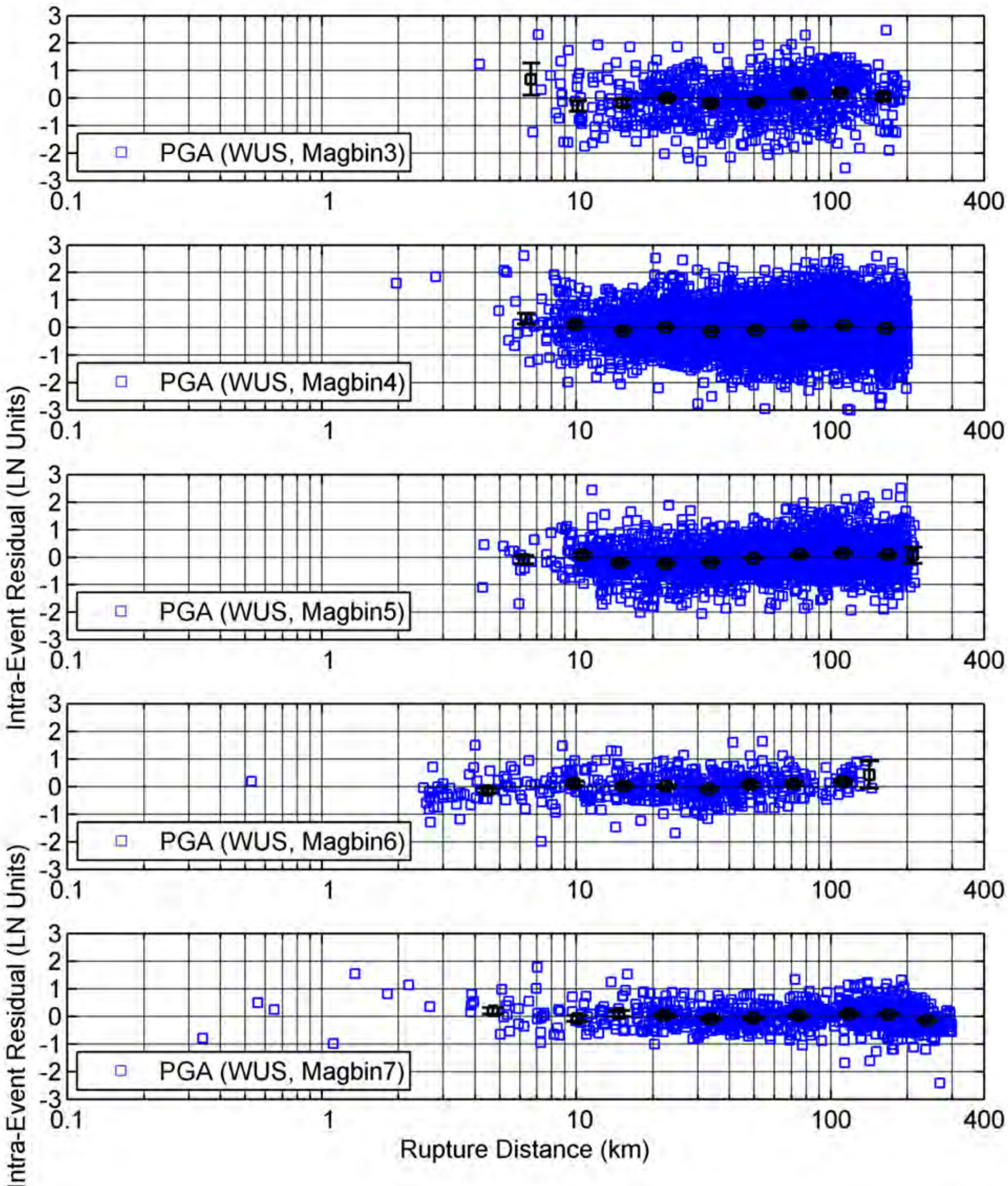

Figure 2.21(a) Distance dependence of the intra-event residuals, WUS only, by magnitude bins, PGA.

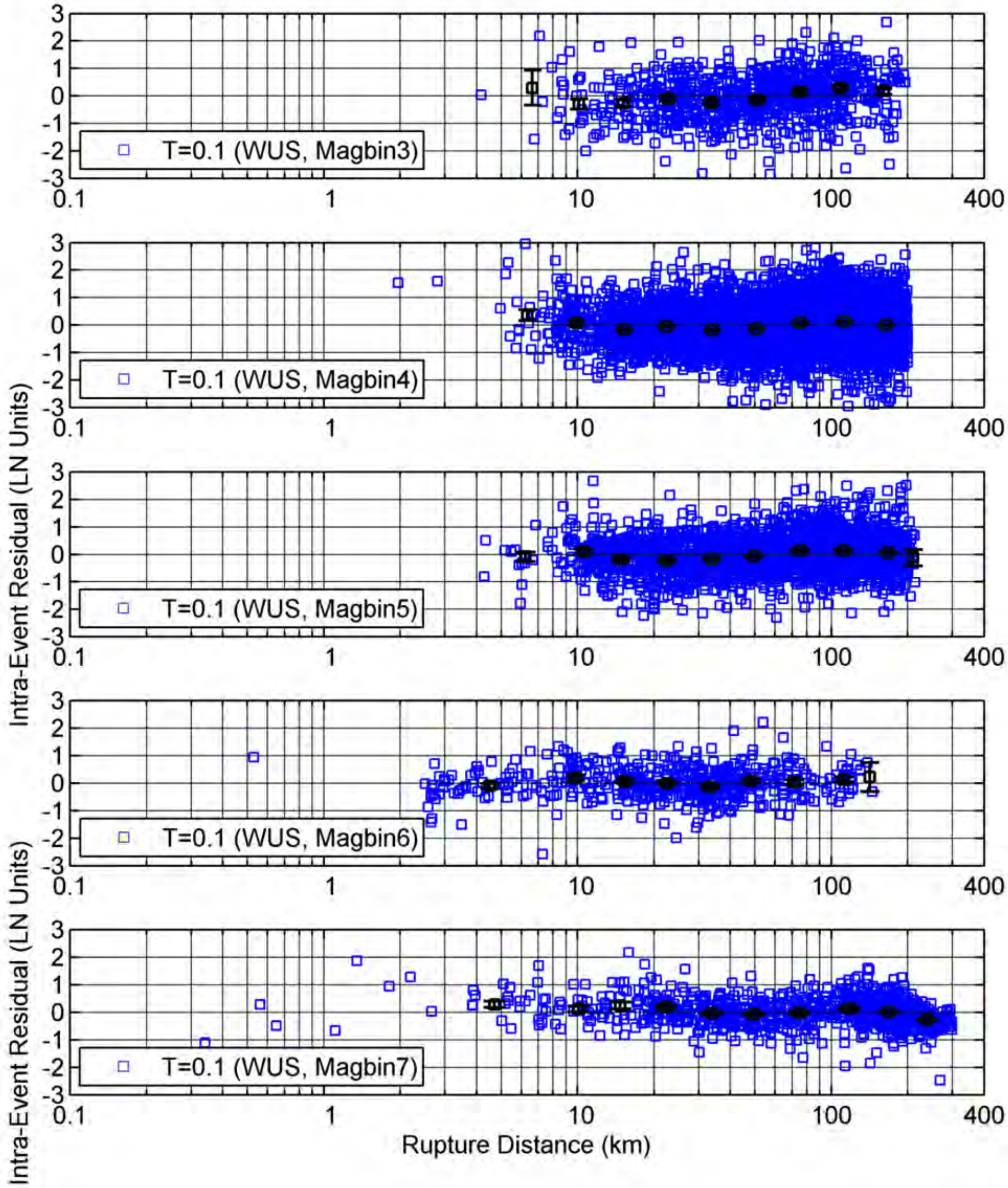

Figure 2.21(b) Distance dependence of the intra-event residuals, WUS only, by magnitude bins, *T* = 0.1 sec.

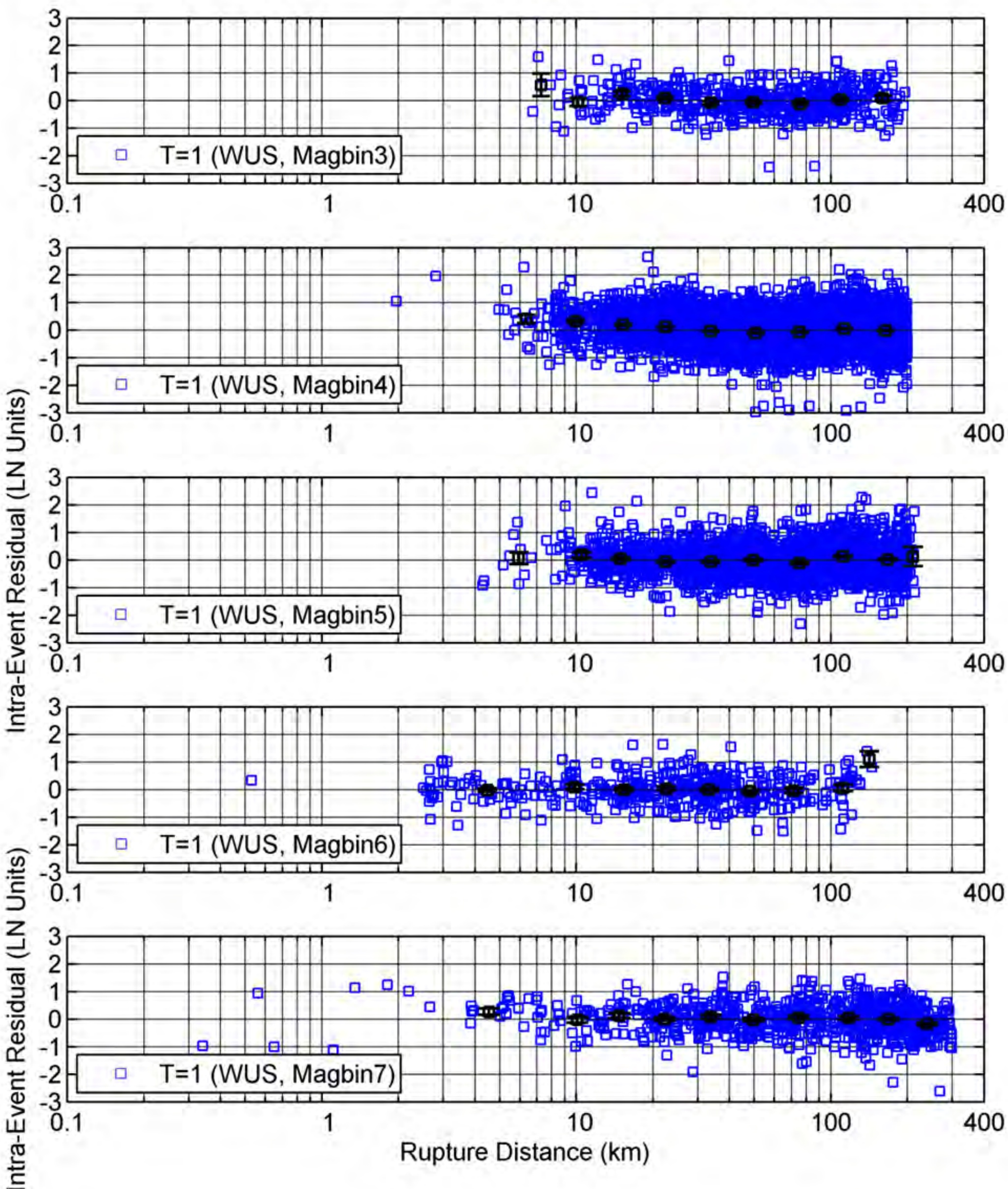

Figure 2.21(c) **Distance dependence of the intra-event residuals, WUS only, by magnitude bins, *T* = 1.0 sec.**

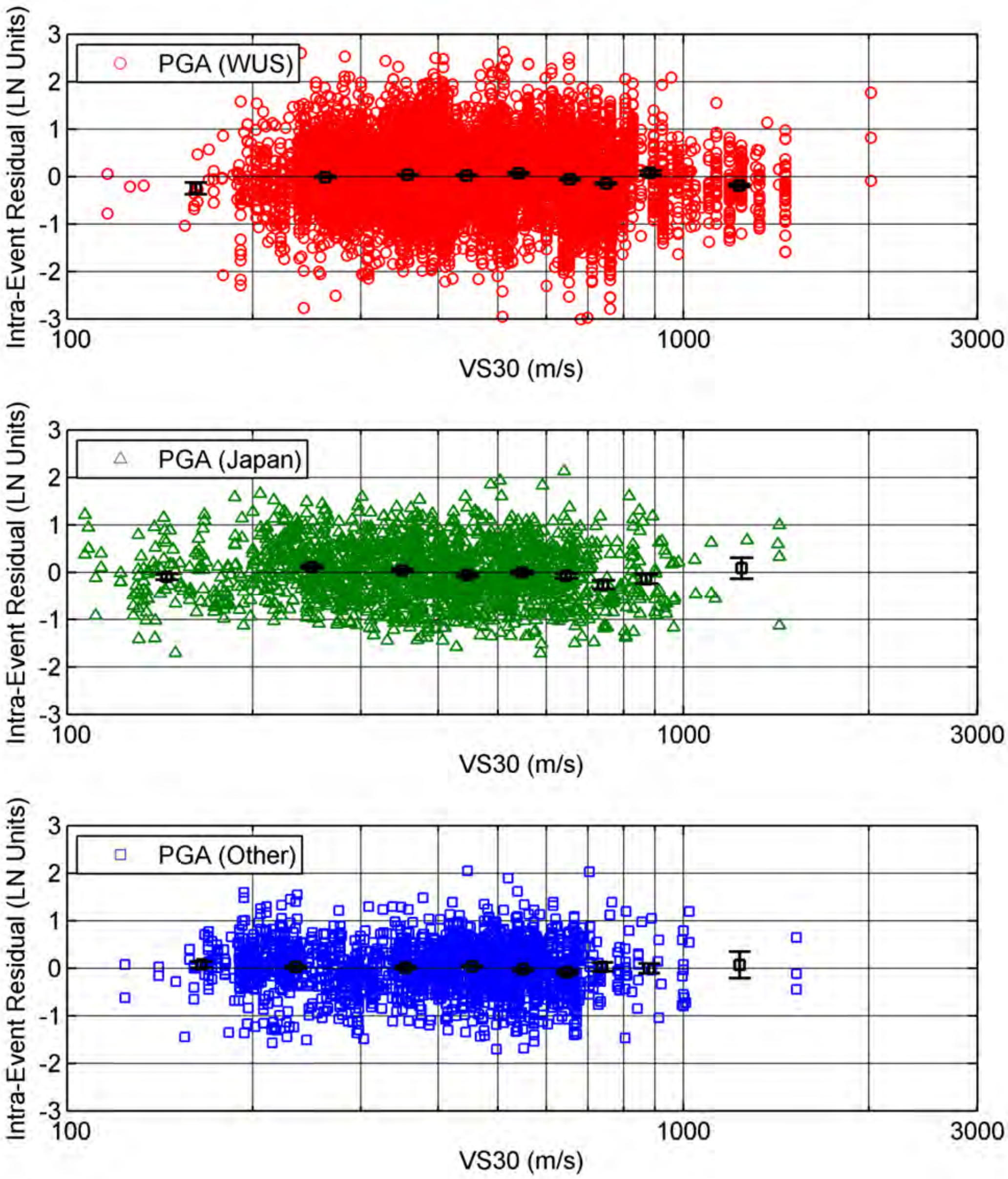

Figure 2.22(a) V_{s30} dependence of the intra-event residuals, PGA.

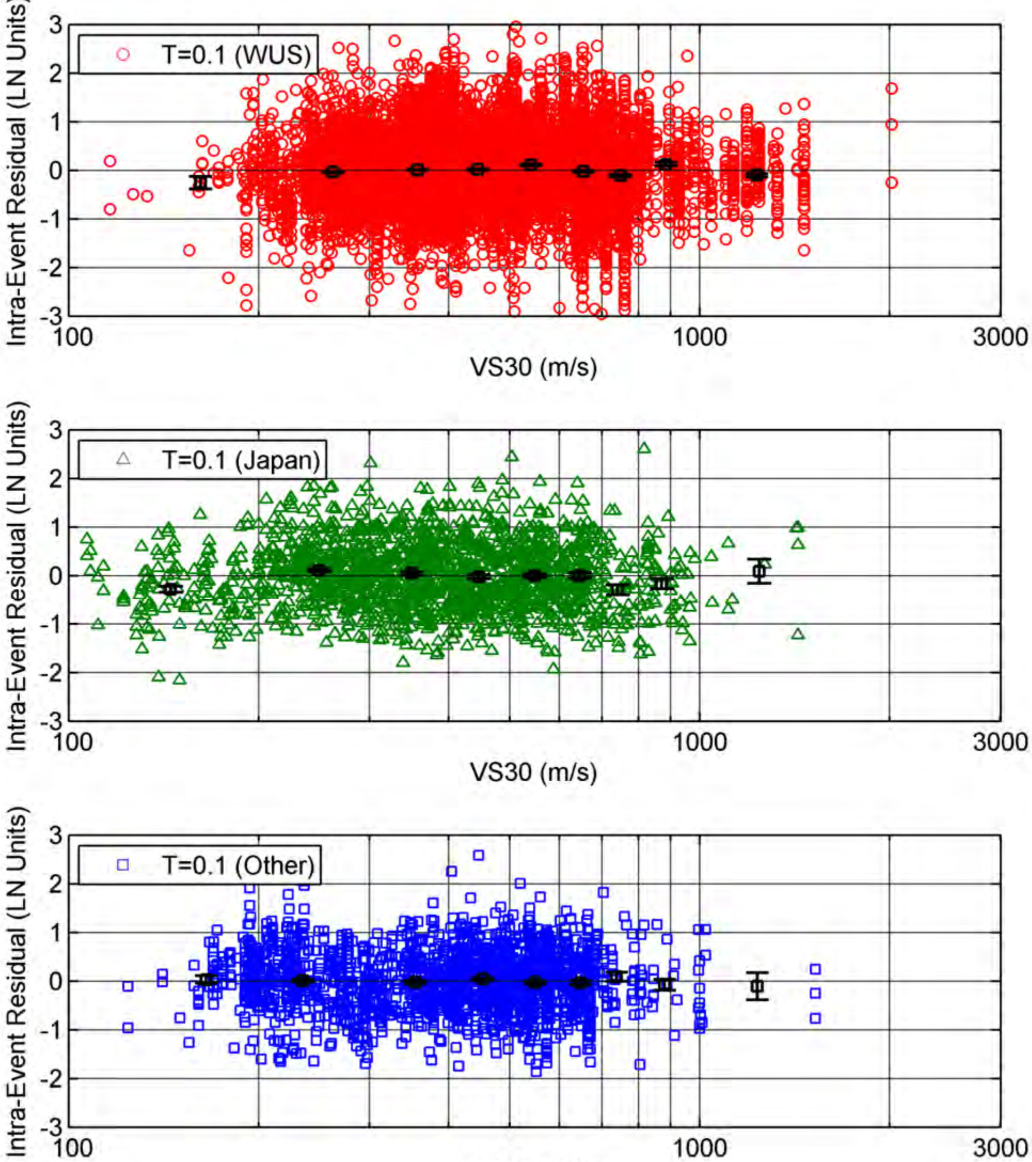

Figure 2.22(b) V_{s30} **dependence of the intra-event residuals,** T **= 0.1 sec.**

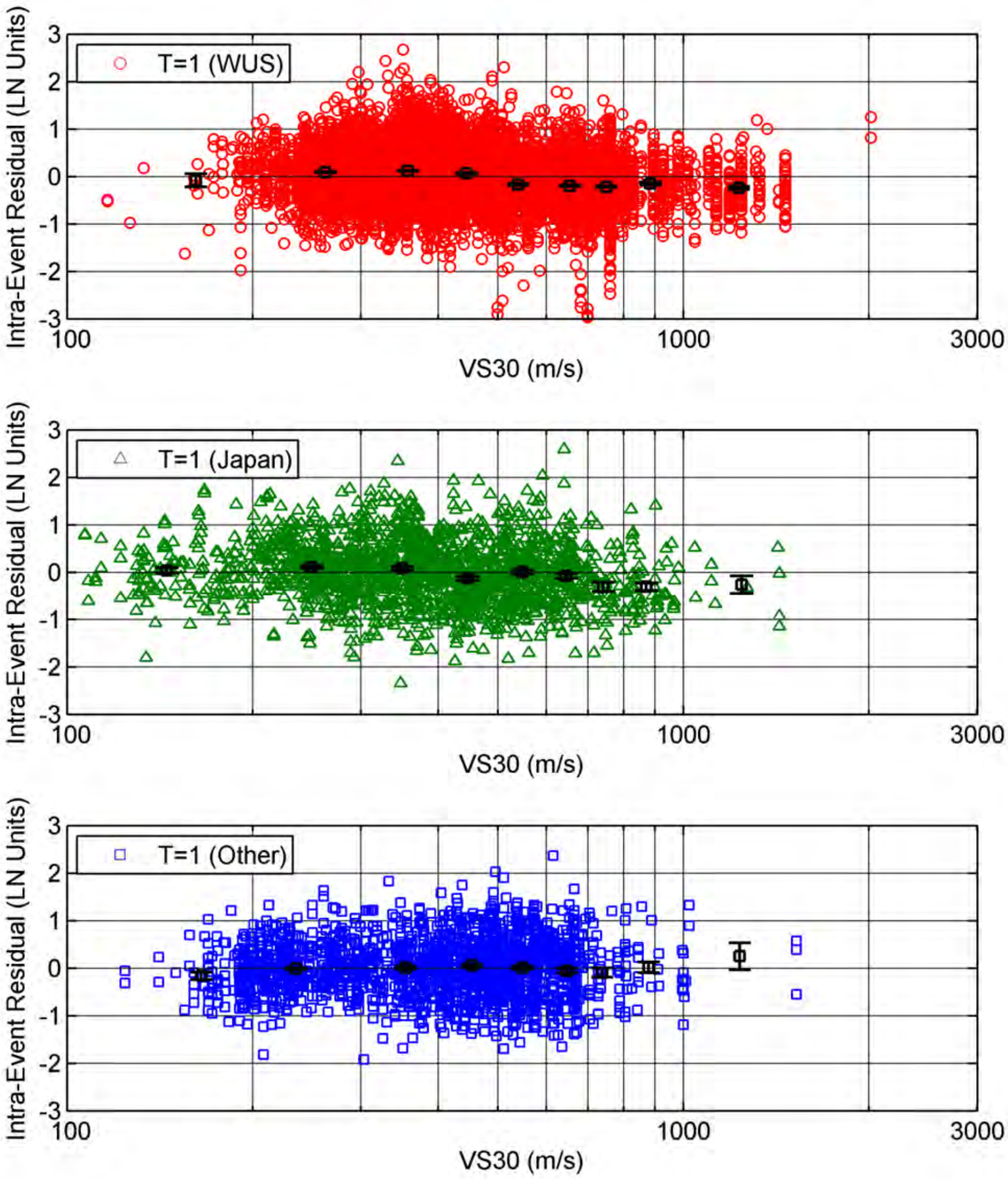

Figure 2.22(c) V_{s30} **dependence of the intra-event residuals,** T **= 1.0 sec.**

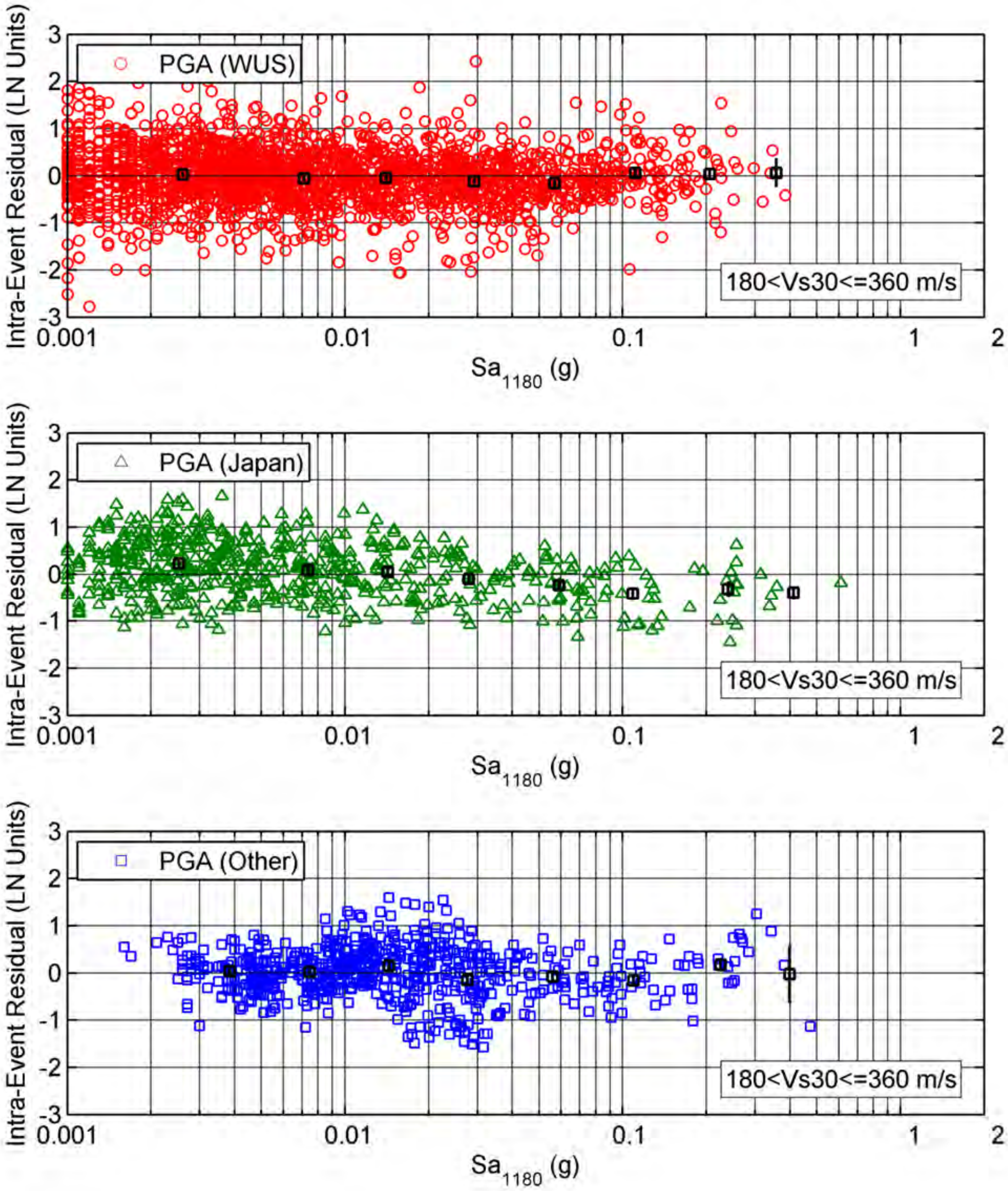

Figure 2.23(a) ***Sa_{1180}* dependence of the Intra-event residuals, PGA.**

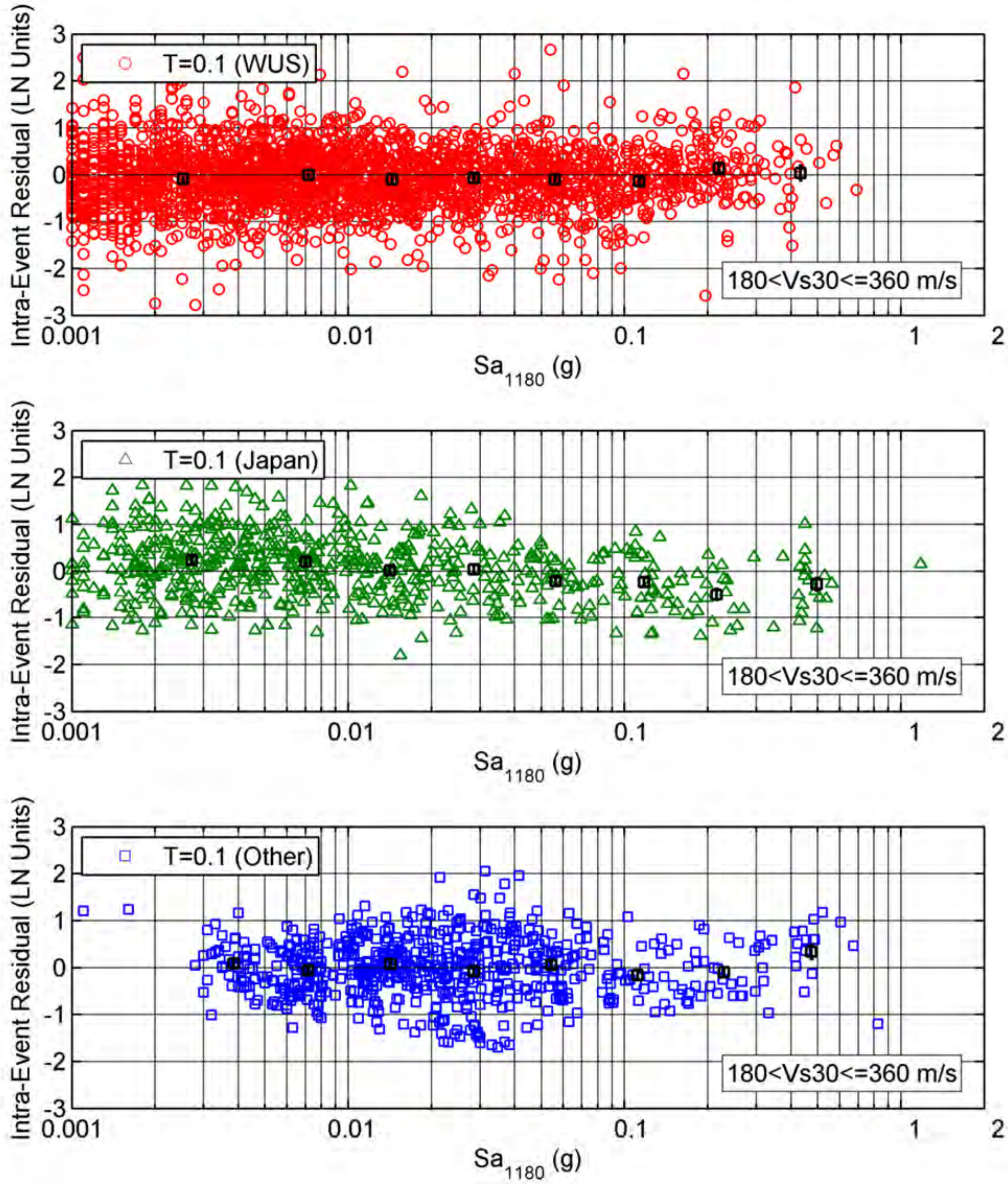

Figure 2.23(b) **Sa_{1180} dependence of the Intra-event residuals, *T* = 0.1 sec.**

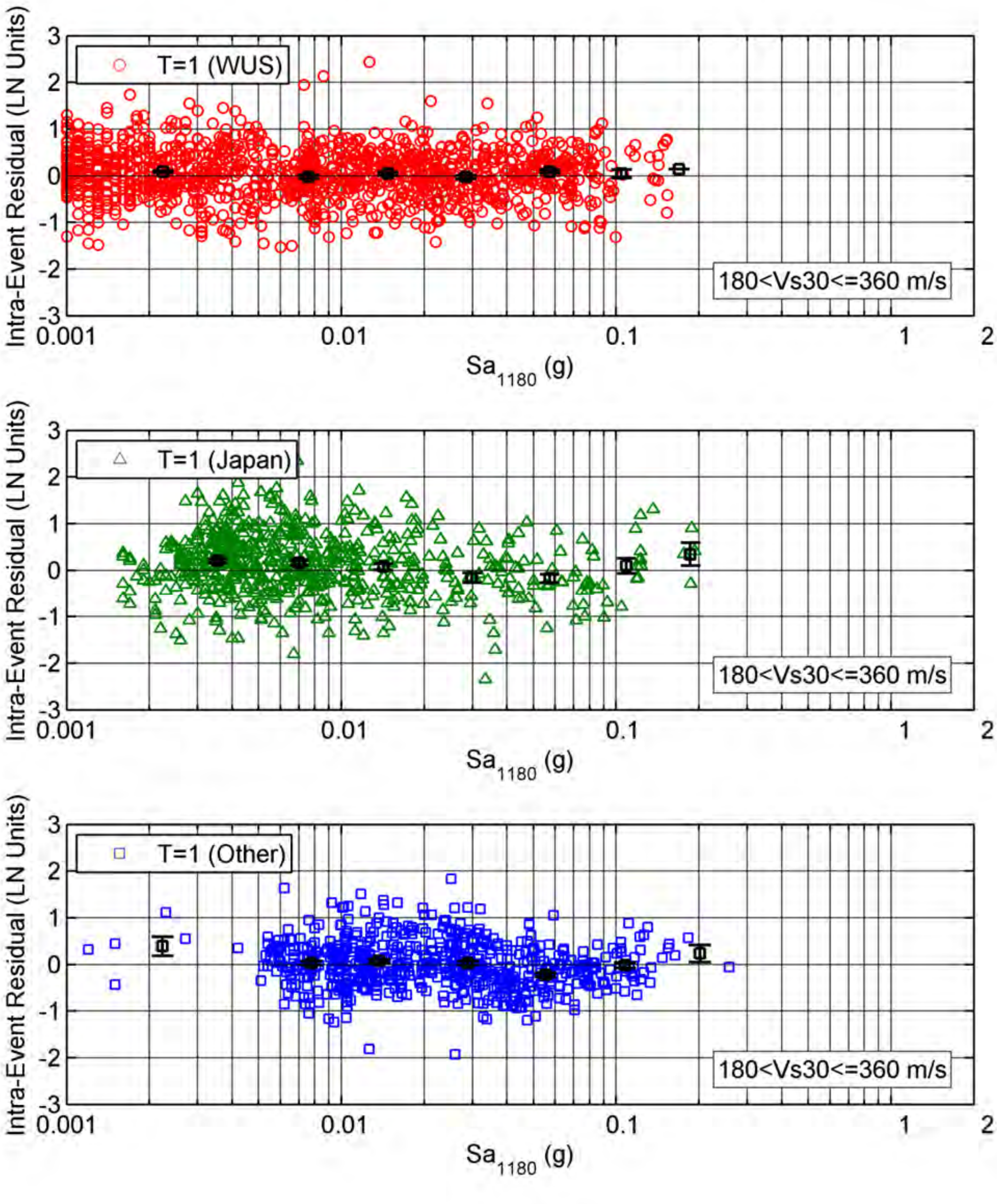

Figure 2.23(c) ***Sa*$_{1180}$ dependence of the Intra-event residuals, *T* = 1.0 sec.**

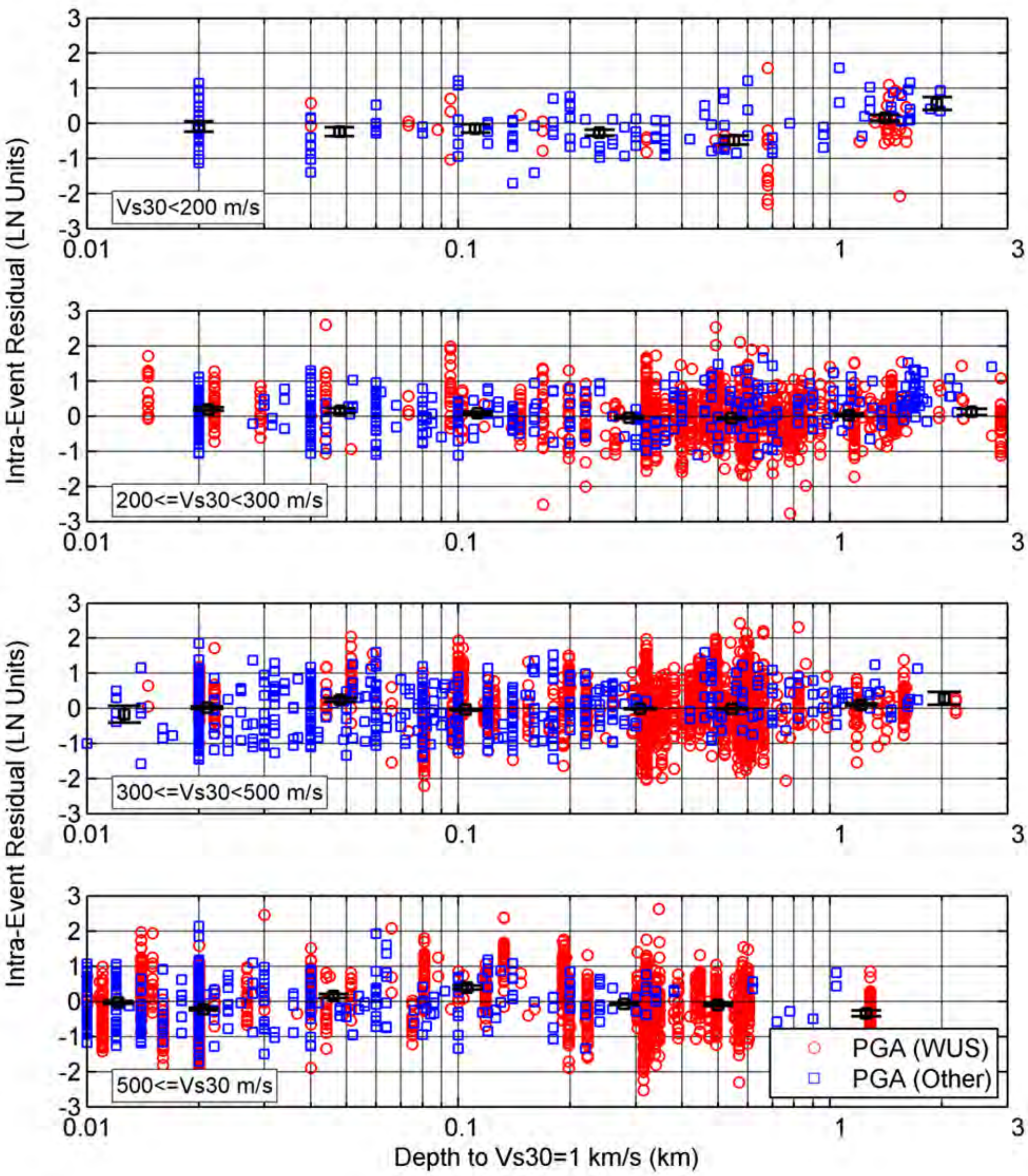

Figure 2.24(a) $\quad$ **Z_1 dependence of the intra-event residuals, PGA.**

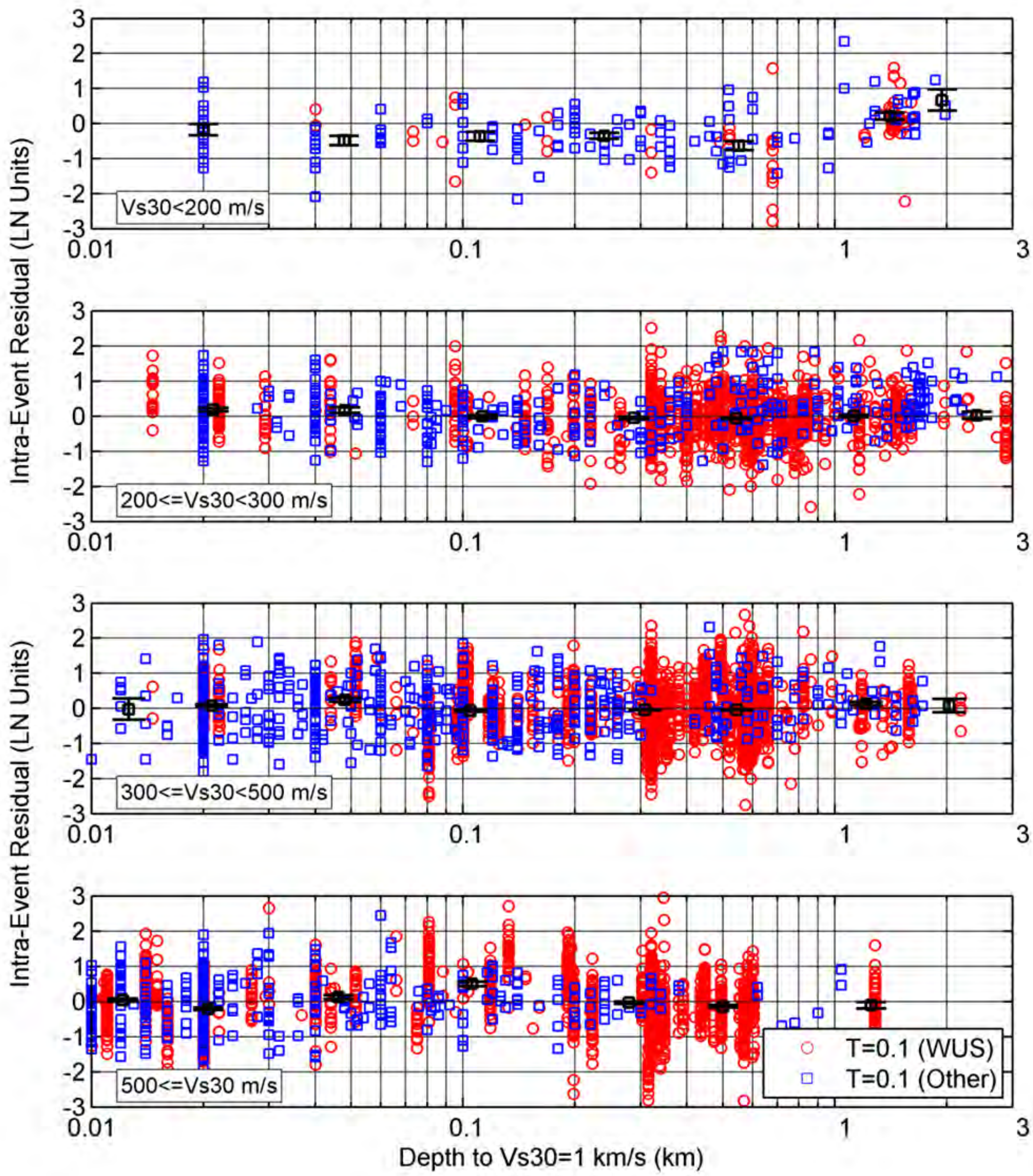

Figure 2.24(b) *Z_1* **dependence of the intra-event residuals,** ***T*** **= 0.1 sec.**

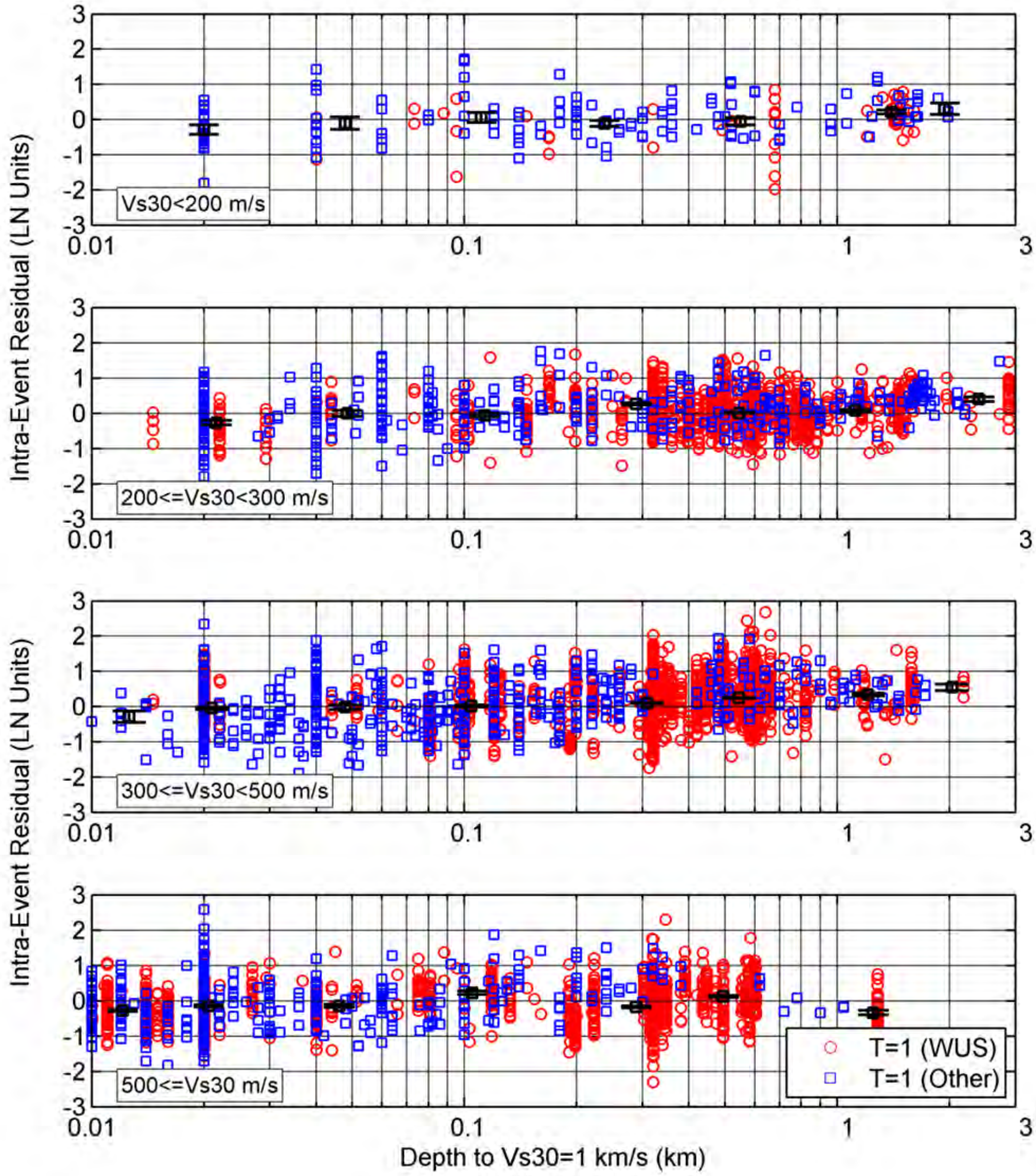

Figure 2.24(c) ***Z_1* dependence of the intra-event residuals, *T* = 1.0 sec.**

2.5 STANDARD DEVIATIONS

The intra-event and inter-event standard deviations are magnitude dependent, as follows:

$$\phi_{A,L}(M) = \begin{cases} s_1 & for\ M < 4 \\ s_1 + \frac{s_2 - s_1}{2}(M-4) & for\ 4 \leq M \leq 6 \\ s_2 & for\ M > 6 \end{cases} \tag{2.18}$$

and

$$\tau_{A,L}(M) = \begin{cases} s_3 & for\ M < 5 \\ s_3 + \frac{s_4 - s_3}{2}(M-5) & for\ 5 \leq M \leq 7 \\ s_4 & for\ M > 7 \end{cases} \tag{2.19}$$

where $\phi_{A,L}$ is the linear intra-event standard deviation and $\tau_{A,L}$ is the linear inter-event standard deviation. The smoothed s_1 through s_4 parameters are provided in Table 2.4 and presented in Figure 2.25.

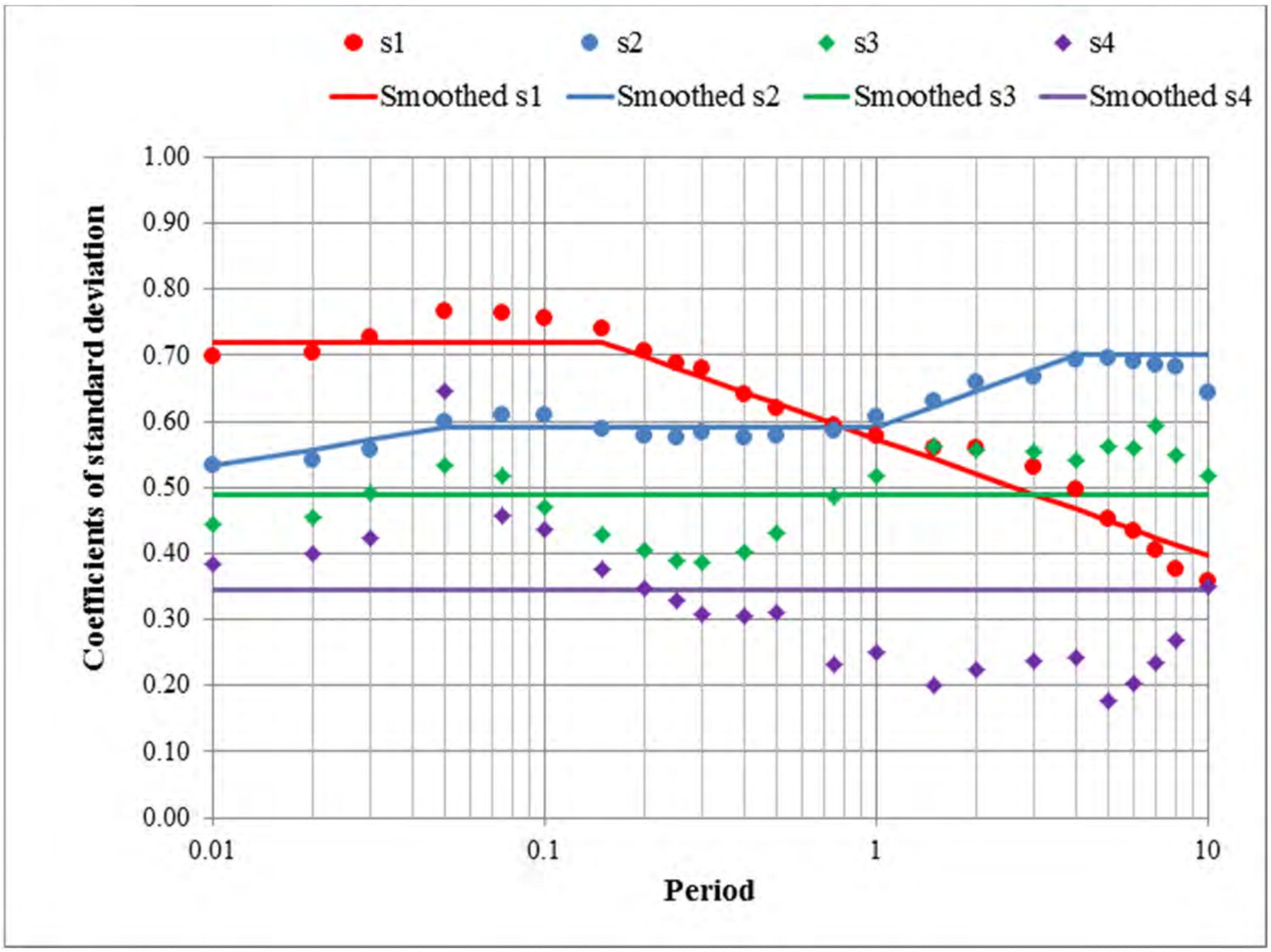

Figure 2.25 Smooth coefficients for the standard deviation models.

Table 2.4 **Coefficients for the standard deviation.**

T (sec)	s_1	s_2	s_3	s_4
PGA	0.720	0.534	0.490	0.345
0.010	0.720	0.534	0.490	0.345
0.020	0.720	0.558	0.490	0.345
0.030	0.720	0.572	0.490	0.345
0.050	0.720	0.590	0.490	0.345
0.075	0.720	0.590	0.490	0.345
0.100	0.720	0.590	0.490	0.345
0.150	0.720	0.590	0.490	0.345
0.200	0.698	0.590	0.490	0.345
0.250	0.681	0.590	0.490	0.345
0.300	0.667	0.590	0.490	0.345
0.400	0.644	0.590	0.490	0.345
0.500	0.627	0.590	0.490	0.345
0.750	0.596	0.590	0.490	0.345
1.000	0.574	0.590	0.490	0.345
1.500	0.543	0.622	0.490	0.345
2.000	0.521	0.645	0.490	0.345
3.000	0.489	0.677	0.490	0.345

2.6 MODEL RESULTS

The median response spectra for the vertical model are compared with the horizontal model (ASK13) in Figures 2.26 through 2.30. Unless noted otherwise, all plots in this section represent the base model (excluding Taiwan, China, and Japan), the Z_{TOR} values are 8, 6.5, 3, and 0 for magnitudes 5, 6, 7, and 8, respectively, and the $Z_{1.0}$ values are set at the Z_{ref} value [Chiou and Youngs 2013] for the given V_{S30}.

Figures 2.26(a) and (b) show a vertical strike-slip scenario at an R_{JB} distance of 30 km and V_{s30} values of 760 m/sec and 270 m/sec, respectively. A similar comparison of the medians at a R_{JB} distance of 1 km is shown in Figure 2.27(a) and (b) for V_{S30} values of 760 m/sec and 270 m/sec. As expected, the peak in the spectra is at shorter periods for the vertical model, especially for soil sites. The sharp peak at $T = 0.1$ sec (especially for the smaller magnitudes) is probably due to insufficient sampling of spectral periods. We will add more periods to the regression in future developments, to be sure to capture the right spectral peak.

While the vertical model is lower than the horizontal for a rock site at a distance of 30 km, the ratio of vertical-to-horizontal (V/H ratio) becomes larger for shorter distances [e.g.,

Figure 2.27(a)] and is clearly larger than one at short periods for soil sites at short distances [e.g., Figure 2.27(b)].

The distance scaling is shown in Figure 2.28 for PGA and spectral periods of 0.1, 1.0, and 3.0 sec. In this figure, the median ground motion from vertical strike-slip earthquakes on rock site conditions (V_{S30} = 760 m/sec) is shown for four different magnitudes.

The magnitude scaling of the current model is shown in Figures 2.29 for vertical strike-slip earthquakes on rock site conditions (V_{S30}=760 m/sec) for T =0.1 and T =3.0 sec. The weak scaling of the short-period motion at short distances reflects the saturation with magnitude.

The site response scaling for **M**7 vertical strike-slip earthquakes at a rupture distance of 30 km is shown in Figure 2.30, presenting the dependence of the spectra on the V_{S30} value.

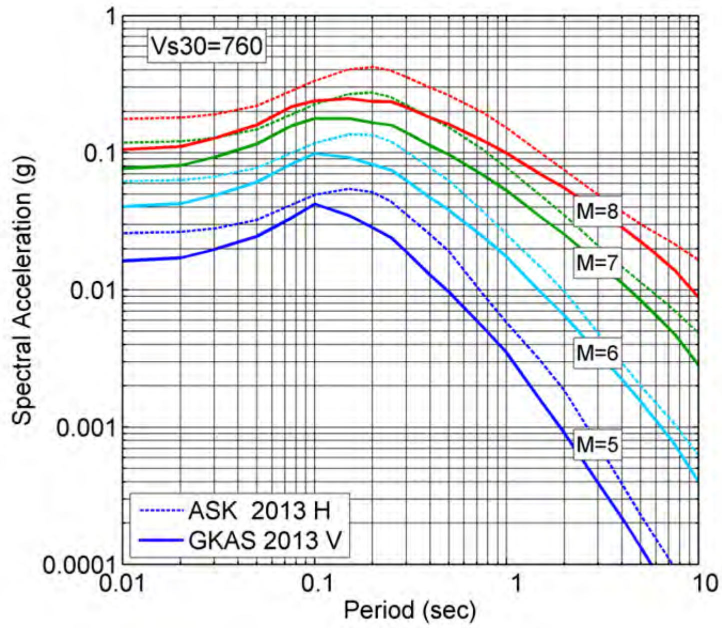

Figure 2.26(a) Comparison of the median spectral acceleration: SS, R_{JB} = 30 km, V_{S30} = 760 m/sec.

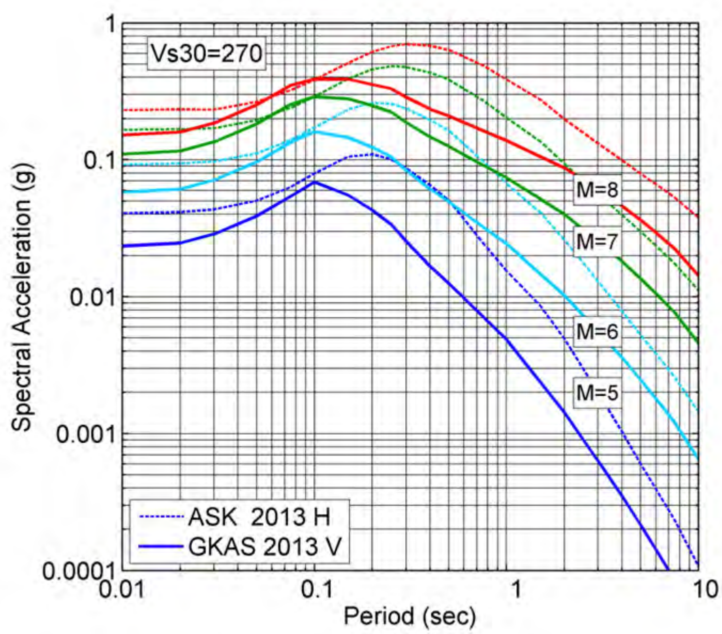

Figure 2.26(b) Comparison of the median spectral acceleration: SS, R_{JB} = 30 km, V_{S30} = 270 m/sec.

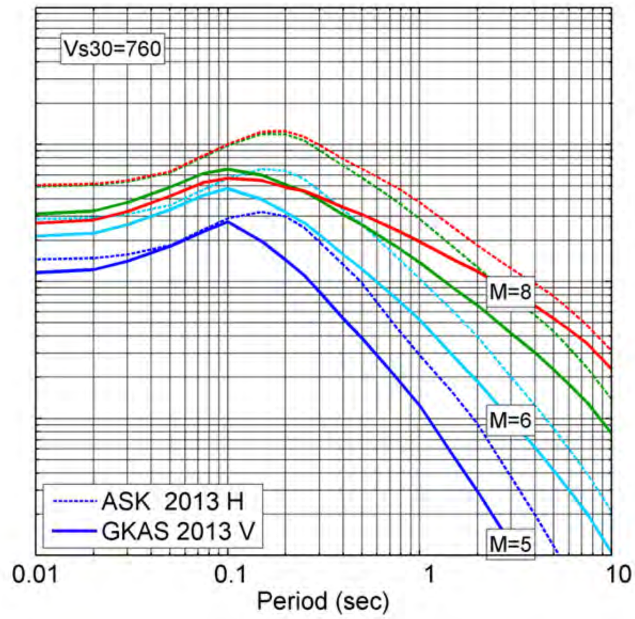

Figure 2.27(a) Comparison of the median spectral acceleration: SS, R_{JB} = 1 km, V_{S30} = 760 m/sec.

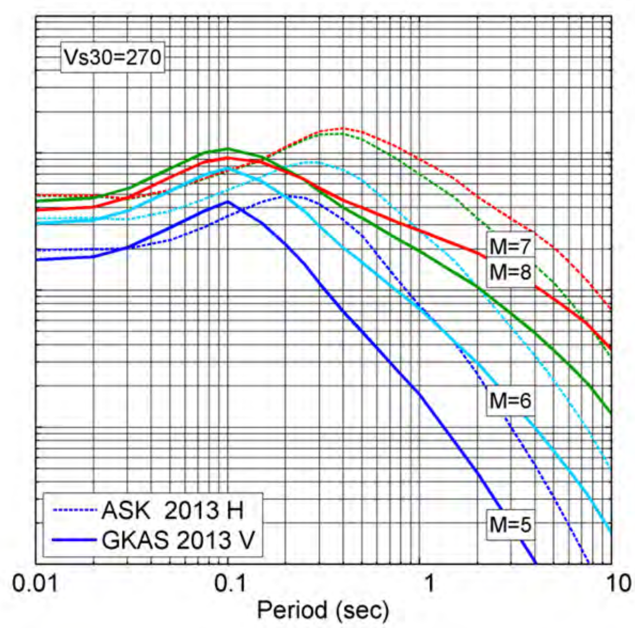

Figure 2.27(b) Comparison of the median spectral acceleration: SS, R_{JB} = 1 km, V_{S30} = 270 m/sec.

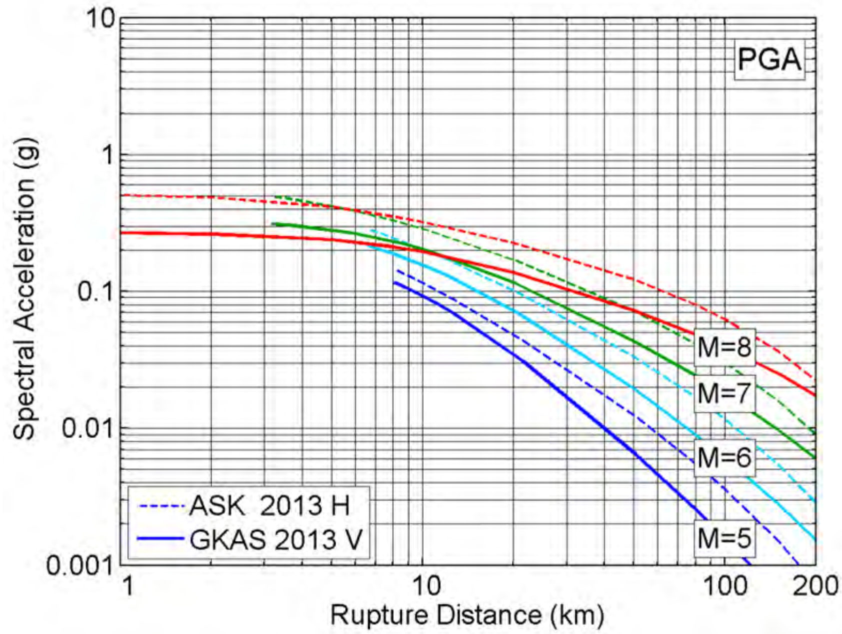

Figure 2.28(a) Comparison of the rupture distance scaling for a vertical strike slip with V_{S30} = 760 m/sec at PGA.

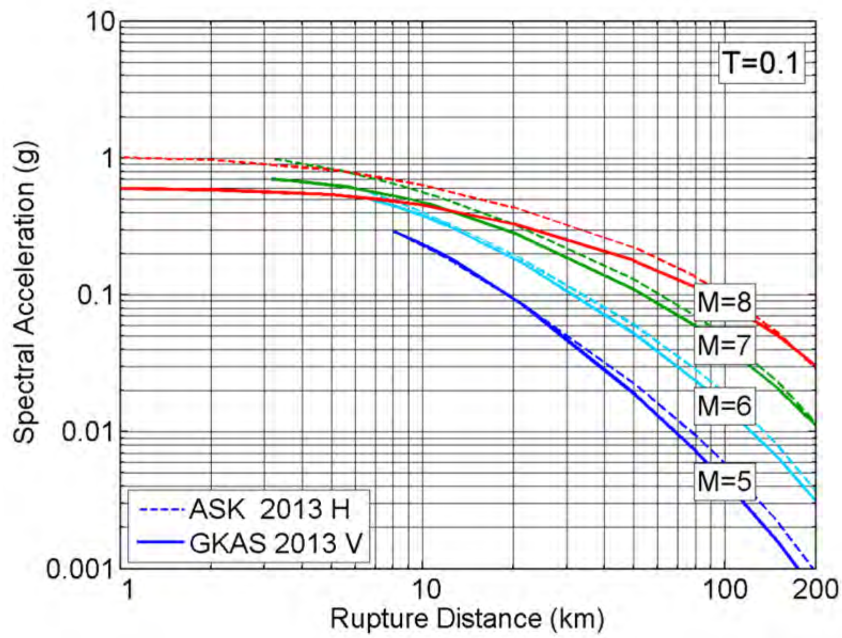

Figure 2.28(b) Comparison of the rupture distance scaling for a vertical strike slip with V_{S30} = 760 m/sec at T = 0.1 sec.

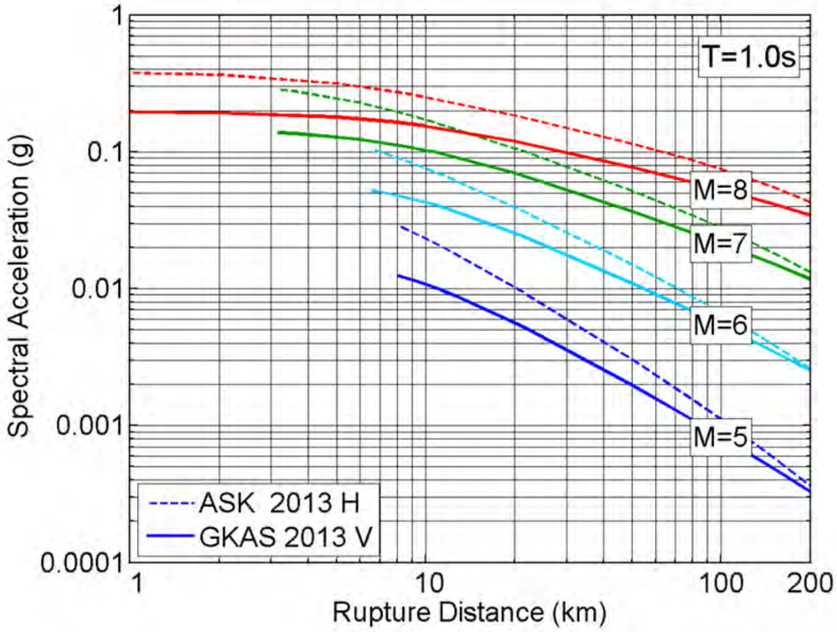

Figure 2.28(c) Comparison of the rupture distance scaling for a vertical strike slip with V_{S30} = 760 m/sec at T = 1 sec.

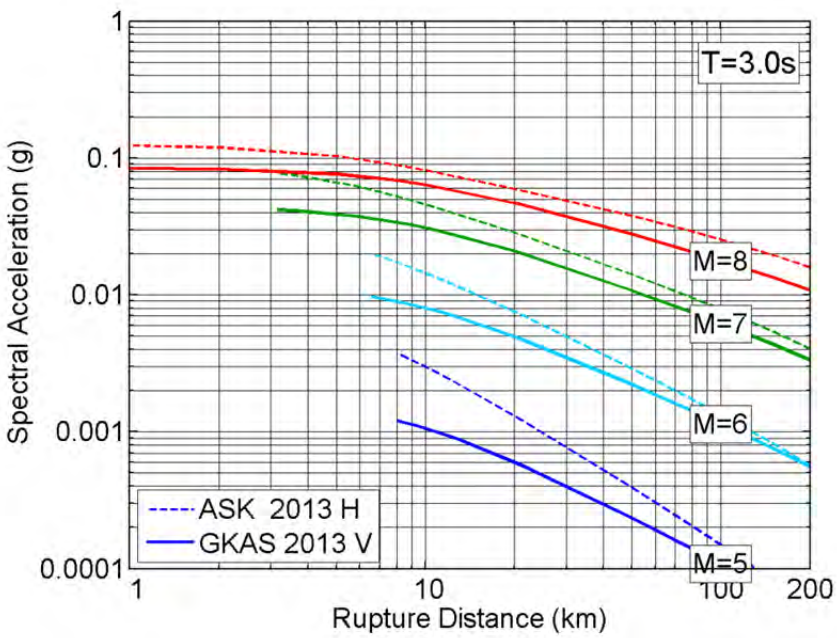

Figure 2.28(d) Comparison of the rupture distance scaling for a vertical strike slip with V_{S30} = 760 m/sec at T = 3 sec.

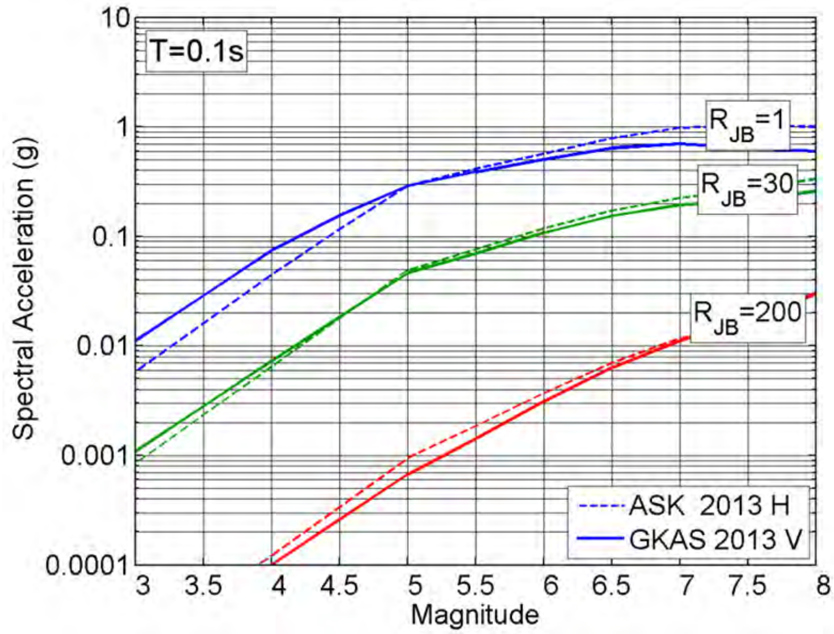

Figure 2.29(a) Comparison of the magnitude scaling for a vertical strike slip with V_{S30} = 760 m/sec at T = 0.1 sec.

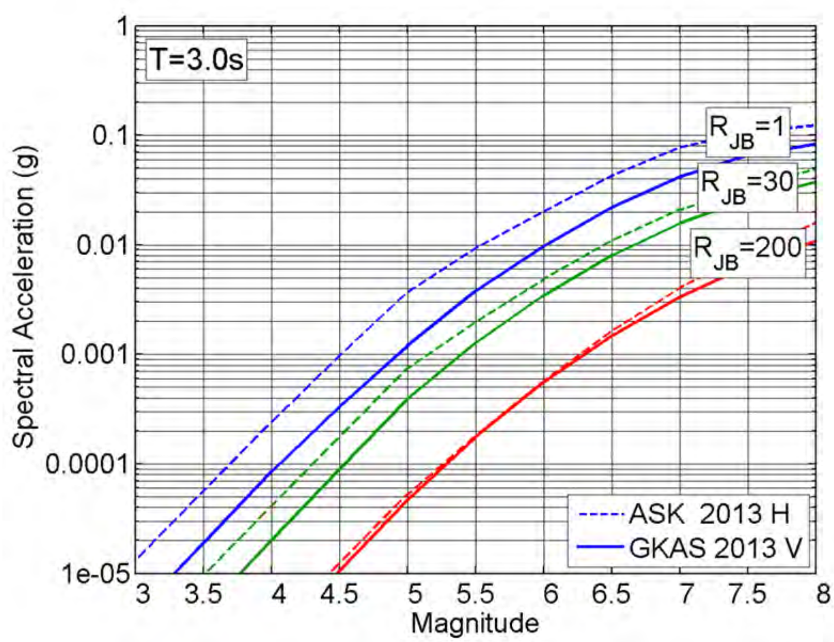

Figure 2.29(b) Comparison of the magnitude scaling for a vertical strike slip with V_{S30} = 760 m/sec at T =3 sec.

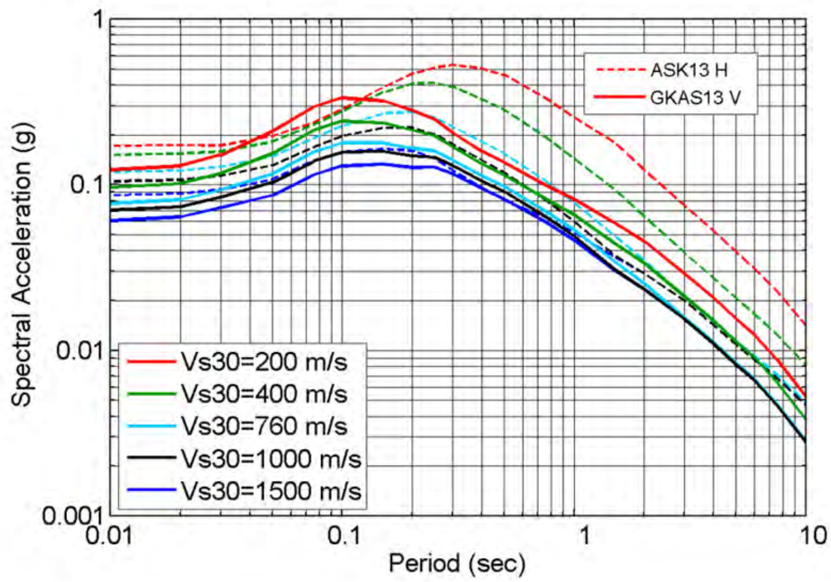

Figure 2.30 Example of VS30 scaling for a strike slip M7 at R_{rup} = 30 km.

2.7 RANGE OF APPLICABILITY

The model is applicable for distances of 0-300 km and magnitudes 3.0–8.5. Although the largest magnitude in the NGA data set is M7.9, we consider that the model can be reliably extrapolated to M8.5. With regards to site conditions, the model is considered applicable for $V_{S30} \geq 180$ m/sec but it is not well constrained for sites with $V_{S30} \geq 1000$ m/sec.

REFERENCES

Abrahamson N.A., Youngs R.R. (1992). A stable algorithm for regression analyses using the random effects model, *Bull. Seismol. Soc. Am*., 82: 505–510.

Abrahamson N.A., Silva W.J. (1997). Empirical response spectral attenuation relations for shallow crustal earthquakes, *Seismol. Res. Lett*., 68: 94–127.

Abrahamson N.A., Silva W.J. (2008). Summary of the Abrahamson and Silva NGA ground-motion relations, *Earthq. Spectra*, 24: 57–69.

Abrahamson N.A., Silva W.J., Kamai R. (2013). Summary of the ASK13 ground-motion relation for active crustal regions, *Earthq. Spectra*, special NGA-West2 issue, submitted.

Ancheta T.D., Darragh R.B., Stewart J.P., Seyhan E., Silva W.J., Chiou B., Wooddell K.E., Graves R.W., Kottke A.R., Boore D.M., Kishida T., Donahue J.L. (2013). PEER NGA-West2 database, *Earthq. Spectra*, special NGA-West2 issue, submitted.

Ambraseys N.N., Douglas J. (2003). Near field horizontal and vertical earthquake ground motions, *Soil Dyn. Earthq. Eng*., 23: 1–18.

Ambraseys N.N., Douglas J., Sarma S.K., Smit P.M. (2005). Equations for the estimation of strong ground motions from shallow crustal earthquakes using data from Europe and the Middle East: Vertical peak ground acceleration and spectral acceleration, *Bull. Earthq. Eng*., 3: 55–73.

Boore D.M., Atkinson G.M. (2008). Ground-motion prediction equations for the average horizontal component of PGA, PGV, and 5%-damped PSA at spectral periods between 0.01s and 10.0 s, *Earthq. Spectra*, 24: 99–139.

Bozorgnia Y., Campbell K.W. (2004). The vertical-to-horizontal response spectral ratio and tentative procedures for developing simplified V/H and vertical design spectra, *J. Earthq. Eng*., 8: 175–207.

Campbell K.W. (1997). Empirical near-source attenuation relationships for horizontal and vertical components of peak ground acceleration, peak ground velocity, and pseudo-absolute acceleration response spectra, *Seismol. Res. Lett*., 68: 154–179.

Campbell K.W., Bozorgnia Y. (2008). NGA ground motion model for the geometric mean horizontal component of PGA, PGV, PGD and 5% damped linear elastic response spectra for periods ranging from 0.01 to 10 s, *Earthq. Spectra*, 24: 139–173.

Chiou B.S.-J., Youngs R.R. (2008). Chiou-Youngs NGA ground motion relations for the geometric mean horizontal component of peak and spectral ground motion parameters, *Earthq. Spectra*, 24: 173–217.

Chiou B.S.-J, Darragh R., Gregor N., Silva W.J. (2008). NGA Project Strong-Motion Database, *Earthq. Spectra*, 24: 23–44.

Donahue J.L., Abrahamson N.A. (2013). Hanging-wall scaling using finite-fault simulations, PEER NGA-West2 database, *Earthq. Spectra*, special NGA-West2 issue, submitted.

Gardner J.K., Knopoff L. (1974). Is the sequence of earthquakes in Southern California, with aftershocks removed, Poissonian?, *Bull. Seismol., Soc. Am*., 64: 1363–1367.

Gulerce Z., Abrahamson N.A., (2010). Vector-valued probabilistic seismic hazard assessment for the effects of vertical ground motions on the seismic response of highway bridges, *Earthq. Spectra*, 26: 999–1016.

Idriss I.M. (2008). An NGA empirical model for estimating the horizontal spectral values generated by shallow crustal earthquakes, *Earthq. Spectra*, 24: 217–243.

Kunnath S.K., Erduran E., Chai Y.-H., Yashinsky M. (2008). Effect of near-fault vertical ground motions on seismic response of highway overcrossings, *J. Bridge Eng*., ASCE, 13: 282–290.

Sadigh C.-Y., Chang J., Egan A., Makdisi F., Youngs R. R. (1997). Attenuation relationships for shallow crustal earthquakes based on California strong motion data, *Bull. Seismol. Soc. Am.*, 68, 180–189.

Wooddell K.E., Abrahamson N.A. (2013). New earthquake classification scheme for mainshocks and aftershocks in the NGA-West2 ground motion prediction equations (GMPEs), *Earthq. Spectra*, special NGA-West2 issue, submitted.

3. SSBA13: Vertical Component Ground Motion Prediction Equations for Active Crustal Regions

JONATHAN P. STEWART[1]

EMEL SEYHAN[1]

DAVID M. BOORE[2]

GAIL M. ATKINSON[3]

3.1 INTRODUCTION

In this chapter we present ground-motion prediction equations (GMPEs) for the vertical component of ground motions in active crustal regions.

Our approach was to begin with the horizontal-component GMPEs described by Boore et al. (2014) (hereafter BSSA14) and then to modify the coefficients as required by trends observed in the residuals. Accordingly, the functional form for the vertical-component GMPEs is very similar to that for our horizontal GMPEs and some of the coefficients remain unchanged. The source, path, and site models have all been modified for the vertical-component GMPEs. The aleatory uncertainty model is also changed. We assume the reader has a working knowledge of the BSSA14 model, and hence the present work is presented concisely.

Subsequent sections of this report chapter provide a complete set of equations for the model, describe the process by which the model coefficients were obtained, and show the ground motion trends revealed by the vertical-component GMPEs. We conclude with a summary and statement of limitations.

[1] Department of Civil and Environmental Engineering, University of California, Los Angeles, California
[2] Earthquake Science Center, U.S. Geological Survey, Menlo Park, California
[3] Department of Earth Sciences, University of Western Ontario, London, Ontario, Canada

3.2 FORM OF THE EQUATIONS

The functional form for the vertical-component GMPEs presented in this report is similar to BSSA14 and is given by the following equation:

$$\ln Y = F_E\left(\mathbf{M}, mech\right) + F_P\left(R_{JB}, \mathbf{M}\right) + F_S\left(V_{S30}, R_{JB}, \mathbf{M}\right) + \varepsilon_n \sigma\left(\mathbf{M}, R_{JB}, V_{S30}\right) \tag{3.1}$$

where ln*Y* represents the natural logarithm of a vertical ground-motion intensity measure (peak acceleration or 5% damped pseudo spectral acceleration; PGA or PSA, respectively); F_E, F_P, and F_S represent period-dependent functions for source ("E" for "event"), path ("P"), and site ("S") effects, respectively; ε_n is the fractional number of standard deviations of a single predicted value of ln*Y* away from the mean (e.g., $\varepsilon_n = -1.5$ is 1.5 standard deviations smaller than the mean); and σ is the total standard deviation of the model. The predictor variables are **M**, *mech*, R_{JB}, and V_{S30}. Parameter *mech* = 0, 1, 2, and 3 for unspecified, *SS*, *NS*, and *RS*, respectively. The units of PGA and PSA are *g* and PGV is cm/s.

3.2.1 Elements of the Median Model (Source, Path, and Site Functions)

The source (event) function is given by:

$$F_E\left(\mathbf{M}, mech\right) = \begin{cases} c_k + e_0 U + e_{1V} SS + e_{2V} NS + e_{3V} RS + \ldots \\ \ldots + e_4\left(\mathbf{M} - \mathbf{M}_h\right) + e_5\left(\mathbf{M} - \mathbf{M}_h\right)^2 & \mathbf{M} \le \mathbf{M}_h \\ c_k + e_0 U + e_{1V} SS + e_{2V} NS + e_{3V} RS + \ldots \\ \ldots + e_6\left(\mathbf{M} - \mathbf{M}_h\right) & \mathbf{M} > \mathbf{M}_h \end{cases} \tag{3.2}$$

where *U*, *SS*, *NS*, and *RS* are dummy variables, with a value of 1 to specify unspecified, strike-slip, normal-slip, and reverse-slip fault types, respectively, and 0 otherwise; the hinge magnitude $\mathbf{M}_h$ is period dependent, and e_0, e_{1V}, e_{2V}, e_{3V}, e_4, e_5, and e_6 are model coefficients. Coefficients with a 'V' in the subscript are modified relative to BSSA14. The only change in the function from BSSA14 is the addition of the c_k term, which approximately represents the period-dependent mean bias between the vertical and average horizontal data. Parameter c_k is estimated through an iterative process described subsequently. Note that there is an ambiguity in equation 3.2, in that any number could be added to c_k and subtracted from e_0, e_{1V}, e_{2V}, and e_{3V} without changing the value of F_E; the coefficients for our GMPEs, determined through an iterative process to be described shortly, are internally consistent, however.

The path function is given by:

$$F_P\left(R_{JB}, \mathbf{M}\right) = \left[c_{1V} + c_{2V}\left(\mathbf{M} - \mathbf{M}_{ref}\right)\right]\ln\left(R / R_{ref}\right) + \left(c_{3V} + \Delta c_{3V}\right) * \left(R - R_{ref}\right) \tag{3.3}$$

where

$$R = \sqrt{R_{JB}^{\ 2} + h^2} \tag{3.4}$$

and c_{1V} , c_{2V} , c_{3V}, Δc_{3V} , $\mathbf{M}_{ref}$, R_{ref} and h are model coefficients. Parameter Δc_{3V} is region-dependent.

The site function is given by:

$$F_S\left(V_{S30},\mathbf{M},R_{JB}\right)=\ln\left(F_{lin}\right)+\ln\left(F_{nl}\right) \tag{3.5}$$

where F_{lin} represents the linear component of site amplification, F_{nl} represents the nonlinear component of site amplification. The basin depth term $F_{\delta z_1}$ that was used in BSSA14 is taken as zero. Both the F_{lin} and F_{nl} terms are changed relative to BSSA14.

The linear component of the model (F_{lin}) describes the scaling of ground motion with V_{S30} for linear soil response conditions (i.e., small strains) as follows:

$$\ln\left(F_{lin}\right)=\begin{cases} c_V \ln\left(\dfrac{V_{S30}}{V_{ref}}\right) & V_{S30}\le V_c \\ c_V \ln\left(\dfrac{V_c}{V_{ref}}\right) & V_{S30}> V_c \end{cases} \tag{3.6}$$

where V_{ref} represents a reference velocity where the amplification is zero (in ln units), V_c is a limiting velocity beyond which there is no further V_{S30}-scaling, and c_V represents the level of V_{S30}-scaling for $V_{S30} < V_c$ and is reduced relative to that in BSSA14 (where a different coefficient c was used). All terms other than c_V in Equation (3.6) are unchanged from BSSA14.

The function for the F_{nl} term is as follows:

$$\ln\left(F_{nl}\right)= f_1+ f_{2V} \ln\left(\frac{PGA_r + f_3}{f_3}\right) \tag{3.7}$$

where f_1, f_{2V} , and f_3 are model coefficients and PGA_r is obtained by evaluating Equation (3.1) for given R_{JB} and $\mathbf{M}$ with V_{S30} = 760 m/sec for the vertical component. Parameter f_{2V} is the only term in Equation (3.7) changed from BSSA14; it represents the degree of nonlinearity for the vertical component and is formulated as:

$$f_{2V} = f_{4V}\left[\exp\left\{ f_5\left(\min\left(V_{s30},760\right)-360\right)\right\}-\exp\left\{ f_5\left(760-360\right)\right\}\right] \tag{3.8}$$

where f_{4V} and f_5 are model coefficients. Parameter f_{4V} is changed from BSSA14 whereas f_5 is unchanged.

3.2.2 Aleatory Uncertainty Function

The total standard deviation σ_V is partitioned into components that represent between-earthquake variability (τ_V) and within-event variability (ϕ_V) as follows:

$$\sigma_V = \sqrt{\phi_V^{\ 2} + \tau_V^{\ 2}} \tag{3.9}$$

At this stage, we have only evaluated τ_V and ϕ_V for the following conditions: $\mathbf{M} > 5.5$, $R_{JB} <$ 100 km, and all V_{S30} conditions.

3.3 EVALUATION OF COEFFICIENTS

3.3.1 Data

We use the 31 May 2013 NGA-West 2 vertical flatfile titled "NGA Flatfile Vertical As-Recorded d050 LgM SMM 05312013". This file contains 21,539 vertical-component ground motions. Our data selection criteria were as follows:

- We use the same magnitude- and distance-dependent cutoff criteria as employed for the horizontal component GMPEs, which are given in Figure 1 of BSSA14.
- We only use events with ≥ 4 recordings, satisfying the limiting distance criteria from the previous bullet.
- We only use data if the "Spectra Quality Flag" under Column JK in the flatfile equals 0.
- We use other data selection criteria described by BSSA14 concerning instrument housing and record reliability (but for vertical component).
- We only use records for oscillator periods less than the inverse of the lowest usable frequency for the vertical component in the flatfile (Column DY).

Application of these criteria results in 15,326 recordings for PGA.

3.3.2 Initial Analysis of Residuals for Adjustment of Site Terms

The initial analyses presented in this section used a subset of the data described in Section 3.3.1 having R_{jb} < 80 km in all regions except Japan, for which we used R_{jb} < 50 km. These distance thresholds were applied to minimize the effects of misfit in anelastic attenuation, which is addressed in the following section. This subset of the data has 8.075 recordings for PGA.

Using that data subset, we calculated residuals relative to the BSSA14 GMPEs (for the horizontal component) as follows:

$$R_{ij} = \ln Z_{ij} - \mu_{ij}\left(\mathbf{M}, R_{JB}, V_{S30}\right) \tag{3.10}$$

Index i refers to the earthquake event and index j refers to the recording within event i. Term Z_{ij} represents the observed vertical-component ground motion and $\mu_{ij}\left(\mathbf{M}, R_{JB}, V_{S30}\right)$ represents the horizontal-component GMPE median in natural log units. We then partition the residuals using mixed effects analysis as follows:

$$R_{ij} = \Delta c_{k1} + \eta_i + \varepsilon_{ij} \tag{3.11}$$

where Δc_{k1} is the mean residual, η_i is an event term, and ε_{ij} is the within-event residual. The number '1' is included in the subscript for Δc_k because this coefficient will be established through multiple iterations as the vertical GMPEs are refined, and Equation (3.11) represents the first iteration. In the iteration procedure we performed a new mixed-effects analysis for each effect that is investigated. There are three of iterations for the site term, which was then fixed. Using that model, we looked at the focal mechanism terms, changed the model, then proceeded to the distance attenuation terms. Each successive iteration required a new mixed effects analysis.

As shown in Figure 3.1, this analysis resulted in significantly non-zero Δc_{k1} terms. Those terms have a clear physical meaning, as they equal the average value of the natural log of the vertical-to-horizontal ratio (i.e., *V/H*) of the intensity measures. For example, Δc_{k1} for PGA and 5% damped PSA at 1 sec are -0.48 and -0.76, which correspond to *V/H* ratios of 0.62 and 0.47, respectively.

Figure 3.2 shows within-event residuals ε_{ij} against V_{S30}. The trends indicate that the vertical-component intensity measures are less sensitive to V_{S30} than the horizontal-component intensity measures. This is accomplished in the GMPEs by reducing the scaling parameter c_V (in an absolute sense) relative to c (the horizontal parameter). The amount of reduction is quantified approximately by a linear fit through the residuals having a slope of Δc_V, as marked in the figures. The number '1' in the subscript refers to this being the first iteration in a process that is repeated. Figure 3.3 shows values of c for the horizontal model and Δc_{V1} established by this first iteration.

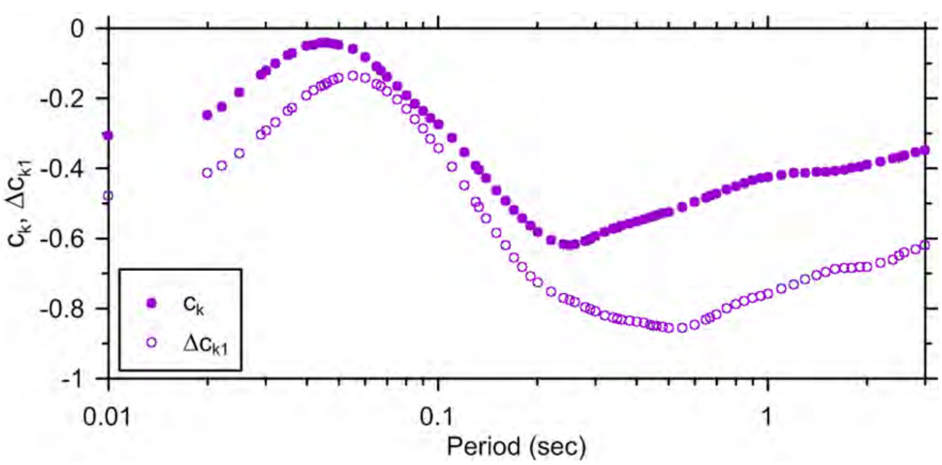

Figure 3.1 **Variation of parameters c_k and Δc_{k1} with period. Parameter c_k is a parameter in the vertical GMPE evaluated from multiple iterations of residuals analysis. Parameter Δc_{k1} represents the mean misfit between vertical data and horizontal model prior to adjustment of any model coefficients (Iteration 1). The results for additional iterations are not shown in this figure.**

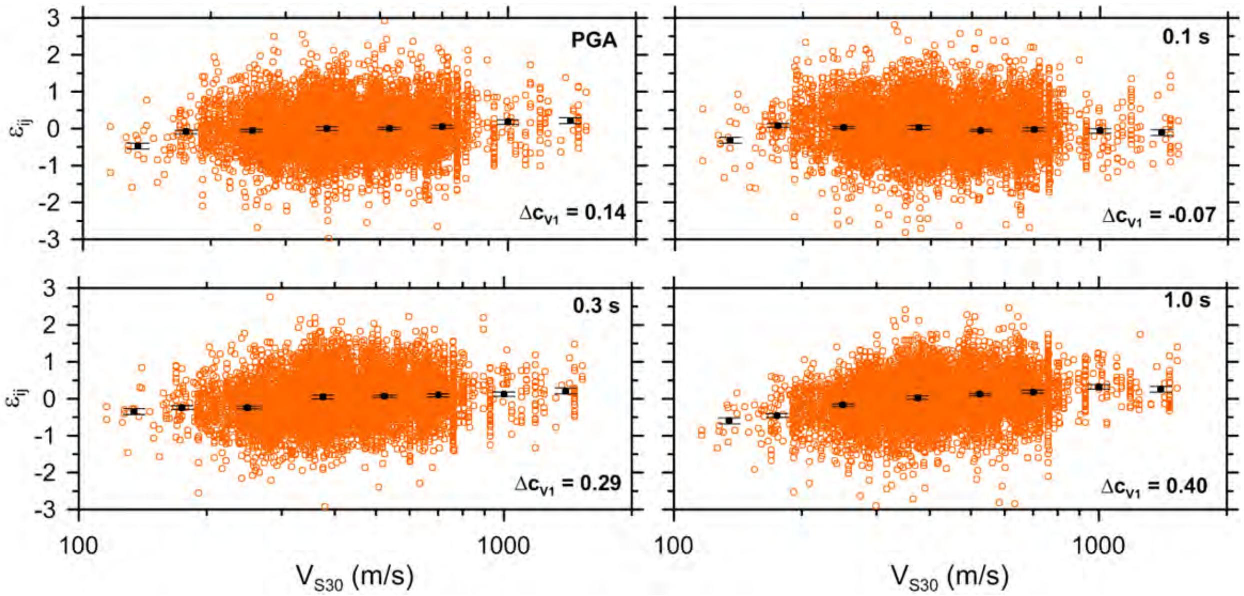

Figure 3.2 **Within-event residuals for vertical data relative to horizontal model. Upward trend indicates slower V_{S30}-scaling of vertical data relative to horizontal. The figure shows the residuals along with the bin means with their 95% confidence intervals.**

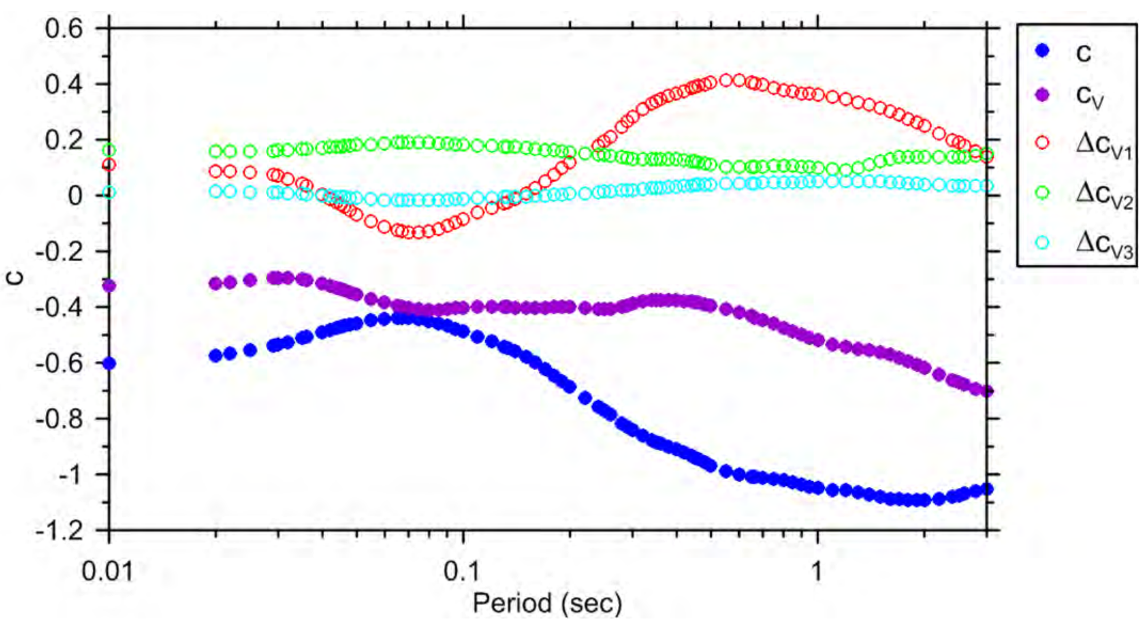

Figure 3.3 **Parameter c_V used in vertical model along with the Δc_{Vi} terms and the final value of c_V recommended for use with the vertical GMPEs.**

We then formulated a preliminary vertical-component GMPE for the purpose of analyzing site effects by using the equations from the previous section with all coefficients set at their horizontal values except for the following values for c_k and c_V:

$$c_k = \sum_{i=1}^{N} \Delta c_{ki} \tag{3.12}$$

$$c_V = c + \sum_{i=1}^{N} \left(\Delta c_{Vi} \right) \tag{3.13}$$

where N=1 at this stage corresponding to the first iteration of residuals analysis. Values for Δc_{k1} and Δc_{V1} are indicated in Figures 3.1 and 3.3, respectively. At this stage we retained the use of f_4 values from the horizontal GMPE. With this preliminary vertical GMPE now defined, we repeated the residuals analysis indicated by Equations (3.10) and (3.11) (but with the preliminary vertical GMPE used in lieu of BSSA14), which led to values of Δc_{V2} in the manner described previously and shown in Figure 3.3.

At this stage, before further analyzing c_V, we investigated whether the vertical data exhibited evidence of nonlinearity. This analysis was undertaken using the methodology described in Seyhan and Stewart [2014]. We evaluate 'rock' residuals (denoted R_{ij}^{r}) relative to the preliminary vertical model with V_{S30} set to 760 m/sec (this turns off the site term). The resulting residuals are plotted in Figure 3.4. We then fit the residuals using Equation (3.7) with f_3 set to 0.1g as in the horizontal model. The objective of this analysis is to establish the parameter f_{2V}, which represents nonlinearity in the vertical-component ground motions. The resulting fits are shown in Figure 3.4 along with the horizontal fits from Seyhan and Stewart [2014] for reference.

The results in Figure 3.4 generally show negligible nonlinearity (f_2 values are nearly zero), except for the slowest V_{S30} bin under 200 m/sec. The resulting f_2 values are plotted against V_{S30} in Figure 3.5 along with the model for f_2 adopted in this study and the values for the horizontal component (shown for reference purposes). The vertical model shown in Figure 3.5 was obtained by reducing parameter f_4, which is denoted f_{4V} in Equation (3.8) and plotted against period in Figure 3.6.

The updating of the model for nonlinearity was not found to appreciably affect the trends of residuals against V_{S30}, as indicated by Δc_{V3} values of nearly zero in Figure 3.3. Hence, no further iterations were performed, and c_V was computed using Equation (3.13) with the result shown in Figure 3.3. Those values of c_V and the values of f_{4V} shown in Figure 3.6 were used in subsequent analysis of residuals and are used in the recommended vertical GMPEs.

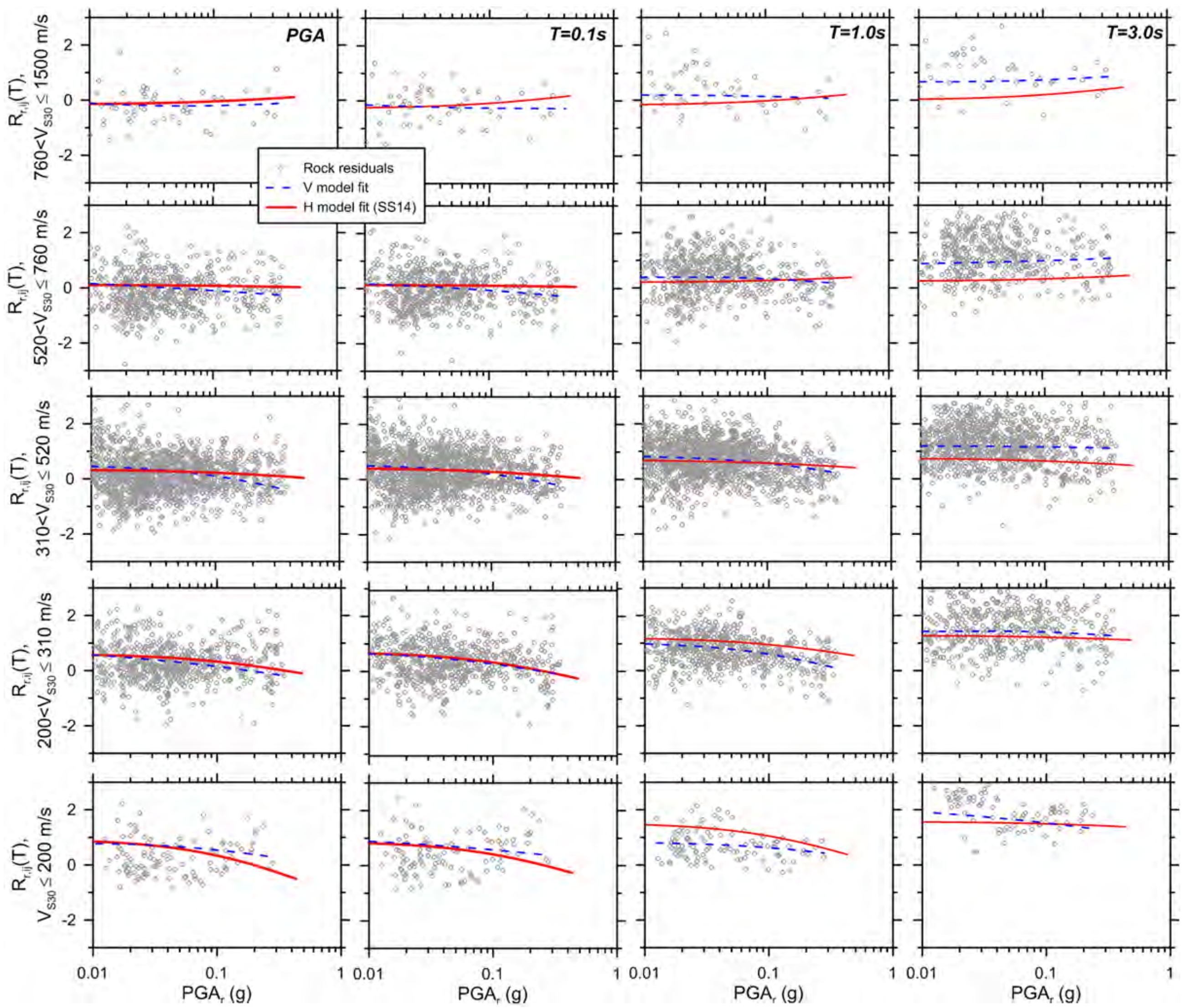

Figure 3.4 **Rock residuals against vertical PGA_r for data in various V_{S30} bins. Rock residuals are computed using vertical data and preliminary version of vertical GMPE with V_{S30} set to reference value of 760 m/s. Fit curve per Equation (3.7) is shown along with fit curve for horizontal component from Seyhan and Stewart (2014). Note: Negligible nonlinearity in all cases except the slowest V_{S30} bin.**

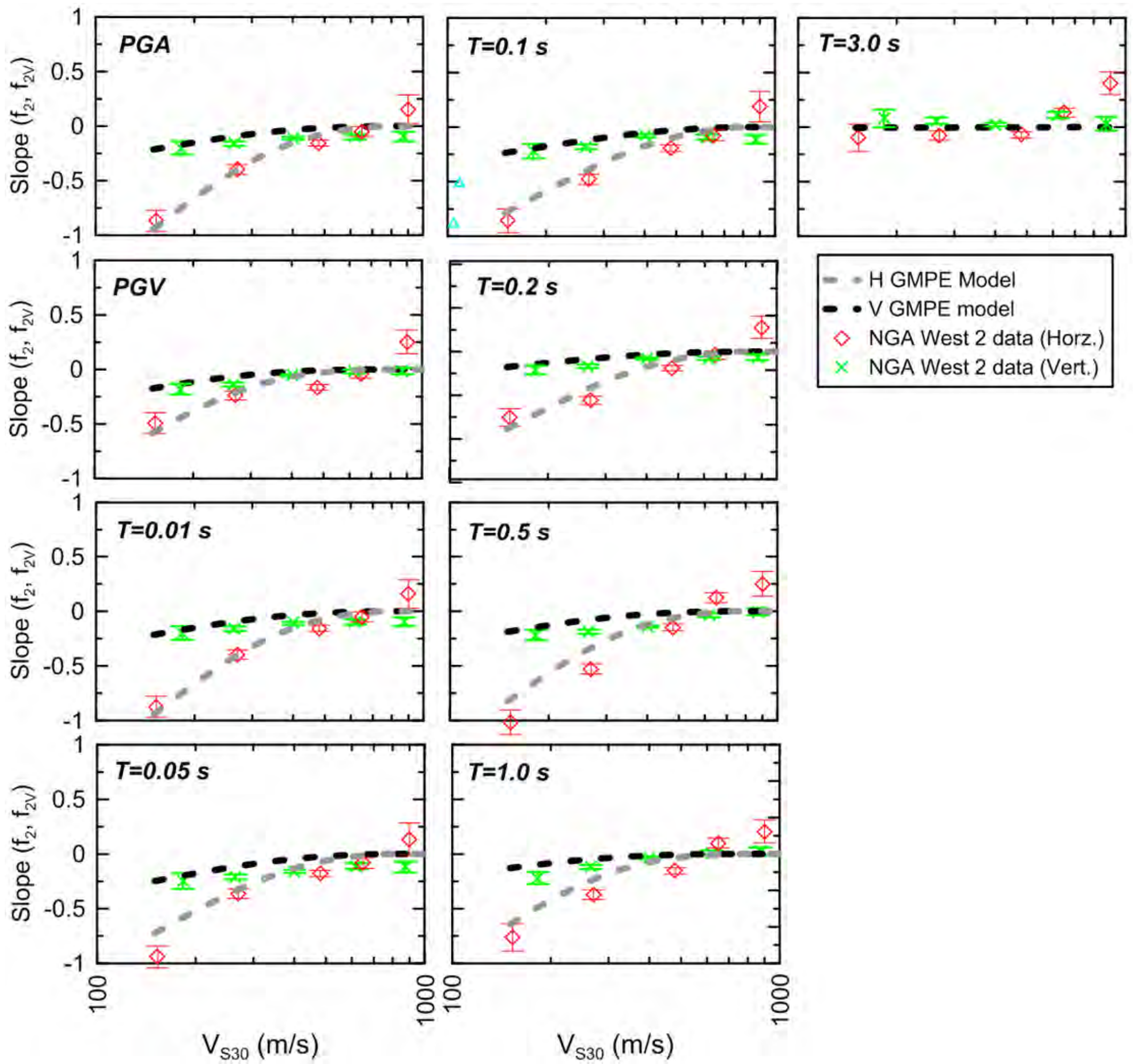

Figure 3.5 **Variation of slope f_2 or f_{2V} with V_{S30} for vertical- and horizontal-component ground motions along with the respective models for representing nonlinearity parameter f_2. Binned means of f_2 or f_{2V} are shown with their 95% confidence intervals.**

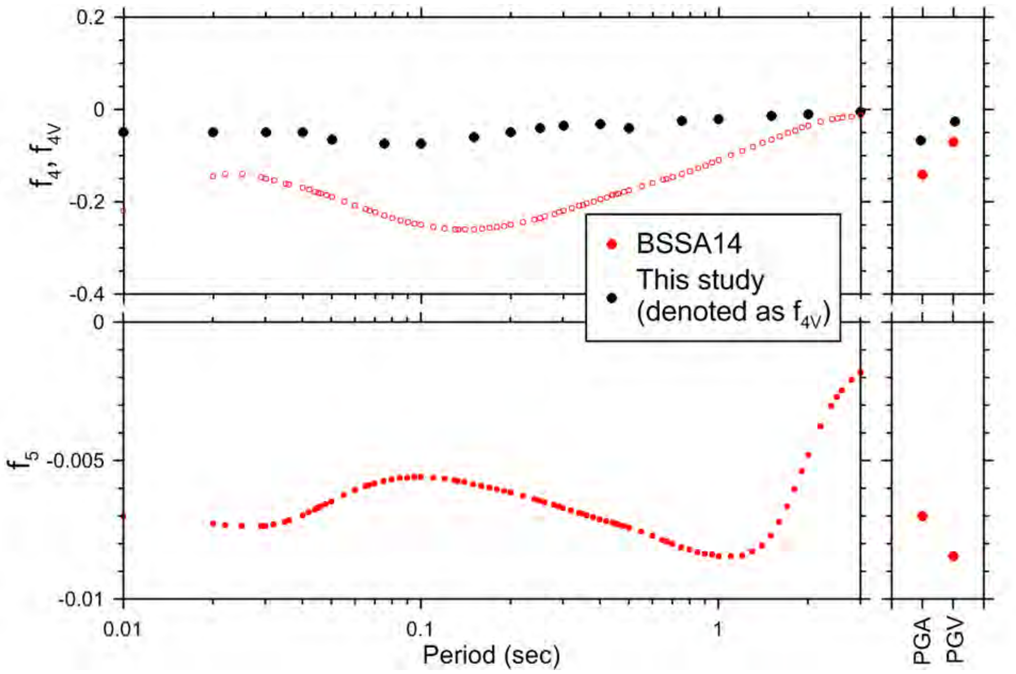

Figure 3.6 Parameters f_4 and f_{4V} for horizontal and vertical site response nonlinearity.

3.3.3 Focal Mechanism

Following some GMPE developers interactions, we suspected that the focal mechanism terms in our horizontal GMPEs may not be applicable to the vertical GMPEs. Accordingly, we took the vertical GMPEs, modified for site terms from the Section 3.3.2, and computed residuals per Equations (3.10) and (3.11). We investigated focal mechanism effects by plotted between-event residuals η_i for the three bins of *SS*, *NS*, and *RS*. Figure 3.7 shows the results along with the bin means and their 95% confidence intervals.

The offset of a bin mean from zero indicates that a correction to the corresponding focal mechanism terms could be made, particularly if zero does not fall within the confidence interval. These changes are made by adding the binned mean to each respective focal mechanism terms (e_1, e_2, and e_3, respectively). As in BSSA14, the values for coefficient e_0 (for an unspecified fault type) are taken as a weighted average of the *SS*, *NS*, and *RS* coefficients. As in BSSA14, the weights used are 0.58, 0.12, and 0.30, respectively, reflecting the relative fractions of events that we use for horizontal-component 1.0 sec PSA.

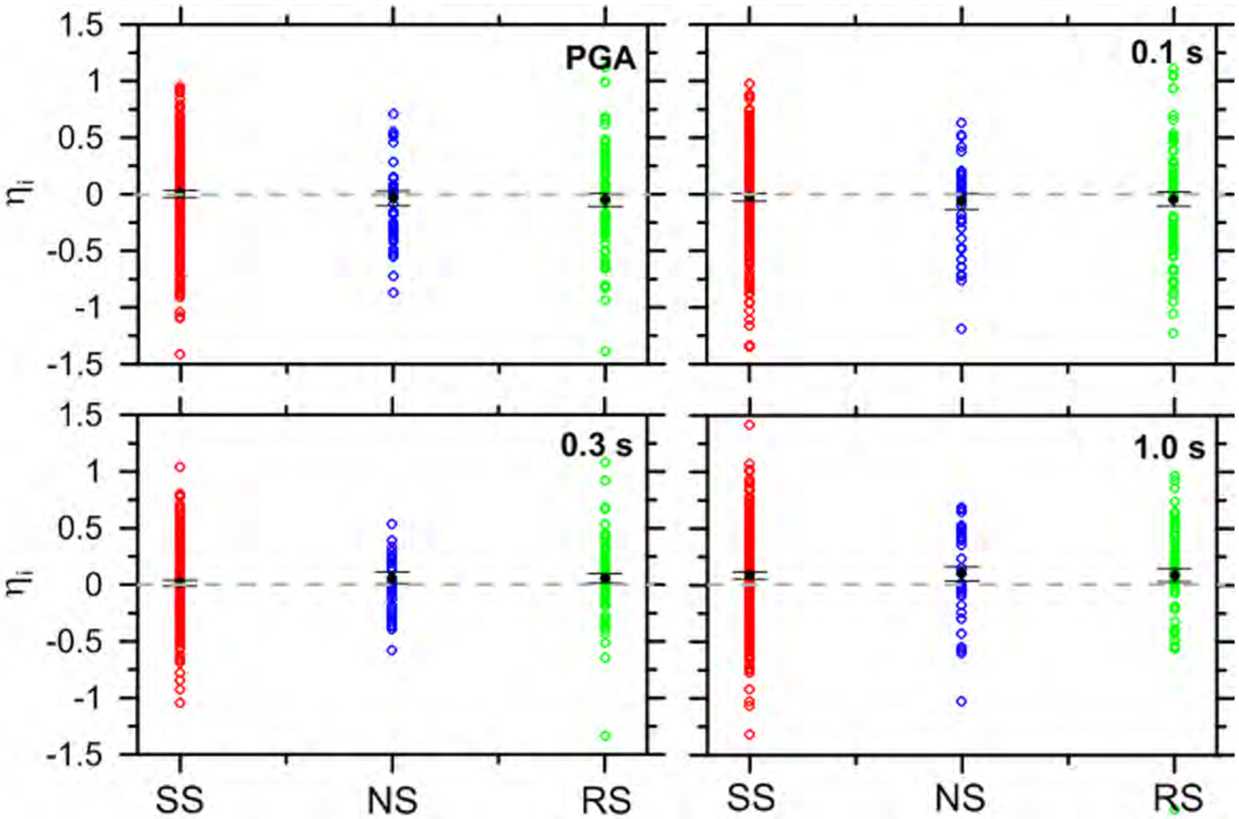

Figure 3.7 **Between-event residuals sorted by focal mechanism. Binned means shown with their 95% confidence intervals.**

3.3.4 Anelastic Attenuation

We next turn to the evaluation of anelastic attenuation coefficients c_3 and Δc_3. We set c_3 using the procedure of BSSA14. In this procedure, we take data from California for **M** < 5.5 as shown in Figure 3.8. After correcting the data for site effects to an equivalent V_{S30} of 760 m/sec, it is plotted against distance as shown for example in Figure 3.9, and an expression with the following form is fit to the data:

$$\ln Z_{ij} = \eta_i' + c_1' \ln\left(R/R_{ref}\right) + c_{3V}\left(R - R_{ref}\right) \tag{3.14}$$

In this expression, c_1' represents apparent geometric spreading within the **M** bin, and c_{3V} represents the apparent anelastic attenuation. Model fits per Equation (3.14) are plotted through the data in Figure 3.9.

The regression results are compiled across the various **M** bins in Figure 3.10, from which we see strong **M** dependence of c_1' but little **M** dependence of c_{3V}. These values of c_{3V} are adopted for use in the vertical GMPEs. Figure 3.11 compares the c_3 values for the horizontal GMPE (BSSA14) with those for the vertical GMPE.

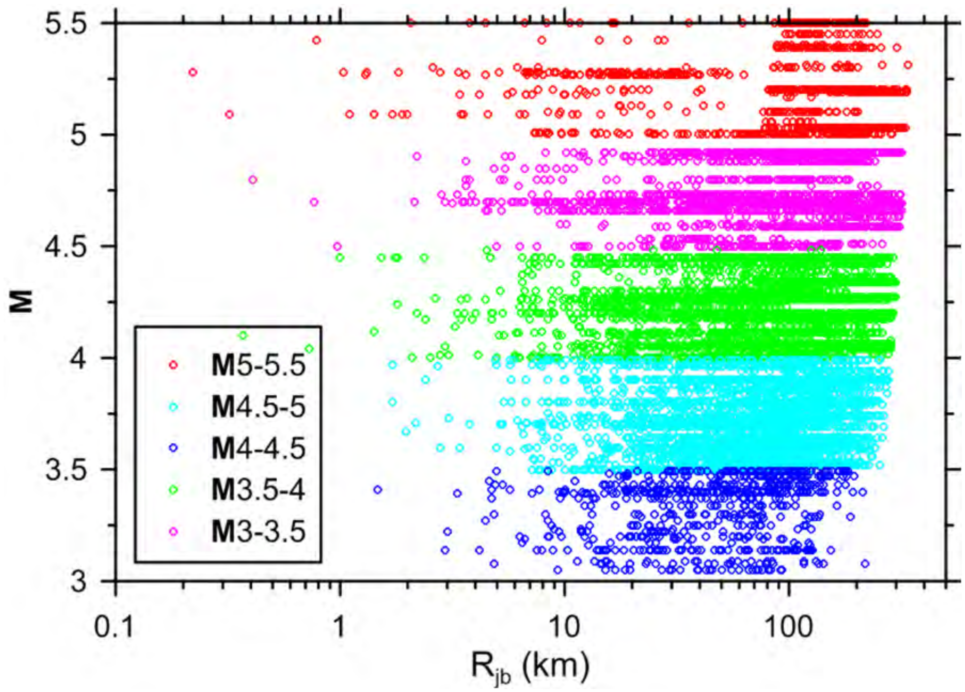

Figure 3.8 Binned groups of California data in NGA-West 2 vertical flatfile used for constraint of apparent anelastic attenuation terms.

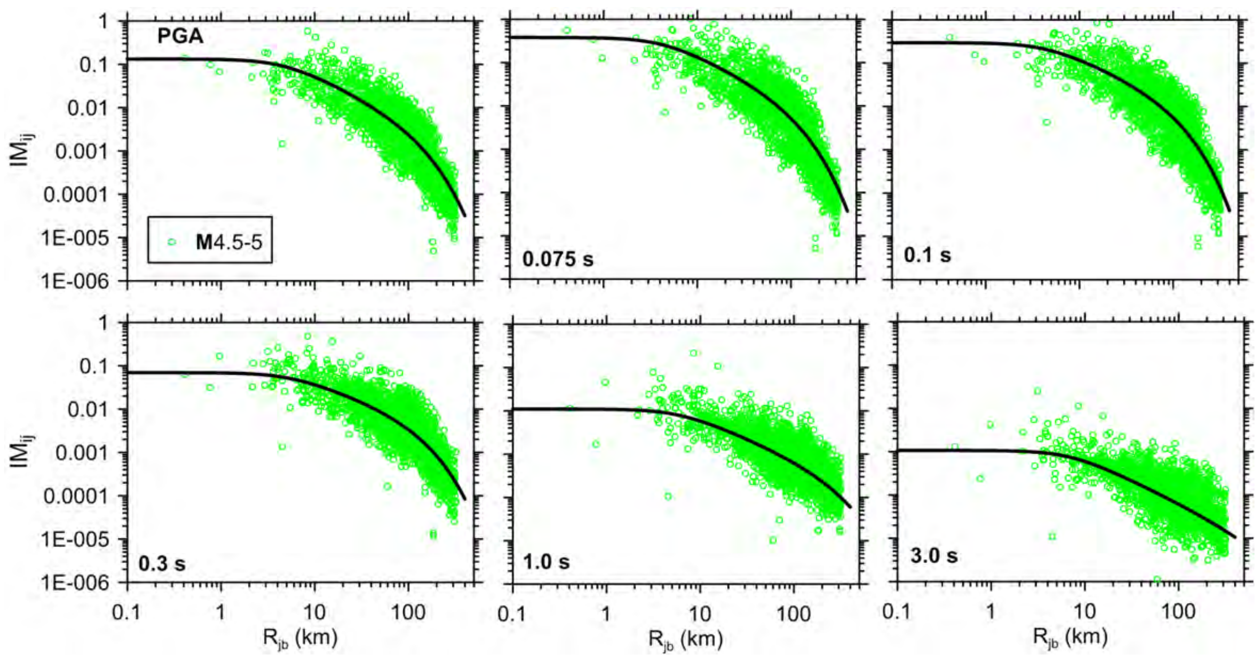

Figure 3.9 California vertical data and fit curve [Equation (3.14)] for M 4.5-5.0 events. Data corrected to V_{S30}=760 m/sec. Results show strong effects of apparent anelastic attenuation at high frequencies and negligible effects for $T \geq 1$ sec.

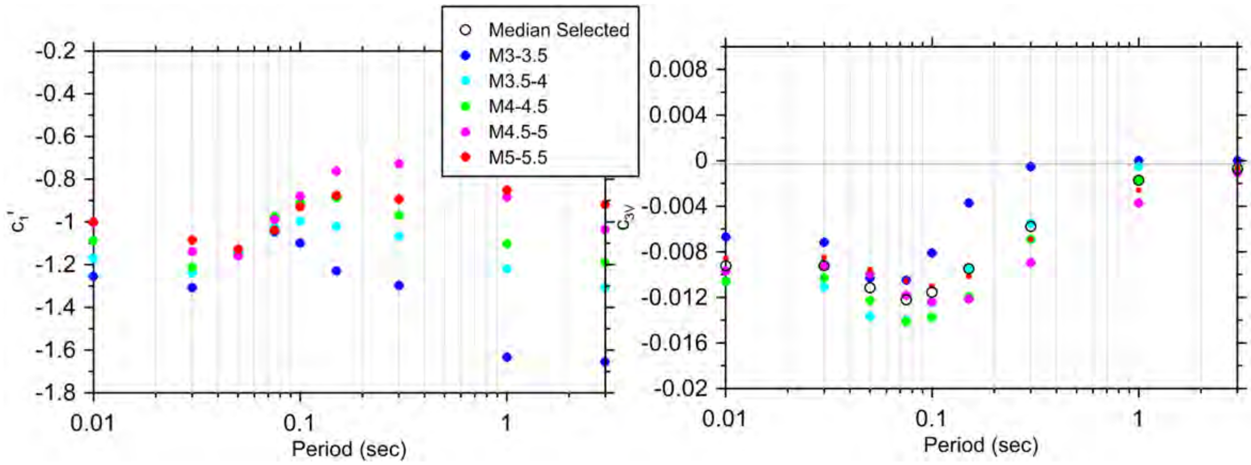

Figure 3.10 **Trends of apparent geometric spreading (c_1') and apparent anelastic attenuation (c_{3V}) terms with period and magnitude. Results show significant M-dependence for c_1' but not for c_3.**

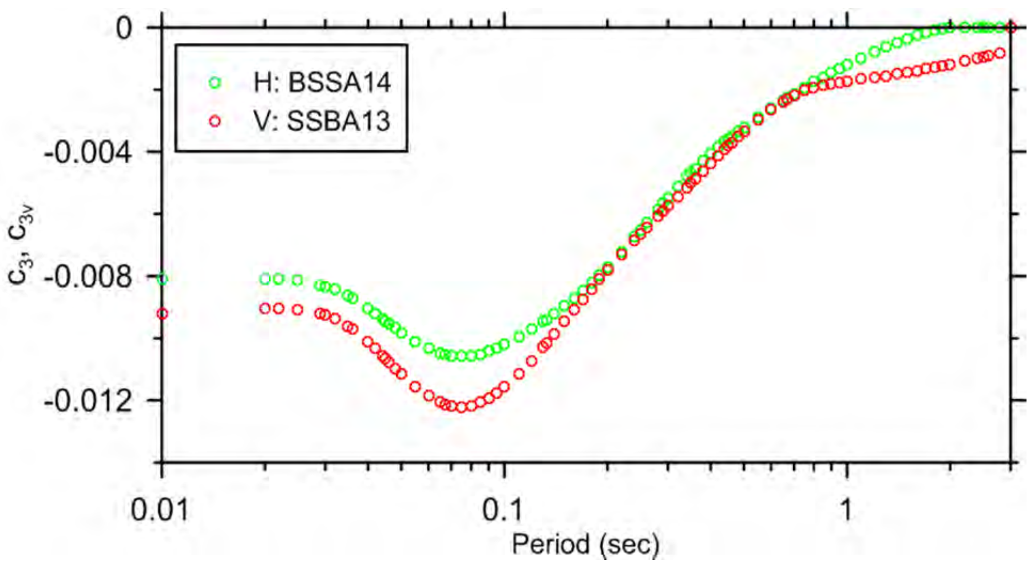

Figure 3.11 **Variation with period of apparent anelastic attenuation terms for horizontal and vertical GMPEs.**

After updating the vertical GMPEs with these c_{3V} values and the site and focal mechanism adjustments from prior sections, we plot within-event residuals against distance for various regions in Figures 3.12. As with the horizontal GMPEs, the anelastic attenuation for the first group (California, Taiwan, and New Zealand) requires no further correction (Δc_{3V} = 0), whereas the second group (Italy and Japan) and third group (China and Turkey) have faster and slower attenuation, respectively. These conditions are marked in the figures as 'Average Q,' 'Low Q,' and 'High Q,' respectively.

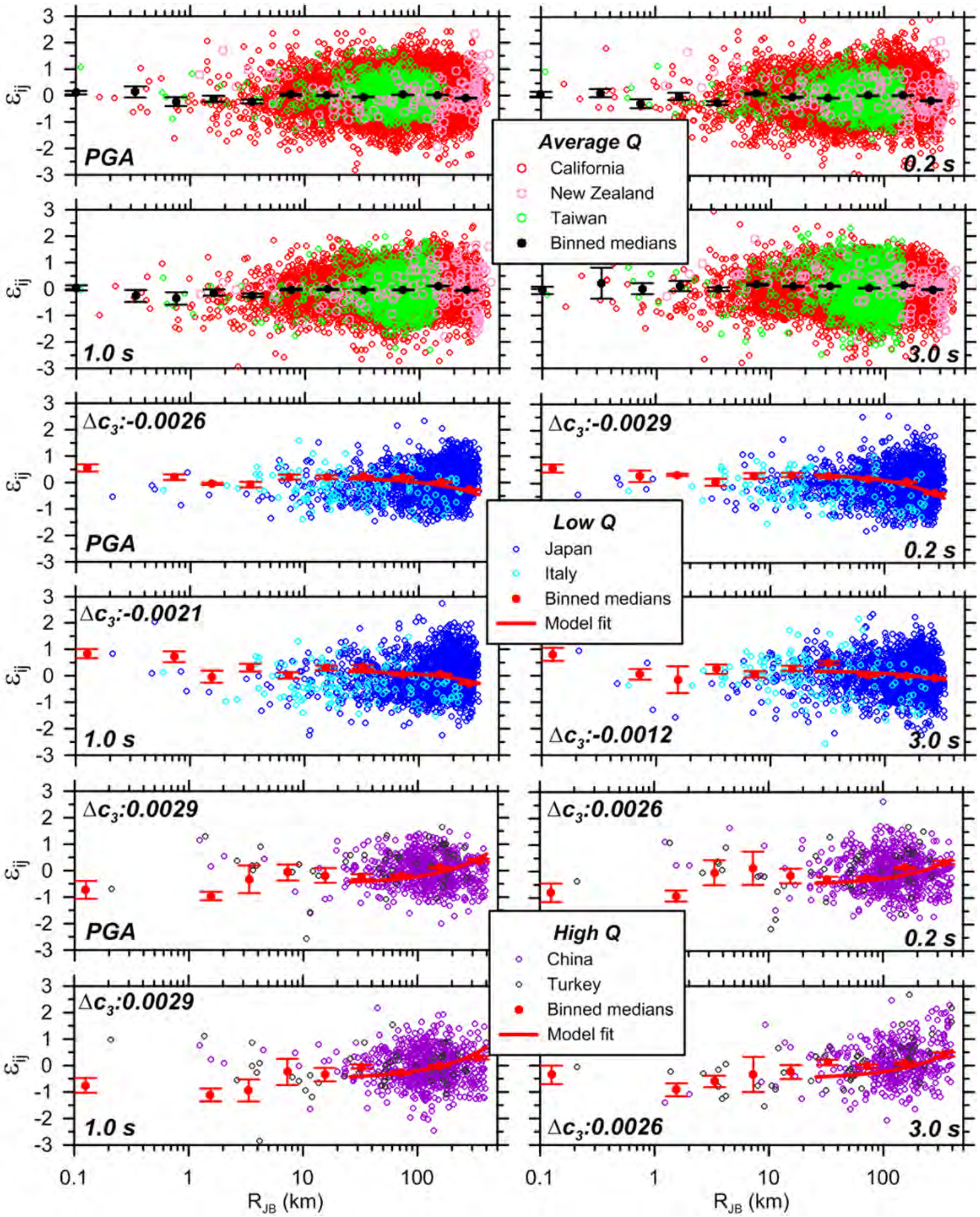

Figure 3.12 Within-event residuals for regions identified as 'Average Q' (California, New Zealand, and Taiwan), 'Low Q' (Japan and Italy), and 'High Q' (China and Turkey). Also shown is the fit line per Equation (3.15) for R_{JB} > 25 km. Means within distance bins are shown along with their 95% confidence intervals.

For the low and high Q cases, we fit a linear expression through the data according to:

$$\varepsilon = \Delta c_{3V}\left(R - R_{ref}\right) + \bar{\varepsilon}_{lR} \tag{3.15}$$

where Δc_{3V} is the additive regional correction to the c_{3V} term from Equation (3.3), and $\bar{\varepsilon}_{lR}$ is the mean value of the residuals at close distance in a given region. In order to prevent the relatively sparse data at the closest distances from affecting the slope Δc_{3V}, we limited the data range used in the regression to $R_{JB} > 25$ km, which captures the 'flat' region in the residuals before anelastic effects become significant (beyond about 80 km) and encompasses the distance range with abundant data. The resulting Δc_{3V} coefficients are recommended for use with the model in the respective regions.

3.3.5 Analysis of Geometric Spreading and Fictitious Depth Terms

We next turn to the evaluation of apparent geometric spreading coefficients c_1 and c_2, and fictitious depth term h. We compute residuals after updating the vertical GMPEs based on the source, site, and path adjustments from the prior three sections. We plot within-event residuals against distance for various bins of **M** in Figures 3.13.

We find evidence for bias in the apparent geometric spreading from these figures. This is evident from non-zero slope in the approximate distance range of 5 to 100 km. We select this distance range because (1) closer distances are largely affected by fictitious depth term h, and (2) further distances are mostly controlled by anelastic terms. For the **M** < 4 data**,** the slopes of the residuals are positive, the trends are generally flat for the **M** 5-6 bin, and for the **M** > 7 bin the slopes are negative for short periods and positive for long periods. The computed slopes for each period and magnitude combination are marked in the figures with the variable θ, which has been computed for additional **M** bins and periods as well, with results for selected periods shown in Figure 3.14. We find that θ varies approximately linearly with **M,** and we fit the trend using a weighted least squares regression (weight proportional to the number of events in each **M** bin) as follows:

$$\theta(\mathbf{M}) = \theta_1 + \theta_2\left(\mathbf{M} - \mathbf{M}_{ref}\right) \tag{3.16}$$

The values of θ_1 and θ_2 in Equation (3.16) represent misfit between geometric spreading in the data and the model. These values are plotted against period in Figure 3.15.

We evaluate the changes in c_1 and c_2 for the vertical GMPEs as:

$$c_{1V} = c_1 + \theta_1 \tag{3.17}$$

$$c_{2V} = c_2 + \theta_2 \tag{3.18}$$

Values of each parameter were smoothed for application as shown in Figure 3.15.

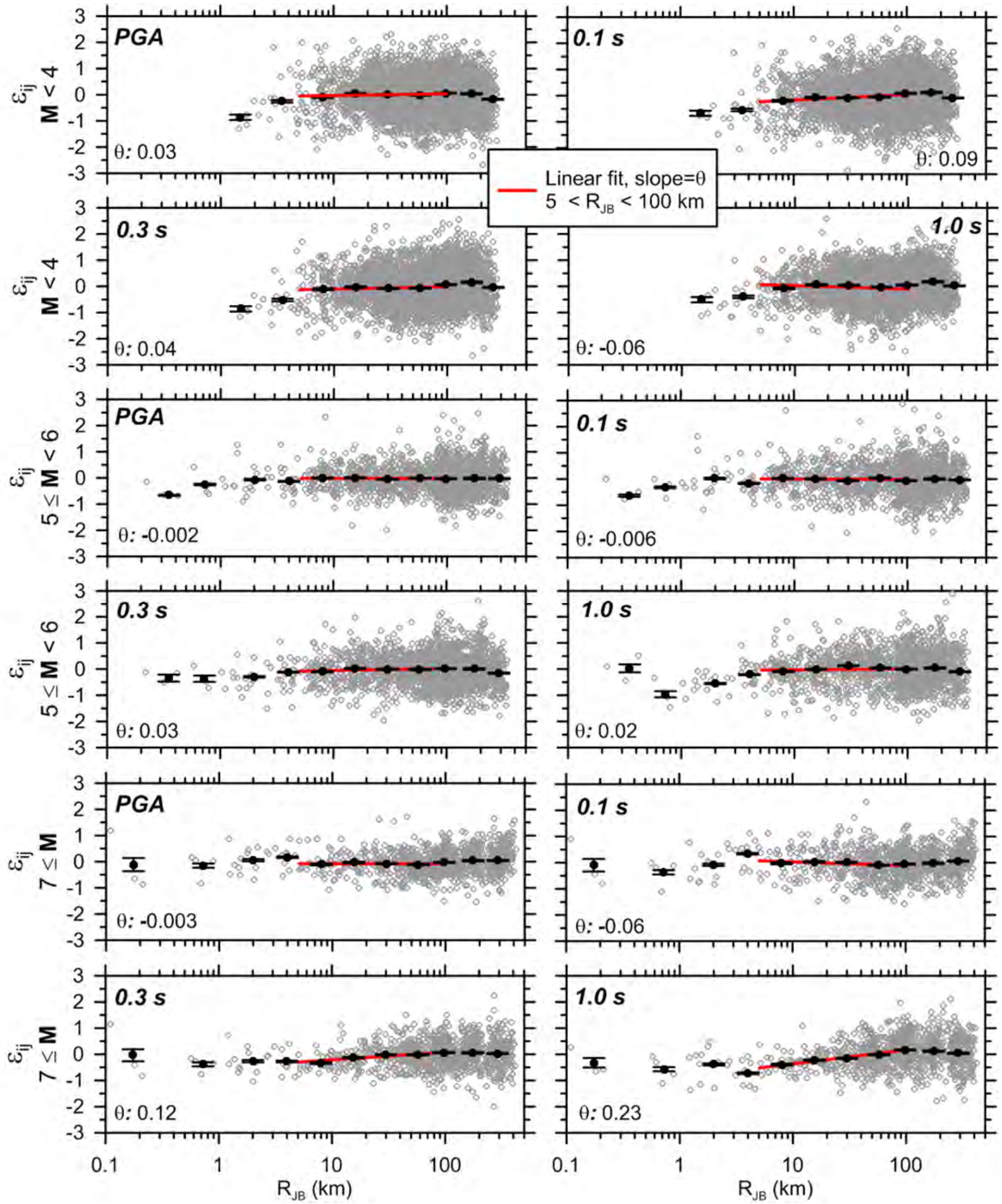

Figure 3.13 Within-event residuals for four M ranges regions. Also shown are fit lines within the distance range of 5 to 100 km. Means within distance bins are shown along with their 95% confidence intervals.

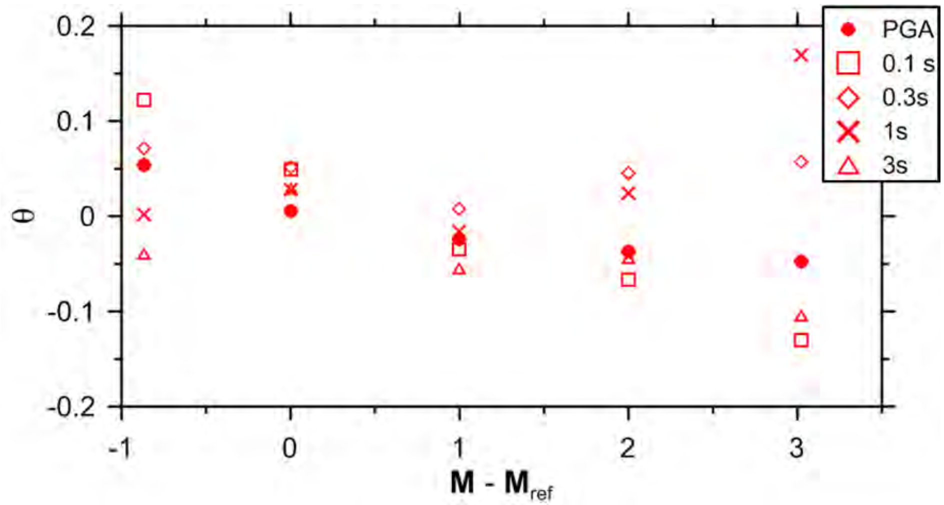

Figure 3.14 **The dependency of the variable θ on M for PGA and PSA at four selected periods for five M ranges.**

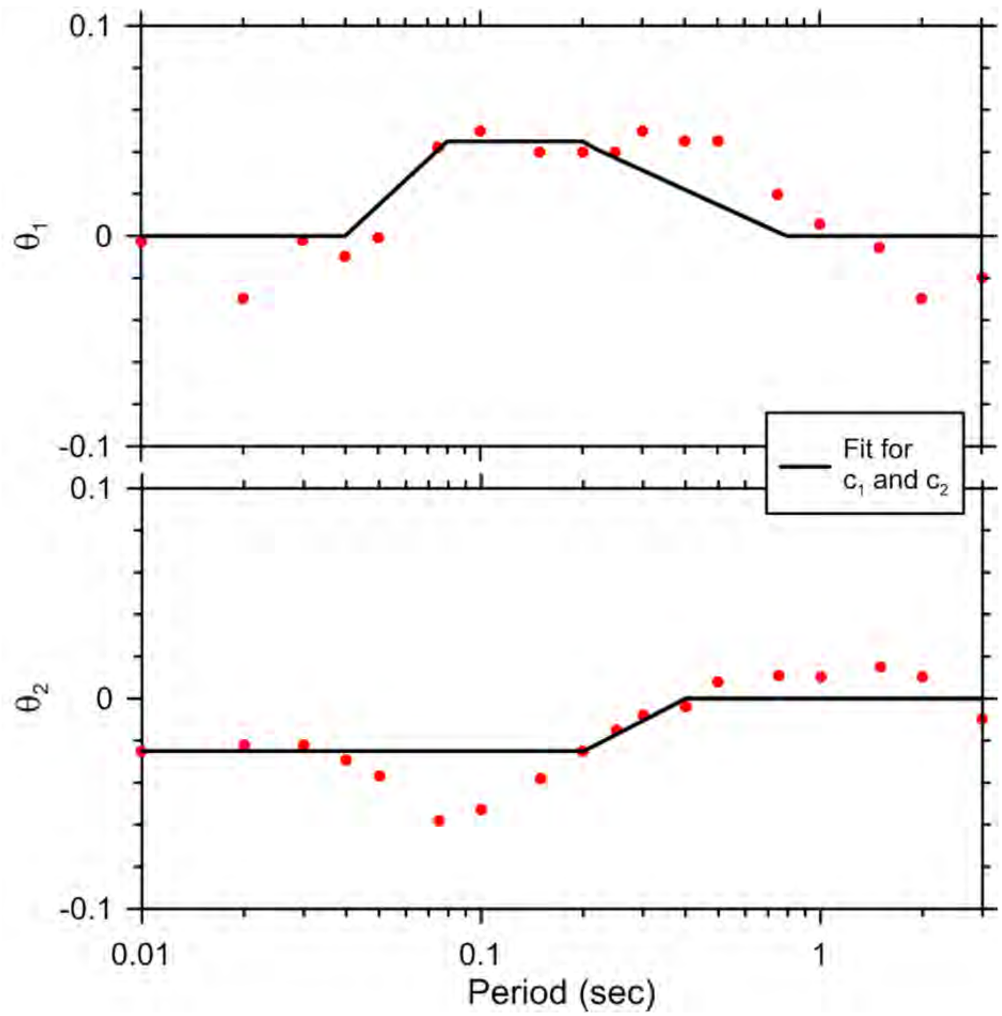

Figure 3.15 **Misfit of M dependent apparent geometric spreading term between vertical data and the c_2 term from the horizontal model.**

The residuals in Figure 3.13 at close distance show evidence of bias at close distance (R_{jb} < ~5–10 km) in some cases. However, we found that after the change of the geometric spreading terms in the GMPEs (from c_1 to c_{1V} and c_2 to c_{2V}), this bias was largely removed. Had there been significant bias, we would have adjusted the fictitious depth term h, but we ultimately decided no change was needed.

3.4 GMPE PERFORMANCE

The recommended GMPEs, as given by the equations in Section 3.2.1, are modified relative to the horizontal model based on the c_k terms and the aforementioned adjustments for parameters describing apparent geometric spreading, apparent anelastic attenuation and its regional dependence, focal mechanism effects, and site effects. The final values of the c_k term reflect each of the incremental adjustments per Equation (3.12) and are shown in Figure 3.1.

Trends of the GMPEs' median predictions are shown in Figure 3.16 in terms of spectra (*PSA* versus *T*) and *V/H* ratios (*V/H* versus *T*), in Figure 3.17 for distance attenuation (*PSA* versus R_{jb}), and Figure 3.18 for magnitude-scaling (*PSA* versus **M**). The plots generally follow the expected patterns. The vertical spectra peak at shorter periods than for horizontal. The attenuation patterns with distance and **M**-scaling patterns are similar to those for the horizontal model.

Residuals of the recommended GMPEs are shown in Figures 3.19 through 3.21. Figure 3.19 shows the trends of between-event residuals with **M**. There are some magnitude ranges with bias as the residuals have peaks and valleys, but overall the trends appear to be reasonably flat, at least for periods of 1.0 sec and less. There are systematic biases at long periods (T > 1 sec) for large magnitudes (**M** > 6.5) that suggest the GMPEs may not be reliable for such conditions. As shown in Figures 3.20 and 3.21, the trends with distance and V_{S30} are generally flat, although there is a negative bias for V_{S30} < 200 m/sec, which suggests the models are likely not reliable for that range of site conditions.

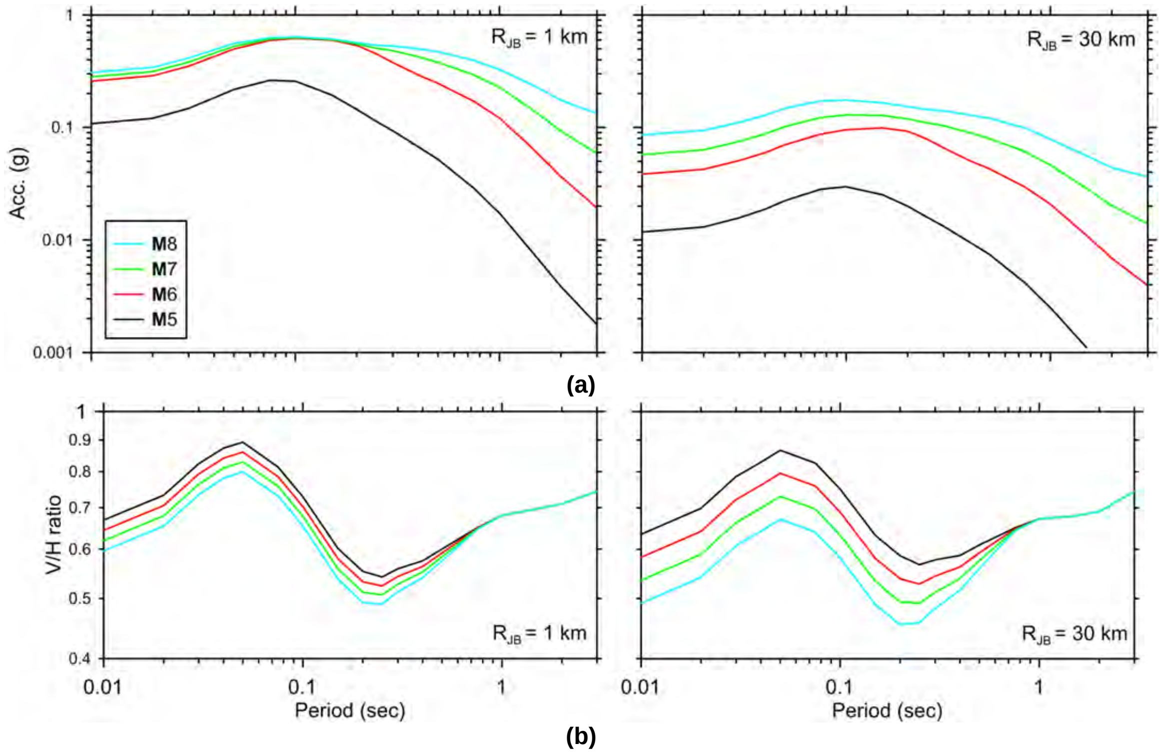

Figure 3.16 (a) Median *PSA* of proposed vertical GMPE for M 5, 6, 7, and 8 strike slip earthquakes for distances R_{JB}=1 and 30 km, and V_{S30} = 760 m/sec; and (b) V/H spectral ratios for the same conditions used to plot spectra.

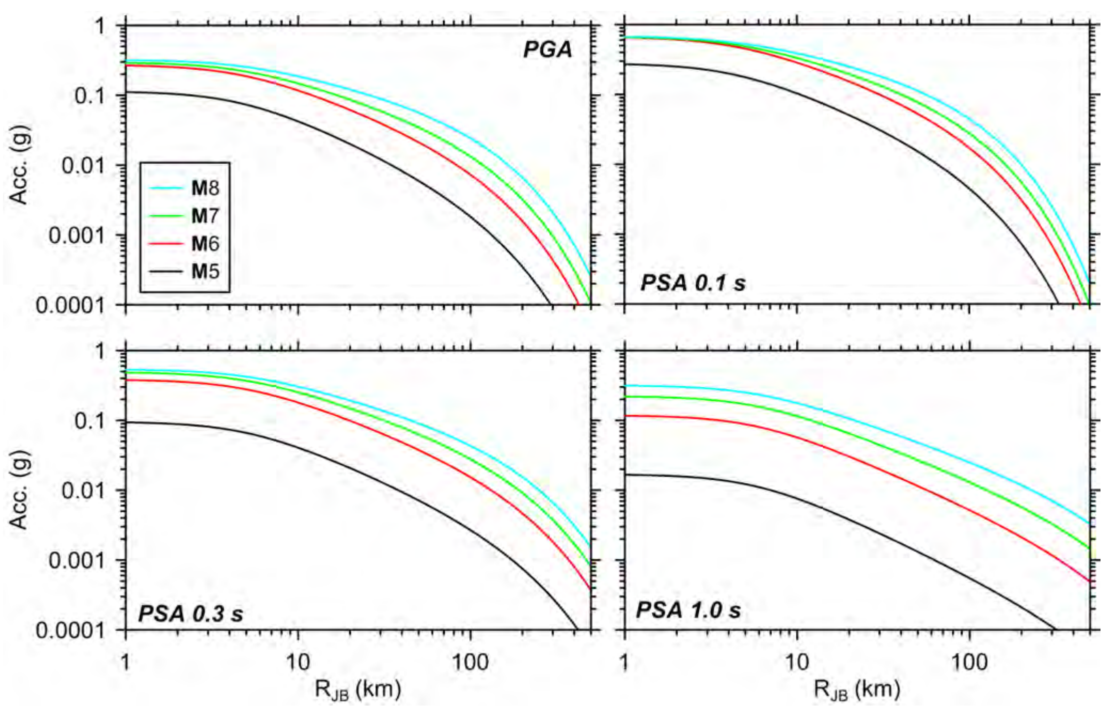

Figure 3.17 Median trends of proposed vertical GMPE as a function of distance for indicated M and strike slip events. V_{S30} = 760 m/sec.

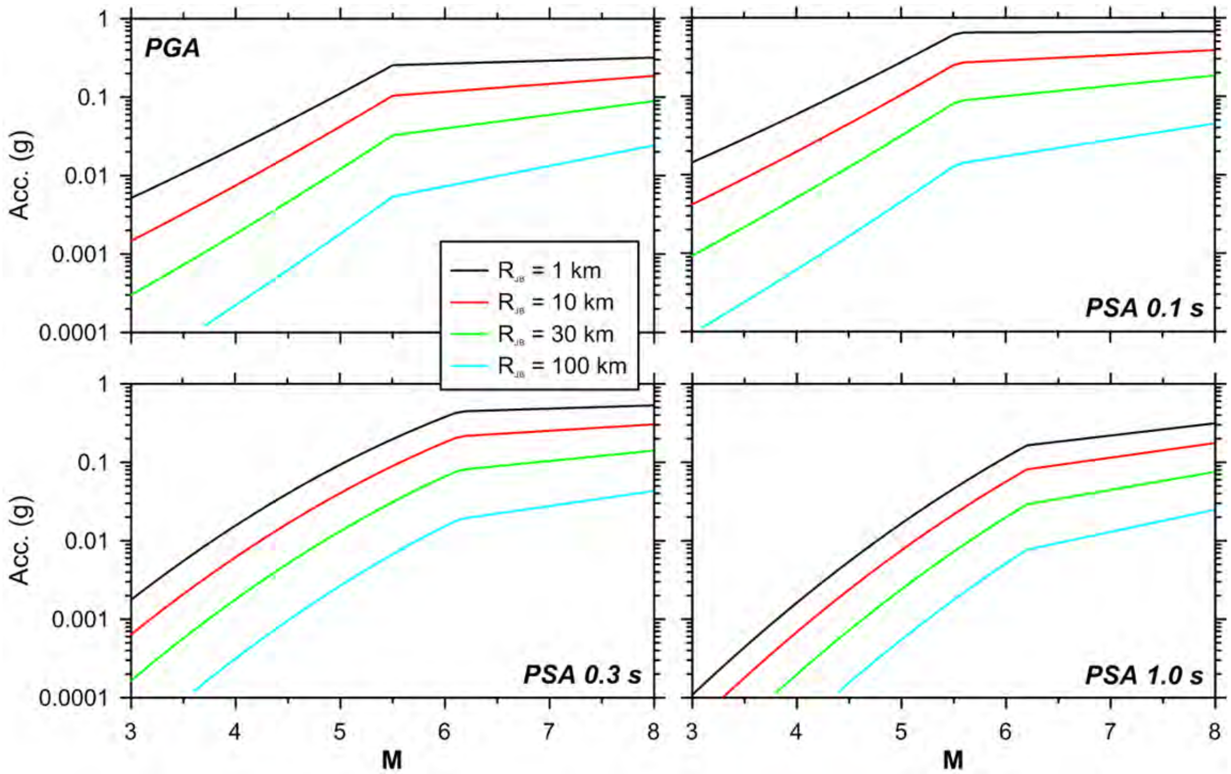

Figure 3.18 **Median trends of proposed vertical GMPE as a function of M for indicated distances and strike slip events. V_{S30} = 760 m/sec.**

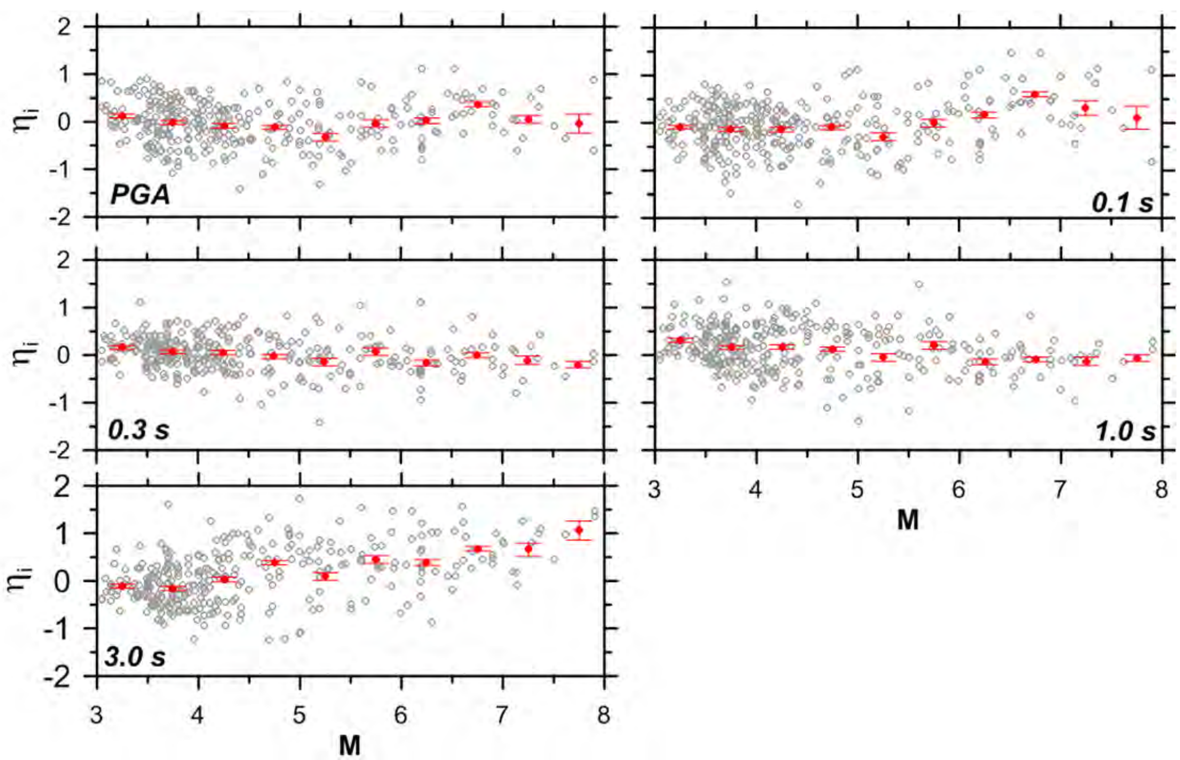

Figure 3.19 **Event terms versus magnitude for PGA and PSA at four selected periods. Means within M bins shown along with their 95% confidence intervals.**

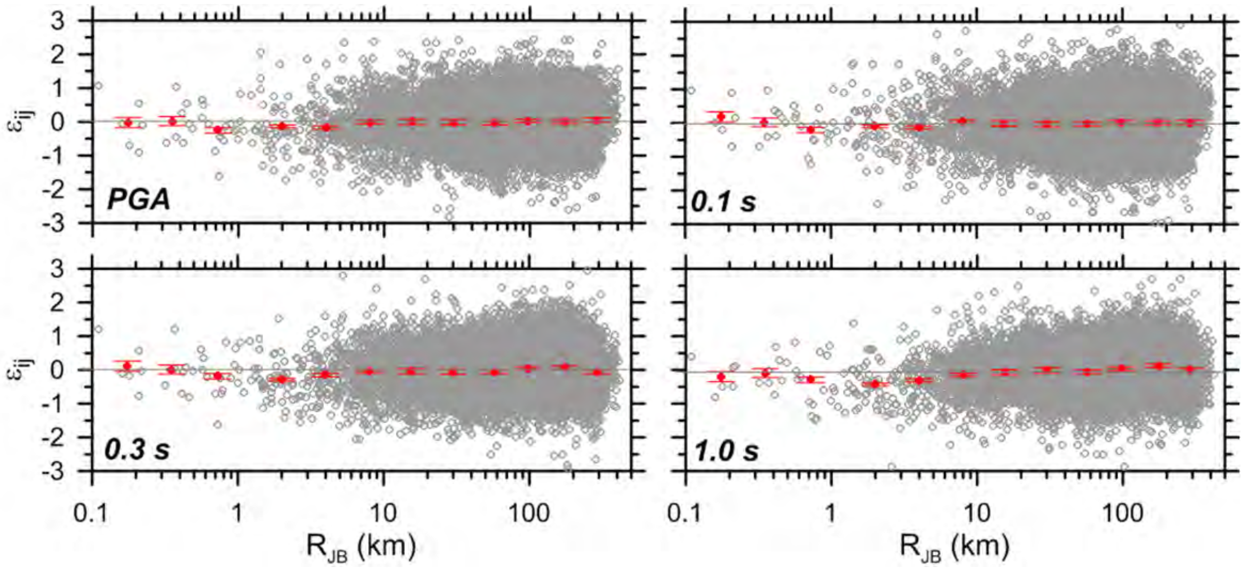

Figure 3.20 **Within-event residuals versus R_{jb} for PGA and PSA at three selected periods. Means within distance bins shown along with their 95% confidence intervals.**

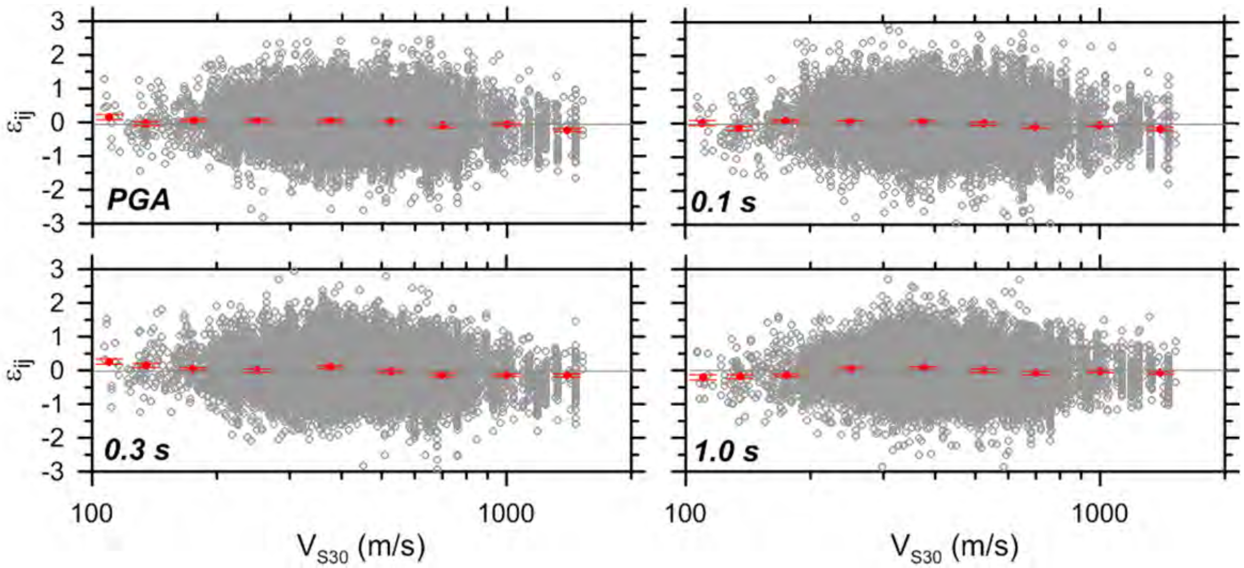

Figure 3.21 **Within-event residuals versus V_{S30} for PGA and PSA at three selected periods. Means within V_{S30} bins are shown along with their 95% confidence intervals.**

Based on GMPE developer interactions, we are aware that our vertical GMPEs produce larger ground motions for the specific condition of mid- to long-periods ($T > \sim 0.3$ sec), large magnitudes ($\mathbf{M} \geq 7$), and close distances ($R_{JB} < \sim 5$ km) than other NGA-West 2 vertical models. For this reason, we present an additional check of our model to test its general performance in this range. In Figure 3.22, we plot the data for the 1999 Chi Chi, Taiwan, (**M** 7.6) event at periods of 1.0 and 3.0 sec. The data are corrected to a site condition of V_{S30} = 760 m/sec using the site model presented in Section 3.2.1. Superimposed on the data is our median model prediction for *RS* earthquakes (no event term is applied). The model performance appears quite good for 1.0 sec PSA, suggesting that our GMPE is not over-predicting this important data set. At 3.0 sec PSA, our model under-predicts the data, which is consistent with the event term in Figure 3.19. Interestingly, since our understanding is that the other models predict considerably lower median ground motions than ours at close distances, those models would likely have a larger offset from the data for this event.

Figure 3.23 presents the aleatory uncertainty terms from the present work (applicable to **M** > 5.5 and R_{JB} < 100 km) for the vertical component as compared to the corresponding terms from BSSA14 for the horizontal component. We find the within-event aleatory uncertainties (ϕ) to be similar for horizontal and vertical, whereas the between-even uncertainties (τ) are lower for vertical at short periods (under around 0.1 sec) and higher at longer periods.

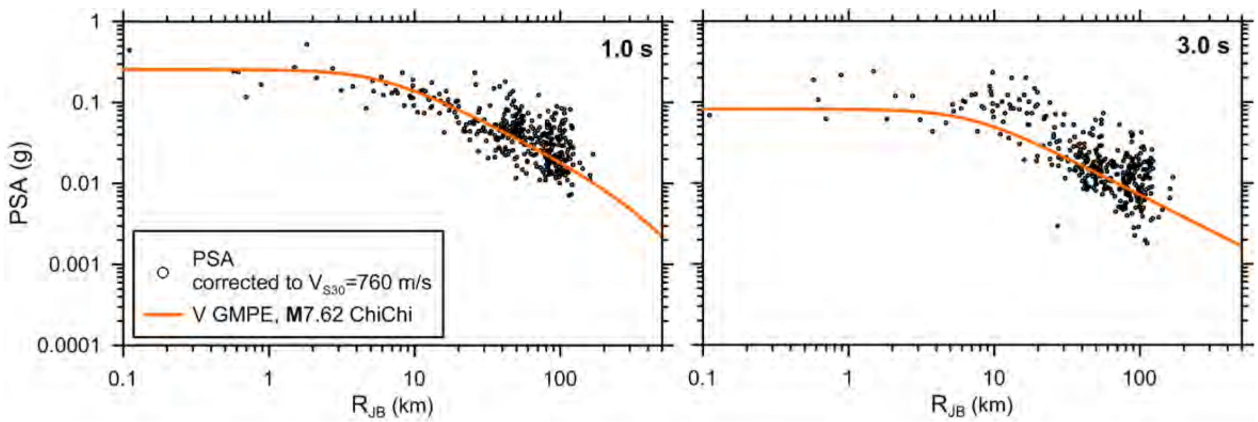

Figure 3.22 NGA-West 2 vertical data for M 7.62 Chi Chi, Taiwan, event, corrected to V_{S30} = 760 m/sec, along with model prediction (without event term) for RS focal mechanism.

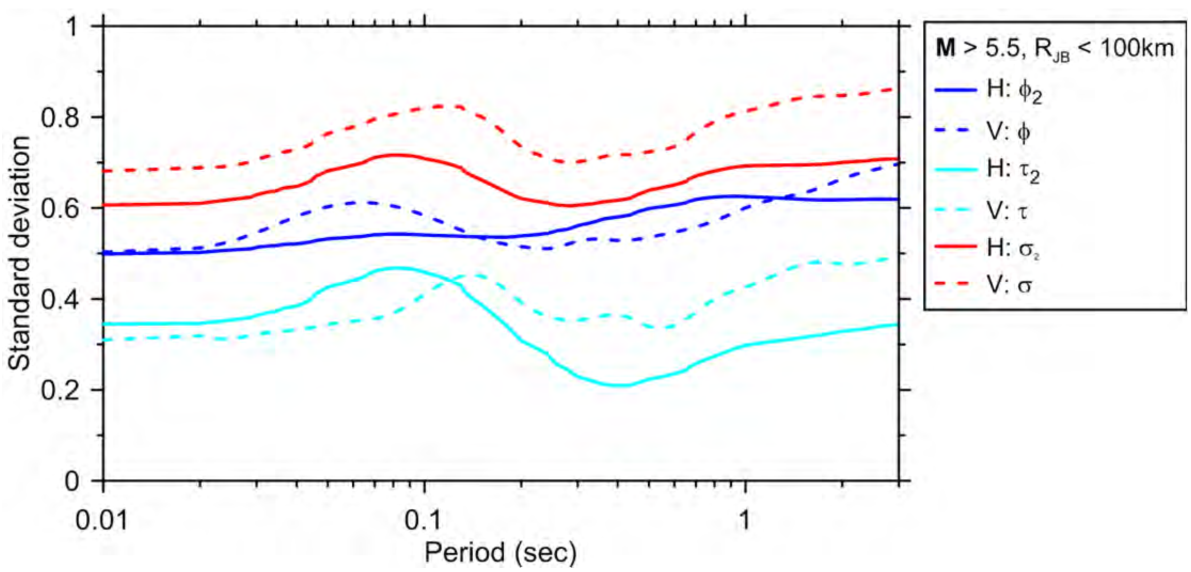

Figure 3.23 Standard deviation terms against period for vertical GMPEs (this study) and horizontal GMPEs BSSA14 for the conditions of M > 5.5 and R_{JB} < 100 km (V_{S30} > 300 m/sec is an additional condition for the horizontal component).

3.5 SUMMARY AND LIMITATIONS

We have presented a set of ground-motion prediction equations that we believe are the simplest formulation demanded by the NGA-West 2 database used for the regressions. The GMPEs presented in this report are *only* recommended for the conditions below:

- Tectonically active crustal regions.
- Strike-slip and reverse-slip earthquakes, **M** = 5 to 8.5.
- Normal-slip earthquakes, **M** = 5 to 7.
- Distance, R_{JB} = 0 to 400 km.
- Spectral periods of PGA to 3.0 sec, with the exception of events with **M** > 6.5, for which we consider the relations to only be valid for PGA to 1.0 sec.
- Time-averaged shear wave velocities of V_{S30} = 200 to 1500 m/sec (the 200 m/sec limit is based on misfits identified from residuals for slower velocities).

Further refinements of these vertical GMPEs are likely. We anticipate performing a fresh set of two-step regressions on the vertical data with subsequent refinements from residuals analysis, which may affect the source and path functions, and reduce the aleatory uncertainties relative to what is presented here.

3.6 COEFFICIENT TABLE

The model parameters that have changed relative to BSSA14 are presented in Table 3.1.

Table 3.1 Coefficients changed relative to BSSA14.

Period (sec)	e_{0V}	e_{1V}	e_{2V}	e_{3V}
PGA	0.45336	0.4499	0.34114	0.50493
PGV	4.96599	5.13000	5.33000	4.50000
0.01	0.4636	0.43243	0.39355	0.55187
0.02	0.49077	0.49282	0.40139	0.52256
0.022	0.5034	0.50645	0.41402	0.53326
0.025	0.52803	0.52944	0.44155	0.55988
0.029	0.56572	0.56269	0.48692	0.60309
0.03	0.57559	0.57162	0.49905	0.61389
0.032	0.59479	0.58965	0.52229	0.6337
0.035	0.62338	0.61801	0.5561	0.66067
0.036	0.63262	0.62743	0.56688	0.66895
0.04	0.66982	0.66587	0.61036	0.70125
0.042	0.68774	0.68442	0.63173	0.71657
0.044	0.70566	0.7029	0.65316	0.73198
0.045	0.71502	0.71252	0.66429	0.74016
0.046	0.72455	0.72228	0.67554	0.74854
0.048	0.74238	0.74051	0.69644	0.76438
0.05	0.761	0.75947	0.71759	0.78132

Period (sec)	e_{0V}	e_{1V}	e_{2V}	e_{3V}
0.055	0.80611	0.80493	0.76563	0.8246
0.06	0.85042	0.84916	0.80816	0.86974
0.065	0.89295	0.8914	0.84522	0.91503
0.067	0.90906	0.90736	0.85866	0.93251
0.07	0.93284	0.9309	0.87806	0.95853
0.075	0.97073	0.96842	0.90878	0.99999
0.08	1.00627	1.0041	0.9381	1.03773
0.085	1.03966	1.03808	0.96606	1.07215
0.09	1.07201	1.0714	0.99335	1.10466
0.095	1.10307	1.10349	1.01981	1.13555
0.1	1.13146	1.13291	1.04438	1.16349
0.11	1.18277	1.18508	1.08951	1.21559
0.12	1.22718	1.2296	1.12953	1.26156
0.13	1.26385	1.266	1.1643	1.2995
0.133	1.27345	1.27556	1.17365	1.30929
0.14	1.29239	1.29436	1.19325	1.32823
0.15	1.31367	1.31592	1.21758	1.34775
0.16	1.32735	1.33062	1.2365	1.35738
0.17	1.33416	1.33901	1.25001	1.35843
0.18	1.3357	1.34241	1.25927	1.35331
0.19	1.33308	1.34166	1.26501	1.34373
0.2	1.32738	1.33747	1.26778	1.33171
0.22	1.31006	1.32153	1.2668	1.30519
0.24	1.28867	1.29888	1.25594	1.28203
0.25	1.27711	1.28564	1.24589	1.27309
0.26	1.26581	1.27206	1.2332	1.26678
0.28	1.24428	1.24504	1.20226	1.25963
0.29	1.23403	1.2322	1.18567	1.25691
0.3	1.22368	1.21977	1.16856	1.25328
0.32	1.20293	1.19681	1.1357	1.24165
0.34	1.18134	1.17521	1.10406	1.22409
0.35	1.16954	1.1639	1.08813	1.21299
0.36	1.15786	1.153	1.073	1.20119
0.38	1.13228	1.12929	1.0423	1.17405
0.4	1.1062	1.10508	1.01301	1.14565
0.42	1.07957	1.07971	0.98461	1.11728
0.44	1.05294	1.0539	0.95687	1.08949
0.45	1.039	1.04027	0.94261	1.07511
0.46	1.0249	1.02648	0.92823	1.06052
0.48	0.99865	1.00068	0.90167	1.03351
0.5	0.97145	0.9743	0.87426	1.0048
0.55	0.90625	0.91241	0.80826	0.93353
0.6	0.84269	0.85384	0.74369	0.86075
0.65	0.78217	0.79904	0.68191	0.78964
0.667	0.76273	0.78154	0.6622	0.76656
0.7	0.72476	0.74719	0.62424	0.72161
0.75	0.6679	0.69501	0.56936	0.65488

Period (sec)	e_{0V}	e_{1V}	e_{2V}	e_{3V}
0.8	0.61179	0.64211	0.51847	0.5905
0.85	0.55637	0.58874	0.47065	0.5281
0.9	0.50044	0.53403	0.42394	0.46608
0.95	0.44423	0.47852	0.37767	0.40456
1	0.39031	0.4251	0.33316	0.3459
1.1	0.2817	0.3172	0.23836	0.23041
1.2	0.17018	0.20598	0.13489	0.11507
1.3	0.05839	0.0941	0.02806	0.00147
1.4	0.04871	0.01335	0.07596	0.10618
1.5	0.15223	0.11741	0.17691	-0.20969
1.6	-0.25092	-0.21699	-0.27189	-0.30815
1.7	-0.3433	-0.31045	-0.35945	-0.40033
1.8	-0.4312	-0.3995	-0.44175	-0.48827
1.9	-0.5138	-0.483	-0.51867	-0.57141
2	-0.58742	-0.55718	-0.58711	-0.64602
2.2	-0.72165	-0.69099	-0.71179	-0.78487
2.4	-0.84801	-0.81601	-0.82716	-0.91822
2.5	-0.90945	-0.87663	-0.88385	-0.98313
2.6	-0.96838	-0.93453	-0.93989	-1.04522
2.8	-1.0813	-1.04509	-1.05165	-1.16318
3	-1.18922	-1.15062	-1.16117	-1.27506

Period (sec)	c_k	c_{1V}	c_{2V}	c_{3V}
PGA	-0.301998	-1.134	0.1667	-0.009224
PGV	-0.589976	-1.180	0.1600	-0.003400
0.01	-0.307103	-1.134	0.1666	-0.009224
0.02	-0.246512	-1.1394	0.16462	-0.009038
0.022	-0.223203	-1.1405	0.16424	-0.009036
0.025	-0.183923	-1.1419	0.16375	-0.009072
0.029	-0.131908	-1.1423	0.16344	-0.009207
0.03	-0.120305	-1.1421	0.16342	-0.009259
0.032	-0.099868	-1.1412	0.1634	-0.009387
0.035	-0.075817	-1.1388	0.16339	-0.009628
0.036	-0.069423	-1.1378	0.16337	-0.009719
0.04	-0.051039	-1.1324	0.16316	-0.010122
0.042	-0.045699	-1.125256	0.16297	-0.010336
0.044	-0.042664	-1.118932	0.16275	-0.010553
0.045	-0.041961	-1.115771	0.16264	-0.01066
0.046	-0.041775	-1.112542	0.16252	-0.010766
0.048	-0.042875	-1.106576	0.1623	-0.010972
0.05	-0.045804	-1.100623	0.16209	-0.011164
0.055	-0.060047	-1.086727	0.16155	-0.011569

Period (sec)	c_k	c_{1V}	c_{2V}	c_{3V}
0.06	-0.08197	-1.073772	0.16082	-0.011868
0.065	-0.108801	-1.061869	0.15985	-0.01207
0.067	-0.120287	-1.057499	0.15942	-0.012126
0.07	-0.13777	-1.051252	0.15869	-0.012183
0.075	-0.166106	-1.041467	0.15725	-0.012216
0.08	-0.191624	-1.0335	0.15552	-0.012176
0.085	-0.214482	-1.0295	0.15356	-0.012078
0.09	-0.235422	-1.0259	0.15143	-0.011934
0.095	-0.255187	-1.0228	0.1492	-0.011757
0.1	-0.274521	-1.0202	0.14703	-0.011562
0.11	-0.313705	-1.0157	0.1427	-0.01115
0.12	-0.353133	-1.0122	0.13852	-0.010726
0.13	-0.391805	-1.0099	0.13482	-0.010299
0.133	-0.40311	-1.0095	0.13382	-0.010172
0.14	-0.42872	-1.0087	0.13172	-0.009878
0.15	-0.462879	-1.0082	0.12901	-0.009475
0.16	-0.493473	-1.0083	0.12658	-0.009096
0.17	-0.52045	-1.0091	0.12448	-0.008742
0.18	-0.543952	-1.0106	0.12268	-0.008411
0.19	-0.564119	-1.0129	0.12116	-0.008103
0.2	-0.581092	-1.0157	0.11989	-0.007815
0.22	-0.605778	-1.025748	0.1193757	-0.007296
0.24	-0.617937	-1.035232	0.1186619	-0.006842
0.25	-0.619222	-1.040139	0.1182967	-0.006636
0.26	-0.617399	-1.044894	0.1179327	-0.006441
0.28	-0.607195	-1.054365	0.1171266	-0.006081
0.29	-0.600407	-1.058888	0.1167083	-0.005913
0.3	-0.593557	-1.063473	0.1162085	-0.005751
0.32	-0.581699	-1.072038	0.1152802	-0.00544
0.34	-0.572202	-1.080078	0.1144214	-0.005145
0.35	-0.568159	-1.084106	0.1140032	-0.005005
0.36	-0.564491	-1.087807	0.1136703	-0.004868
0.38	-0.557988	-1.095237	0.1130535	-0.004606
0.4	-0.552119	-1.102179	0.1126268	-0.00436
0.42	-0.5464	-1.10854	0.112275	-0.004129
0.44	-0.540724	-1.114629	0.1120024	-0.003913
0.45	-0.537899	-1.117548	0.1118969	-0.00381
0.46	-0.535079	-1.120451	0.1117925	-0.00371
0.48	-0.52945	-1.125713	0.1117186	-0.003521
0.5	-0.52383	-1.130919	0.1116734	-0.003346
0.55	-0.509781	-1.142369	0.1117089	-0.00296

Period (sec)	c_k	c_{1V}	c_{2V}	c_{3V}
0.6	-0.495999	-1.152354	0.1115151	-0.002644
0.65	-0.4828	-1.161015	0.1108959	-0.002391
0.667	-0.478502	-1.163641	0.1106506	-0.002318
0.7	-0.470505	-1.168586	0.1101099	-0.002194
0.75	-0.459435	-1.175694	0.1093617	-0.002043
0.8	-0.449838	-1.1819	0.10873	-0.001932
0.85	-0.441663	-1.1854	0.10709	-0.001852
0.9	-0.434789	-1.1884	0.10548	-0.001796
0.95	-0.429091	-1.1909	0.10389	-0.001756
1	-0.424447	-1.193	0.10248	-0.001724
1.1	-0.417828	-1.1966	0.10016	-0.001665
1.2	-0.413951	-1.1996	0.098482	-0.001606
1.3	-0.411835	-1.2018	0.097375	-0.001549
1.4	-0.4105	-1.2039	0.096743	-0.001494
1.5	-0.408967	-1.2063	0.096445	-0.001439
1.6	-0.40646	-1.2086	0.096338	-0.001386
1.7	-0.403029	-1.2106	0.096254	-0.001334
1.8	-0.398928	-1.2123	0.096207	-0.001283
1.9	-0.394411	-1.2141	0.096255	-0.001232
2	-0.389734	-1.2159	0.096361	-0.001183
2.2	-0.380577	-1.219	0.096497	-0.001086
2.4	-0.371794	-1.2202	0.096198	-0.000992
2.5	-0.367543	-1.2201	0.096106	-0.000946
2.6	-0.363385	-1.2198	0.096136	-0.0009
2.8	-0.355348	-1.218	0.096667	-0.000809
3	-0.347682	-1.217	0.097638	0

Period (sec)	Δc_{3V} (***CATWNZ,Global***)	Δc_{3V} (***CHTur***)	Δc_{3V} (***ItJP***)
PGA	0.00	0.0029	-0.0026
PGV	0.00	0.0044	-0.0003
0.01	0.00	0.0028	-0.0026
0.02	0.00	0.0028	-0.0022
0.022	0.00	0.0027	-0.0022
0.025	0.00	0.0027	-0.0022
0.029	0.00	0.0027	-0.0022
0.03	0.00	0.0027	-0.0022
0.032	0.00	0.0027	-0.0021
0.035	0.00	0.0028	-0.0021

Period (sec)	Δc_{3V} (*CATWNZ,Global*)	Δc_{3V} (*CHTur*)	Δc_{3V} (*ItJP*)
0.036	0.00	0.0028	-0.0021
0.04	0.00	0.0028	-0.0020
0.042	0.00	0.0029	-0.0020
0.044	0.00	0.0029	-0.0020
0.045	0.00	0.0029	-0.0020
0.046	0.00	0.0029	-0.0020
0.048	0.00	0.0030	-0.0020
0.05	0.00	0.0030	-0.0020
0.055	0.00	0.0030	-0.0020
0.06	0.00	0.0030	-0.0020
0.065	0.00	0.0030	-0.0020
0.067	0.00	0.0030	-0.0020
0.07	0.00	0.0030	-0.0021
0.075	0.00	0.0029	-0.0021
0.08	0.00	0.0029	-0.0022
0.085	0.00	0.0029	-0.0023
0.09	0.00	0.0029	-0.0023
0.095	0.00	0.0029	-0.0024
0.1	0.00	0.0029	-0.0024
0.11	0.00	0.0029	-0.0025
0.12	0.00	0.0029	-0.0026
0.13	0.00	0.0028	-0.0026
0.133	0.00	0.0028	-0.0027
0.14	0.00	0.0028	-0.0027
0.15	0.00	0.0028	-0.0027
0.16	0.00	0.0028	-0.0027
0.17	0.00	0.0028	-0.0028
0.18	0.00	0.0028	-0.0028
0.19	0.00	0.0028	-0.0028
0.2	0.00	0.0027	-0.0029
0.22	0.00	0.0026	-0.0030
0.24	0.00	0.0025	-0.0032
0.25	0.00	0.0024	-0.0032
0.26	0.00	0.0024	-0.0033
0.28	0.00	0.0023	-0.0033
0.29	0.00	0.0022	-0.0033
0.3	0.00	0.0022	-0.0033
0.32	0.00	0.0021	-0.0034
0.34	0.00	0.0020	-0.0033
0.35	0.00	0.0020	-0.0033

Period (sec)	Δc_{3V} (*CATWNZ,Global*)	Δc_{3V} (*CHTur*)	Δc_{3V} (*ItJP*)
0.36	0.00	0.0020	-0.0033
0.38	0.00	0.0020	-0.0033
0.4	0.00	0.0021	-0.0032
0.42	0.00	0.0021	-0.0032
0.44	0.00	0.0022	-0.0031
0.45	0.00	0.0022	-0.0031
0.46	0.00	0.0022	-0.0031
0.48	0.00	0.0023	-0.0030
0.5	0.00	0.0023	-0.0030
0.55	0.00	0.0024	-0.0028
0.6	0.00	0.0025	-0.0027
0.65	0.00	0.0026	-0.0027
0.667	0.00	0.0026	-0.0026
0.7	0.00	0.0026	-0.0026
0.75	0.00	0.0027	-0.0025
0.8	0.00	0.0027	-0.0025
0.85	0.00	0.0028	-0.0024
0.9	0.00	0.0029	-0.0024
0.95	0.00	0.0029	-0.0023
1	0.00	0.0030	-0.0022
1.1	0.00	0.0030	-0.0021
1.2	0.00	0.0031	-0.0019
1.3	0.00	0.0031	-0.0017
1.4	0.00	0.0030	-0.0016
1.5	0.00	0.0030	-0.0014
1.6	0.00	0.0030	-0.0013
1.7	0.00	0.0030	-0.0012
1.8	0.00	0.0031	-0.0011
1.9	0.00	0.0031	-0.0011
2	0.00	0.0031	-0.0011
2.2	0.00	0.0030	-0.0010
2.4	0.00	0.0029	-0.0011
2.5	0.00	0.0028	-0.0011
2.6	0.00	0.0027	-0.0012
2.8	0.00	0.0025	-0.0012
3	0.00	0.0024	-0.0013

Period (sec)	c_V	$f4_V$
PGA	-0.33	-0.1500
PGV	-0.52	-0.2010
0.01	-0.33	-0.1483
0.02	-0.32	-0.1471
0.022	-0.31	-0.1477
0.025	-0.3	-0.1496
0.029	-0.3	-0.1525
0.03	-0.29	-0.1549
0.032	-0.3	-0.1574
0.035	-0.3	-0.1607
0.036	-0.3	-0.1641
0.04	-0.32	-0.1678
0.042	-0.33	-0.1715
0.044	-0.33	-0.176
0.045	-0.34	-0.181
0.046	-0.34	-0.1862
0.048	-0.35	-0.1915
0.05	-0.36	-0.1963
0.055	-0.37	-0.2014
0.06	-0.39	-0.2066
0.065	-0.4	-0.212
0.067	-0.4	-0.2176
0.07	-0.4	-0.2232
0.075	-0.41	-0.2287
0.08	-0.41	-0.2337
0.085	-0.41	-0.2382
0.09	-0.41	-0.2421
0.095	-0.4	-0.2458
0.1	-0.4	-0.2492
0.11	-0.4	-0.2519
0.12	-0.4	-0.254
0.13	-0.4	-0.2556
0.133	-0.4	-0.2566
0.14	-0.4	-0.2571
0.15	-0.4	-0.2571
0.16	-0.4	-0.2562
0.17	-0.4	-0.2544
0.18	-0.4	-0.2522
0.19	-0.4	-0.2497
0.2	-0.4	-0.2466
0.22	-0.4	-0.2432

Period (sec)	c_V	$f4_V$
0.24	-0.41	-0.2396
0.25	-0.41	-0.2357
0.26	-0.41	-0.2315
0.28	-0.4	-0.2274
0.29	-0.39	-0.2232
0.3	-0.39	-0.2191
0.32	-0.38	-0.2152
0.34	-0.38	-0.2112
0.35	-0.38	-0.207
0.36	-0.37	-0.2033
0.38	-0.37	-0.1996
0.4	-0.38	-0.1958
0.42	-0.38	-0.1922
0.44	-0.38	-0.1884
0.45	-0.38	-0.184
0.46	-0.39	-0.1793
0.48	-0.39	-0.1749
0.5	-0.39	-0.1704
0.55	-0.41	-0.1658
0.6	-0.42	-0.161
0.65	-0.43	-0.1558
0.667	-0.44	-0.1503
0.7	-0.45	-0.1446
0.75	-0.46	-0.1387
0.8	-0.47	-0.1325
0.85	-0.49	-0.1262
0.9	-0.5	-0.1197
0.95	-0.51	-0.1126
1	-0.52	-0.1052
1.1	-0.53	-0.0977
1.2	-0.54	-0.0902
1.3	-0.55	-0.0827
1.4	-0.56	-0.0753
1.5	-0.56	-0.0679
1.6	-0.57	-0.0604
1.7	-0.58	-0.0534
1.8	-0.59	-0.047
1.9	-0.61	-0.0414
2	-0.62	-0.0361
2.2	-0.64	-0.0314
2.4	-0.66	-0.0271

Period (sec)	c_V	$f4_V$
2.5	-0.67	-0.0231
2.6	-0.68	-0.0196
2.8	-0.69	-0.0165
3	-0.7	-0.0136

Period (sec)	ϕ_V	τ_V
PGA	0.502	0.440
PGV	0.479	0.438
0.01	0.503	0.446
0.02	0.512	0.439
0.022	0.517	0.442
0.025	0.527	0.450
0.029	0.542	0.464
0.03	0.546	0.468
0.032	0.554	0.476
0.035	0.565	0.487
0.036	0.569	0.490
0.04	0.582	0.502
0.042	0.587	0.507
0.044	0.592	0.511
0.045	0.594	0.513
0.046	0.596	0.514
0.048	0.600	0.517
0.05	0.603	0.519
0.055	0.608	0.522
0.06	0.611	0.524
0.065	0.612	0.523
0.067	0.612	0.522
0.07	0.611	0.520
0.075	0.608	0.516
0.08	0.604	0.512
0.085	0.600	0.506
0.09	0.595	0.500
0.095	0.589	0.493
0.1	0.584	0.486
0.11	0.572	0.472
0.12	0.562	0.458
0.13	0.551	0.446
0.133	0.548	0.442

Period (sec)	ϕ_V	τ_V
0.14	0.542	0.435
0.15	0.534	0.426
0.16	0.528	0.420
0.17	0.524	0.417
0.18	0.520	0.414
0.19	0.517	0.412
0.2	0.515	0.409
0.22	0.512	0.398
0.24	0.511	0.387
0.25	0.512	0.382
0.26	0.514	0.380
0.28	0.521	0.378
0.29	0.524	0.379
0.3	0.527	0.380
0.32	0.531	0.381
0.34	0.532	0.382
0.35	0.532	0.382
0.36	0.531	0.383
0.38	0.530	0.384
0.4	0.529	0.385
0.42	0.529	0.388
0.44	0.530	0.391
0.45	0.530	0.392
0.46	0.531	0.394
0.48	0.533	0.398
0.5	0.536	0.401
0.55	0.541	0.410
0.6	0.547	0.418
0.65	0.552	0.425
0.667	0.554	0.428
0.7	0.558	0.432
0.75	0.565	0.440
0.8	0.572	0.447
0.85	0.579	0.455
0.9	0.587	0.462
0.95	0.594	0.470
1	0.600	0.477
1.1	0.611	0.490
1.2	0.618	0.502
1.3	0.623	0.512
1.4	0.628	0.523

Period (sec)	ϕ_V	τ_V
1.5	0.632	0.534
1.6	0.638	0.546
1.7	0.644	0.558
1.8	0.651	0.571
1.9	0.658	0.582
2	0.664	0.592
2.2	0.674	0.606
2.4	0.681	0.615
2.5	0.684	0.617
2.6	0.687	0.619
2.8	0.692	0.621
3	0.697	0.624

REFERENCES

Ancheta T.D., Darragh R.B., Stewart J.P., Seyhan E., Silva W.J., Chiou B.S.J., Wooddell K.E. Graves R.W., Kottke A.R., Boore D.M., Kishida T., Donahue J.L. (2014). NGA-West2 database, *Earthq. Spectra*, submitted.

Boore D.M., Stewart J.P., Seyhan E., Atkinson G.M. (2014). NGA-West 2 equations for predicting PGA, PGV, and 5%-damped PSA for shallow crustal earthquakes, *Earthq. Spectra*, submitted.

Seyhan E., Stewart J.P. (2014). Semi-empirical nonlinear site amplification from NGA-West 2 data and simulations, *Earthq. Spectra*, submitted.

4. BC13: Ground Motion Model for the Vertical Component of PGA, PGV, and Pseudo-Acceleration Response Spectra

YOUSEF BOZORGNIA[1]
KENNETH W. CAMPBELL[2]

4.1 INTRODUCTION

This chapter summarizes the development of the NGA-West2 Bozorgnia-Campbell (BC13) empirical ground motion prediction equation (GMPE) for the vertical component. This GMPE updates and supersedes the GMPE developed by Campbell and Bozorgnia [2003], which pre-dated the NGA research program. We used the extensive and expanded PEER NGA-West2 ground motion database recorded from shallow crustal earthquakes in active tectonic domains to develop a GMPE for the vertical component of peak ground acceleration (PGA), peak ground velocity (PGV), and 5%-damped elastic pseudo-absolute acceleration response spectral ordinates (PSA) at periods ranging from 0.01 to 3 sec, which is the NGA-West2 consensus period range for the vertical component.

As in our NGA-West2 GMPE for the average horizontal component [Campbell and Bozorgnia 2013; 2014], we included terms and predictor variables that modeled magnitude scaling, magnitude-dependent geometric attenuation, magnitude-dependent style of faulting, magnitude-dependent rupture dip, magnitude-dependent hypocentral depth, hanging-wall (HW) effects, regionally dependent shallow linear site response, regionally dependent shallow basin response, regionally dependent anelastic attenuation, and magnitude-dependent between-event and within-event standard deviations. We did not include nonlinear vertical site response or deep basin response of the vertical component, as the simulation results for these effects had not reached the level of confidence to be included in our new GMPE and we did not find any empirical evidence that such effects are important.

Our new vertical GMPE is considered valid for estimating vertical ground motions from shallow continental earthquakes occurring worldwide in active tectonic domains for magnitudes

[1] Pacific Earthquake Engineering Research Center, University of California, Berkeley
[2] EQECAT, Inc., Beaverton, Oregon

ranging from 3.3 to as large as 8.5, depending on the style of faulting, and distances as far as 300 km from the source.

In the last three decades there have been major advances in our understanding and quantification of the characteristics of vertical ground motion (e.g., Campbell [1982]; Niazi and Bozorgnia, [1991, 1992]; Bozorgnia et al. [1995]; Silva [1997]; Beresnev et al. [2002]; Bozorgnia and Campbell [2004]; and Gülerce and Abrahamson [2010]; Bommer at el. [2011]; among others). These studies established that vertical-to-horizontal spectral ratio (V/H) is primarily a function of spectral period and source-to-site distance, with short periods exhibiting higher ratios than long periods, and is generally higher on soil sites than on rock sites. Bozorgnia and Campbell [2004] also developed simplified vertical design and V/H spectra, and their recommendations were adopted for the first time in the U.S. as part of the NEHRP Provisions for seismic design [BSSC 2009].

4.2 GROUND MOTION DATABASE

The ground motion database used in this study is a subset of the PEER ground motion database that was updated as part of the PEER NGA-West2 Project [Ancheta et al. 2013; 2014]. An electronic version of the PEER NGA-West2 database can be accessed from the PEER website. The NGA-West2 database includes over 21,000 three-component recordings from worldwide earthquakes with moment magnitudes ranging from 3.0 to 7.9. More details are provided in Ancheta et al. [2013; 2014].

We excluded from the larger PEER NGA-West2 database the following earthquakes, recordings, or seismic stations in order to meet our general selection criteria and project requirements:

1. recordings having only one horizontal component or only a vertical component. This was carried out in order to make the database consistent with that used for the average horizontal component [Campbell and Bozorgnia 2013; 2014];
2. recording sites with no measured or estimated value of V_{S30}, which precludes modeling shallow site effects;
3. earthquakes with no rake or focal mechanism, which precludes modeling style-of-faulting effects;
4. earthquakes with the hypocenter or a significant amount of the fault rupture located in the lower crust (below about 20 km), in an oceanic plate, or in a stable continental region (SCR), which are not consistent with the desired tectonic domain;
5. the Lamont Doherty Geologic Observatory recordings from the 1999 Düzce, Turkey, earthquake, which are considered to be unreliable because of their odd spectral shapes;
6. recordings from instruments designated quality D from the 1999 Chi-Chi, Taiwan, earthquake according to the quality designation of Lee et al. [2001], which are considered to be unreliable because of their poor quality;
7. "aftershocks" located in the immediate vicinity of the inferred mainshock rupture plane and defined as a "Class 2" event with $CR_{JB} < 10$ km according to criteria given in Ancheta

et al. [2012; 2013] and Wooddell and Abrahamson [2012], which are potentially considered to have below-average stress drops;

8. rupture distances (R_{RUP}) greater than 80 km to isolate the effects of geometric attenuation; however, to model anelastic attenuation we used a separate database with recordings at distances as far as 500 km;
9. an earthquake considered to be poorly recorded according to the criteria (a) $\mathbf{M} < 5.5$ and $N < 5$ or (b) $5.5 \le \mathbf{M} < 6.5$ and $N < 3$ (i.e., note that singly recorded events with large magnitudes are included), where $\mathbf{M}$ is moment magnitude and N is the number of recordings with $R_{RUP} \le 80$ km;
10. a seismic station not representative of free-field site conditions, which we define as an instrument that is: (a) in the basement of a building, (b) embedded more than a few meters below the ground surface, or (c) on a dam crest, embankment, or toe (note that abutment recordings were included if sited on rock in order to supplement the limited number of firm and hard rock sites in the database); and
11. recordings from the Pacoima Dam upper-left abutment and the Tarzana Cedar Hill Nursery that have been shown to exhibit strong topographic effects.

The application of the above criteria, as described further below, resulted in selecting a total of 15,161 recordings from 321 earthquakes for the development of our vertical GMPE. This includes 6989 near-source ($R_{RUP} \le 80$ km) recordings from 282 earthquakes. The distribution of our selected recordings with respect to magnitude and distance is shown in Figure 4.1. The list of the selected earthquakes and recording sites for the vertical component is essentially the same as that used for the development of our horizontal GMPE [Campbell and Bozorgnia 2013], except, obviously, excluding the recordings that had a missing vertical intensity measure (IM).

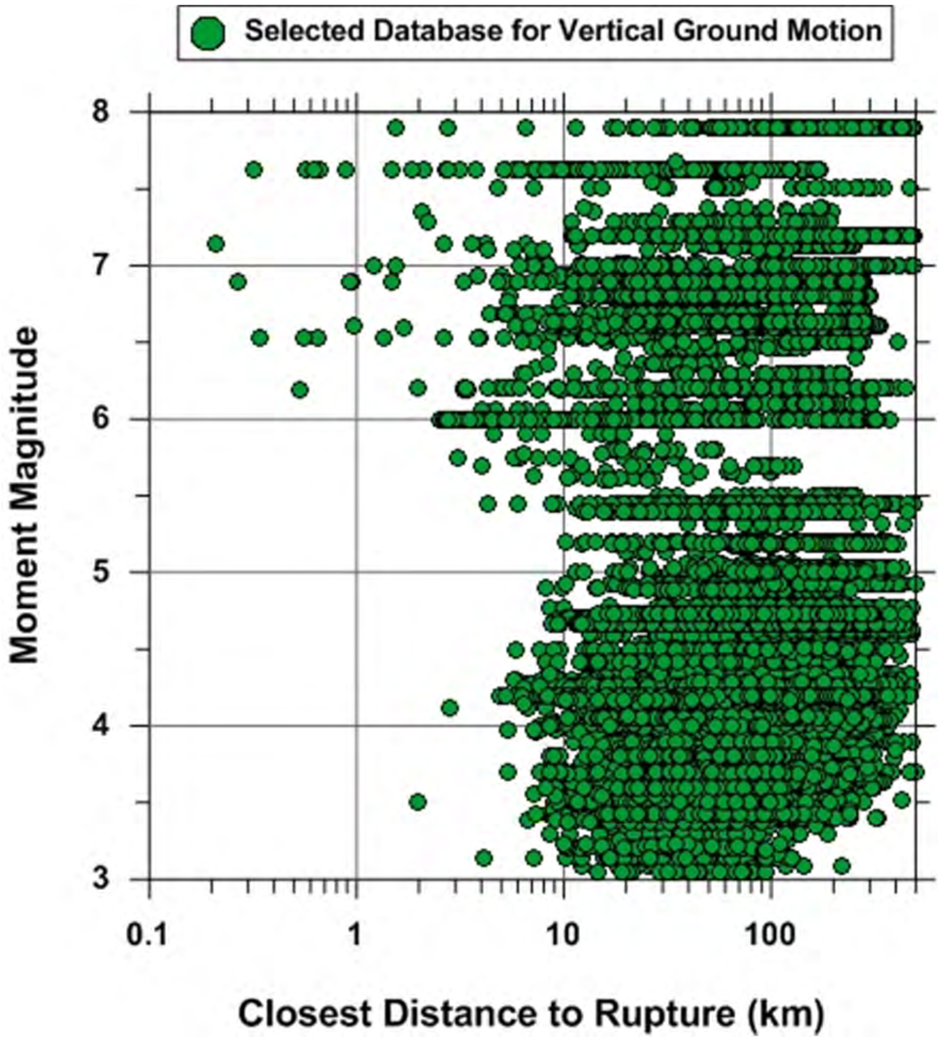

Figure 4.1 **Distribution of recordings with magnitude and distance for the BC13 vertical ground motion database.**

4.3 GROUND MOTION MODEL

The functional forms used in our NGA-West2 vertical GMPE were the same as those used for our horizontal GMPE, as described in Campbell and Bozorgnia [2013, 2014]. The appropriateness of using these functional forms for the vertical component was verified through analysis of residuals, as elaborated in the following sections. Although part of the functional forms were not used, we retained them for consistency with the horizontal GMPE. The parts that were not used are turned-off by setting certain coefficients to zero.

4.3.1 Regression Analysis Approach

Similar to the case of the horizontal component, the regression analysis using the near-source database ($R_{RUP} \leq 80$ km) was performed on a subset of spectral periods using the two-stage weighted regression procedure of Joyner and Boore [1993]. The only exception to this procedure was that our analysis used nonlinear rather than linearized regression. In Stage 1, all of the mathematical terms involving individual recordings were fit by the method of nonlinear least squares using all of the selected recordings. Each earthquake was constrained to have a zero mean residual by including a "source" (a.k.a, between-event, inter-event, or simply event) term for each earthquake. The terms included in Stage 1 were f_{dis}, f_{hng}, f_{site}, and f_{sed} in the GMPE presented in the next section. In Stage 2, all of the mathematical terms involving the earthquake source were fit by the method of weighted least squares using the source terms from Stage 1. Each source term was assigned a weight that was inversely proportional to its variance from Stage 1. The Stage 2 terms included f_{mag}, f_{flt}, f_{hyp}, and f_{dip} in the GMPE presented in the next section. Once the functional forms of all of the mathematical terms were established, a final regression analysis was performed for the larger set of spectral periods using random-effects regression [Abrahamson and Youngs 1992]. After the near-source GMPE was developed, we used random-effects regression in conjunction with the far-source database to develop a regionally-dependent anelastic attenuation term. Finally, we did a limited amount of smoothing of the coefficients in order to remove roughness in predicted response spectra.

4.3.2 Strong-Motion Intensity Measures

The IMs addressed in this study are the vertical components of PGA, PGV, and PSA at 17 oscillator periods (*T*) ranging from 0.01 to 3 sec. The specific spectral periods are 0.01, 0.02, 0.03, 0.05, 0.075, 0.1, 0.15, 0.2, 0.25, 0.3, 0.4, 0.5, 0.75, 1, 1.5, 2, and 3 sec. As indicated previously, we have also reviewed results for longer periods; however, the consensus of the NGA-West2 group was that the behavior of vertical ground motion at longer periods needs to be further investigated. Additionally, similar to the case of the horizontal motion, the consensus of the NGA-West2 GMPE developers was to exclude peak ground displacement (PGD) as an IM because of its strong dependence on the low-pass filter used to process the strong-motion recordings.

The vertical spectra, and the associated new GMPE, are for a 5% damping ratio. Scaling spectral values for the vertical components to damping values ranging from 0.5% to 30% can be obtained from the spectral value at 5% damping using the spectral damping factors developed by Rezaeian et al. [2012].

4.3.3 Median Ground Motion Model

Examination of the vertical ground motion data revealed that we could adopt the functional forms that we developed for the NGA-West2 horizontal GMPE, except that certain coefficients were set to zero in order to turn-off those parts of the functional forms that were not needed. This is explained in more detail in the section on the justification of the functional forms.

The natural logarithm of the vertical ground motion component of PGA (*g*), PGV (cm/sec), and PSA (*g*) is given by the equation

$$\ln Y = \begin{cases} \ln \mathrm{PGA}; & Y < \mathrm{PGA},\ T < 0.25 \\ f_{mag} + f_{dis} + f_{flt} + f_{hng} + f_{site} + f_{sed} + f_{hyp} + f_{dip} + f_{atn}; & \text{Otherwise} \end{cases} \tag{4.1}$$

where Y is the IM of interest and the f-terms represent the scaling of ground motion with respect to earthquake magnitude, geometric attenuation, style of faulting, HW geometry, shallow site response, shallow basin response, hypocentral depth, rupture dip, and anelastic attenuation. Note that PGA is the true value of peak ground acceleration and is not equivalent to PSA at $T = 0.01$ sec, although the two have very similar amplitudes. Note also that there are some combinations of predictor variable values, especially at large distances, for which the calculated value of PSA at periods of $T < 0.25$ sec can fall below the value of PGA. Since this is an artifact of the numerical analysis and is not possible given the definition of pseudo-absolute acceleration, the calculated value of PSA is set equal to the value of PGA when this occurs.

4.3.4 Magnitude Term

$$f_{mag} = \begin{cases} c_0 + c_1\mathbf{M}; & \mathbf{M} \le 4.5 \\ c_0 + c_1\mathbf{M} + c_2(\mathbf{M} - 4.5); & 4.5 < \mathbf{M} \le 5.5 \\ c_0 + c_1\mathbf{M} + c_2(\mathbf{M} - 4.5) + c_3(\mathbf{M} - 5.5); & 5.5 < \mathbf{M} \le 6.5 \\ c_0 + c_1\mathbf{M} + c_2(\mathbf{M} - 4.5) + c_3(\mathbf{M} - 5.5) + c_4(\mathbf{M} - 6.5); & \mathbf{M} > 6.5 \end{cases} \tag{4.2}$$

4.3.5 Geometric Attenuation Term

$$f_{dis} = (c_5 + c_6\mathbf{M})\ln\left(\sqrt{R_{RUP}^2 + c_7^2}\right) \tag{4.3}$$

4.3.6 Style-of-Faulting Term

$$f_{flt} = f_{flt,F}\, f_{flt,M} \tag{4.4}$$

$$f_{flt,F} = c_8 F_{RV} + c_9 F_{NM} \tag{4.5}$$

$$f_{flt,M} = \begin{cases} 0; & \mathbf{M} \le 4.5 \\ \mathbf{M} - 4.5; & 4.5 < \mathbf{M} \le 5.5 \\ 1; & \mathbf{M} > 5.5 \end{cases} \tag{4.6}$$

4.3.7 Hanging-Wall Term

$$f_{hng} = c_{10}\, f_{hng,R_X}\, f_{hng,R_{RUP}}\, f_{hng,M}\, f_{hng,Z}\, f_{hng,\delta} \tag{4.7}$$

$$f_{hng,R_X} = \begin{cases} 0; & R_X < 0 \\ f_1(R_X); & 0 \le R_X < R_1 \\ \max[f_2(R_X), 0]; & R_X \ge R_1 \end{cases} \tag{4.8}$$

$$f_1(R_X) = h_1 + h_2(R_X / R_1) + h_3(R_X / R_1)^2 \tag{4.9}$$

$$f_2(R_X) = h_4 + h_5\left(\frac{R_X - R_1}{R_2 - R_1}\right) + h_6\left(\frac{R_X - R_1}{R_2 - R_1}\right)^2 \tag{4.10}$$

$$R_1 = W\cos(\delta) \tag{4.11}$$

$$R_2 = 62\mathbf{M} - 350 \tag{4.12}$$

$$f_{hng,R_{RUP}} = \begin{cases} 1; & R_{RUP} = 0 \\ (R_{RUP} - R_{JB}) / R_{RUP}; & R_{RUP} > 0 \end{cases} \tag{4.13}$$

$$f_{hng,M} = \begin{cases} 0; & \mathbf{M} \le 5.5 \\ (\mathbf{M} - 5.5)[1 + a_2(\mathbf{M} - 6.5)]; & 5.5 < \mathbf{M} \le 6.5 \\ 1 + a_2(\mathbf{M} - 6.5); & \mathbf{M} > 6.5 \end{cases} \tag{4.14}$$

$$f_{hng,Z} = \begin{cases} 1 - 0.06Z_{TOR}; & Z_{TOR} \le 16.66 \\ 0; & Z_{TOR} > 16.66 \end{cases} \tag{4.15}$$

$$f_{hng,\delta} = (90 - \delta) / 45 \tag{4.16}$$

4.3.8 Shallow Site Response Term

$$f_{site} = f_{site,G} + S_J f_{site,J} \tag{4.17}$$

$$f_{site,G} = \begin{cases} c_{11}\ln\left(\frac{V_{S30}}{k_1}\right) + k_2\left\{\ln\left[A_{1100} + c\left(\frac{V_{S30}}{k_1}\right)^n\right] - \ln\left[A_{1100} + c\right]\right\}; & V_{S30} \le k_1 \\ (c_{11} + k_2 n)\ln\left(\frac{V_{S30}}{k_1}\right); & V_{S30} > k_1 \end{cases} \tag{4.18}$$

$$f_{site,J} = \begin{cases} (c_{12} + k_2 n)\left[\ln\left(\frac{V_{S30}}{k_1}\right) - \ln\left(\frac{200}{k_1}\right)\right]; & V_{S30} \le 200 \\ (c_{13} + k_2 n)\ln\left(\frac{V_{S30}}{k_1}\right); & \text{All } V_{S30} \end{cases} \tag{4.19}$$

4.3.9 Basin Response Term

$$f_{sed} = \begin{cases} (c_{14} + c_{15}S_J)(Z_{2.5} - 1); & Z_{2.5} \le 1 \\ 0; & 1 < Z_{2.5} \le 3 \\ c_{16}k_3 e^{-0.75}[1 - \exp(-0.25(Z_{2.5} - 3)]; & Z_{2.5} > 3 \end{cases} \tag{4.20}$$

4.3.10 Hypocentral Depth Term

$$f_{hyp} = f_{hyp,H} f_{hyp,M} \tag{4.21}$$

$$f_{hyp,H} = \begin{cases} 0; & Z_{HYP} \le 7 \\ Z_{HYP} - 7; & 7 < Z_{HYP} \le 20 \\ 13; & Z_{HYP} > 20 \end{cases} \tag{4.22}$$

$$f_{hyp,M} = \begin{cases} c_{17}; & \mathbf{M} \le 5.5 \\ [c_{17} + (c_{18} - c_{17})(\mathbf{M} - 5.5)]; & 5.5 < \mathbf{M} \le 6.5 \\ c_{18}; & \mathbf{M} > 6.5 \end{cases} \tag{4.23}$$

4.3.11 Rupture Dip Term

$$f_{dip} = \begin{cases} c_{19}\delta; & \mathbf{M} \le 4.5 \\ c_{19}(5.5 - \mathbf{M})\delta; & 4.5 < \mathbf{M} \le 5.5 \\ 0; & \mathbf{M} > 5.5 \end{cases} \tag{4.24}$$

4.3.12 Anelastic Attenuation Term

$$f_{atn} = \begin{cases} (c_{20} + \Delta c_{20})(R_{RUP} - 80); & R_{RUP} > 80 \\ 0; & R_{RUP} \le 80 \end{cases} \tag{4.25}$$

4.3.13 Definitions of Predictor Variables

The definitions of the predictor variables appearing in the equations given in the previous sections are defined as follows:

- $\mathbf{M}$ is moment magnitude
- R_{RUP} (km) is closest distance to the coseismic rupture plane
- R_{JB} (km) is closest distance to the surface projection of the coseismic rupture plane (Joyner-Boore distance)
- R_X (km) is closest distance to the surface projection of the top edge of the coseismic rupture plane measured perpendicular to its average strike [Ancheta et al. 2013; 2014]
- W (km) is the down-dip width of the rupture plane
- λ (°) is rake defined as the average angle of slip measured in the plane of rupture between the strike direction and the slip vector (e.g., Ancheta et al. [2013; 2014]; Lay and Wallace [1995])

- F_{RV} is an indicator variable representing reverse and reverse-oblique faulting where $F_{RV} = 1$ for $30° < \lambda < 150°$ and $F_{RV} = 0$ otherwise
- F_{NM} is an indicator variable representing normal and normal-oblique faulting where $F_{NM} = 1$ for $-150° < \lambda < -30°$ and $F_{NM} = 0$ otherwise
- Z_{TOR} (km) is the depth to the top of the coseismic rupture plane
- δ (°) is the average dip of the rupture plane
- V_{S30} (m/sec) is the time-averaged shear-wave velocity in the top 30 m of the site
- A_{1100} (g) is the median predicted value of vertical PGA on rock with $V_{S30} = 1100$ m/sec (rock PGA)
- S_J is an indicator variable representing regional site effects where $S_J = 1$ for sites located in Japan and $S_J = 0$ otherwise
- $Z_{2.5}$ (km) is depth to the 2.5 km/sec shear-wave velocity horizon beneath the site (sediment depth)
- Z_{HYP} (km) is the hypocentral depth of the earthquake

4.3.14 Model Coefficients

The coefficients appearing in the equations given in the previous sections are defined as follows:

- c and n are period-independent, numerically constrained model coefficients
- a_2, h_i and k_i are period-dependent, numerically constrained model coefficients. As indicated previously, the effects of vertical nonlinear soil response are not considered in the current study; thus, this is equivalent of assigning k_2=0. Similarly, since the effects of deep basins are not explicitly considered for the vertical component, k_3 = 0 and c_{16} = 0
- c_i and Δc_{20} are empirically derived model coefficients.

4.3.15 Treatment of Missing Values

Similar to the case of the horizontal component, when predictor variables for selected recordings were missing from the PEER database, they were either estimated using proxies or the regression analysis involving the terms that included those variables was performed using only the recordings for which values were available. Sediment depth ($Z_{2.5}$) was the only predictor variable that had missing values and no credible proxies to substitute for these missing values. When values of V_{S30} were missing, they were replaced with proxy values derived from surface geological units, geotechnical site categories, ground slope, geomorphology, or elevation based on relationships given in Stewart et al. [2012] and Ancheta et al. [2013; 2014]. When finite rupture models were not available, the distance variables R_{RUP}, R_{JB}, and R_X, and the source variables W, Z_{HYP}, and δ were derived from focal mechanism or moment tensor information and source dimension versus magnitude relationships [Ancheta et al. 2013; 2014].

4.4 ALEATORY VARIABILITY MODEL

Consistent with the random-effects regression analysis used to derive the median value of *Y*, the aleatory variability model for the vertical component is defined by the equation

$$y_{ij} = Y_{ij} + \eta_i + \varepsilon_{ij} \tag{4.26}$$

where η_i is the between-event (inter-event) residual for event *i* and y_{ij}, Y_{ij}, and ε_{ij} are the observed value, estimated value, and within-event (intra-event) residual for recording *j* of event *i*, respectively. The independent normally distributed variables η_i and ε_{ij} have zero means and estimated between-event and within-event standard deviations on reference rock ($V_{S30} = 1100$ m/sec) or on soil represented by linear site response, $\tau_{\ln Y}$ and $\phi_{\ln Y}$, given by the magnitude-dependent equations

$$\tau_{\ln Y} = \begin{cases} \tau_1; & \mathbf{M} \le 4.5 \\ \tau_2 + (\tau_1 - \tau_2)(5.5 - \mathbf{M}); & 4.5 < \mathbf{M} < 5.5 \\ \tau_2; & \mathbf{M} \ge 5.5 \end{cases} \tag{4.27}$$

$$\phi_{\ln Y} = \begin{cases} \phi_1; & \mathbf{M} \le 4.5 \\ \phi_2 + (\phi_1 - \phi_2)(5.5 - \mathbf{M}); & 4.5 < \mathbf{M} < 5.5 \\ \phi_2; & \mathbf{M} \ge 5.5 \end{cases} \tag{4.28}$$

where τ_i and ϕ_i are empirically derived standard deviations.

The final model standard deviations that incorporate the effects of nonlinear soil response for completeness are given by the equations

$$\tau = \sqrt{\tau^2_{\ln Y_B} + \alpha^2 \tau^2_{\ln PGA_B} + 2\alpha \rho_{\ln PGA, \ln Y} \tau_{\ln Y_B} \tau_{\ln PGA_B}} \tag{4.29}$$

$$\phi = \sqrt{\phi^2_{\ln Y_B} + \phi^2_{\ln AF} + \alpha^2 \phi^2_{\ln PGA_B} + 2\alpha \rho_{\ln PGA, \ln Y} \phi_{\ln Y_B} \phi_{\ln PGA_B}} \tag{4.30}$$

where $\tau_{\ln Y_B} = \tau_{\ln Y}$ and $\tau_{\ln PGA_B} = \tau_{\ln PGA}$ are the between-event standard deviations for the IM of interest and for PGA at the base of the site profile; $\phi_{\ln Y_B} = (\phi^2_{\ln Y} - \phi^2_{\ln AF})^{1/2}$ and $\phi_{\ln PGA_B} = (\phi^2_{\ln PGA} - \phi^2_{\ln AF})^{1/2}$ are the within-event standard deviations for the IM of interest and for PGA at the base of the site profile; $\phi_{\ln AF}$ is the estimated standard deviation of the logarithm of the site amplification factor f_{site} for linear site response; $\rho_{\ln PGA, \ln Y}$ is the correlation coefficient between the within-event residuals of the IM of interest and PGA; and α is the linearized functional relationship between f_{site} and $\ln A_{1100}$. Since the effects of vertical soil nonlinearity is not included in this study, we assign $\alpha = 0$.

The total aleatory standard deviation is given by combining the between-event and within-event standard deviations by square-root of sum of squares (SRSS) according to the equation

$$\sigma = \sqrt{\tau^2 + \phi^2} \tag{4.31}$$

4.5 RESULTS

The model coefficients k_i and $c_0 - c_{19}$ are listed in Table 4.1 and the hanging-wall model coefficients h_i are listed in Table 4.2. Table 4.3 lists the anelastic attenuation coefficients c_{20} and Δc_{20}, where the latter captures the regional differences in anelastic attenuation for those regions where sufficient data are available to determine a separate anelastic attenuation coefficient. The regions used to derive c_{20} for the base model includes California, Taiwan, the Middle East and similar active tectonic regions. The regions used to derive Δc_{20} include Japan and Italy as one region (JI) and eastern China as another region (CH). The aleatory standard deviations τ_i and ϕ_i are listed in Table 4.4. Note that the values for the nonlinear model coefficients $c = 1.88$ and $n = 1.18$ do not have any influence as we assigned $k_2 = 0$.

In order to evaluate the validity of the median GMPE, it is useful to plot the between-event and within-event residuals as defined in Abrahamson and Youngs [1992]. Residual plots for PGA, PGV, and PSA at spectral periods of 0.1, 0.2, 1, and 3 sec are shown in Figures 4.2 to 4.11. In these plots a positive residual indicates the underestimation of a recording by the model and a negative residual indicates overestimation of a recording by the model. Figures 4.2 to 4.5 show between-event residuals as a function of magnitude, hypocentral depth, rake, and rupture dip. Figures 4.6 to 4.11 show within-event residuals as a function of magnitude, rupture distance, horizontal distance from the top edge of the rupture plane for sites located directly over the rupture plane (hanging-wall effects), 30-m shear-wave velocity, vertical rock PGA, and sediment depth. The plots show that there are no systematic trends or biases in the residuals that would indicate that the model is inconsistent with the data.

Figures 4.12 to 4.19 present a series of plots that show how our median ground motion model scales with rupture distance, magnitude, site effects, and spectral period. The values of the predictor variables used to calculate the ground motions are listed in the title at the top of each plot. Figure 4.12 shows the scaling of vertical PGA with distance (attenuation) for magnitudes of 3.5, 4.5, 5.5, 6.5, and 7.5 for a strike-slip fault. Figure 4.13 shows similar plots comparing our NGA-West2 vertical model (BC13) with our NGA-West2 horizontal model (CB13). Figure 4.14 shows similar plots to Figure 4.13 for PSA at $T = 1$ sec. Figure 4.15 shows scaling of PGA with distance for sites over the hanging-wall of a reverse fault. Consistent with the horizontal component, hanging-wall effects are strong over the bottom edge of the rupture plane.

Figure 4.16 shows the scaling of PGA with magnitude for rupture distances of 5, 10, 40, and 80 km for a strike-slip fault. In the process of model development for the vertical component, we investigated and compared the magnitude scaling between vertical and horizontal motions and concluded the magnitude scaling behavior of the two motions are similar, as presented in Figure 4.16. Figure 4.17 shows similar plots for PSA at $T = 1$ sec.

Figure 4.18 shows the scaling of PSA with magnitude for rupture distances of 5, 10, 40, and 80 km. There is a modest shift in the peak of the spectra at short distances as magnitude increases, but this shift is much less than was found for the horizontal model. There is also a noticeable shift at larger distances where the spectral peak shifts to longer periods at small magnitudes and broadens considerably at large magnitudes.

Figure 4.19 shows how PSA behaves for NEHRP site categories B ($V_{S30} = 1070$ m/sec), C ($V_{S30} = 525$ m/sec), D ($V_{S30} = 255$ m/sec), and E ($V_{S30} = 150$ m/sec). This figure does not show the strong shift in the spectral peak to longer periods and the associated reduction in spectral amplitude for the softer site conditions (NEHRP D and E) that was found for the horizontal component.

Figure 4.20 compares the between-event, within-event, and total aleatory standard deviations between the BC13 vertical and CB13 horizontal models. Overall, the standard deviations of the two models for $\mathbf{M} < 4.5$ are consistent. For $\mathbf{M} >$ 5.5, the standard deviation for vertical motion is higher at short periods, but lower at long periods, than that for horizontal motion.

Figure 4.21 presents the (V/H) spectral ratio for $V_{S30} = 760$ and $V_{S30} = 255$ m/sec, and for rupture distances of 5, 10, 40, and 80 km. In this figure, “V” represents the vertical BC13 model and “H” represents the horizontal CB13 model. This figure shows that at short periods V/H is generally higher for soil than for rock, and, for the soil sites, the short-period V/H is sensitive to the rupture distance. These observations are consistent with those of the previous studies listed in the Introduction to this chapter.

Table 4.1 Median ground motion model coefficients.

T (sec)	c_0	c_1	c_2	c_3	c_4	c_5	c_6	c_7	c_8	c_9	c_{10}	c_{11}
0.010	-4.674	0.977	0.533	-1.485	-0.445	-2.665	0.214	7.136	0	-0.229	0.759	-0.354
0.020	-4.548	0.976	0.549	-1.488	-0.453	-2.699	0.215	6.936	0	-0.270	0.768	-0.344
0.030	-4.050	0.931	0.628	-1.494	-0.464	-2.772	0.216	7.235	0	-0.315	0.766	-0.297
0.050	-3.435	0.887	0.674	-1.388	-0.552	-2.760	0.202	8.334	0	-0.329	0.764	-0.363
0.075	-3.435	0.902	0.726	-1.469	-0.543	-2.575	0.177	8.761	0	-0.290	0.795	-0.427
0.10	-3.930	0.993	0.698	-1.572	-0.470	-2.461	0.166	9.049	0	-0.203	0.842	-0.429
0.15	-5.505	1.267	0.510	-1.669	-0.452	-2.349	0.164	8.633	0	-0.203	0.736	-0.421
0.20	-6.280	1.366	0.447	-1.750	-0.435	-2.335	0.175	8.742	0	-0.203	0.801	-0.429
0.25	-6.789	1.458	0.274	-1.711	-0.410	-2.332	0.183	8.400	0	-0.203	0.715	-0.438
0.30	-7.400	1.528	0.193	-1.770	-0.305	-2.297	0.190	7.643	0	-0.203	0.708	-0.421
0.40	-8.750	1.739	-0.020	-1.594	-0.446	-2.219	0.185	7.059	0	-0.203	0.683	-0.401
0.50	-9.740	1.872	-0.121	-1.577	-0.489	-2.205	0.191	6.375	0	-0.203	0.704	-0.417
0.75	-11.050	2.021	-0.042	-1.757	-0.530	-2.143	0.188	5.166	0.016	-0.203	0.602	-0.490
1.0	-12.184	2.180	-0.069	-1.707	-0.624	-2.092	0.176	5.642	0.032	-0.115	0.394	-0.539
1.5	-13.451	2.270	0.047	-1.621	-0.686	-1.913	0.144	5.963	0.128	-0.005	0.328	-0.611
2.0	-13.700	2.271	0.149	-1.512	-0.840	-1.882	0.126	7.584	0.255	0.120	0.112	-0.630
3.0	-13.900	2.150	0.368	-1.315	-0.853	-1.789	0.105	8.645	0.284	0.170	0.011	-0.562
PGA	-4.729	0.984	0.537	-1.499	-0.443	-2.666	0.214	7.166	0	-0.230	0.759	-0.356
PGV	-3.860	1.510	0.270	-1.299	-0.379	-2.383	0.196	6.274	0.111	-0.128	0.140	-0.395

Table 4.1 Continued.

T (sec)	c_{12}	c_{13}	c_{14}	c_{15}	c_{16}	c_{17}	c_{18}	c_{19}	k_1	k_2	k_3
0.010	1.015	0.372	-0.1193	-0.094	0.000	0.1026	0.0452	0.00784	865	0	0
0.020	0.950	0.400	-0.1454	-0.081	0.000	0.1059	0.0427	0.00786	865	0	0
0.030	1.056	0.394	-0.1957	-0.091	0.000	0.1175	0.0410	0.00815	908	0	0
0.050	1.316	0.422	-0.1870	-0.290	0.000	0.1238	0.0408	0.00783	1054	0	0
0.075	1.758	0.336	-0.0950	-0.261	0.000	0.1088	0.0516	0.00726	1086	0	0
0.10	1.411	0.314	-0.0999	-0.091	0.000	0.0918	0.0559	0.00644	1032	0	0
0.15	1.227	0.289	0.0017	-0.092	0.000	0.0720	0.0447	0.00745	878	0	0
0.20	0.987	0.290	0.0402	-0.081	0.000	0.0602	0.0485	0.00789	748	0	0
0.25	0.577	0.303	0.0468	0.011	0.000	0.0500	0.0416	0.00629	654	0	0
0.30	0.279	0.336	0.0255	0.092	0.000	0.0382	0.0438	0.00524	587	0	0
0.40	0.358	0.358	0.0606	0.122	0.000	0.0264	0.0307	0.00522	503	0	0
0.50	0.229	0.432	0.0904	0.287	0.000	0.0163	0.0287	0.00539	457	0	0
0.75	0.574	0.459	0.1776	0.292	0.000	-0.0016	0.0277	0.00501	410	0	0
1.0	0.980	0.442	0.2389	0.316	0.000	-0.0072	0.0277	0.00506	400	0	0
1.5	0.819	0.520	0.2758	0.450	0.000	-0.0262	0.0293	0.00353	400	0	0
2.0	0.044	0.566	0.3051	0.424	0.000	-0.0408	0.0221	0.00220	400	0	0
3.0	-0.396	0.562	0.3482	0.300	0.000	-0.0512	0.0321	-0.00137	400	0	0
PGA	1.019	0.373	-0.1172	-0.097	0.000	0.1020	0.0442	0.00784	865	0	0
PGV	0.338	0.407	-0.0016	0.382	0.000	0.0581	0.0294	0.00761	400	0	0

Note: c = 1.88 and n = 1.18; however, for vertical component they have no effect as k_2 = 0.

Table 4.2 Constrained hanging-wall coefficients.

T (sec)	a_2	h_1	h_2	h_3	h_4	h_5	h_6
0.010	0.168	0.242	1.471	-0.714	1.000	-0.336	-0.270
0.020	0.166	0.244	1.467	-0.711	1.000	-0.339	-0.263
0.030	0.167	0.246	1.467	-0.713	1.000	-0.338	-0.259
0.050	0.173	0.251	1.449	-0.701	1.000	-0.338	-0.263
0.075	0.198	0.260	1.435	-0.695	1.000	-0.347	-0.219
0.10	0.174	0.259	1.449	-0.708	1.000	-0.391	-0.201
0.15	0.198	0.254	1.461	-0.715	1.000	-0.449	-0.099
0.20	0.204	0.237	1.484	-0.721	1.000	-0.393	-0.198
0.25	0.185	0.206	1.581	-0.787	1.000	-0.339	-0.210
0.30	0.164	0.210	1.586	-0.795	1.000	-0.447	-0.121
0.40	0.160	0.226	1.544	-0.770	1.000	-0.525	-0.086
0.50	0.184	0.217	1.554	-0.770	1.000	-0.407	-0.281
0.75	0.216	0.154	1.626	-0.780	1.000	-0.371	-0.285
1.0	0.596	0.117	1.616	-0.733	1.000	-0.128	-0.756
1.5	0.596	0.117	1.616	-0.733	1.000	-0.128	-0.756
2.0	0.596	0.117	1.616	-0.733	1.000	-0.128	-0.756
3.0	0.596	0.117	1.616	-0.733	1.000	-0.128	-0.756
PGA	0.167	0.241	1.474	-0.715	1.000	-0.337	-0.270
PGV	0.596	0.117	1.616	-0.733	1.000	-0.128	-0.756

Table 4.3 Regional anelastic attenuation coefficients.

T (sec)	c_{20}	Δc_{20}		
		CA	JI	CH
0.010	-0.0053	0	-0.0018	0.0039
0.020	-0.0052	0	-0.0018	0.0036
0.030	-0.0052	0	-0.0020	0.0033
0.050	-0.0062	0	-0.0026	0.0039
0.075	-0.0072	0	-0.0021	0.0048
0.10	-0.0072	0	-0.0018	0.0050
0.15	-0.0066	0	-0.0018	0.0048
0.20	-0.0056	0	-0.0022	0.0041
0.25	-0.0049	0	-0.0025	0.0034
0.30	-0.0046	0	-0.0027	0.0031
0.40	-0.0037	0	-0.0024	0.0024
0.50	-0.0031	0	-0.0025	0.0021
0.75	-0.0021	0	-0.0025	0.0020
1.0	-0.0012	0	-0.0023	0.0012
1.5	-0.0004	0	-0.0013	0.0004
2.0	0	0	-0.0004	0
3.0	0	0	0	0
PGA	-0.0053	0	-0.0018	0.0039
PGV	-0.0019	0	0.0005	0.0019

Note: CA represents California and similar active tectonic domains, JI represents Japan and Italy, and CH represents eastern China (Wenchuan earthquake).

Table 4.4 Aleatory variability model standard deviations.

T (sec)	τ_1	τ_2	ϕ_1	ϕ_2	$\phi_{\ln AF}$	σ	
						M ≤ 4.5	**M** ≥ 5.5
0.010	0.462	0.345	0.695	0.494	0.300	0.834	0.602
0.020	0.474	0.375	0.700	0.508	0.300	0.846	0.632
0.030	0.529	0.416	0.722	0.536	0.300	0.895	0.679
0.050	0.576	0.468	0.751	0.584	0.300	0.947	0.749
0.075	0.523	0.427	0.740	0.578	0.300	0.906	0.719
0.10	0.461	0.390	0.723	0.570	0.300	0.858	0.691
0.15	0.391	0.343	0.731	0.536	0.300	0.829	0.636
0.20	0.363	0.308	0.701	0.510	0.300	0.789	0.596
0.25	0.355	0.288	0.687	0.507	0.300	0.773	0.583
0.30	0.355	0.265	0.668	0.514	0.300	0.757	0.579
0.40	0.360	0.280	0.628	0.521	0.300	0.723	0.591
0.50	0.376	0.284	0.606	0.526	0.300	0.713	0.598
0.75	0.416	0.322	0.568	0.536	0.300	0.704	0.625
1.0	0.472	0.311	0.536	0.550	0.300	0.714	0.632
1.5	0.507	0.329	0.511	0.559	0.300	0.719	0.649
2.0	0.539	0.345	0.507	0.571	0.300	0.740	0.667
3.0	0.515	0.335	0.474	0.557	0.300	0.700	0.650
PGA	0.461	0.347	0.694	0.493	0.300	0.833	0.603
PGV	0.334	0.240	0.608	0.442	0.300	0.694	0.503

Note: All standard deviations are in natural logarithmic units and are for linear site conditions.

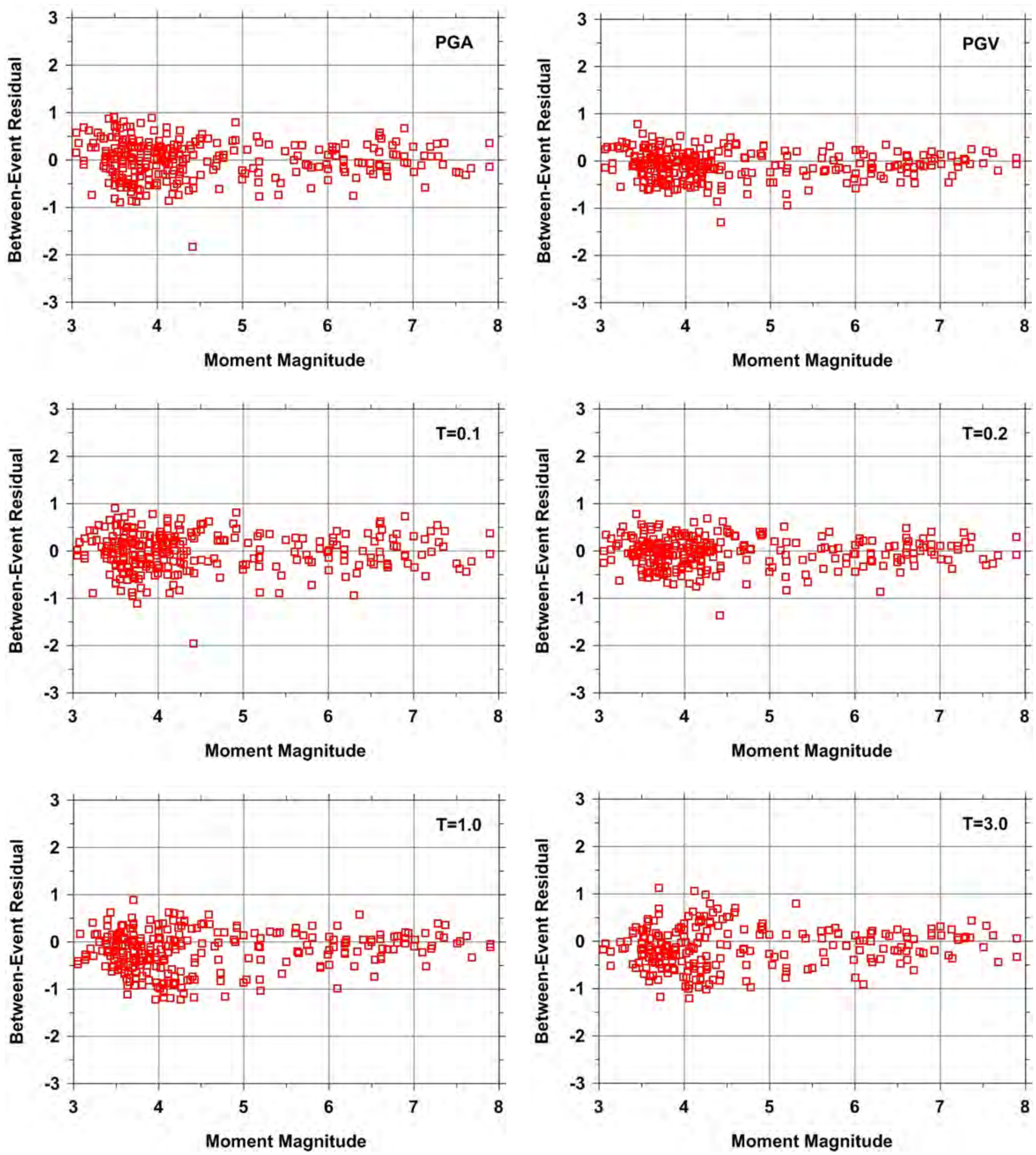

Figure 4.2 Dependence of between-event residuals on earthquake magnitude.

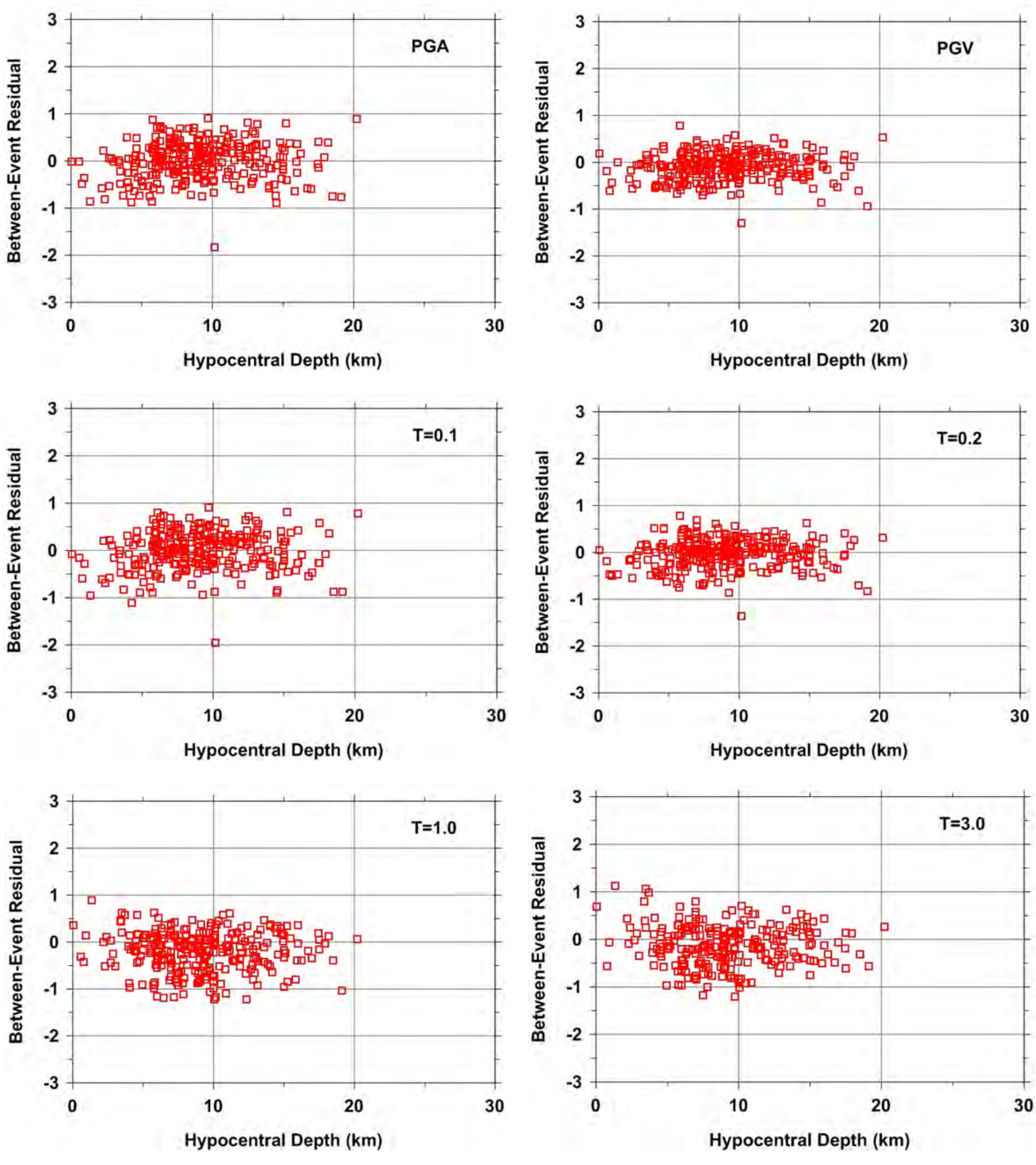

Figure 4.3 Dependence of between-event residuals on hypocentral depth.

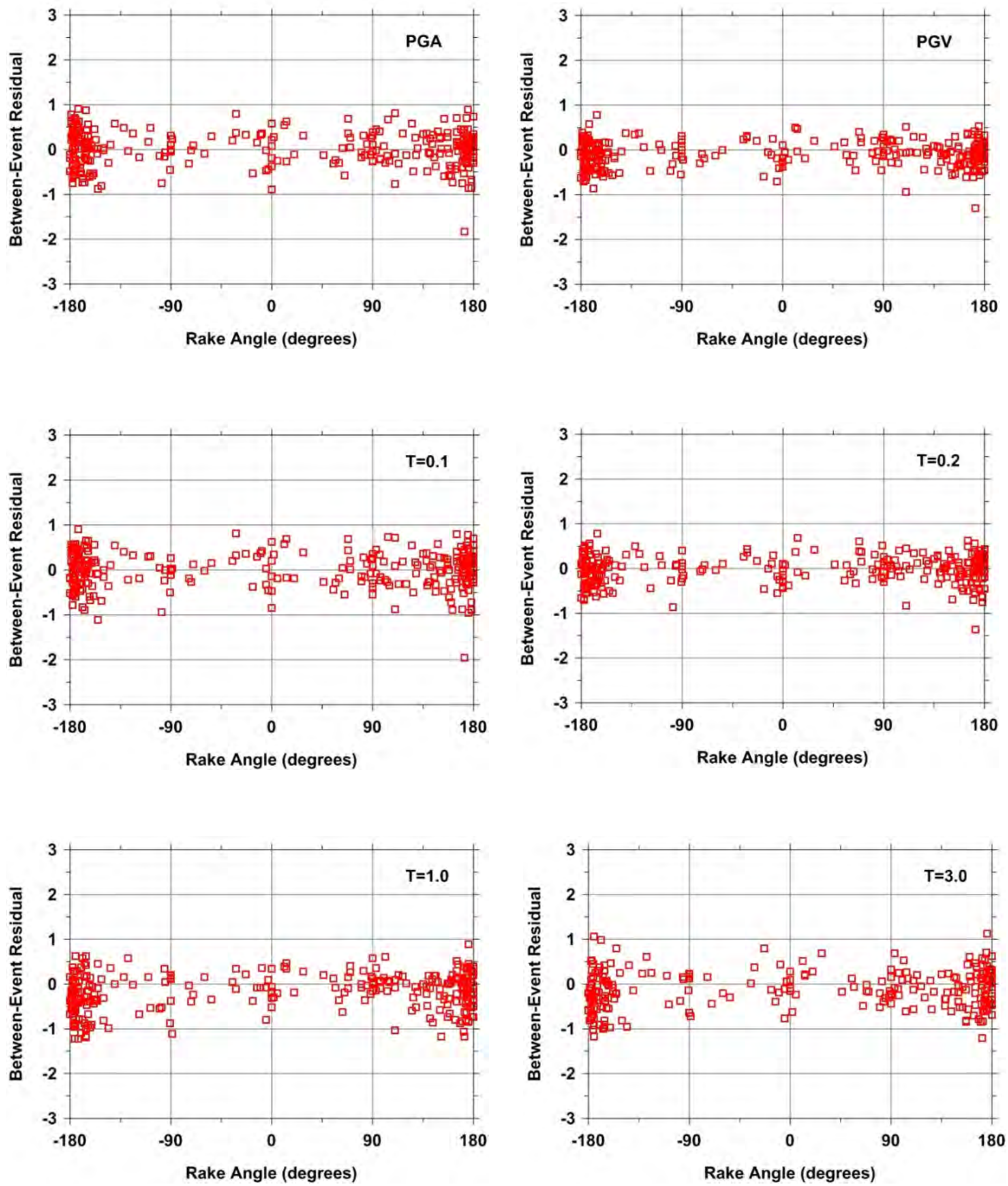

Figure 4.4 Dependence of between-event residuals on rake.

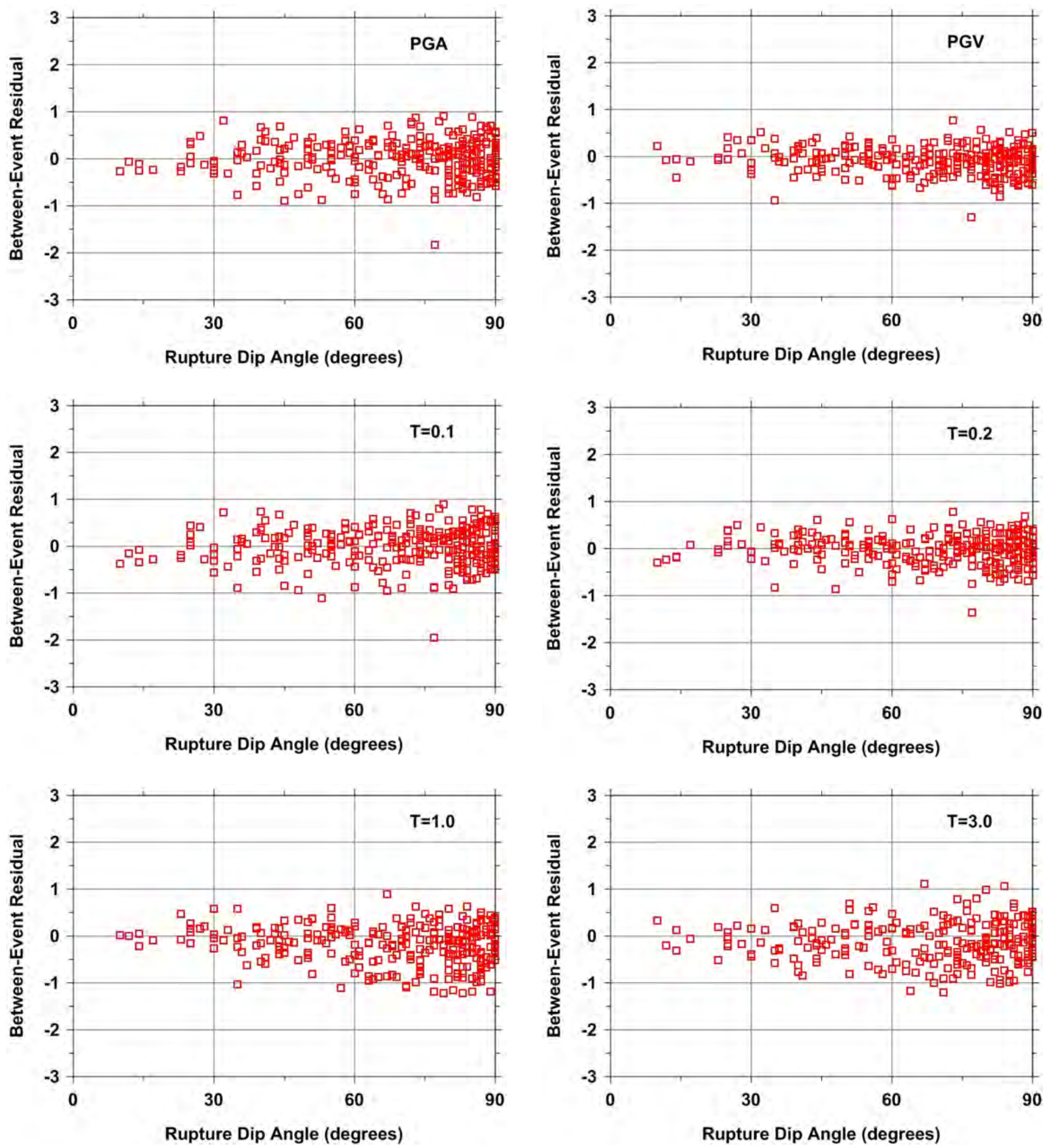

Figure 4.5 **Dependence of between-event residuals on rupture dip.**

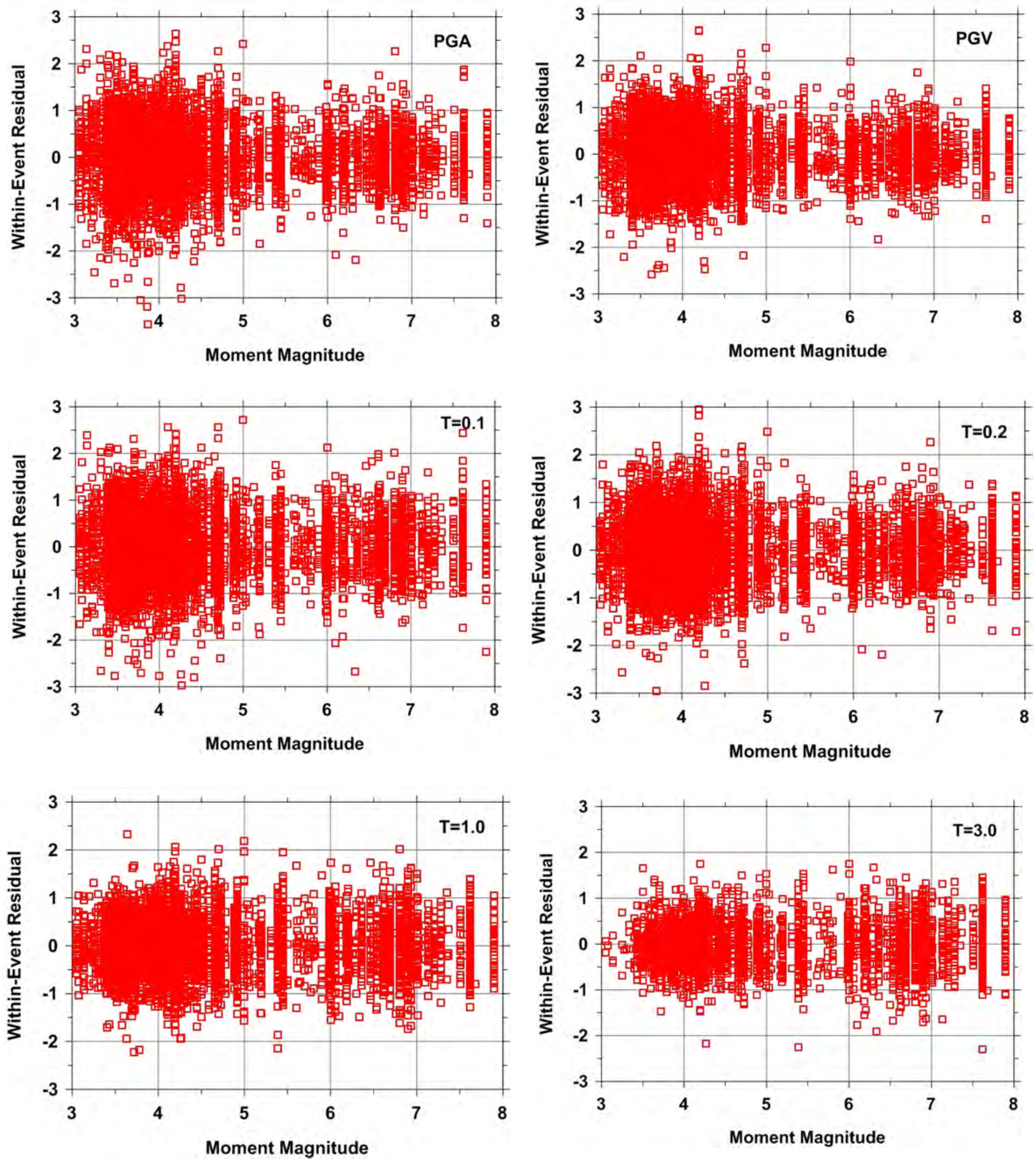

Figure 4.6 **Dependence of within-event residuals on earthquake magnitude.**

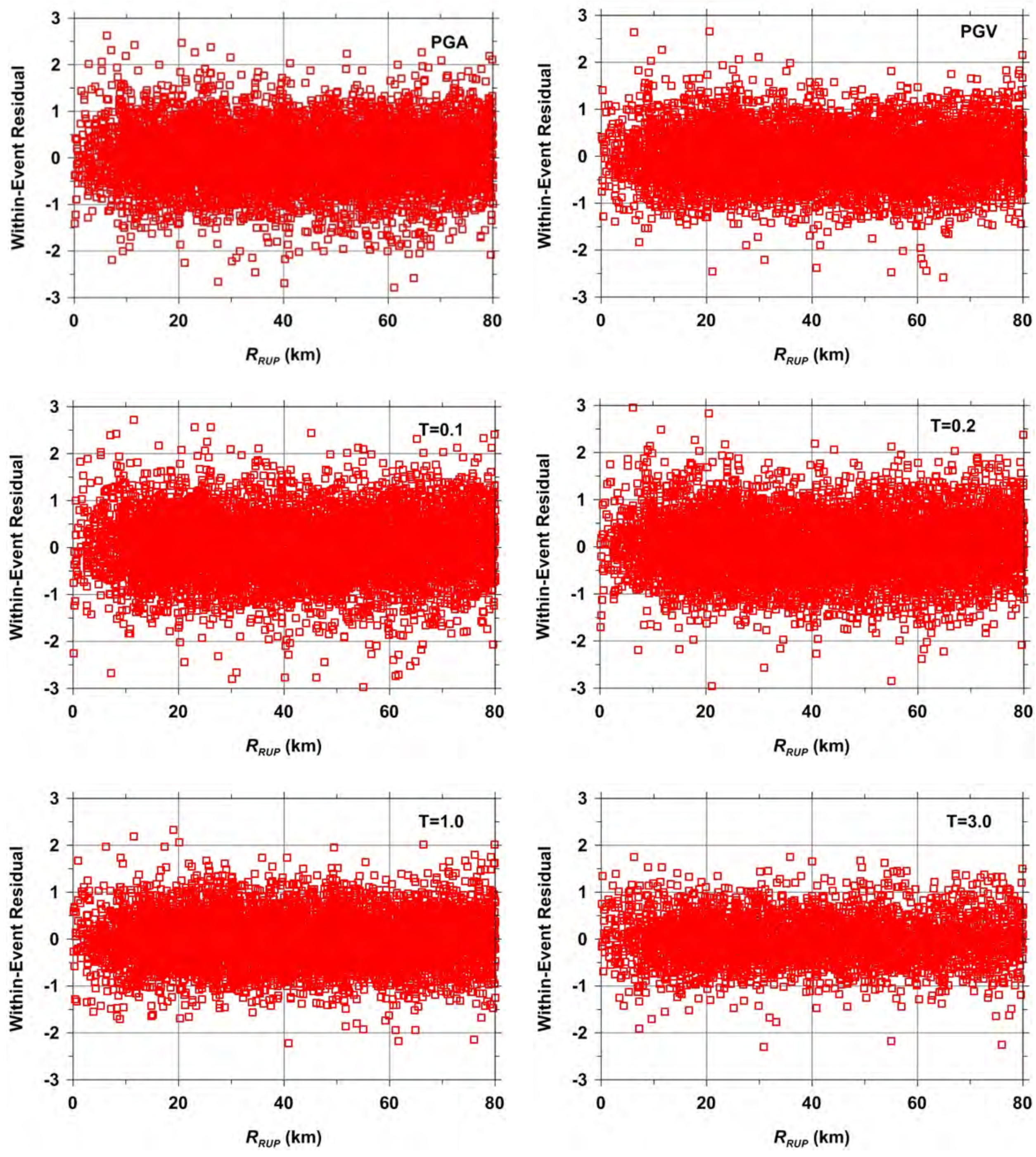

Figure 4.7a Dependence of within-event residuals on rupture distance for distances ranging from 0 to 80 km.

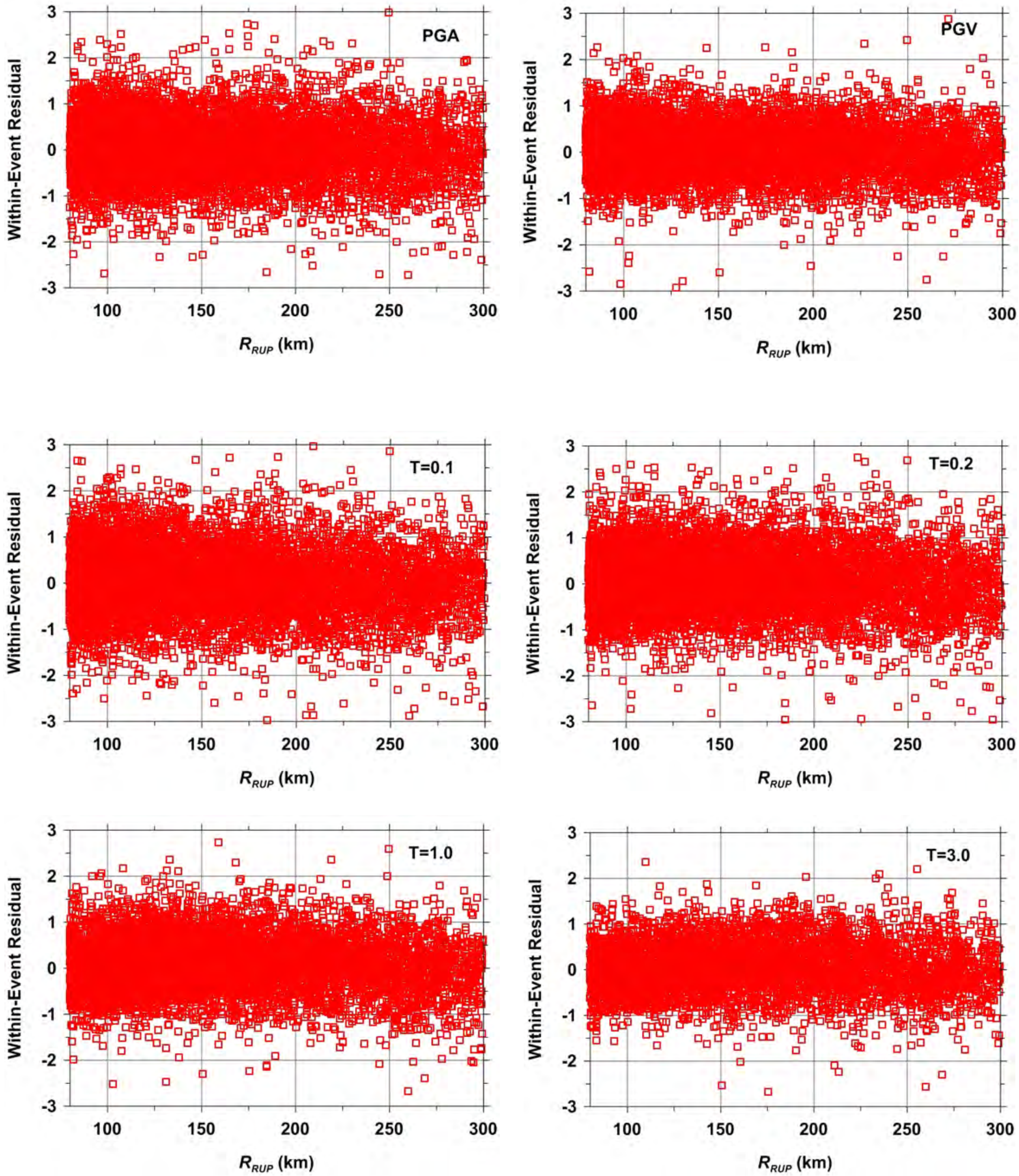

Figure 4.7b **Dependence of within-event residuals on rupture distance for distances ranging from 80 to 300 km.**

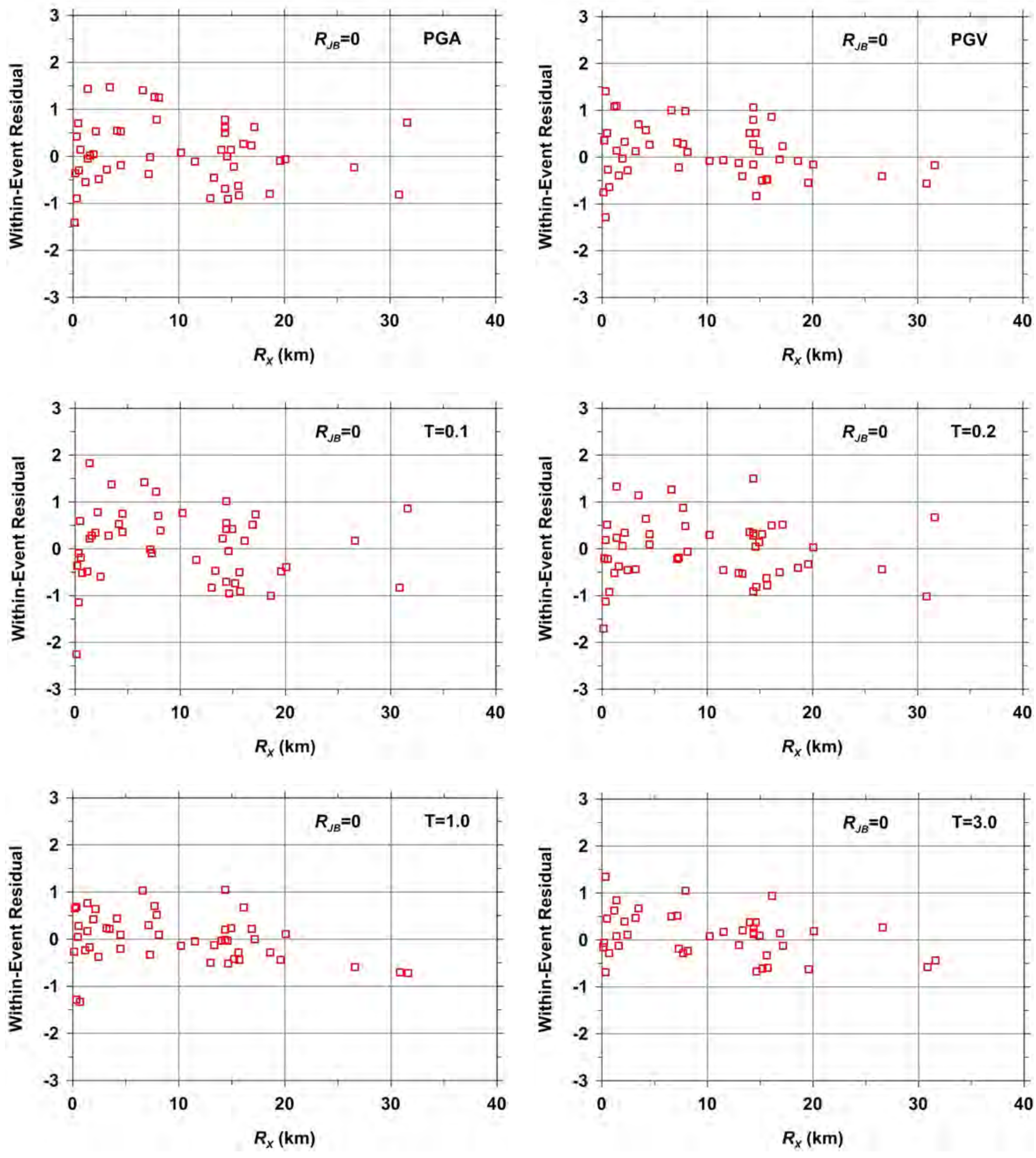

Figure 4.8 Dependence of within-event residuals on horizontal distance for sites located over the rupture plane.

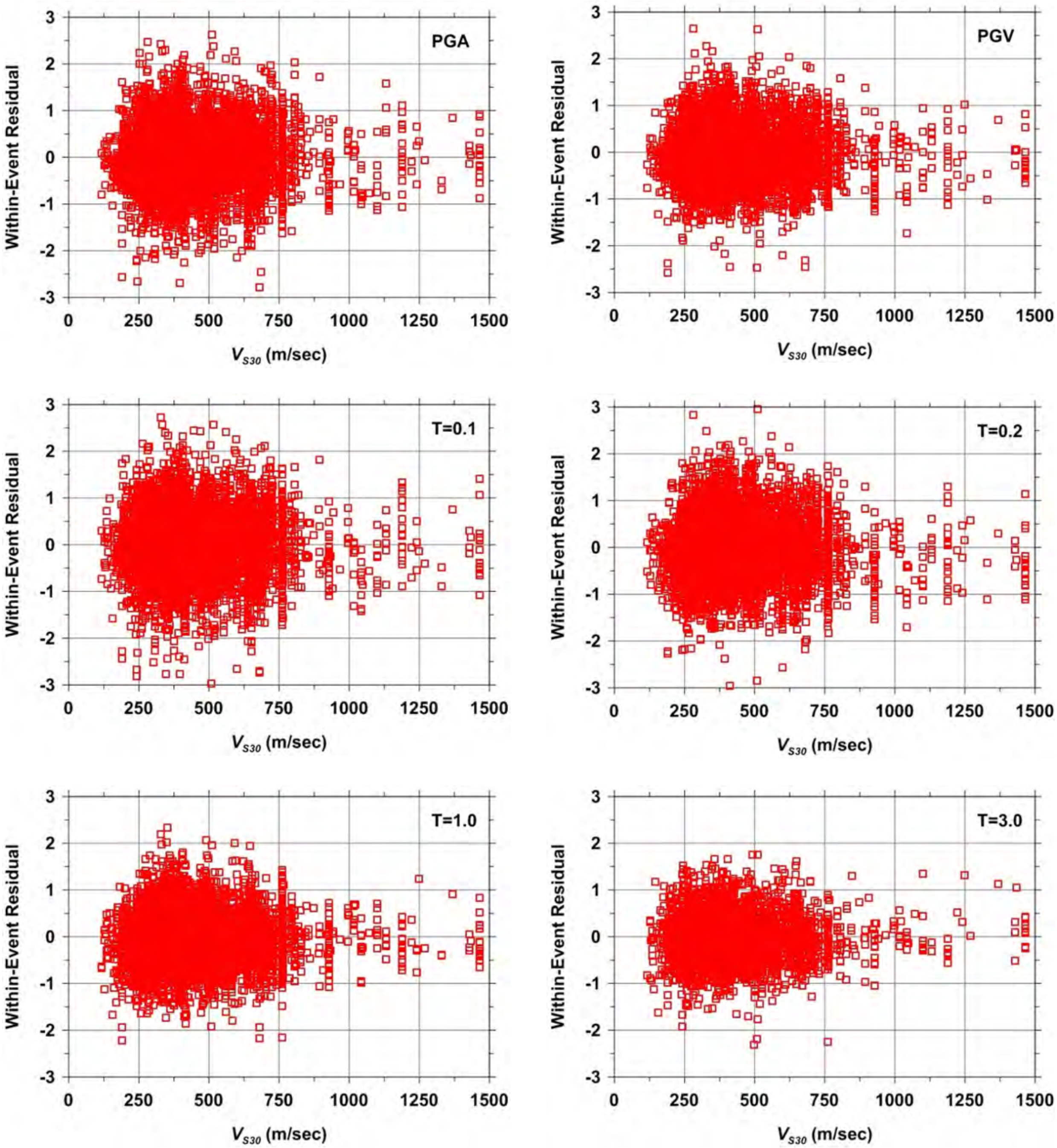

Figure 4.9 Dependence of within-event residuals on 30-m shear-wave velocity.

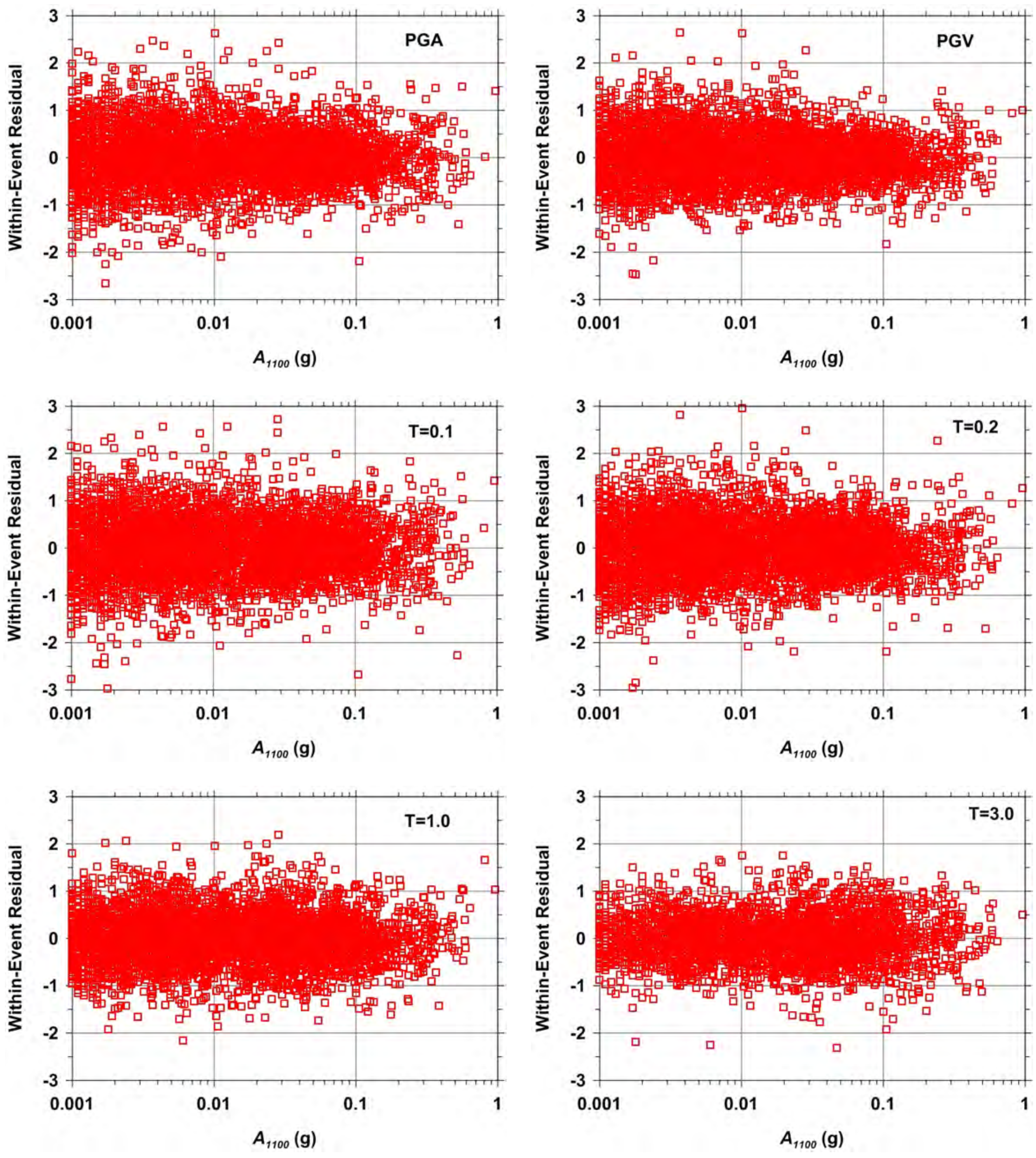

Figure 4.10 Dependence of within-event residuals on vertical A_{1100}.

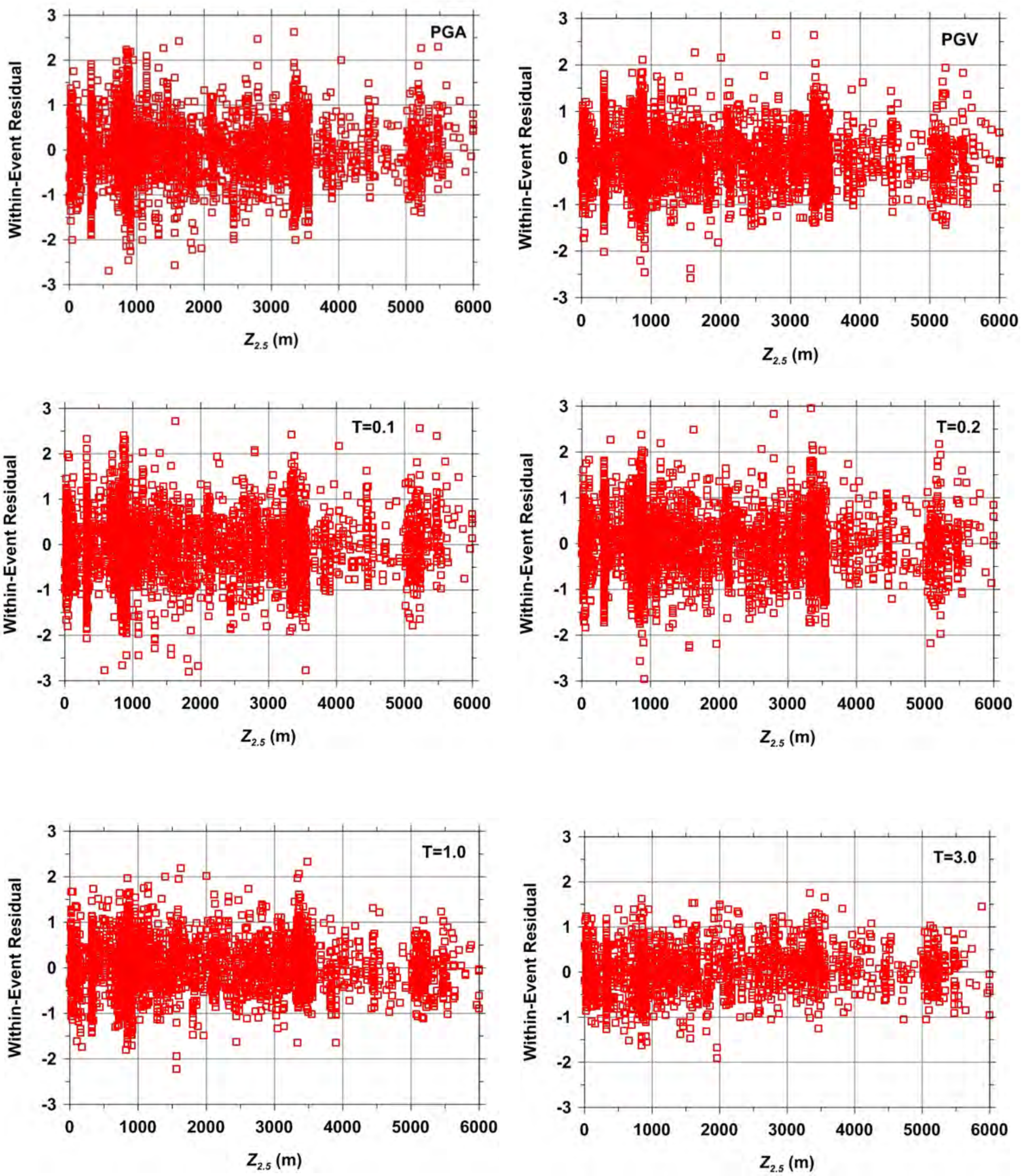

Figure 4.11 Dependence of within-event residuals on sediment basin depth.

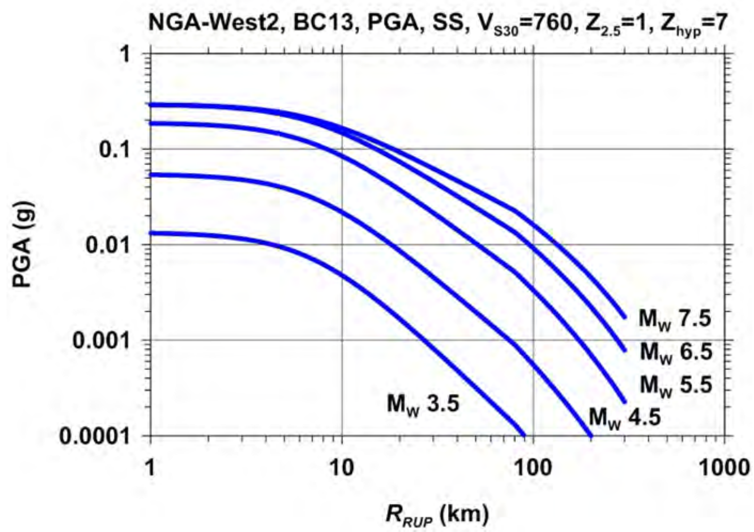

Figure 4.12 Scaling of PGA with distance for the BC13 model.

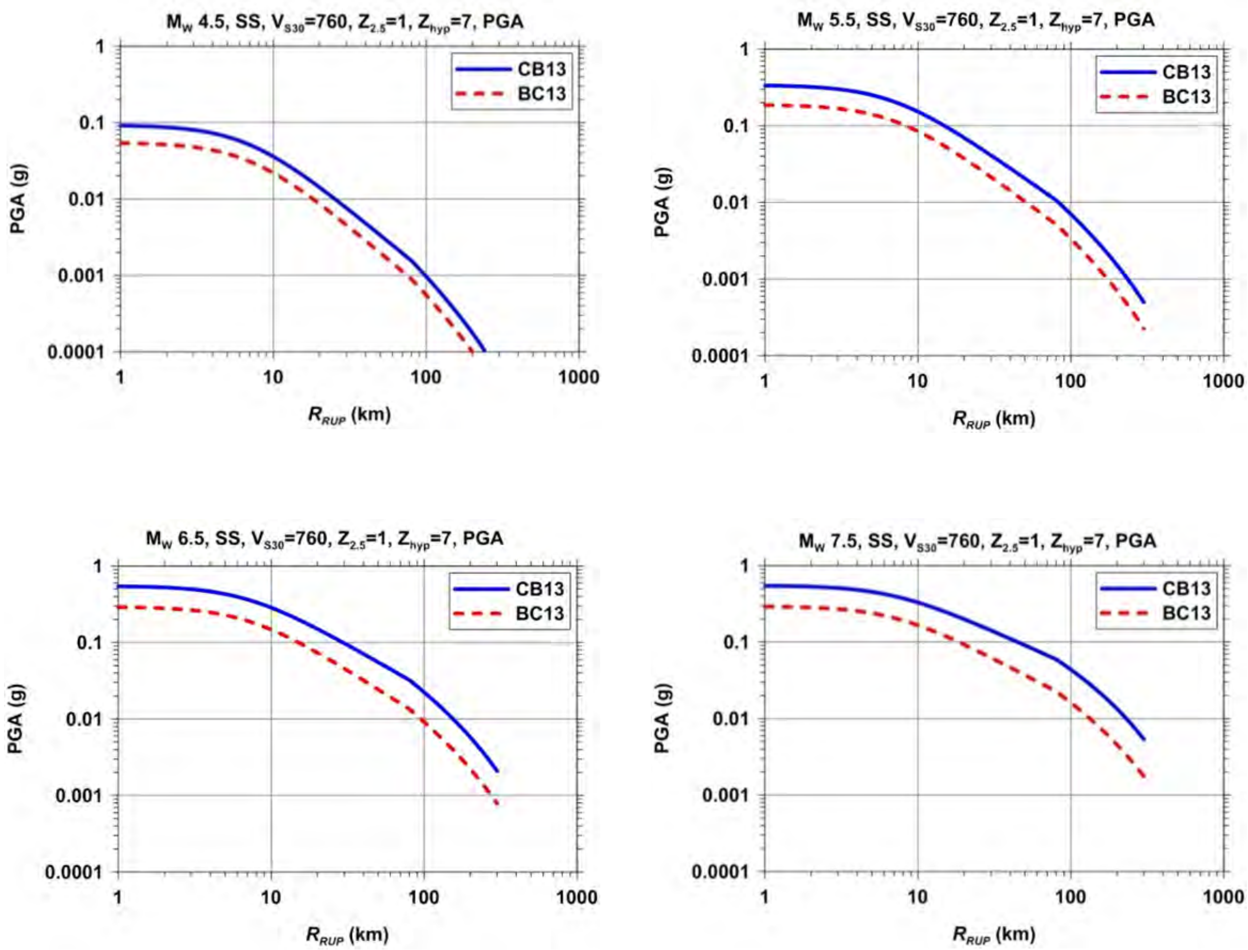

Figure 4.13 **Scaling of PGA with distance for strike-slip faults comparing the BC13 vertical and CB13 horizontal models.**

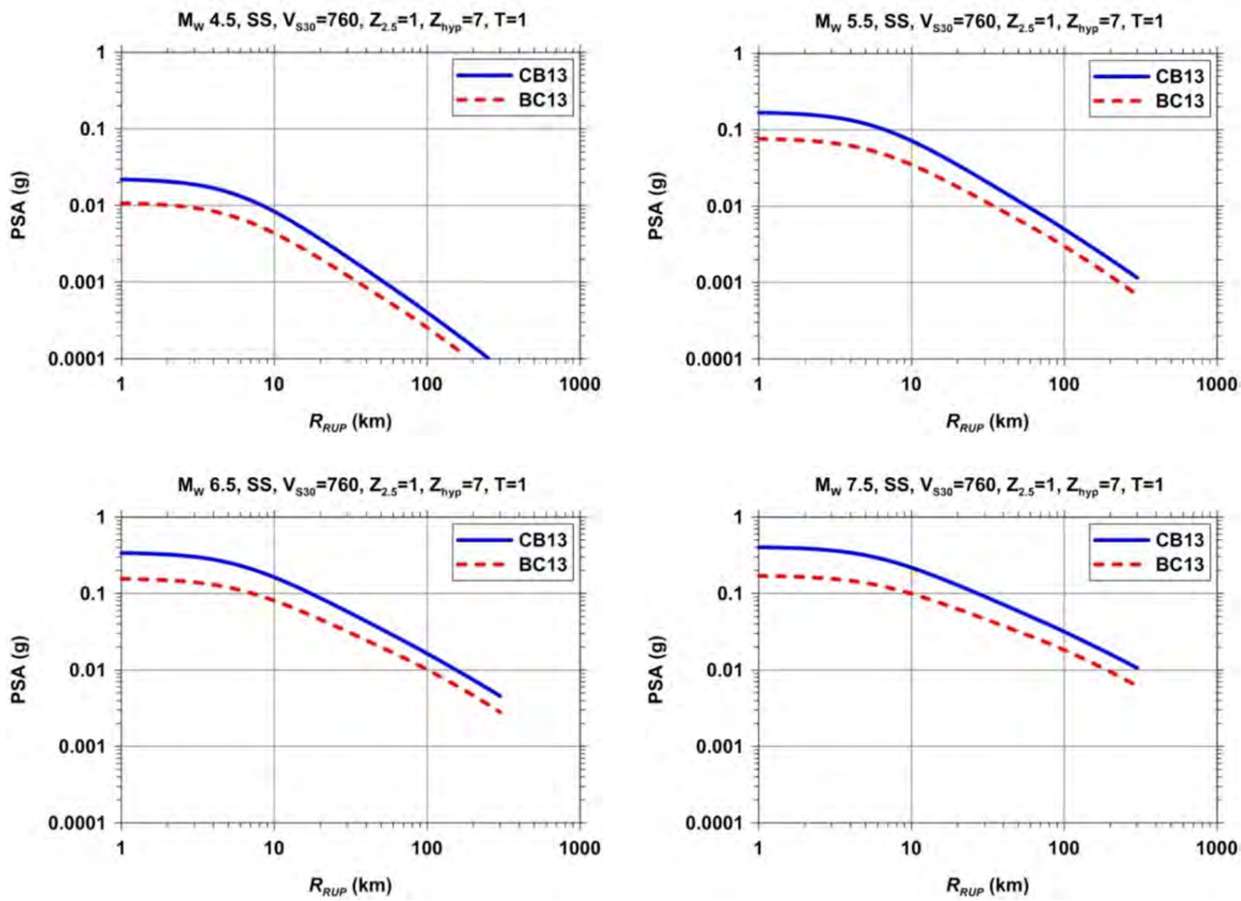

Figure 4.14 **Scaling of PSA (T = 1 sec) with distance for strike-slip faults comparing the BC13 vertical and CB13 horizontal models.**

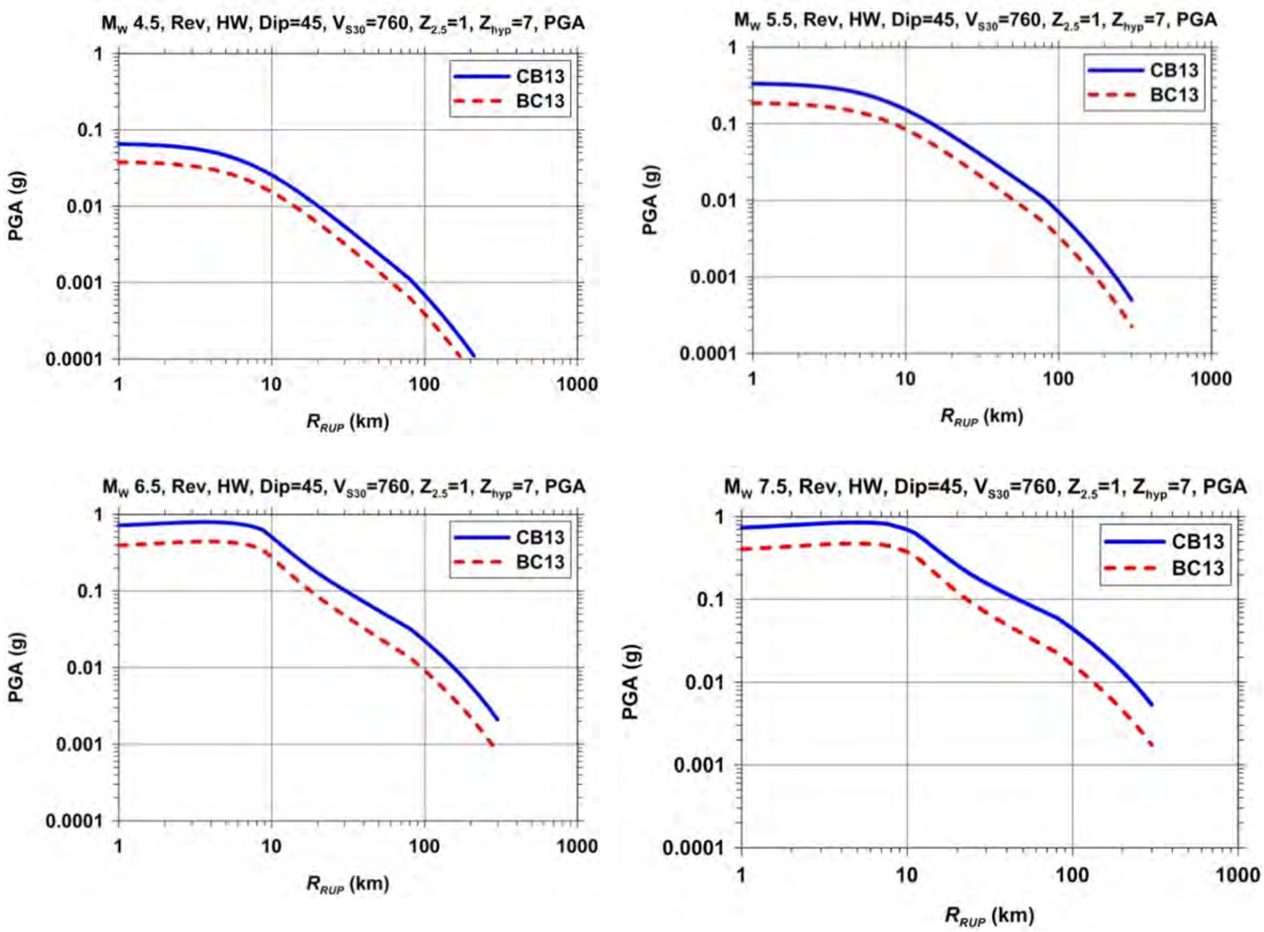

Figure 4.15 Scaling of PGA with distance for reverse faults comparing the BC13 vertical and CB13 horizontal models.

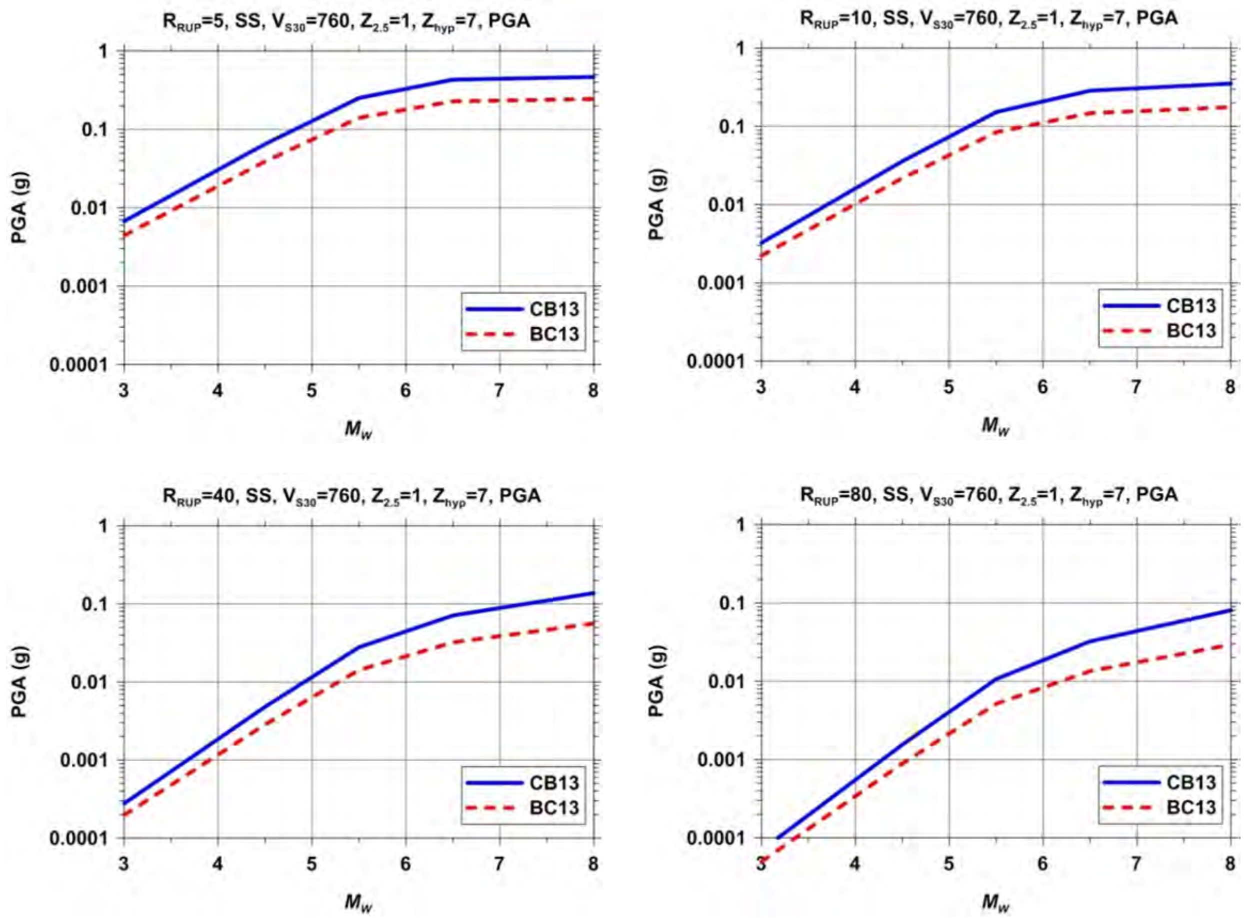

Figure 4.16 Scaling of PGA with magnitude for strike-slip faults comparing the BC13 vertical and CB13 horizontal models.

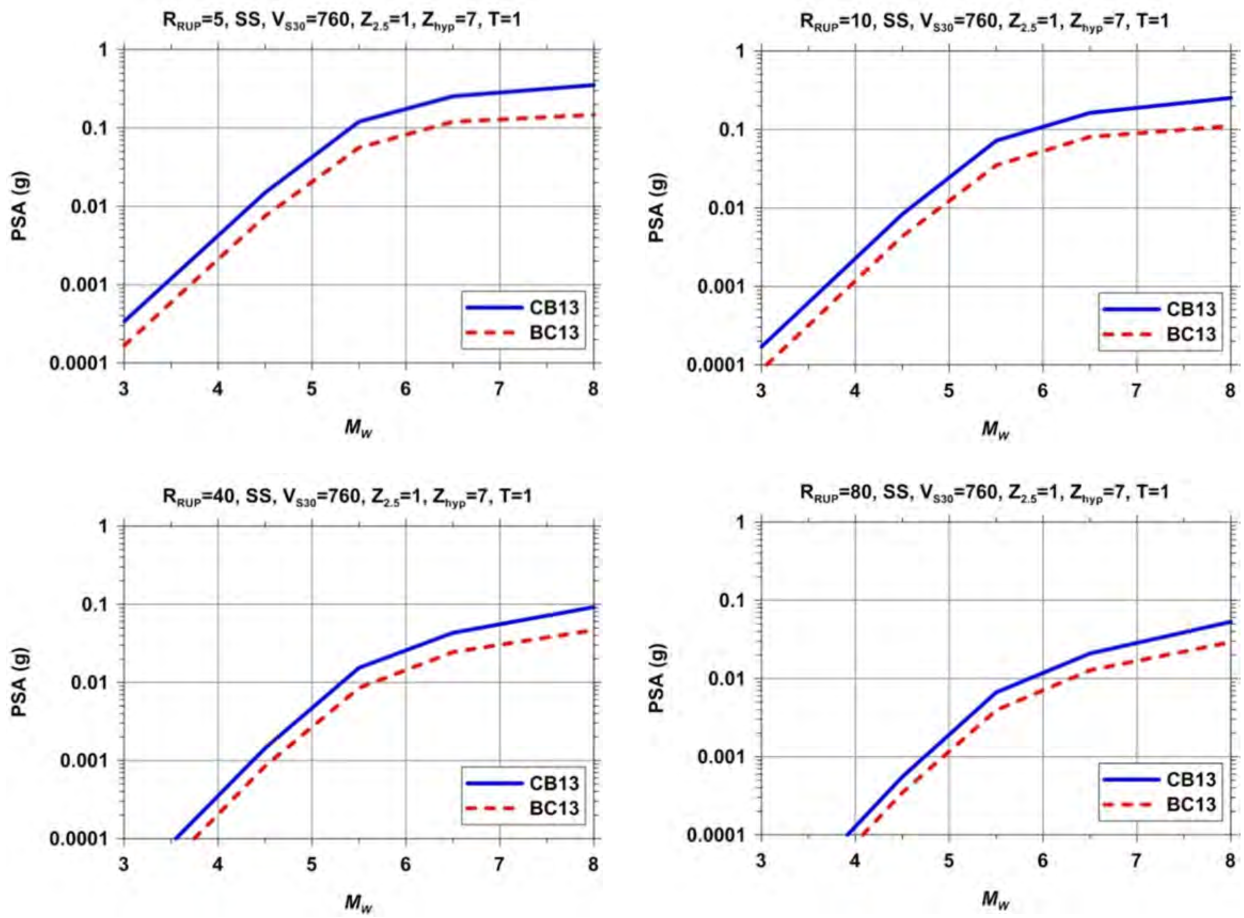

Figure 4.17 Scaling of PSA (T = 1 sec) with magnitude for strike-slip faults comparing the BC13 vertical and CB13 horizontal models.

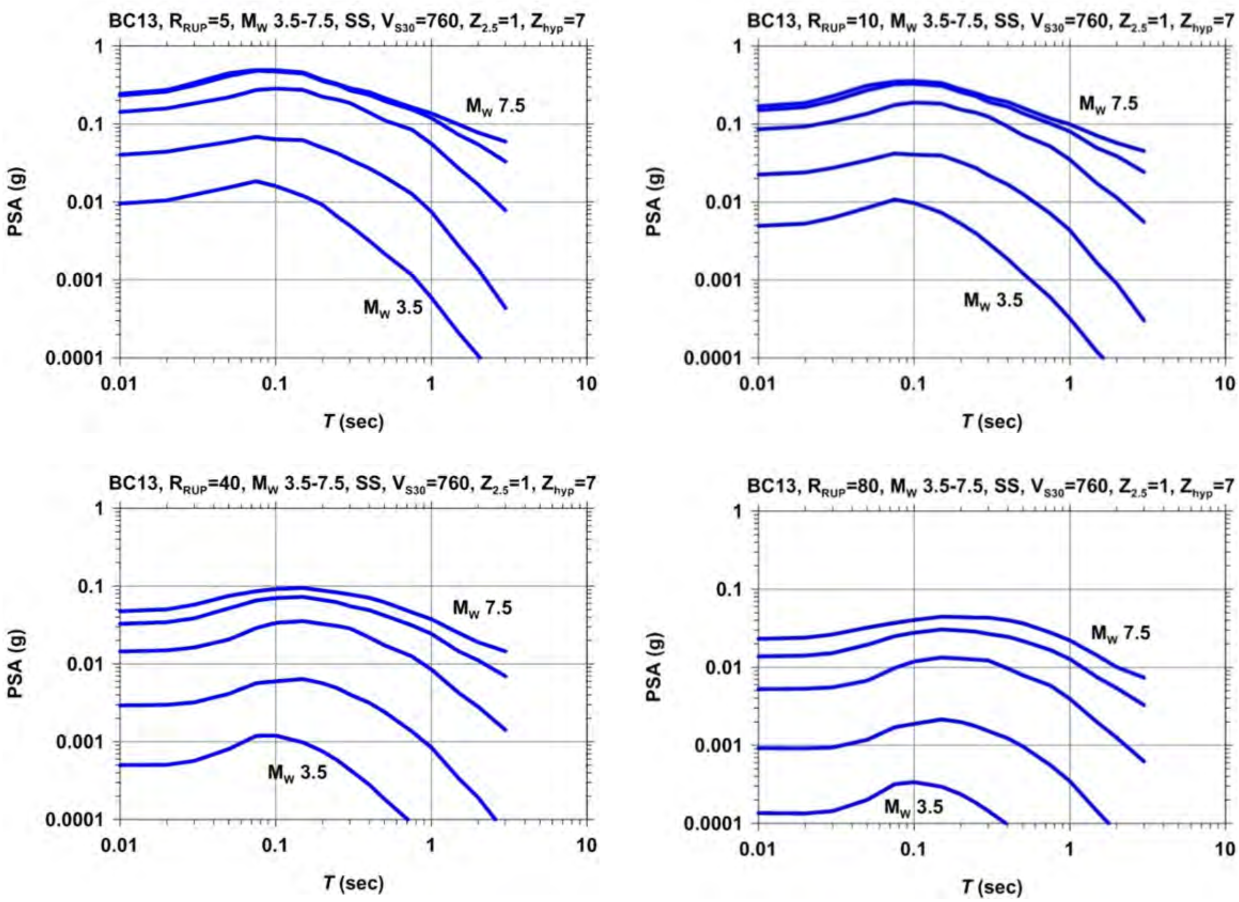

Figure 4.18 Scaling of PSA with magnitude (M3.5, 4.5, 5.5, 6.5, and 7.5) for the BC13 vertical model.

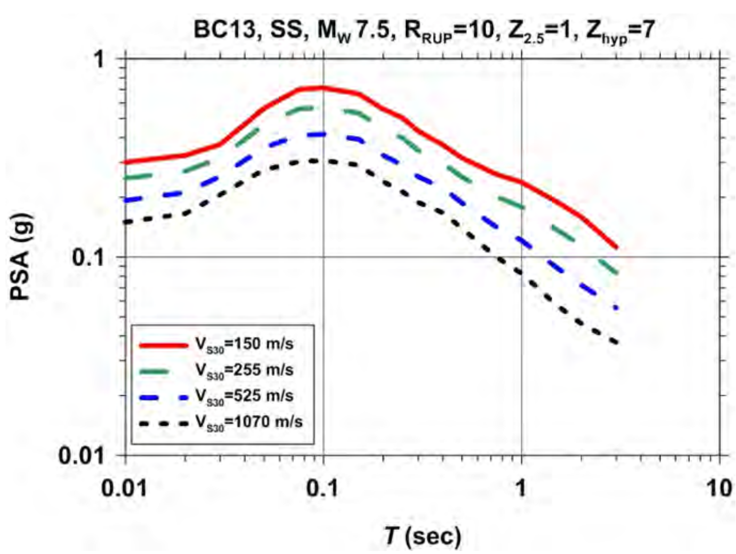

Figure 4.19 Scaling of PSA with site conditions for the BC13 vertical model.

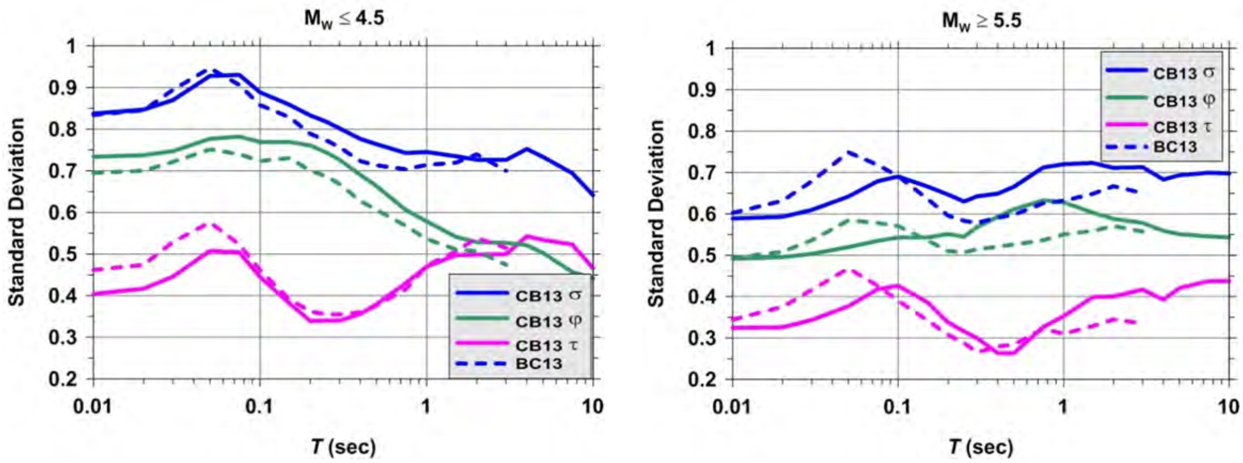

Figure 4.20 Aleatory standard deviations for τ (purple), ϕ (green) and σ (blue) comparing the BC13 vertical and CB13 horizontal models.

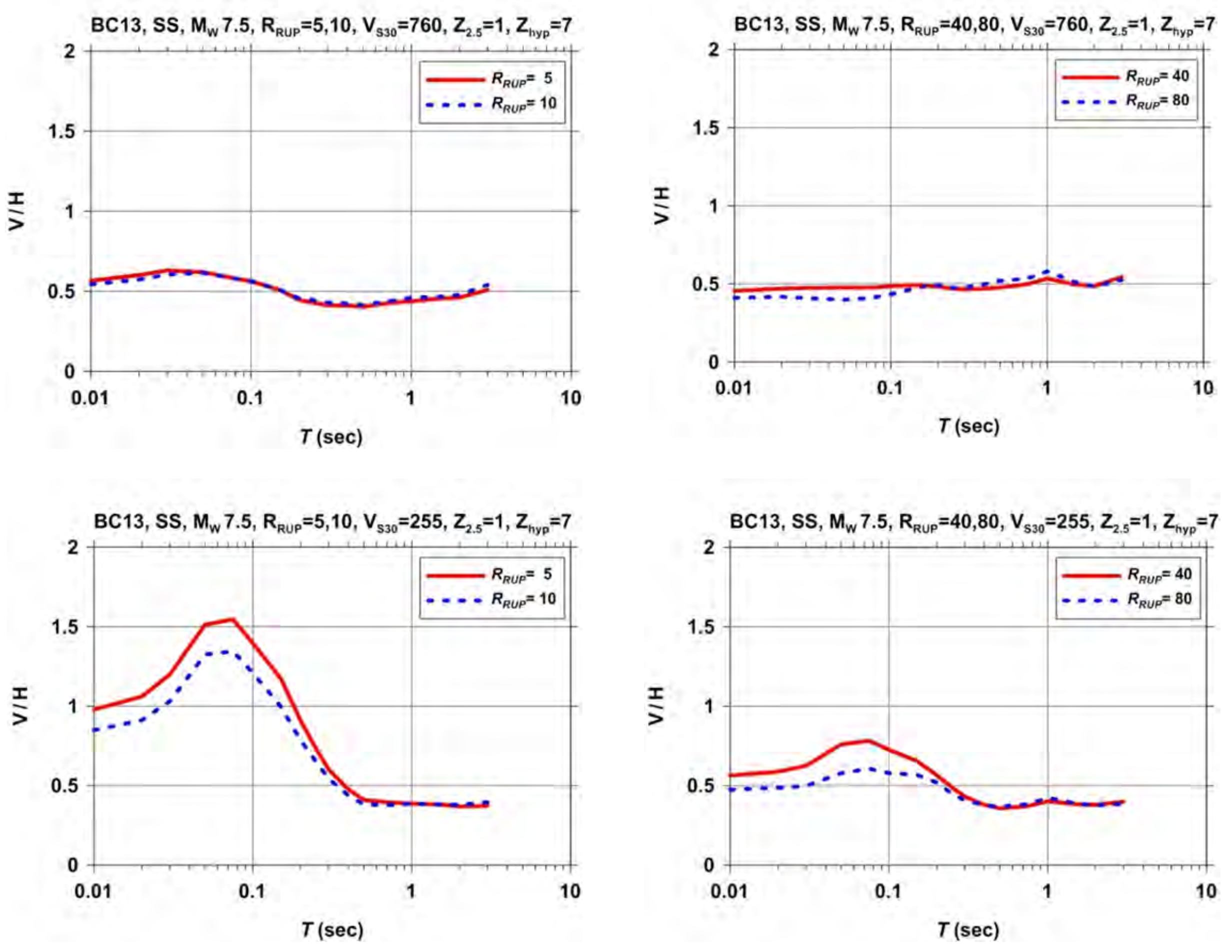

Figure 4.21 Vertical (BC13) to horizontal (CB13) spectral ratio (V/H) for four distances and for $V_{S30} = 760$ m/sec (top) and $V_{S30} = 255$ m/sec (bottom).

4.6 JUSTIFICATION OF FUNCTIONAL FORMS

This section presents the justification for the functional forms of the predictor variable terms used to develop our median ground motion and aleatory variability models. Sections include a discussion of the magnitude term, the geometric attenuation term, the style-of-faulting term, the hanging-wall term, the shallow site response term, the shallow basin response term, the hypocentral depth term, the rupture dip term, and the anelastic attenuation term.

As mentioned previously, examination of the vertical ground motion data revealed that we could adopt the functional forms that we developed for the NGA-West2 horizontal GMPE with some coefficients set to zero, as noted in the following sub-sections.

4.6.1 Magnitude Term

We adopted the same quadrilinear functional form used to model f_{mag} for the horizontal component. Qualitatively similar to the horizontal component, the regression analysis using the quadrilinear magnitude term predicted "oversaturation" (i.e., decreasing ground motion with increasing magnitude) for PGA and short-period PSA for large magnitudes and short distances. This behavior was not allowed in our model and we conservatively decided to constrain f_{mag} to remain constant (i.e., saturate but not oversaturate) at $\mathbf{M} > 6.5$ and $R_{RUP} = 0$ when oversaturation was indicated by the regression analysis. This constraint is equivalent to setting $c_4 = -c_1 - c_2 - c_3 - c_6 \ln(c_7)$ in Equation (4.2). Additional details are provided in Campbell and Bozorgnia [2013; 2014].

4.6.2 Geometric Attenuation and Style-of-Faulting Terms

The functional form of our source-to-site distance term f_{dis} and style-of-faulting term f_{flt} for the vertical component are the same as those for the horizontal motion. Analysis of residuals for the vertical ground motion indicated that these functional forms fit well with the empirical data. Details of these functional forms are presented in Campbell and Bozorgnia [2013; 2014].

4.6.3 Hanging-Wall Term

Donahue and Abrahamson [2013] showed that their HW scaling model, developed based on analysis of "physics-based" simulation data, works well for both the horizontal and vertical components. As a result, we used the same functional form for our vertical model. Details of the functional form are given in Campbell and Bozorgnia [2013; 2014].

4.6.4 Shallow Site Response Term

To assess the effects of nonlinear vertical site response, the NGA-West2 project initiated a task on simulation of site amplifications due to soil nonlinear response. The results of the vertical nonlinear site response were inconclusive; therefore, the consensus of the NGA-West2 researchers was that the task needs to be expanded and investigated more in the future. Thus, the current version of our GMPE for the vertical component includes only linear site response. We do not consider this as a serious constraint of the applicability of the vertical GMPE, especially considering the fact that the vertical soil response can remain effectively linear over a wide range of rock motion, even when the horizontal soil response becomes nonlinear. Analysis of the residuals has also confirmed that this assumption is not very restrictive. We implement the assumption of linear vertical site response by assigning $k_2 = 0$ in Equations (4.18) and (4.19).

Similar to our horizontal model, the linear behavior of our current model was calibrated by empirically fitting the model coefficients c_{11} through c_{13} in the regression analysis. The first of these coefficients applies to all recording sites except for those in Japan. We found that the linear V_{S30} scaling for sites in Japan was different than for sites outside of Japan, which come primarily from California. We also found that the V_{S30} scaling in Japan was especially different for softer sites defined as $V_{S30} < 200$ m/sec than for harder sites. The way that f_{site} is defined means that the scaling in Japan represents the difference between Japan and non-Japan regions, so that the coefficients are additive, meaning that the total model coefficient for the harder sites in Japan is equal to $c_{11} + c_{13}$ and that for the softer sites in Japan is equal to $c_{11} + c_{12} + c_{13}$.

4.6.5 Basin Response Term

The functional form used to model f_{sed} has two parts: (1) a term to model 3D basin effects for $Z_{2.5} > 3$ km; and (2) a term to model shallow sediment effects for $Z_{2.5} < 1$ km. For the evaluation of deep basin effects, an analysis of vertical response using the numerical simulations conducted by Day et al. [2008] was carried out. The simulation results in the vertical direction were inconclusive; thus, the consensus of the NGA-West2 team and S. Day (personal communication) was to postpone the inclusion of deep vertical 3D basin effects. To implement this, we assigned $k_3 = 0$ and $c_{16} = 0$ in Equation (4.20). Considering that such effects may primarily be at long vertical periods and the majority of structural components and systems have short vertical periods [e.g., Bozorgnia et al., 1998], excluding the 3D basin effects in the vertical direction may not pose a serious practical limitation. Furthermore, the residuals plotted in Figure 4.11 also do not reveal a strong trend at the spectral periods included in this study suggesting that there is no significant empirical evidence for including a deep basin response term.

We modeled the shallow sediment term based on an analysis of residuals. We found that the data were sufficient to empirically constrain this trend. As in our horizontal model, we found that the shallow basin response term was different for sites in Japan than for sites outside of Japan. The model coefficient c_{14} for non-Japan recording sites is based primarily on California sites because of a lack of sediment-depth information for other regions. A different coefficient was found for recording sites in Japan. Since this coefficient is additive, the total Japan coefficient is equal to $c_{14} + c_{15}$.

4.6.6 Hypocentral Depth and Rupture Dip Terms

We found that the same functional form used in our horizontal GMPE could be used to model the effects of hypocentral depth and rupture dip angle on vertical ground motion prediction. An analysis of residuals supports this modeling. Details of these functional forms are given in Campbell and Bozorgnia [2013; 2014].

4.6.7 Anelastic Attenuation Term

There is a strong regional dependence of attenuation beyond the 80 km distance used to develop our near-source NGA-West2 vertical model. This implies that there is a regional dependence to the anelastic attenuation we observe. We have modeled this decay with a new anelastic attenuation term f_{atn} and model coefficients c_{20} and Δc_{20}. We fit the anelastic attenuation term by holding all of the other coefficients constant and using the far-source database $(80 < R_{RUP} \leq 500$ km) to derive the anelastic attenuation coefficients using random-effects regression.

Similar to the case of the horizontal component, we used an analysis of residuals together with iterative random-effects regression to determine which regions had both a sufficient number of far-source recordings to derive a reliable anelastic attenuation coefficient and a significant difference in this coefficient. This analysis indicated that California, Taiwan, the Middle East, and other similar active tectonic regions could be used to represent a base anelastic attenuation region. Japan and Italy was found to have relatively stronger attenuation and eastern China (i.e., the Wenchuan earthquake region) relatively weaker attenuation than that of the base region.

4.6.8 Aleatory Variability Term

The overall formulation of the aleatory variability is similar to that for the horizontal motion (see Campbell and Bozorgnia [2013; 2014]); however, since our vertical model is restricted to linear vertical site response, the formulation is significantly simplified, as in Equations (4.29) and (4.30) many of the terms become zero because $\alpha = 0$.

4.7 USER GUIDANCE

Because of the relatively complex nature of the functional forms that comprise our NGA-West2 vertical ground motion model, and because of the inclusion of many new predictor variables, this section presents guidelines to users on how one might evaluate the model for engineering applications.

Generally speaking, and similar to our NGA-West2 horizontal GMPE, our vertical ground motion model is considered to be valid for shallow crustal earthquakes occurring worldwide in active tectonic regimes for which the following conditions apply:

- Minimum magnitudes of $\mathbf{M} \geq 3.3$
- Maximum magnitude limits of $\mathbf{M} \leq 8.5$ for strike-slip faults, $\mathbf{M} \leq 8.0$ for reverse faults, and $\mathbf{M} \leq 7.5$ for normal faults
- Distances of $R_{RUP} = 0-300$ km
- Shear-wave velocities of $V_{S30} = 150-1500$ m/sec (NEHRP site categories B, C, D, and E)
- Sediment depths of $Z_{2.5} = 0-10$ km
- Depths to top of rupture of $Z_{TOR} = 0-20$ km
- Hypocentral depths of $Z_{HYP} = 0-20$ km
- Rupture dips of $\delta = 15-90\,°$.

The model is not uniformly valid over the entire range of predictor variables listed above. Statistical prediction errors are smallest for values of predictor variables near their mean and increase as these values diverge from this mean. These errors can become large when the model is extrapolated beyond the data limits of the predictor variable and should be used with caution under such conditions. The applicable range of some predictor variables have been extended beyond the limits of the data when the model has been constrained theoretically.

Details of the applicable limits and guidance on estimating various parameters used in our vertical GMPE are the same as for our horizontal model and can be found in Campbell and Bozorgnia [2013; 2014].

REFERENCES

Abrahamson N.A., Youngs R.R. (1992). A stable algorithm for regression analyses using the random effects model, *Bull. Seismol. Soc. Am.*, 100**:** 1288–92.

Ancheta T.D., Darragh R., Stewart J.P., Seyhan E., Silva W.J., Chiou B.S.-J., Wooddell K.E., Graves R.W, Kottke A.R., Boore D.M., Kishida T., Donahue J.L. (2013). PEER NGA-West2 database, *Report PEER 2013/03*, Pacific Earthquake Engineering Research Center, University of California, Berkeley, CA.

Ancheta T.D., Darragh R., Stewart J.P., Seyhan E., Silva W.J., Chiou B.S.-J., Wooddell K.E., Graves R.W, Kottke A.R., Boore D.M., Kishida T., Donahue J.L. (2014). NGA-West2 database, *Earthq. Spectra*, submitted.

Beresnev I.A., Nightengale A.M., Silva W.J. (2002). Properties of vertical ground motions, *Bull. Seismol. Soc. Am.*, 92: 3152-3164.

Bommer J.J., Akkar S., Kale O. (2011). A model for vertical-to-horizontal response spectral ratios for Europe and the Middle East, *Bull. Seismol. Soc. Am.*, 101: 1783–1806.

Bozorgnia Y., Campbell K.W. (2004). The vertical-to-horizontal response spectral ratio and tentative procedures for developing simplified V/H and vertical design spectra, *J. Earthq. Eng*., 8: 175–207.

Bozorgnia Y., Mahin S.A., Brady A.G. (1998). Vertical response of twelve structures recorded during the Northridge earthquake, *Earthq. Spectra*, 14: 411-432.

Bozorgnia Y., Niazi M., Campbell K.W. (1995). Characteristics of free-field vertical ground motion during the Northridge earthquake, *Earthq. Spectra*, 11: 515–525.

Bozorgnia Y., Abrahamson N.A., Campbell K.W., Rowshandel B., Shantz T. (2012). NGA-West2: A comprehensive research program to update ground motion predictions equations for shallow crustal earthquakes in active tectonic regions, *Proceedings, 15th World Conference on Earthquake Engineering*, Paper No. 2572, Lisbon, Portugal.

Bozorgnia Y., Abrahamson N.A., Al Atik L., Ancheta T.D., Atkinson G.M., Baker J.W., Baltay A., Boore D.M., Campbell K.W., Chiou B.S.-J., Darragh R., Day S., Donahue J., Graves R.W., Gregor N., Hanks T., Idriss I.M., Kamai R., Kishida T., Kottke A., Mahin S.A., Rezaeian S., Rowshandel B., Seyhan E., Shahi S., Shantz T., Silva W., Spudich P., Stewart J.P., Watson-Lamprey J., Wooddell K.E., Youngs R.R. (2014). NGA-West2 research project, *Earthq. Spectra,* submitted.

BSSC (2009). NEHRP recommended seismic provisions for new buildings and other structures (*FEMA P-750*), 2009 edition, Report prepared for the Federal Emergency Management Agency (FEMA). Washington, D.C., Building Seismic Safety Council, National Institute of Building Sciences.

Campbell K.W. (1982). A study of the near-source behavior of peak vertical acceleration. *EOS*, 63, p. 1037.

Campbell K.W., Bozorgnia Y. (2013). NGA-West2 Campbell-Bozorgnia ground motion model for the horizontal components of PGA, PGV and 5%-damped elastic pseudo-acceleration response spectra for periods ranging from 0.01 to 10 sec, *Report PEER 2013/06*, Pacific Earthquake Engineering Research Center, University of California, Berkeley, CA.

——— (2014). NGA-West2 ground motion model for the average horizontal components of PGA, PGV and 5%-damped linear response spectra, *Earthq. Spectra,* submitted.

——— (2003). Updated near-source ground motion (attenuation) relations for the horizontal and vertical components of peak ground acceleration and acceleration response spectra, *Bull. Seismol. Soc. Am.,* 93**:** 314–331.

Day S.M., Graves R., Bielak J., Dreger. D., Larsen S., Olsen. K.B., Pitarka A., Ramirez-Guzman L. (2008). Model for basin effects on long-period response spectra in southern California, *Earthq. Spectra,* 24: 257–277.

Donahue J., Abrahamson N.A. (2013). Hanging-wall scaling using finite-fault simulations, *Report PEER 2013/14*, Pacific Earthquake Engineering Research Center, University of California, Berkeley, CA.

Joyner W.B., Boore D.M. (1993). Methods for regression analysis of strong-motion data, *Bull. Seismol. Soc. Am.*, 83: 469–487.

Gülerce Z., Abrahamson N.A., (2010). Vector-valued probabilistic seismic hazard assessment for the effects of vertical ground motions on the seismic response of highway bridges, *Earthq. Spectra,* 26, 999–1016.

Lay T., Wallace T.C. (1995). *Modern Global Seismology*, Academic Press, 521 pgs.

Lee W.H K., Shin T.C., Kuo K.W., Chen K.C., Wu C.F. (2001). Data files from "CWB free-field strong-motion data from the 21 September Chi-Chi, Taiwan, earthquake," *Bull. Seismol. Soc. Am.* 91**:** 1390.

Niazi M., Bozorgnia Y. (1991). Behavior of near-source peak vertical and horizontal ground motions over SMART-1 array, Taiwan, *Bull. Seismol. Soc. Am.,* 81: 715–732.

——— (1992). Behavior of near-source vertical and horizontal response spectra at SMART-1 array, Taiwan, *Earthq. Eng. Struct. Dyn.*, 21: 37–50.

Rezaeian S., Bozorgnia Y., Idriss I.M., Campbell K.W., Abrahamson N.A., Silva W.J. (2012). Spectral damping scaling factors for shallow crustal earthquakes in active tectonic regions, *Report PEER 2012/01*, Pacific Earthquake Engineering Research Center, University of California, Berkeley, CA.

Silva W.J. (1997). Characteristics of vertical strong ground motions for applications to engineering design, FHWA/NCEER Workshop on the National Representation of Seismic Ground Motion for New and Existing Highway Facilities; Burlingame; CA; Proceedings, *Technical Report NCEER-97-0010*, National Center for Earthquake Engineering Research, Buffalo, New York.

Stewart J.P., Seyhan E., Boore D.M., Campbell K.W., Erdik M., Silva W.J., Di Alessandro C., Bozorgnia Y. (2012). Site effects in parametric ground motion models for the GEM-PEER global GMPEs project, *Proceedings, 15th World Conference on Earthquake Engineering*, Paper No. 2554, Lisbon, Portugal.

Wooddell K.E., Abrahamson N.A. (2012). New earthquake classification scheme for mainshocks and aftershocks in the NGA-West2 ground motion prediction equations (GMPEs), *Proceedings, 15th World Conference on Earthquake Engineering*, Paper No. 3872, Lisbon, Portugal.

5. CY13: Ground Motion Prediction Model for Vertical Component of Peak Ground Motions and Response Spectra

BRIAN S.-J. CHOIU[1]

ROBERT R. YOUNGS[2]

In this chapter, we present an NGA model for estimating vertical ground-motion amplitudes caused by shallow crustal earthquakes occurring in active tectonic environments. This vertical model, similar to the 2013 horizontal NGA model of Chiou and Youngs, is based on statistical analysis of 5%-damped response spectra of the NGA-West2 vertical ground-motion database and seismological simulations of vertical ground motions. The developed vertical model has the functional form of the accompanying horizontal ground motion prediction equation (GMPE), with one modification related to linear soil response term. As in the horizontal GMPE, we model regional differences in far-source distance attenuation and site effects between California and other active tectonic regions. The vertical-to-horizontal (V/H) response spectral ratios computed using the developed vertical GMPE and the accompanying horizontal GMPE show the well-known shape peaking around 0.05-sec period. The peak ratio varies with V_{S30} and, to a lesser extent, also with rupture distance and magnitude. The aleatory variability for the vertical component was found to have similar values and similar magnitude dependence to those of the horizontal component.

5.1 INTRODUCTION

This chapter presents the development of a vertical GMPE by Chiou and Youngs. This vertical GMPE was based on analysis of a large ground-motion database for vertical components of free-field recordings [Ancheta et al. 2013] and an extensive set of ground-motion simulations [Donahue and Abrahamson 2013], both were provided by PEER as part of the NGA-West2 Project [Bozorgnia et al. 2014]. The development of our site effect model also benefited from the amplification factors resulted from an equivalent-linear site response analysis of vertical

[1] Division of Research and Innovation, California Department of Transportation, Sacramento, California.

[2] AMEC, Oakland, California

component of motions by Silva (http://peer.berkeley.edu/ngawest2_wg/site-response-working-group/data-sire).

Initial evaluations of the NGA-West2 vertical data indicated that, except for the term of linear soil response, the functional form for horizontal component is suitable for use in modeling the vertical ground motions. Hence, our vertical GMPE borrowed abundantly from the accompanying horizontal GMPE [Chiou and Youngs 2013] for both functional form and model coefficient values. Modifications were made where there are important differences between the two components of motions. Our modeling decisions are summarized in Table 5.1. As in horizontal motion, regional differences in anelastic attenuation and scaling with V_{S30} (the travel-time-averaged shear-wave velocity of the top 30 m of soil) were observed and included in the final vertical GMPE.

Table 5.1 Summary of Modeling Decisions for the Vertical GMPE.

	Horizontal GMPE Functional Form	Coefficients Borrowed from Horizontal GMPE	Coefficients Estimated from Vertical Data
M-Scaling	Kept	c_2, c_{M}, c_n	c_3
Style of Faulting	Kept	$c_{1\mathrm{a}}$, c_{1b}, c_{1c}, c_{1d}	
Rupture Depth Scaling	Kept		c_7, $c_{7\mathrm{b}}$
Near-Source Scaling	Kept		c_5, c_6
Geometric Spreading	Kept	c_4, c_{4a}, c_{RB}	
Crustal Anelastic Damping	Kept	γ_3	γ_1, γ_2, $\gamma_{Jp\text{-}It}$, γ_{Wn}
Directivity Effect	Removed		
Hanging Wall Effect	Kept	c_9, $c_{9\mathrm{a}}$, $c_{9\mathrm{b}}$	
Linear Soil Response	Revised		ϕ_1, ϕ_{1Jp}, ϕ_{1Tw} ϕ_{1a}, ϕ_{1aJP} ϕ_{1b}, ϕ_{1bJp}
Nonlinear Soil Response	Removed		
Sediment Depth	Kept	ϕ_6, ϕ_{6Jp}	ϕ_5, ϕ_{5Jp}

In the following, we first describe the selection of vertical data used in the regression analysis. We then describe the modifications made to the horizontal GMPE to improve fits to vertical data, followed by evaluations of the developed vertical model and comparisons to the accompanying horizontal GMPE in the form of vertical-to-horizontal (V/H) spectra ratio. The GMPE presented herein does not include effects of fault rupture directivity. The effects due to soil nonlinear response was found to be insignificant in the NGA-West2 vertical data, therefore the final model does not include terms for nonlinear soil response. Finally, we offer guidance on model applicability of the developed vertical GMPE.

5.2 GROUND MOTION DATA

5.2.1 Data Selection

The vertical dataset were selected for the same records that were used to develop the 2013 Chiou and Youngs horizontal GMPE. These data were then further reduced to remove vertical components of questionable quality or with issues of late P-wave trigger as identified in the PEER NGA-West2 vertical motion database. We supplemented the NGA-West2 database with imputed values of missing metadata that were developed for the horizontal motions, as described in Chiou and Youngs [2013].

After applying the selections described above, a total of 11,889 records obtained from 296 earthquakes were used in the development of vertical GMPE. The smaller data size, compared to our horizontal GMPE, is mainly due to the fact that there are more late P-wave trigger records than late S-wave trigger records in the NGA-West2 database. A total of 2564 records were selected from eighteen well-recorded non-California earthquakes. Figure 5.1 shows a scatter plot of the distance-magnitude-region distribution of our selected dataset. Figure 5.2 shows the number of usable data as a function spectral period.

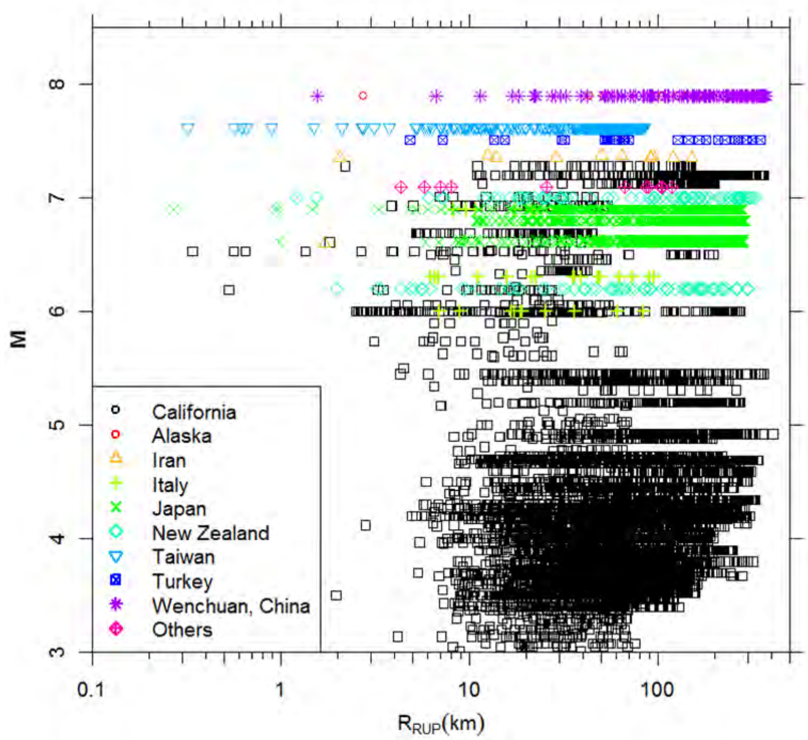

Figure 5.1 **Magnitude-distance-region distribution of selected records of vertical motion.**

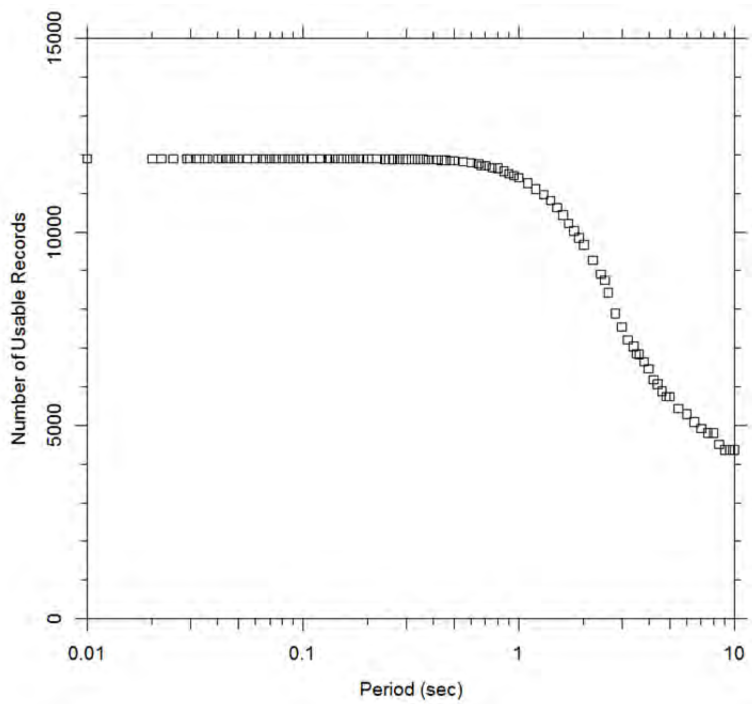

Figure 5.2 Number of usable records as a function of spectral period.

5.2.2 $Z_{1.0}$ - V_{s30} Relationship

For horizontal motion, the thickness of near-surface sediments is represented in our GMPE by the depth to the shear-wave velocity horizon of 1.0 km/sec, $Z_{1.0}$. The NGA-West2 database contains $Z_{1.0}$ for recording sites within the Southern California Earthquake Center three-dimensional basin model, for sites within the USGS velocity model for the San Francisco Bay area, for Japanese sites within the NIED (National Institute for Earth Science and Disaster Prevention) velocity model, and for sites where measured shear-wave velocity profiles reached the 1.0 km/sec horizontal.

As was done for our 2013 horizontal GMPE, we estimated $Z_{1.0}$ for sites without reported values using relationships between $Z_{1.0}$ and V_{S30}. Data in the NGA-West2 database show a clear difference in $Z_{1.0}$-V_{S30} relationship between California and Japan. Therefore, we used separate relationship for the two regions.

For California:

$$\ln(Z_{1.0}) = \frac{-7.15}{4}\ln\left(\frac{V_{S30}^4 + 571^4}{1360^4 + 571^4}\right) \tag{5.1}$$

For Japan:

$$\ln(Z_{1.0}) = \frac{-5.23}{2}\ln\left(\frac{V_{S30}^2 + 412^2}{1360^2 + 412^2}\right) \tag{5.2}$$

5.3 MODEL DEVELOPMENT

We borrowed heavily from the accompanying 2013 horizontal GMPE [Chiou and Youngs 2013] for both model formulation and coefficient values. Development of our vertical GMPE consisted of two steps. First, we took the horizontal GMPE as an initial model and evaluated its adequacy against vertical data. We found that the basic horizontal component formulations for ground-motion scaling with distance and source parameters performed well for the vertical component. Consequently, these formulations were adopted without change. However, soil amplification of vertical motions shows a clear flattening of $\ln(V_{S30})$ scaling at $V_{S30} < 360$ m/sec in both data and site response analysis results. The linear $\ln(V_{S30})$ relationship adopted by the horizontal GMPE was thus modified to reflect the observed trends in vertical data. Evidence of nonlinear soil response in the vertical data was not found; hence we assumed linear soil response for the vertical component and did not include effects of nonlinear soil behavior in the vertical GMPE. In addition, the rupture directivity term was removed from the vertical GMPE because there is little knowledge about directivity effects on the vertical component. While some horizontal model coefficients were kept, others were modified in the second step of model development to improve fits to vertical ground-motion data. These modeling decisions are summarized in Table 5.1 and discussed in sections below.

5.3.1 Magnitude Scaling

Development of the magnitude scaling formulation in our horizontal GMPE was guided by the results of simulation using seismological models for the source excitation of shear-waves. We evaluated the suitability of this magnitude scaling formulation against the vertical component, which is composed of both compressional-waves and shear-waves. Our analysis indicated that the horizontal component model performed well, requiring just a slight change to coefficient c_3 to improve fits to $\mathbf{M} < 5$ spectral data at short (< 0.1 sec) and long (> 3 sec) periods.

5.3.2 Distance Scaling

Our 2013 horizontal GMPE adopted a magnitude- and period-independent near-source geometric spreading, coupled with an **M**-dependent additive distance to capture the effects of extended ruptures. This near-source distance scaling was then gradually transitioned to a far-source geometric spreading of -1/2 $\ln(R_{RUP})$ in order to model the transition from body-wave geometric spreading near the source to surface/*Lg* wave geometric spreading at larger distances. In addition, we included an **M**-dependent attenuation term $[\gamma(\mathbf{M},T) \times R_{RUP}]$ to model the effects of anelastic attenuation and scattering (i.e., the effects of crustal Q). Results of our analysis indicated that this distance-scaling formulation is also adequate for the modeling of distance scaling of vertical motion in the distance range of 0 to 300 km. Consequently, we adopted the formulation for distance scaling used for the horizontal component without change, but changed coefficients c_5, c_6, $c_{\gamma 1}$, and $c_{\gamma 2}$, as discussed below.

5.3.2.1 Additive Distance in Near-Source Distance Scaling

We estimated for each of the well-recorded earthquakes the additive distance that controlled the near-source distance scaling of vertical motions. The results indicated that at $T < 0.1$ sec the estimated additive distances for vertical component are smaller than the estimates for horizontal component, but at $T > 0.2$ sec the opposite is true. This finding prompted us to modify coefficients c_5 and c_6 as part of the vertical model development. It should be noted that the differences in additive distance between horizontal and vertical components is one of the important factors that determines the shape of V/H spectral ratios.

5.3.2.2 Regional Variance in γ

Previously, we found from the analysis of a worldwide dataset of horizontal motions that there are significant regional differences in γ for active tectonic regions [Chiou and Youngs 2012; 2013]. The γ estimates for New Zealand, Taiwan, and Turkey are similar to those obtained for California earthquakes. The values for Italy and Japan indicate more rapid attenuation with distance than California. The data for the Wenchuan, China, earthquake shows slower distance attenuation. Regional γ differences were also found in NGA-West2 vertical data. To account for the observed regional γ differences, we applied multiplicative adjustment factors ($\gamma_{Jp\text{-}It}$, γ_{Wn}) to the California γ.

5.3.3 Scaling with Style of Faulting

In our 2013 horizontal GMPE, style of faulting scaling varies with **M**. Specifically, style-of-faulting effect is weaker for **M** < 5 earthquakes than for **M** > 6 earthquakes. We adopted the horizontal functional form for style of faulting effects and found the estimated effects for vertical component to be statistically similar to the effects for horizontal component. As a result, we retained both the functional form and model coefficients (c_{1a}, c_{1b}, c_{1c}, and c_{1d}) from our 2013 horizontal GMPE.

5.3.4 Scaling with Centered Z_{TOR}

As in the 2013 horizontal GMPE, source depth scaling in the vertical GMPE is defined based on the value of $\Delta Z_{TOR} = Z_{TOR} - E[Z_{TOR}]$, where $E[Z_{TOR}]$ is the mean Z_{TOR} given by Equation (5.3) for the reverse and reverse oblique faulting,

$$E[Z_{TOR}] = \max[2.704 - 1.226\max(\mathbf{M} - 5.849, 0), 0]^2 \tag{5.3}$$

and by Equation (5.4) for the combined strike-slip and normal faulting,

$$E[Z_{TOR}] = \max[2.673 - 1.136\max(\mathbf{M} - 4.970, 0), 0]^2 \tag{5.4}$$

Our analyses indicated that the horizontal component formulation for ΔZ_{TOR} scaling is applicable to vertical component. One important difference from the horizontal component is that the ΔZ_{TOR} scaling for **M** > 6 earthquakes is much weaker. Estimated values of coefficient c_7 are statistically indistinguishable from zero so we set it to zero for all periods.

5.3.5 Fault Dip Effect

In our 2013 GMPE, amplitudes for **M** < 5 earthquakes increase with $\cos(\delta)^2$, but not for **M** > 5 earthquakes. Our analysis indicated that fault dip effect is also insignificant for vertical data from **M** > 5 earthquakes. For dip effect, we retained both the functional form and the model coefficients (c_{11} and c_{11b}) of horizontal GMPE.

5.3.6 Hanging-Wall Effect

For R_{JB} = 0 (region inside the surface projection of the ruptured area), there is very limited data in NGA-West2 database (for both horizontal and vertical components) that can be used to define the trend of hanging-wall (HW) amplification with R_X (the horizontal distance from the top of the rupture measured perpendicular to strike). In the 2013 horizontal GMPE we used simulated data to develop the HW amplification model. The numerical simulations were conducted as part of the NGA-West2 project and are described in Donahue and Abrahamson [2014]. Using the same set of simulations, Donahue [personal communication] found similar HW amplification between the horizontal and vertical components. Based on her findings, we adopted the horizontal component HW effects (the functional form and the accompanying coefficients c_9, c_{9a}, and c_{9b}) for vertical GMPE in regions of both R_{JB} = 0 and R_{JB} > 0. It should be noted that HW amplification in the 2013 horizontal GMPE for the R_{JB} = 0 region was constrained by numerical simulations, not by empirical data.

5.3.7 V_{S30} Scaling

In our 2013 horizontal GMPE, amplification of soil motion under weak loading condition is adequately modeled by a linear function of $\ln(V_{S30})$ in the range of $180 \leq V_{S30} \leq 1100$ m/sec. For vertical component, however, the relationship between rock and soil motion is not as clear, as evidenced in the analysis of empirical data as well as theoretical site response analysis [Kamai, personal communication]. To empirically characterize the difference in linear soil response between vertical and horizontal components, we computed the within-earthquake residuals of vertical data with respect to reference (V_{S30}=1130 m/sec) motion predicted by our 2013 horizontal GMPE, after correcting for a constant V/H ratio. Figure 5.3 shows the resulting within-earthquake residuals against $\ln(V_{S30})$ for recordings under weak loading condition (weak reference rock motion) for peak ground acceleration (*pga*), 0.2-, 1-, and -sec spectra. These plots indicate that there are differences between horizontal and vertical components in both the amplification level and the trend with $\ln(V_{S30})$. In particular, for vertical component, trend with $\ln(V_{S30})$ is flatter at low V_{S30} than at higher V_{S30}. Similar trend was also noted in the site response analysis results for vertical motion [Kamai, personal communication].

To capture the flattening of V_{S30} trends at low V_{S30}, we proposed a new functional form for use in vertical GMPE for linear soil response,

$$f_{Site} = \frac{\phi_1}{1+\left(\frac{V_{S30}}{\phi_{1a}}\right)^{\phi_{1b}}} \tag{5.5}$$

In Equation (5.5), parameter ϕ_1 represents the asymptotic amplification level at very low V_{S30} ($\ll \phi_{1a}$), parameter ϕ_{1a} represents the V_{S30} value at which amplification is half of ϕ_1, and parameter ϕ_{1b} represents the curvature of amplification curve, a measure of how fast the amplification factor drops from ϕ_1 to 1 as V_{S30} increases. Depending on the values of ϕ_{1a} and ϕ_{1b}, this site response model may not constrain ground motion amplification factors to be 1 for V_{S30} greater than 1130 m/sec, and it also may get very close to 1 before 1130 m/sec.

The existence and degree of nonlinear soil response for vertical motion are uncertain. Vertical site response analysis conducted for the NGA-West2 project suggested that for $T > 0.3$ sec, soil response is primarily linear. For $T < 0.3$sec, nonlinear soil effect is present but much weaker than the horizontal component, requiring a large threshold input motion to induce nonlinear soil behavior [Kamai 2012]. We did not find strong evidence of nonlinear soil response in the vertical data. Based on the above discussions, we assumed linear soil response for all spectral periods and did not include effects of nonlinear soil behavior in the vertical GMPE.

Regional differences in linear soil response between Japan, Taiwan (Chi Chi earthquake), and California were found in the NGA-West2 vertical data (Figure 5.3). This difference was modeled in the final vertical GMPE by allowing for region-specific ϕ_1 for Japan and Taiwan (ϕ_{1Jp}, ϕ_{1Tw}) and region-specific ϕ_{1a} and ϕ_{1b} for Japan (ϕ_{1aJp} and ϕ_{1bJp}).

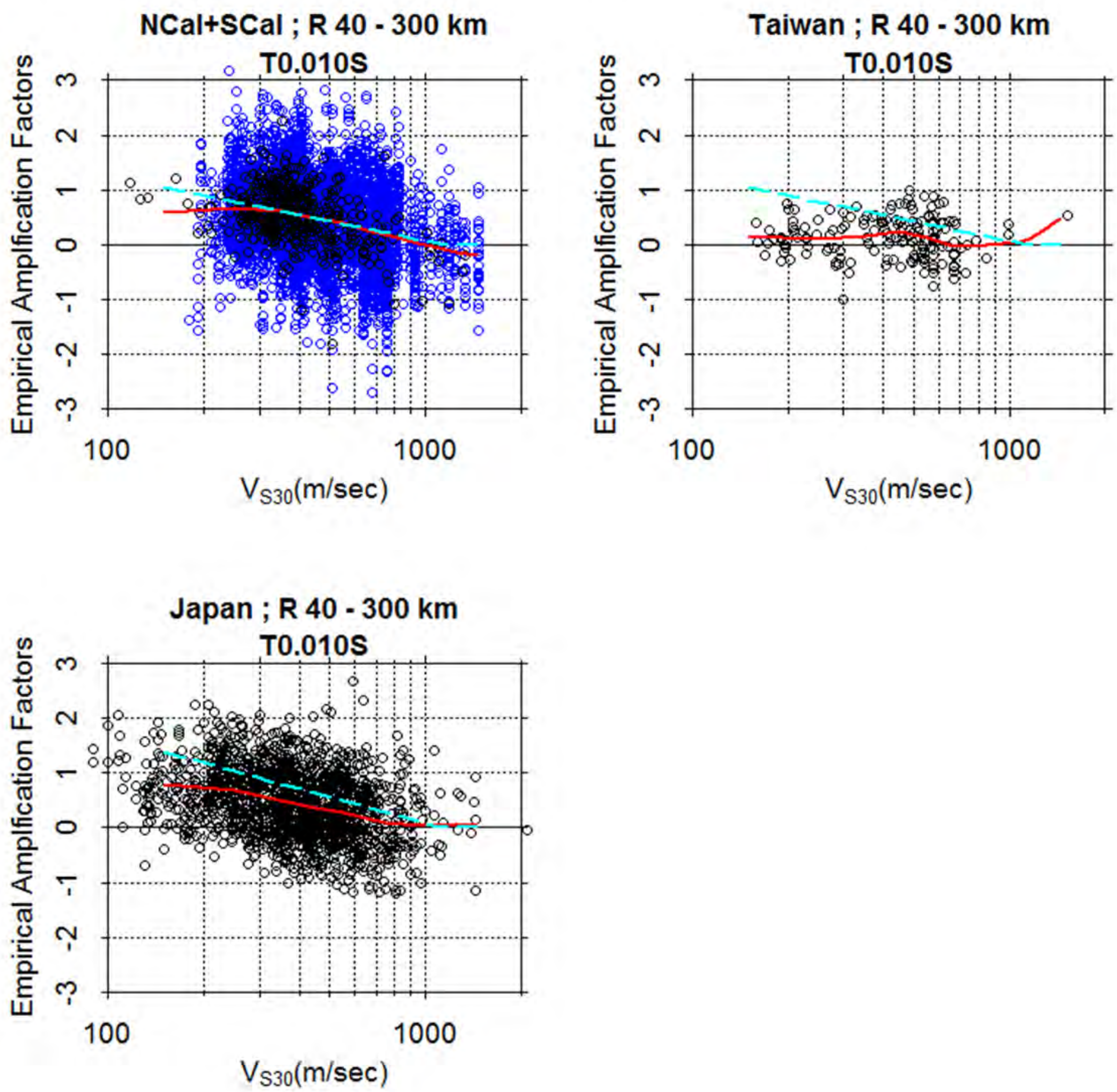

Figure 5.3 **Within-earthquake residuals (empirical soil amplification factor) plotted versus V_{S30}. These residuals are from distant records (R_{RUP} > 40 km) computed with respect to predictions for 1130 m/sec condition. Data from M > 6 earthquakes are shown in black; data from M < 6 are in blue. A smoothed trend (computed using the local linear regression method *loess* in statistical package R) is shown as the solid red line. For comparison, amplification from our horizontal GMPE is shown as the long dash curve.**

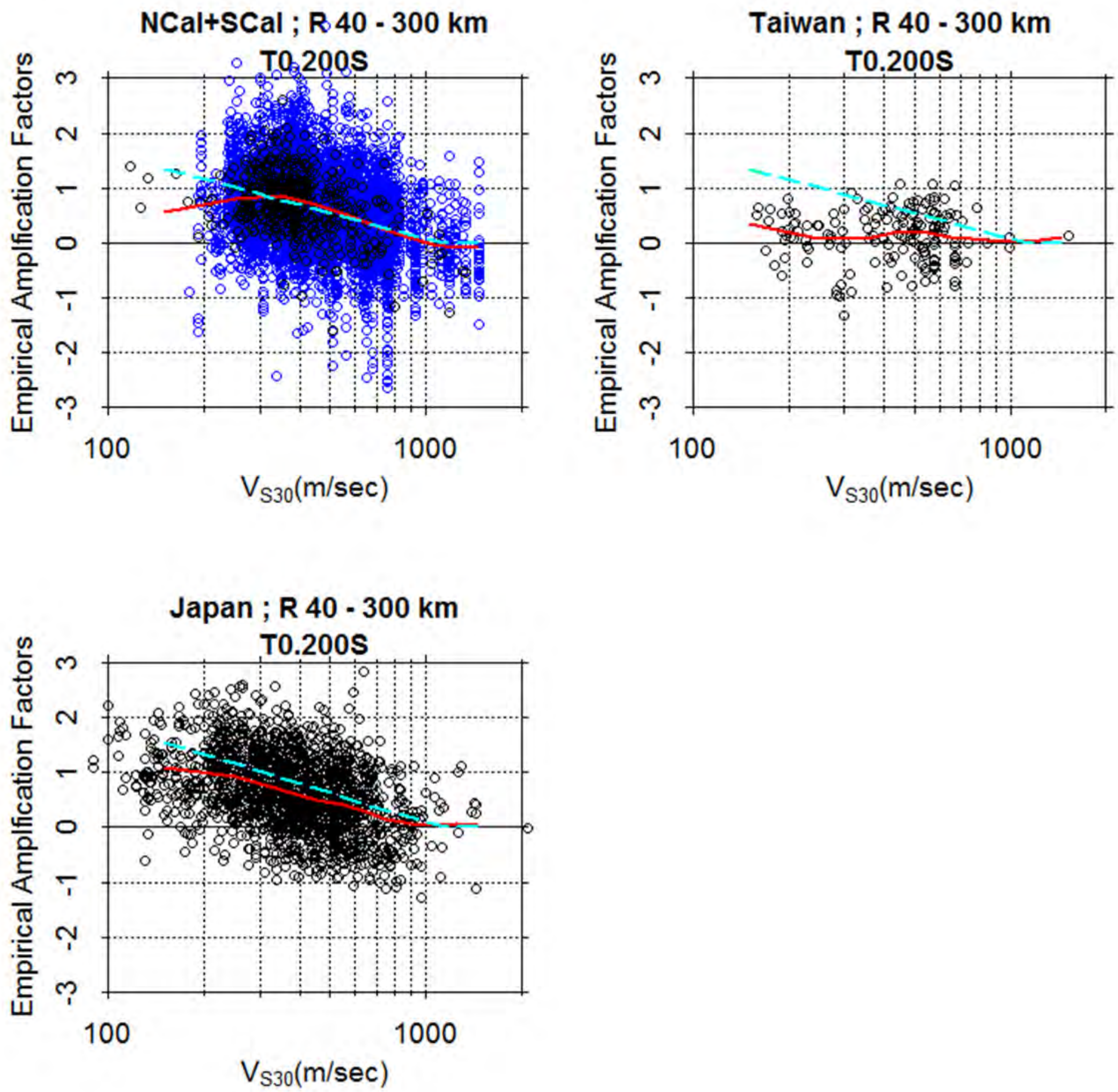

Figure 5.3 Continued.

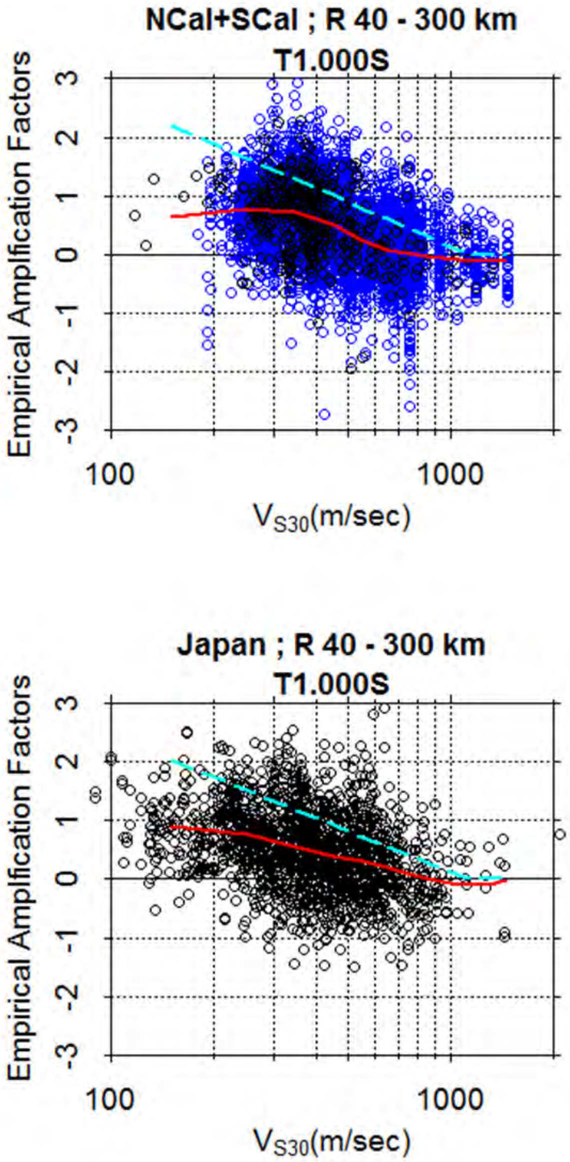

Figure 5.3 Continued.

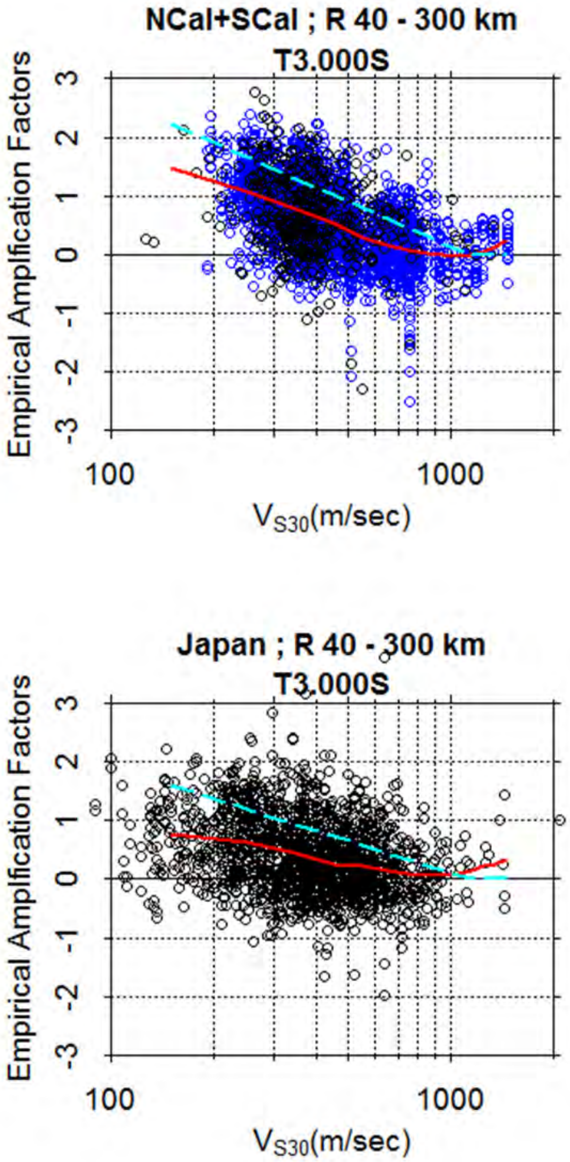

Figure 5.3 Continued.

5.3.8 Scaling with $\Delta Z_{1.0}$

In our 2013 horizontal GMPE, amplification (deamplification) of horizontal motion for sites with larger (smaller) than average sediment thickness is modeled as a function of $\Delta Z_{1.0}$, $\Delta Z_{1.0} = Z_{1.0} - E[Z_{1.0}]$. Given by Equations (5.1) or (5.2), $E[Z_{1.0}]$ is the mean $Z_{1.0}$ at a specified V_{S30}. The adequacy of the horizontal formulation for $\Delta Z_{1.0}$ scaling of vertical motion is illustrated in Figure 5.4. The figure also indicates a much stronger $\Delta Z_{1.0}$ scaling for positive $\Delta Z_{1.0}$ in Japan than in California, suggesting a need for regionalization of sediment thickness effects.

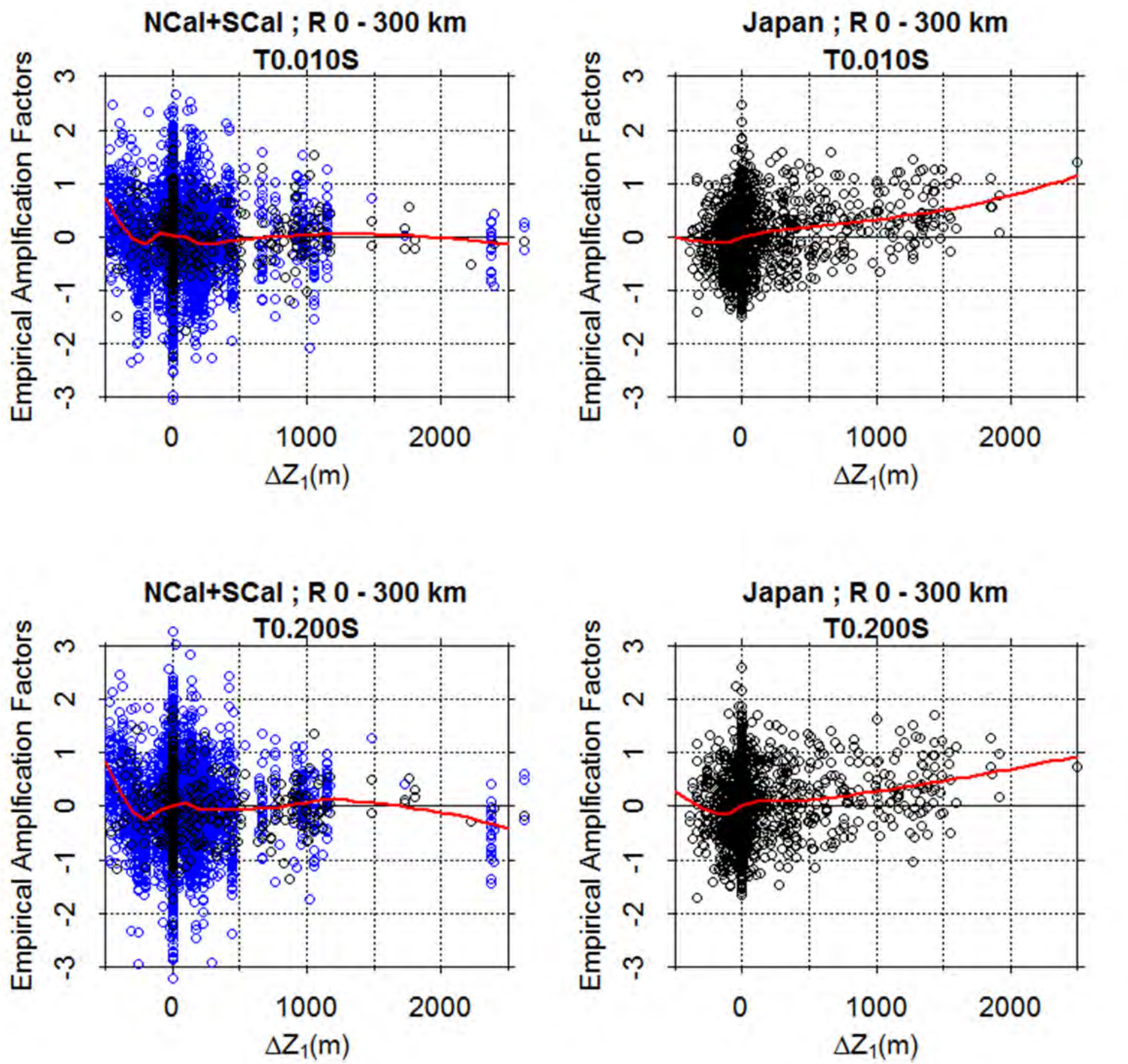

Figure 5.4 **Within-earthquake residuals plotted versus $\Delta Z_{1.0}$. These residuals are computed using a model without $\Delta Z_{1.0}$ term in order to show the effects of $\Delta Z_{1.0}$. A smoothed trend (computed using the local linear regression method) is shown as the solid line.**

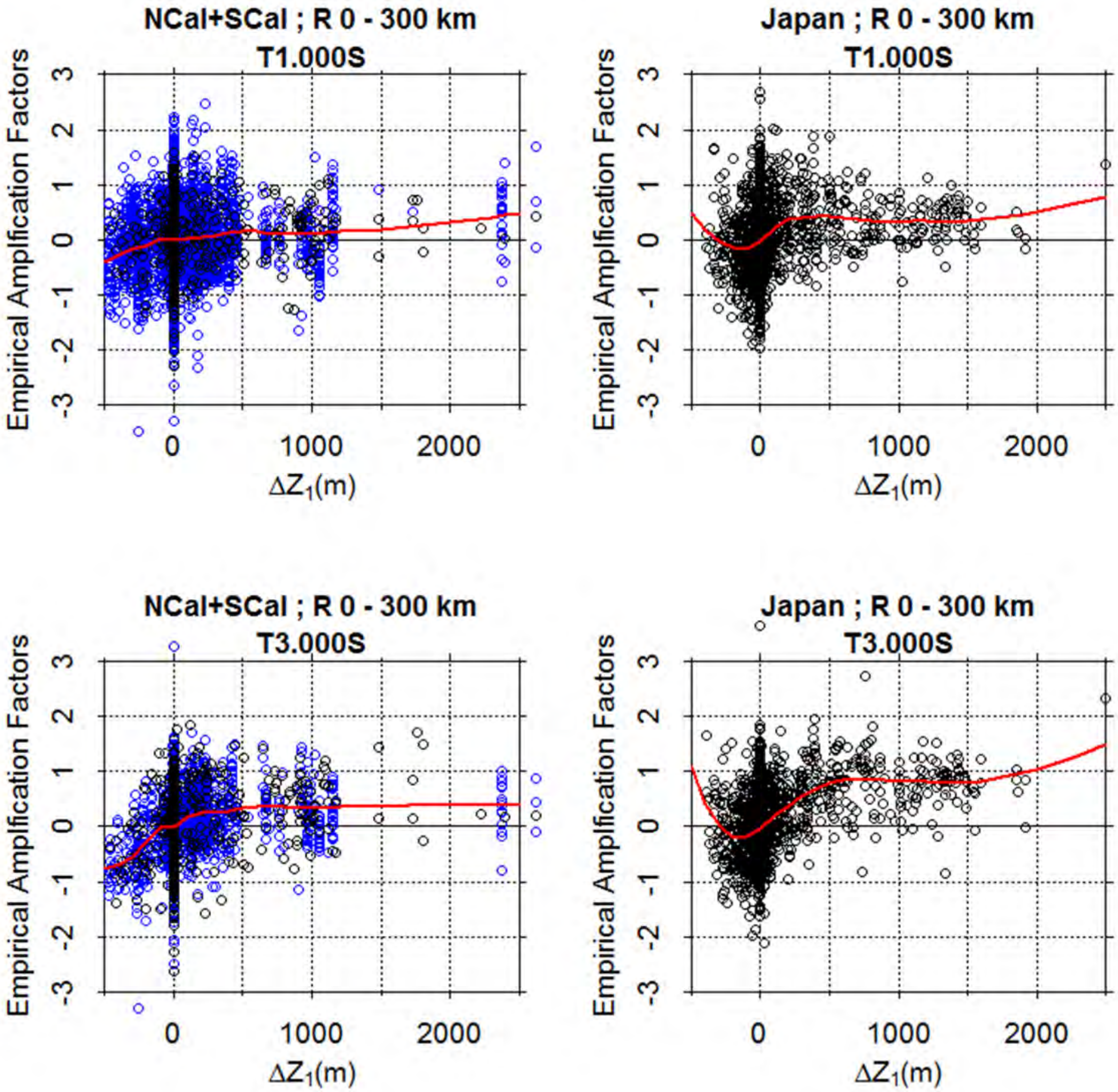

Figure 5.4 **Continued.**

5.4 RESULTS OF DEVELOPED VERTICAL GMPE

The GMPE formulation for vertical motion is given by Equations (5.6) and (5.7).

$$
\begin{aligned}
\ln\left(y_{refij}\right) = c_1 & \\
& + \left\{ c_{1a} + \frac{c_{1c}}{\cosh(2 \cdot \max(\mathbf{M}_i - 4.5,\ 0))} \right\} F_{RVi} \\
& + \left\{ c_{1b} + \frac{c_{1d}}{\cosh(2 \cdot \max(\mathbf{M}_i - 4.5,\ 0))} \right\} F_{NMi} \\
& + \left\{ c_7 + \frac{c_{7b}}{\cosh(2 \cdot \max(\mathbf{M}_i - 4.5,\ 0))} \right\} \Delta Z_{TORi} \\
& + \left\{ c_{11} + \frac{c_{11b}}{\cosh(2 \cdot \max(\mathbf{M}_i - 4.5,\ 0))} \right\} (\cos \delta_i)^2 \\
& + c_2 \ (\mathbf{M}_i - 6) + \frac{c_2 - c_3}{c_n} \ln\left(1 + e^{c_n (c_M - \mathbf{M}_i)}\right) \\
& + c_4 \ln\left(R_{RUPij} + c_5 \cosh\left(c_6 \cdot \max(\mathbf{M}_i - c_{HM}, 0)\right)\right) \\
& + \left(c_{4a} - c_4\right) \ \ln\left(\sqrt{R_{RUPij}^2 + c_{RB}^2}\right) \\
& + \left\{ c_{\gamma 1} + \frac{c_{\gamma 2}}{\cosh\left(\max(\mathbf{M}_i - c_{\gamma 3},\ 0)\right)} \right\} R_{RUPij} \\
& + c_9 \ F_{HWij} \cos \delta_i \left\{ c_{9a} + (1 - c_{9a}) \tanh\left(\frac{R_{Xij}}{c_{9b}} \right) \right\} \left\{ 1 - \frac{\sqrt{R_{JBij}^2 + Z_{TORi}^2}}{R_{RUPij} + 1} \right\}
\end{aligned}
\tag{5.6}
$$

$$
\ln\left(y_{ij}\right) = \ln\left(y_{ref_{ij}}\right) + \frac{\phi_1}{1 + \left(\frac{V_{S30}}{\phi_{1a}}\right)^{\phi_{1b}}} + \phi_5 \left(1 - e^{-\Delta Z_{1.0j} / \phi_6}\right) + \eta_i + \varepsilon_{ij} \tag{5.7}
$$

Random variables η_i (between-earthquake residual) and ε_{ij} (within-earthquake residual) in Equation (5.7) represent the two modeling errors that contribute to the aleatory variability of predicted motion. The predictor variables of the vertical GMPE are:

- $\mathbf{M}$ = Moment magnitude.
- R_{RUP} = Closest distance (km) to the ruptured plane.
- R_{JB} = Joyner-Boore distance (km) to the ruptured plane.
- R_X = Site coordinate (km) measured perpendicular to the fault strike from the fault line, with the down-dip direction being positive.
- F_{HW} = Hanging-wall flag: 1 for $R_X \geq 0$ and 0 for $R_X < 0$.
- δ = Fault dip angle.
- Z_{TOR} = Depth (km) to the top of ruptured plane.
- ΔZ_{TOR} = Z_{TOR} centered on the $\mathbf{M}$-dependent average Z_{TOR}.
- F_{RV} = Reverse-faulting flag: 1 for $30° \leq \lambda \leq 150°$ (combined reverse and reverse-oblique), 0 otherwise; λ is the rake angle.
- F_{NM} = Normal faulting flag: 1 for $-120° \leq \lambda \leq -60°$ (excludes normal-oblique), 0 otherwise.
- V_{S30} = Travel-time averaged shear-wave velocity (m/sec) of the top 30 m of soil.
- $Z_{1.0}$ = Depth (m) to shear-wave velocity of 1.0 km/sec.
- $\Delta Z_{1.0}$ = $Z_{1.0}$ centered on the V_{S30}–dependent average $Z_{1.0}$.

The GMPE coefficients (variable names starting with the letter c or ϕ) are listed in Tables 5.2 to 5.4. In the tables, we underlined coefficients whose values were unmodified from our 2013 horizontal GMPE. Because Class 2 earthquakes (aftershocks) were excluded, we did not include aftershock terms.

To simplify, Equations (5.6) and (5.7) were written for application in California, although our regression analysis included regionalization to account for the observed regional difference in anelastic attenuation and site effects. To apply our GMPE to regions where differences from California were accounted for in regression, one should use the region-specific coefficients or adjustment factors given in Table 5.5. Also, in application to sites in Japan, the Japan-specific average Z1.0 model given by Equation (5.2) should be used to center $Z_{1.0}$.

Table 5.2 Period-independent coefficients of model for ln(*y*): Equation (5.6).

$\underline{c_2}$	$\underline{c_4}$	$\underline{c_{4a}}$	$\underline{c_{RB}}$
1.06	-2.1	-0.5	50

Table 5.3 Period-dependent coefficients of model for ln(y_{ref}): Equation (5.6).

Period (sec)	c_1	$\underline{c_{1a}}$	$\underline{c_{1b}}$	$\underline{c_{1c}}$	$\underline{c_{1d}}$	$\underline{c_n}$	$\underline{c_M}$	c_3	c_5	$\underline{c_{HM}}$	c_6
0.01	-2.2621	0.1650	-0.3729	-0.1650	0.1977	16.0875	4.9993	1.8616	5.4530	3.0956	0.508
0.02	-2.2629	0.1650	-0.3772	-0.1650	0.2180	15.7118	4.9993	1.8523	5.0265	3.0963	0.508
0.03	-2.1389	0.1650	-0.4429	-0.1650	0.3484	15.8819	4.9993	1.807	4.5820	3.0974	0.508
0.04	-1.9451	0.1650	-0.5122	-0.1650	0.4733	16.4556	4.9993	1.786	4.4501	3.0988	0.508
0.05	-1.7424	0.1650	-0.5544	-0.1650	0.5433	17.6453	4.9993	1.7827	4.6504	3.1011	0.508
0.075	-1.3529	0.1650	-0.5929	-0.1650	0.5621	20.1772	5.0031	1.8426	5.8073	3.1094	0.508
0.1	-1.2191	0.1650	-0.5760	-0.1650	0.4633	19.9992	5.0172	1.9156	6.9412	3.2381	0.508
0.12	-1.2007	0.1650	-0.5583	-0.1650	0.4000	18.7106	5.0315	1.9704	7.6152	3.3407	0.508
0.15	-1.2392	0.1650	-0.5345	-0.1650	0.3337	16.6246	5.0547	2.0474	8.3585	3.4300	0.508
0.17	-1.2856	0.1650	-0.5188	-0.1650	0.2961	15.3709	5.0704	2.0958	8.7181	3.4688	0.508
0.2	-1.3599	0.1650	-0.4944	-0.1650	0.2438	13.7012	5.0939	2.1638	9.1170	3.5146	0.508
0.25	-1.4633	0.1650	-0.4517	-0.1650	0.1620	11.2667	5.1315	2.2628	9.5761	3.5746	0.5068
0.3	-1.5533	0.1650	-0.4122	-0.1650	0.0881	9.1908	5.1670	2.3439	9.8569	3.6232	0.505
0.4	-1.7318	0.1650	-0.3532	-0.1650	-0.0287	6.5459	5.2317	2.4636	10.1521	3.6945	0.5007
0.5	-1.9025	0.1650	-0.3101	-0.1650	-0.1158	5.2305	5.2893	2.5461	10.2969	3.7401	0.4961
0.75	-2.274	0.1650	-0.2219	-0.1650	-0.2708	3.7896	5.4109	2.6723	10.4613	3.7941	0.4846
1	-2.5805	0.1650	-0.1694	-0.1650	-0.3527	3.3024	5.5106	2.7479	10.5397	3.8144	0.4704
1.5	-3.047	0.1650	-0.1376	-0.1650	-0.3454	2.8498	5.6705	2.8355	10.5992	3.8284	0.4401
2	-3.3941	0.1645	-0.1218	-0.1645	-0.2605	2.5417	5.7981	2.8806	10.6045	3.8330	0.4264
3	-3.8807	0.1168	-0.1053	-0.1168	-0.0914	2.1488	5.9983	2.9304	10.6005	3.8361	0.4183

Table 5.3 (Continued). Period-dependent coefficients of model for ln(y_{ref}): Equation (5.6).

Period (sec)	c_7	c_{7b}	c_9	c_{9a}	c_{9b}	c_{11}	c_{11b}	$c_{\gamma 1}$	$c_{\gamma 2}$	$c_{\gamma 3}$
0.01	0	0.0855	0.9228	0.1202	6.8607	0.0	-0.4536	-0.00842	-0.00481	4.2542
0.02	0	0.0871	0.9296	0.1217	6.8697	0.0	-0.4536	-0.00848	-0.00489	4.2386
0.03	0	0.0957	0.9396	0.1194	6.9113	0.0	-0.4536	-0.00893	-0.00508	4.2519
0.04	0	0.1032	0.9661	0.1166	7.0271	0.0	-0.4536	-0.0097	-0.00491	4.2960
0.05	0	0.1066	0.9794	0.1176	7.0959	0.0	-0.4536	-0.01048	-0.00467	4.3578
0.075	0	0.0952	1.0260	0.1171	7.3298	0.0	-0.4536	-0.01169	-0.00370	4.5455
0.1	0	0.0829	1.0177	0.1146	7.2588	0.0	-0.4536	-0.01206	-0.00260	4.7603
0.12	0	0.075	1.0008	0.1128	7.2372	0.0	-0.4536	-0.01182	-0.00211	4.8963
0.15	0	0.0654	0.9801	0.1106	7.2109	0.0	-0.4536	-0.01116	-0.00175	5.0644
0.17	0	0.0601	0.9652	0.1150	7.2491	0.0	-0.4536	-0.01072	-0.00161	5.1371
0.2	0	0.0531	0.9459	0.1208	7.2988	0.0	-0.4440	-0.01017	-0.00144	5.1880
0.25	0	0.043	0.9196	0.1208	7.3691	0.0	-0.3539	-0.00946	-0.00118	5.2164
0.3	0	0.034	0.8829	0.1175	6.8789	0.0	-0.2688	-0.00892	-0.00091	5.1954
0.4	0	0.0183	0.8302	0.1060	6.5334	0.0	-0.1793	-0.00805	-0.00047	5.0899
0.5	0	0.0056	0.7884	0.1061	6.5260	0.0	-0.1428	-0.00727	-0.00035	4.7854
0.75	0	-0.0158	0.6754	0.1000	6.5000	0.0	-0.1138	-0.00554	-0.00089	4.3304
1	0	-0.028	0.6196	0.1000	6.5000	0.0	-0.1062	-0.00434	-0.00149	4.1667
1.5	0	-0.0422	0.5101	0.1000	6.5000	0.0	-0.1020	-0.00289	-0.00224	4.0029
2	0	-0.0511	0.3917	0.1000	6.5000	0.0	-0.1009	-0.00209	-0.00257	3.8949
3	0	-0.0573	0.1244	0.1000	6.5000	0.0	-0.1003	-0.00153	-0.00251	3.7928

Table 5.4 Coefficients of site response model for ln(y): Equation (5.7).

Period (sec)	ϕ_1	ϕ_{1a}	ϕ_{1b}	ϕ_5	ϕ_6
0.01	0.8700	660.7	3.000	0.000	300
0.02	0.8700	660.6	3.000	0.000	300
0.03	0.8700	660.3	3.000	0.000	300
0.04	0.8700	660.0	3.000	0.000	300
0.05	0.8700	659.5	3.000	0.000	300
0.075	0.8700	657.9	3.005	0.000	300
0.1	0.8700	655.6	3.360	0.000	300
0.12	0.8700	653.2	4.062	0.000	300
0.15	0.8700	648.8	4.929	0.000	300
0.17	0.8700	645.4	5.262	0.000	300
0.2	0.8700	639.6	5.553	0.000	300
0.25	0.8652	628.5	5.854	0.000	300
0.3	0.8434	616.3	6.061	0.000	300
0.4	0.7698	590.8	6.292	0.000	300
0.5	0.7263	566.9	6.379	0.000	300
0.75	0.7360	522.2	6.360	0.046	300
1	0.7960	496.2	6.220	0.110	300
1.5	0.9023	472.3	5.716	0.199	300
2	1.0001	462.7	4.952	0.260	300
3	1.1271	455.7	3.347	0.312	300

Table 5.5 GMPE coefficients for non-California regions.

Period (sec)	$\gamma_{Jp\text{-}It}$	γ_{Wn}	ϕ_{1Jp}	ϕ_{1Tw}	ϕ_{1aJp}	ϕ_{1bJp}	ϕ_{5Jp}	ϕ_{6Jp}
0.01	1.2818	0.6771	0.7780	0.2000	460.5	3.000	0.477	800
0.02	1.2769	0.6730	0.7598	0.2000	461.9	3.000	0.473	800
0.03	1.2764	0.6712	0.7062	0.2000	461.3	3.000	0.468	800
0.04	1.2769	0.6704	0.6572	0.2000	460.5	3.000	0.462	800
0.05	1.2652	0.6701	0.6389	0.2000	459.9	3.000	0.458	800
0.075	1.2172	0.6694	0.7371	0.2000	460.6	2.995	0.451	800
0.1	1.1700	0.6650	0.8740	0.2000	461.7	2.940	0.448	800
0.12	1.1615	0.6586	0.9769	0.2000	459.8	2.842	0.447	800
0.15	1.1710	0.6461	1.1222	0.2000	451.7	2.652	0.445	800
0.17	1.1785	0.6372	1.2109	0.2000	443.1	2.478	0.445	800
0.2	1.1845	0.6240	1.3421	0.2000	427.7	2.155	0.444	800
0.25	1.1864	0.6036	1.5379	0.2000	399.8	1.698	0.445	800
0.3	1.1846	0.5849	1.6771	0.2000	373.9	1.436	0.447	800
0.4	1.1858	0.5494	1.7600	0.2000	340.0	1.206	0.456	800
0.5	1.2158	0.5156	1.7310	0.2000	336.1	1.140	0.470	800
0.75	1.3014	0.4429	1.4999	0.2000	391.8	1.370	0.521	800
1	1.4162	0.3886	1.2900	0.2000	435.5	1.600	0.591	800
1.5	1.7863	0.3315	1.0539	0.2140	454.1	2.088	0.757	800
2	2.0498	0.0000	0.9199	0.3285	455.7	2.422	0.924	800
3	2.1545	0.0000	0.7245	0.6632	454.4	2.824	1.157	800

5.4.1 Aleatory Variability

The formulation for aleatory variability developed in our 2013 horizontal GMPE includes dependence on magnitude and degree of nonlinear soil response. In this study, we updated both the functional form and the coefficients of aleatory variability model to reflect the changes brought upon by the vertical data and the absence of effects of nonlinear soil behavior in vertical GMPE.

The current terminology used to express the components of variability use the symbol τ for the between-earthquake component and the symbol ϕ for the within-earthquake component, with the symbol σ used for total aleatory variability, such that $\sigma^2 = \tau^2 + \phi^2$. However, to avoid confusion with our use of the symbol ϕ for the coefficients of site amplification model, we retain the symbols used in Chiou and Youngs [2013]: τ for the between-earthquake component and σ for within-earthquake component, with the symbol σ_T used for the total aleatory variability.

Examination of the residuals for vertical motions indicated similar behavior to that found for the horizontal component. Therefore, the same function form was adopted. The total variance, σ^2_T, for forward prediction of ground motion is given as

$$\sigma_T^2 = \tau^2 + \sigma^2$$

$$\tau = \tau_1 + \frac{\tau_2 - \tau_1}{1.5}\left(\min\left(\max(\mathbf{M},5),6.5\right)-5\right) \tag{5.8}$$

$$\sigma = \sigma_1 + \frac{\sigma_2 - \sigma_1}{1.5}\left(\min\left(\max(\mathbf{M},5),6.5\right)-5\right)\times\sqrt{\sigma_3 F_{Inferred} + 0.7F_{Measured} + 1}$$

Equation (5.8) has been simplified from the aleatory variance model for the horizontal component because of the absence of soil nonlinearity in the vertical GMPE. The estimated values of coefficients τ_1, τ_2, σ_1, and σ_2 are listed in Table 5.6, along with the Japan-specific estimates for σ_2.

Table 5.6 Coefficients of variance model: Equation (5.8).

Period (sec)	τ_1	τ_2	σ_1	σ_2	$\underline{\sigma_3}$	σ_{2Jp}
0.01	0.4200	0.3300	0.4912	0.3762	0.8000	0.4528
0.02	0.4230	0.3289	0.4904	0.3762	0.8000	0.4551
0.03	0.4271	0.3273	0.4988	0.3849	0.8000	0.4571
0.04	0.4309	0.3259	0.5049	0.3910	0.8000	0.4642
0.05	0.4341	0.3247	0.5096	0.3957	0.8000	0.4716
0.075	0.4404	0.3223	0.5179	0.4043	0.8000	0.5022
0.1	0.4450	0.3206	0.5236	0.4104	0.8000	0.5230
0.12	0.4479	0.3195	0.5221	0.4109	0.8000	0.5235
0.15	0.4514	0.3182	0.5202	0.4116	0.8000	0.5209
0.17	0.4533	0.3175	0.5191	0.4119	0.8000	0.5187
0.2	0.4558	0.3166	0.5177	0.4124	0.8000	0.5152
0.25	0.4590	0.3154	0.5159	0.4130	0.7999	0.5100
0.3	0.4615	0.3144	0.5143	0.4135	0.7997	0.5059
0.4	0.4652	0.3130	0.5119	0.4144	0.7988	0.5002
0.5	0.4679	0.3120	0.5100	0.4150	0.7966	0.4959
0.75	0.4724	0.3103	0.4973	0.4256	0.7792	0.4985
1	0.4753	0.3093	0.4882	0.4331	0.7504	0.4998
1.5	0.4788	0.3079	0.4755	0.4436	0.7136	0.5001
2	0.4811	0.3071	0.4681	0.4511	0.7035	0.4979
3	0.4838	0.3061	0.4617	0.4617	0.7006	0.4917

5.4.2 Evaluation of Vertical GMPE

Figure 5.5 shows the event term η_i (between-earthquake residual) for spectral periods of $T = 0.01$ (*pga*), 0.2, 1, and 3 sec. In the range of $3.5 \leq \mathbf{M} \leq 8$, the event terms do not exhibit a significant trend with **M** or a large offset from zero. The vertical model tends to under-predict for $\mathbf{M} < 3.5$ earthquakes, as evidenced by their positive event terms.

Figures 5.6 through 5.9 show the within-earthquake residuals ε_{ij} plotted versus **M**, R_{RUP}, V_{S30}, and $\Delta Z_{1.0}$ for spectral periods of 0.01, 0.2, 1 and 3 sec, respectively. In general, these residuals do not exhibit a significant trend within the body of a predictor, but some show trends near the ends of predictor domain. We note our $\Delta Z_{1.0}$ model under-predicts the data for $\Delta Z_{1.0} < -350$ m sites, which are mostly located in the San Francisco Bay area (NCal), suggesting that additional regionalization of sediment depth effects for soft sites within California may be warranted.

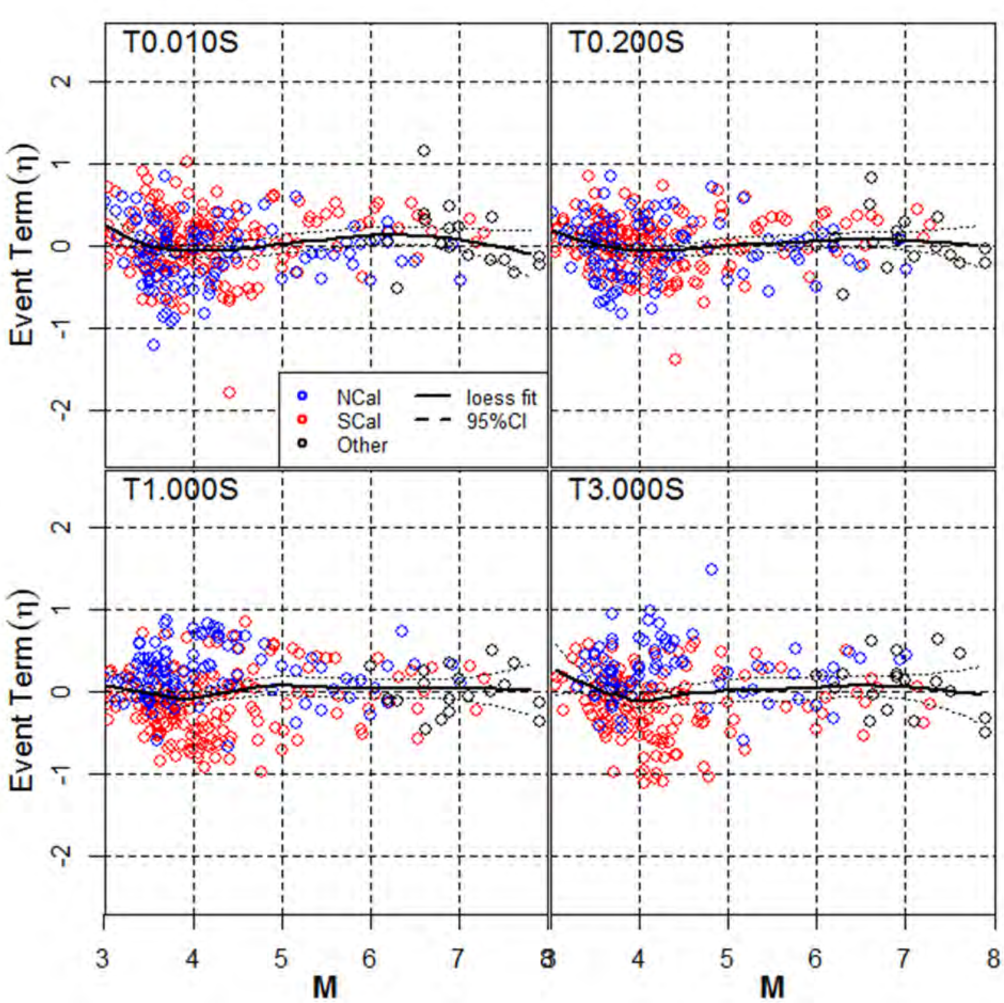

Figure 5.5 Between-earthquake residuals (event terms) for spectral periods of 0.01 sec (*pga*), 0.2, 1, and 3 sec.

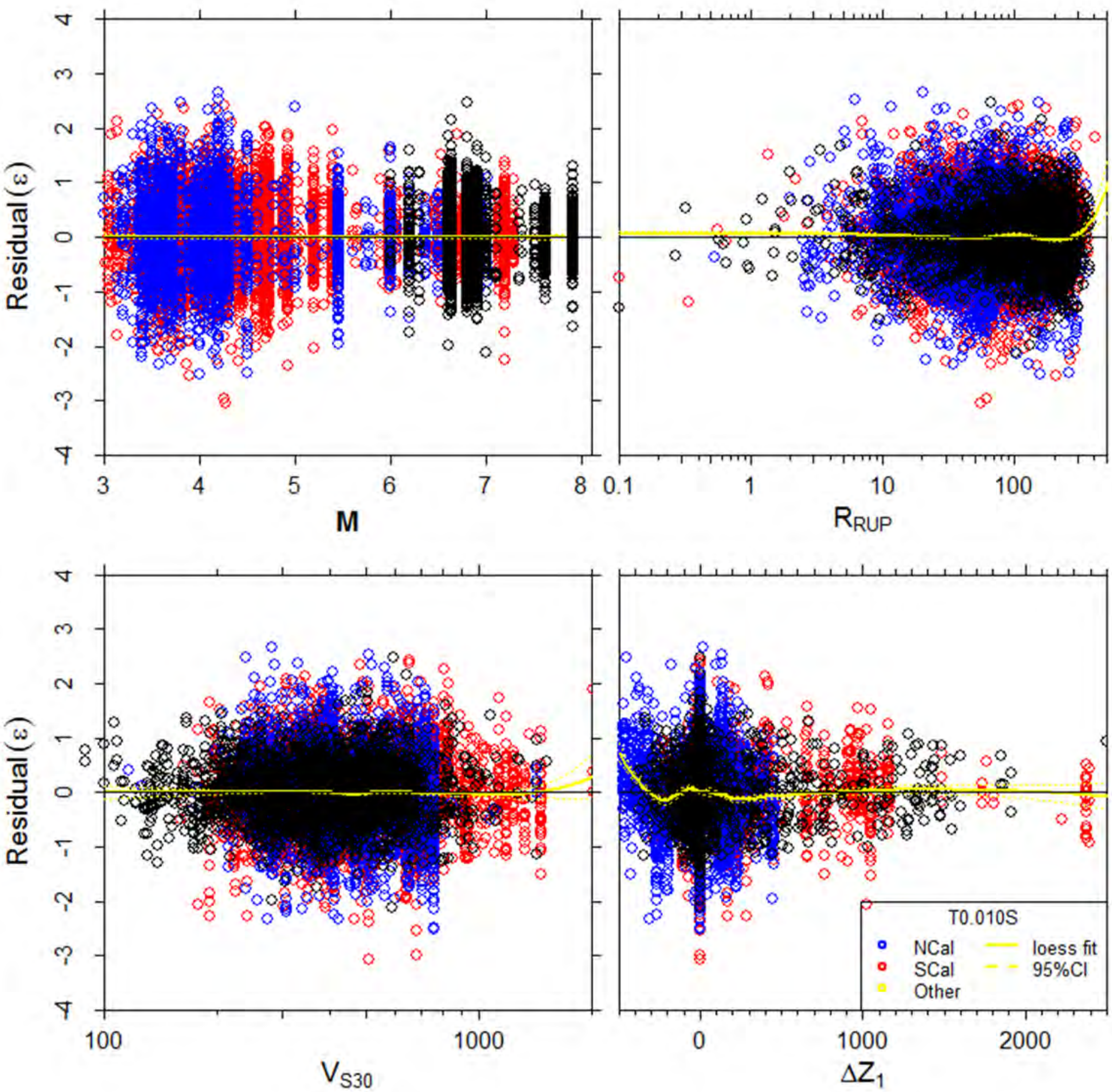

Figure 5.6 **Within-earthquake residuals for spectral period of 0.01 second (*pga*) plotted against M, R_{RUP}, V_{S30}, and $\Delta Z_{1.0}$**

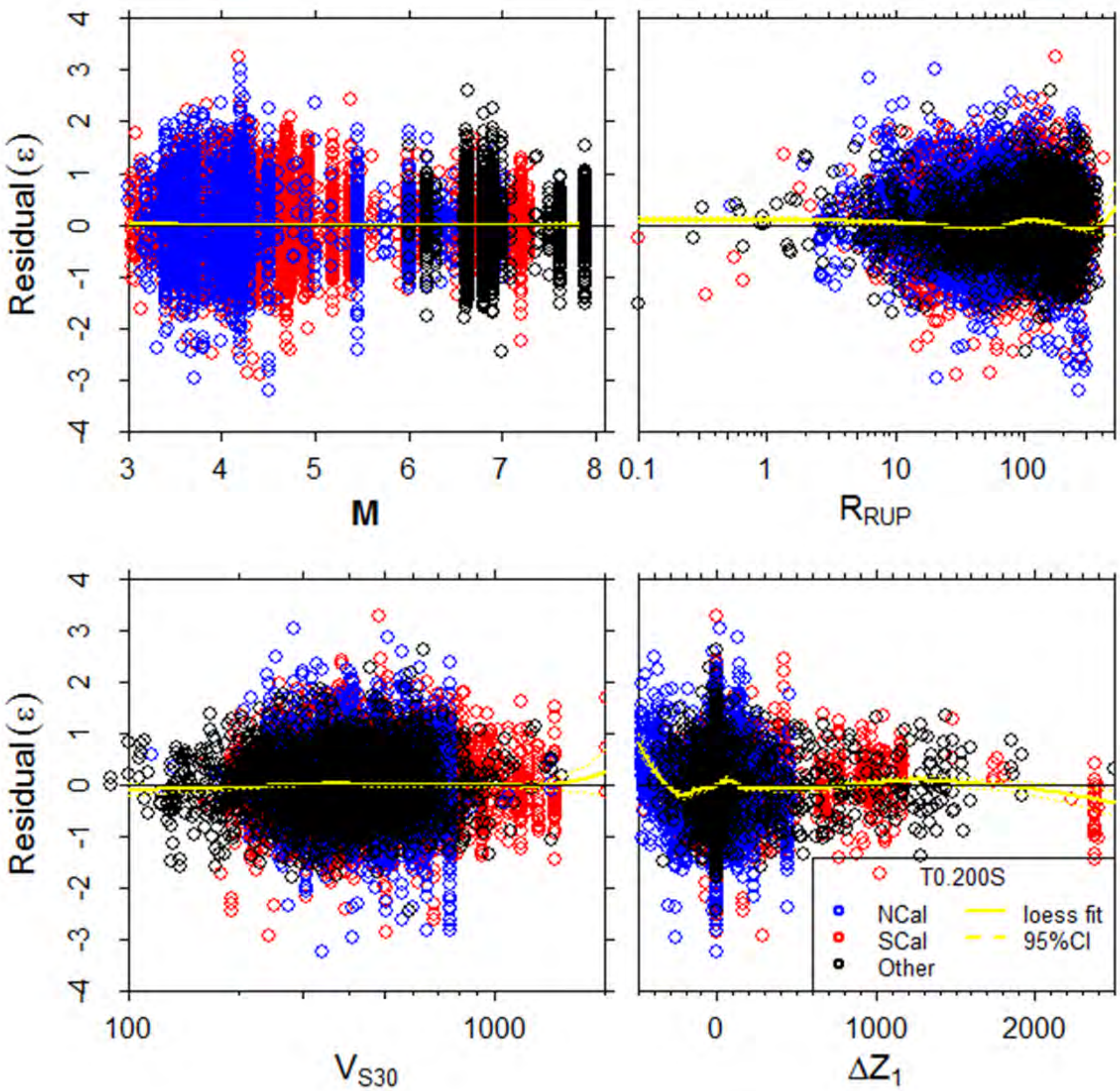

Figure 5.7 **Within-earthquake residuals for spectral period of 0.2 sec plotted against M, R_{RUP}, V_{S30}, and $\Delta Z_{1.0}$.**

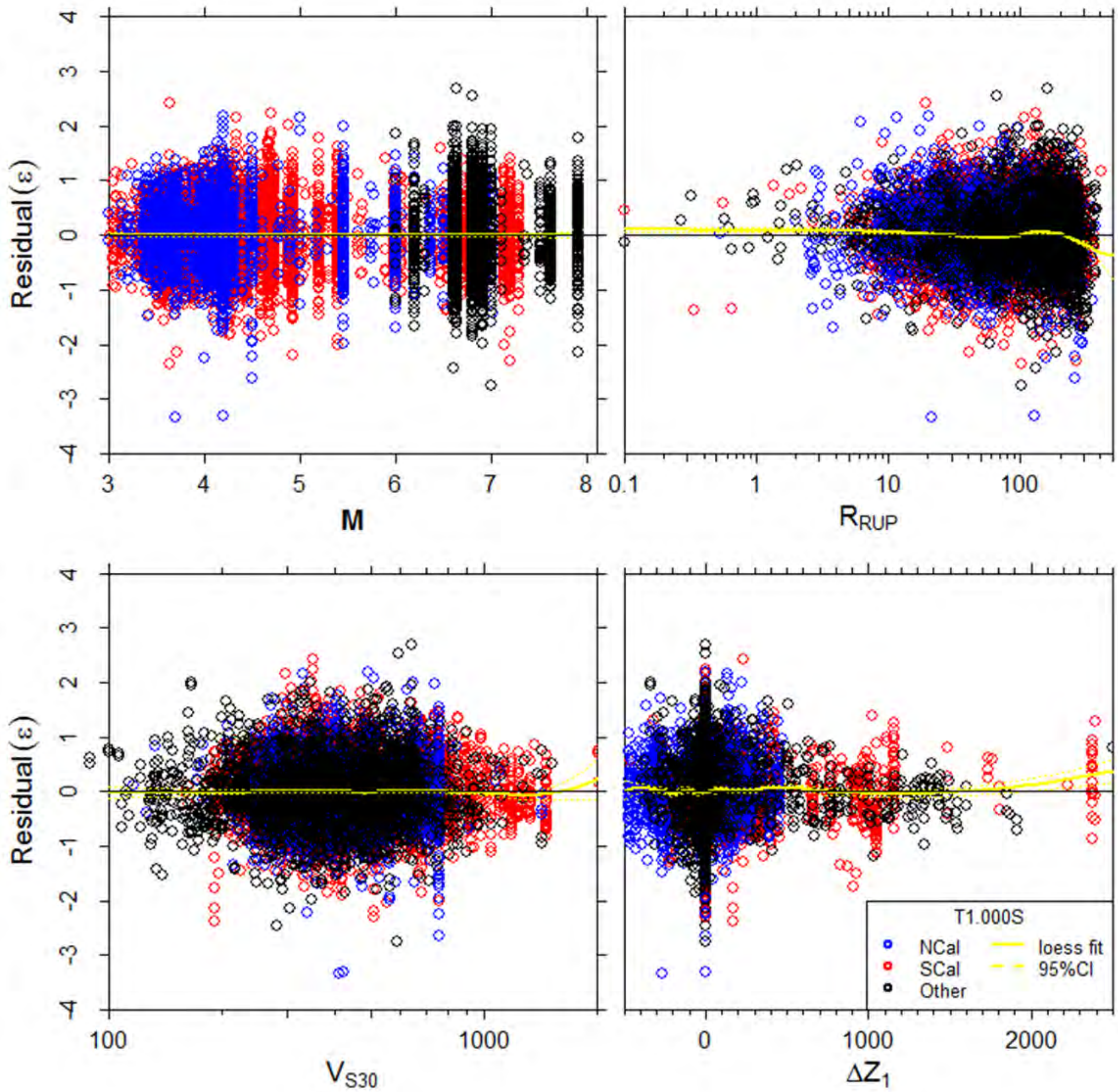

Figure 5.8 Within-earthquake residuals for spectral period of 1 sec plotted against M, R_{RUP}, V_{S30}, and $\Delta Z_{1.0}$.

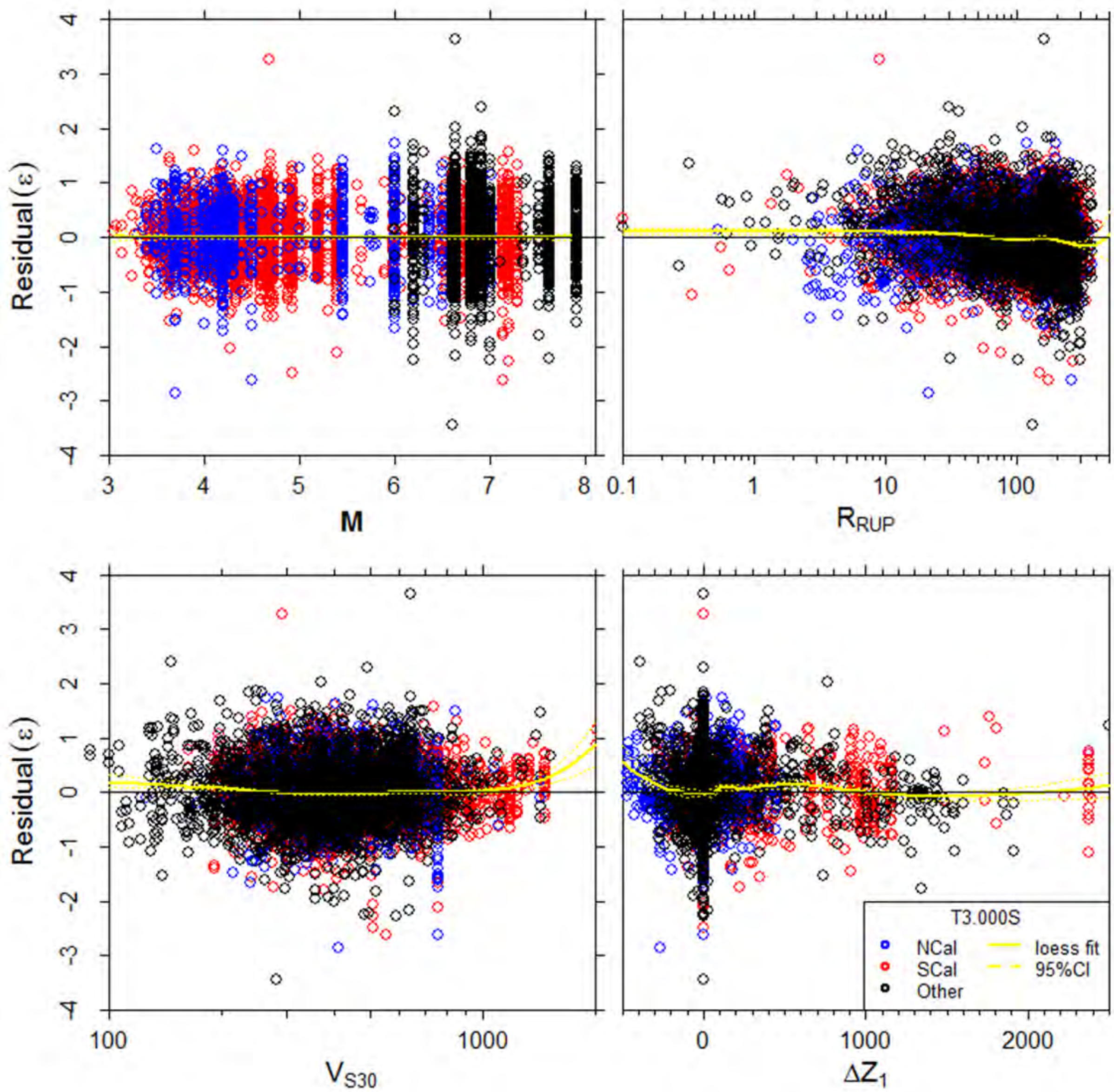

Figure 5.9 Within-earthquake residuals for spectral period of 3 sec plotted against M, R_{RUP}, V_{S30}, and $\Delta Z_{1.0}$.

The adequacy of not including effects of nonlinear soil response in our GMPE is demonstrated in Figure 5.10. Data points shown in the figure are T = 0.2 sec within-earthquake residuals from California computed with respect to predictions for the reference condition of V_{S30} = 1130 m/sec. These residuals can be loosely interpreted as empirical soil amplification relative to the event-specific median reference motion [$y_{ref}\exp(\eta)$]. The empirical amplification factors are grouped by the levels of reference motion and plotted against V_{S30} in Figure 5.10. Linear soil response predicted by our vertical GMPE is shown in the figure as the thick solid red curve. The good match between the linear soil response model and the empirical soil amplification for all levels of loading confirms the adequacy of excluding nonlinear soil response term in our vertical GMPE.

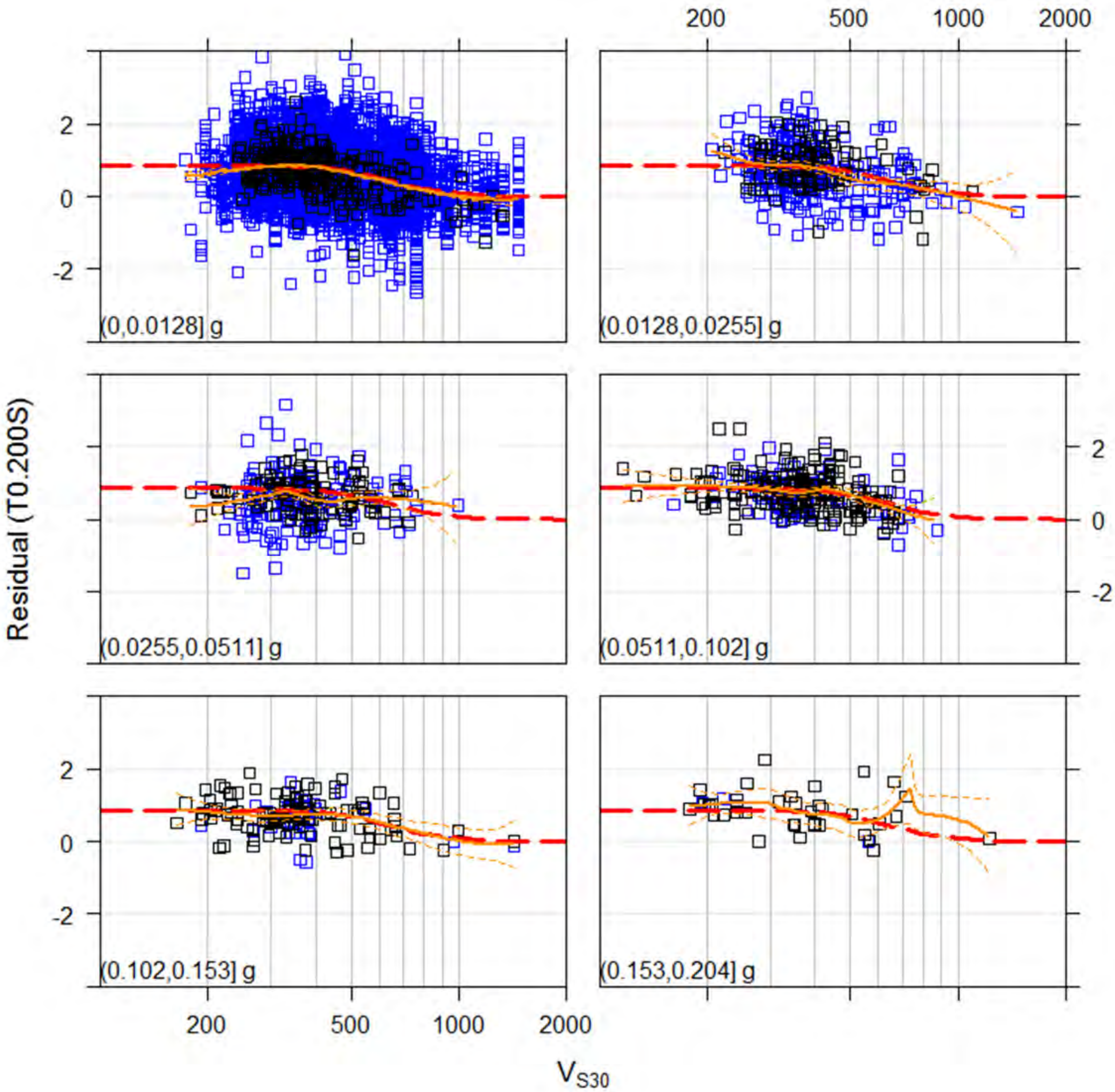

Figure 5.10 **Within-earthquake residuals (empirical soil amplification factor) plotted versus V_{S30}. These residuals are for California data and computed with respect to predictions for reference condition of 1130 m/sec condition. Data from M > 6 earthquakes are shown in black, and data from M < 6 are in blue. Each panel contains residuals for the range of reference motion indicated in the bottom left corner. A smoothed trend (computed using the local linear regression method loess in statistical package R) is shown as the solid orange line. For comparison, linear soil response predicted by our vertical GMPE is shows as the long dash (red) curve.**

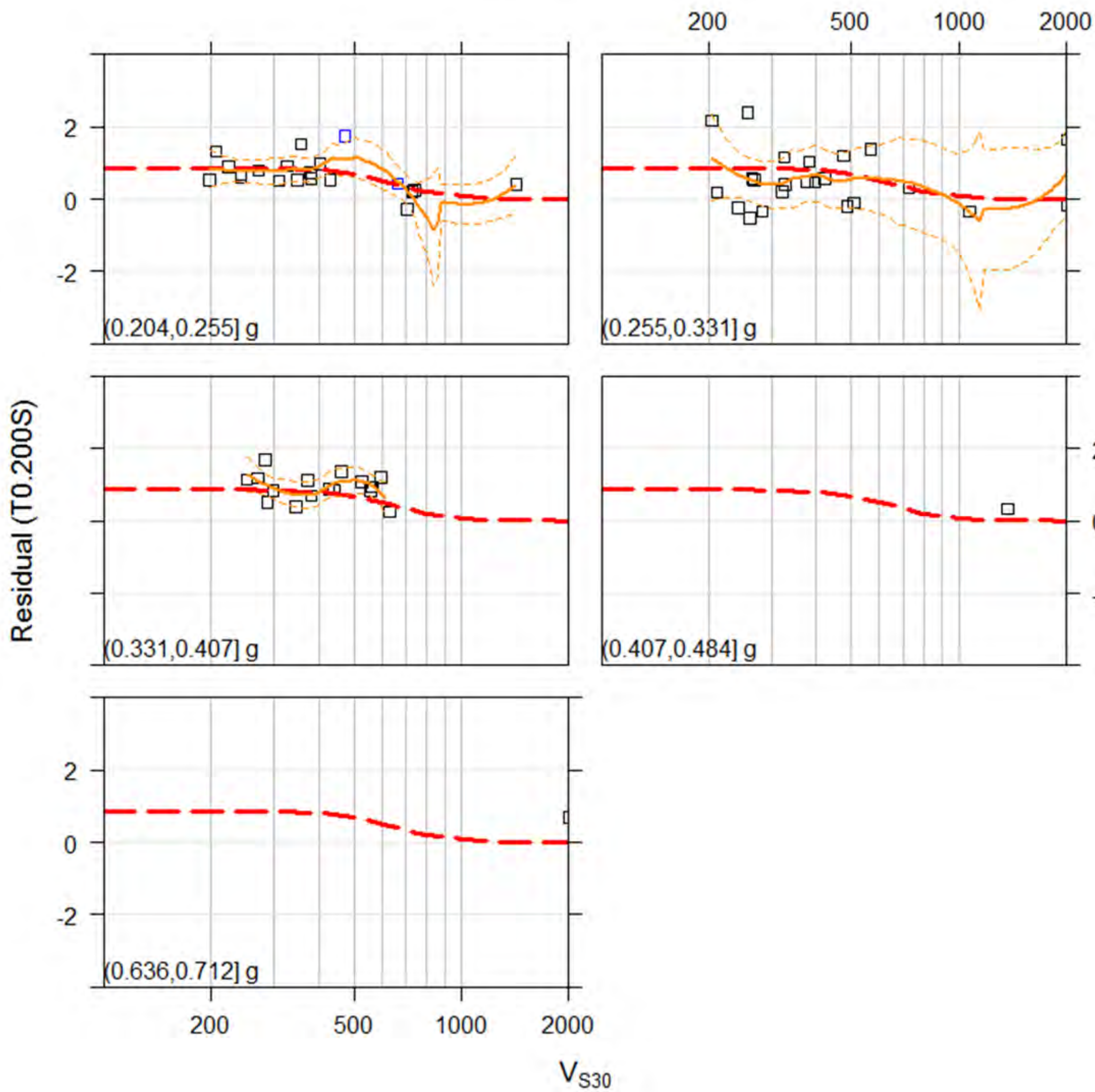

Figure 5.10 Continued.

5.4.3 Vertical-To-Horizontal Spectral Ratio

The left panels of Figure 5.11 compare the predicted median motions between horizontal and vertical components at distances of 1 and 20 km from strike-slip earthquakes on rock condition of V_{S30} = 760 m/sec. For these predictions, we set ΔZ_{TOR} and $\Delta Z_{1.0}$ to 0. The right panels of Figure 5.11 show the V/H ratio of median predictions. Figure 5.12 shows similar comparisons but for two HW sites of 45°-dipping reverse earthquakes. Figures 5.13 and 5.14 compare predicted median response spectra for V_{S30} = 450 and 250 m/sec, respectively.

Difference in additive distance between vertical and horizontal component is partly responsible for creating the near-source (1 km distance) shape of V/H spectral ratio shown in these figures. The peak of V/H ratio occurs near $T = 0.05$ sec and its amplitude increases as V_{S30} decreases, both features are well-known from past studies.

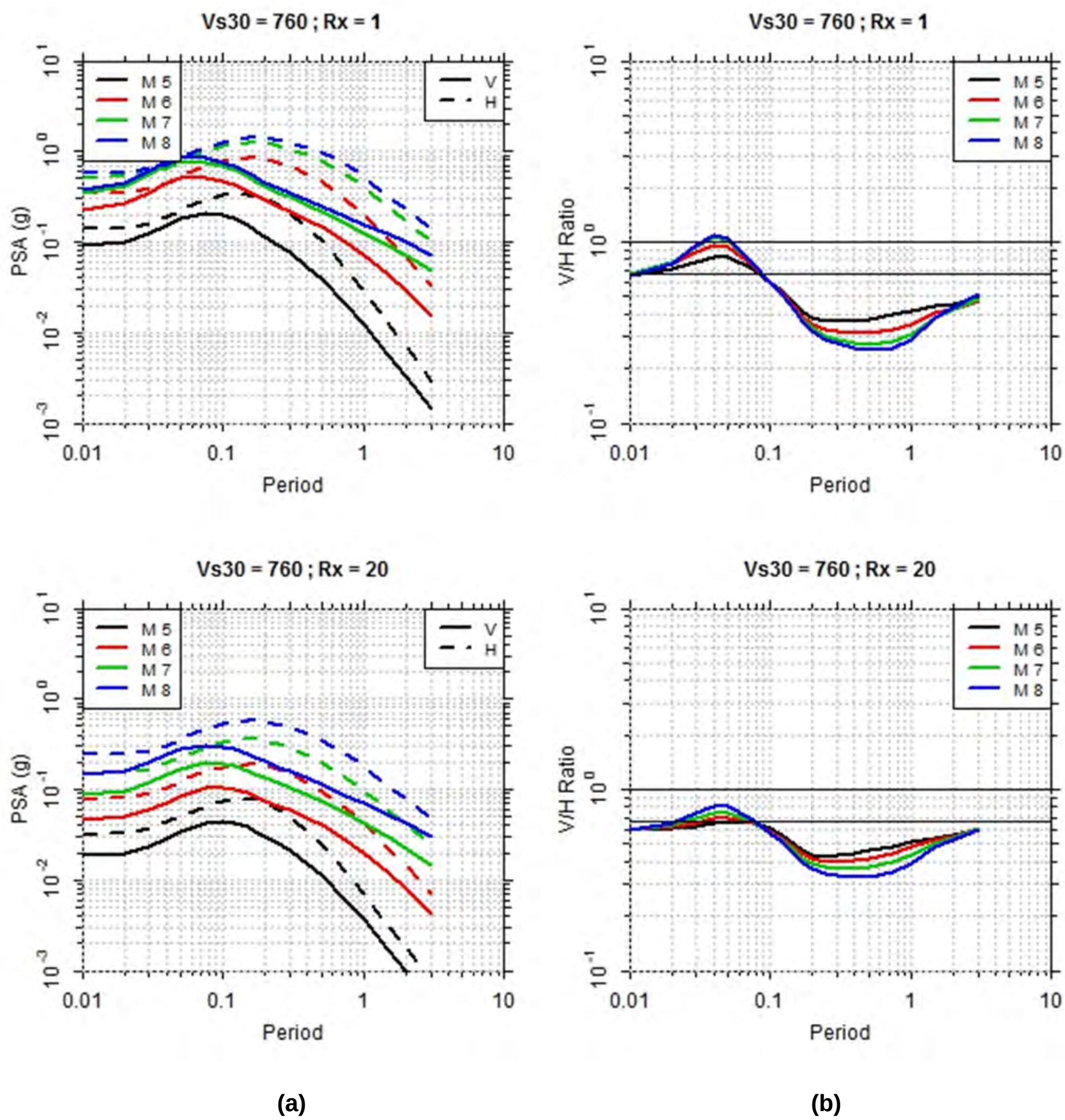

Figure 5.11 (a) Predicted median motions by the vertical GMPE developed in this study and our 2013 horizontal GMPE for vertical strike-slip earthquakes on rock (V_{S30} = 760 m/sec) at R_X distances of 1 and 20 km; and (b) V/H ratios of median motions.

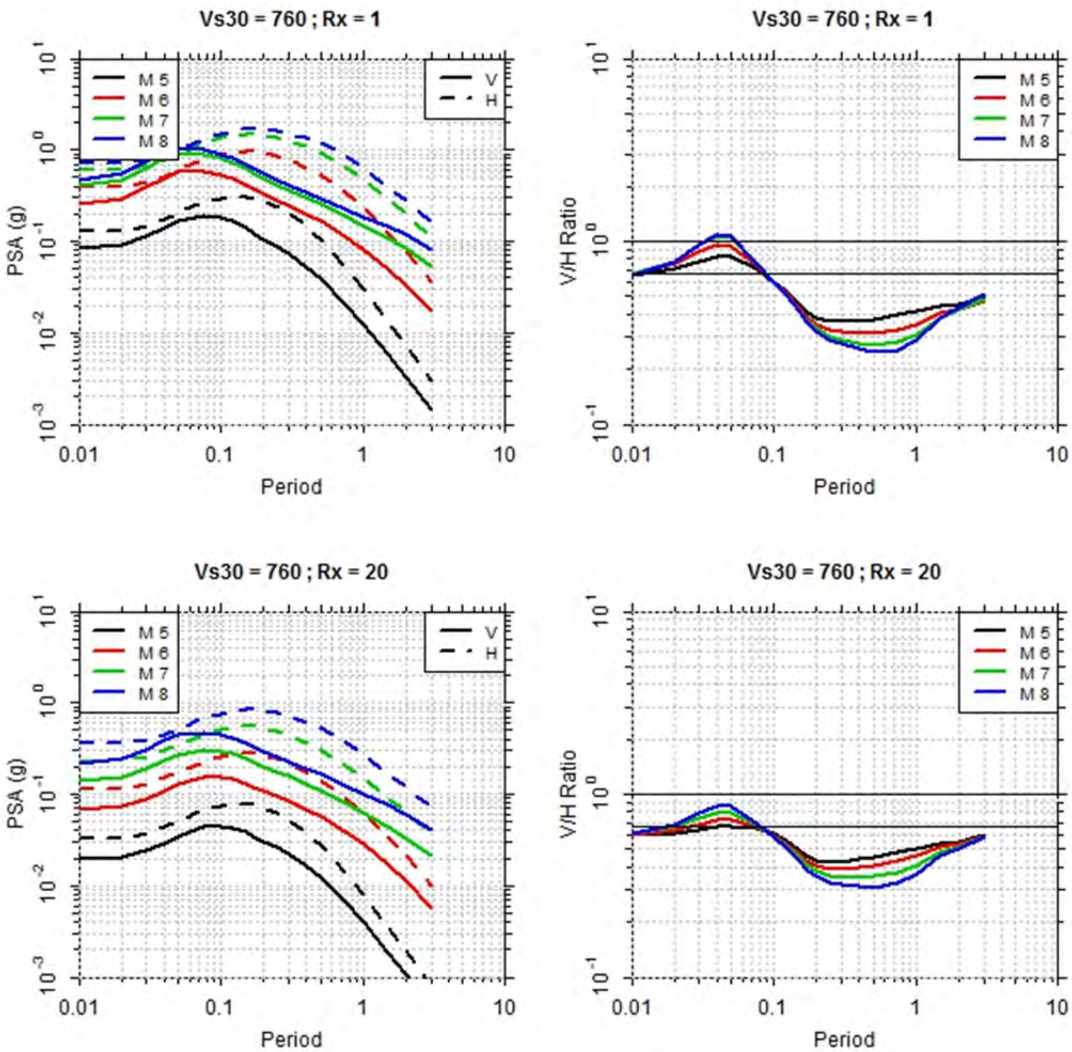

(a) (b)

Figure 5.12 **(a) Predicted median motions by the vertical GMPE developed in this study and our 2013 horizontal GMPE for 45° dipping reverse earthquakes on rock (V_{S30} = 760 m/sec) at R_X distances of 1 and 20 km on hanging wall; and (b) V/H ratios of median motions.**

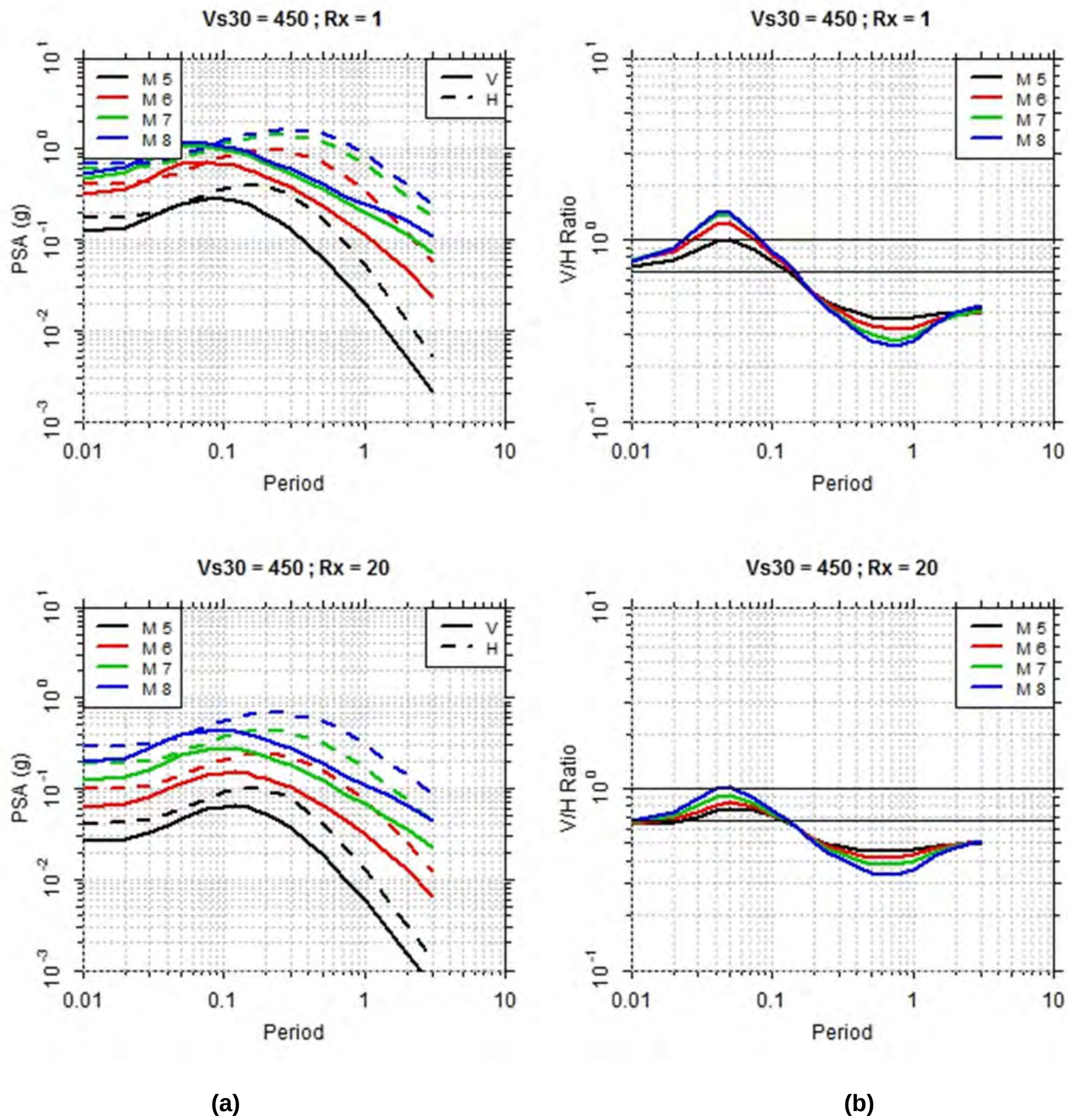

Figure 5.13 **(a) Predicted median motions by the vertical GMPE developed in this study and our 2013 horizontal GMPE for vertical strike-slip earthquakes on soil (V_{S30} = 450 m/sec) at R_X distances of 1 and 20 km; (b) V/H ratios of median motions.**

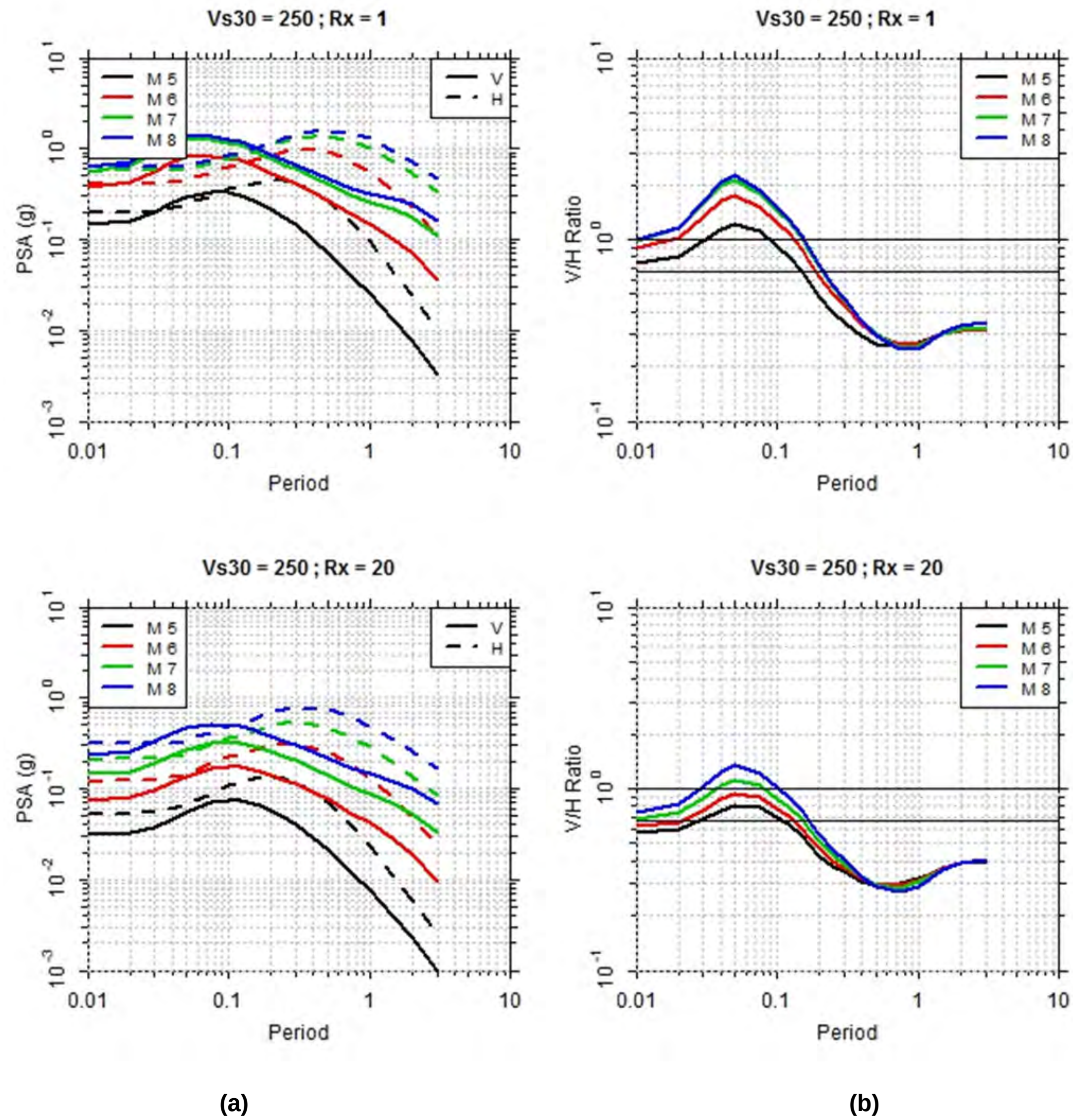

Figure 5.14 **(a) Predicted median motions by the vertical GMPE developed in this study and our 2013 horizontal GMPE for vertical strike-slip earthquakes on soil (V_{S30} = 250 m/sec) at R_X distances of 1 and 20 km; and (b) V/H ratios of median motions.**

5.5 MODEL APPLICABILITY

Since the vertical GMPE developed in this study largely mirrored our 2013 horizontal GMPE in terms of data and functional form, the applicable ranges of the vertical GMPE also mirrored our recommendations for the 2013 horizontal GMPE. The developed vertical GMPE is considered to be applicable for estimating pseudo-spectral accelerations (5% of critical damping) and peak motions for earthquakes in active tectonic regions in which the following conditions apply:

- $3.5 \leq \mathbf{M} \leq 8.5$ for strike-slip earthquakes
- $3.5 \leq \mathbf{M} \leq 8.0$ for reverse and normal faulting earthquake
- $Z_{TOR} \leq 20$ km
- $0 \leq R_{RUP} \leq 300$ km
- 180 m/sec $\leq V_{S30} \leq$ 1500 m/sec

Because all **M** < 6 earthquakes were from California, our GMPE may not be applicable to small-to-moderate earthquakes in other active tectonic regions. For application in other active tectonic regions where earthquakes at distances greater than about 50 km contribute significantly to the hazard, adjustments to the $\gamma\,(\mathbf{M},T)$ model may be warranted. These adjustments can be made using the hybrid approach developed by Campbell [2003]. In making such adjustments, we stress the need for the user to obtain estimates of Q for the two regions that are based on geometric spreading models consistent with the one used in this study.

As the rock velocity increases we expect shallow crustal damping (i.e., kappa) to decrease, resulting in increases in high-frequency motion. Data for such sites were not sampled in the NGA-West2 database in sufficient quantity to allow us to reliably estimate this effect, and it was thus not included in the vertical model. However, users should consider such effects if the model is applied to sites with V_{S30} greater than 1500 m/sec.

The updated model was developed using recordings from earthquakes with a maximum Z_{TOR} of 20 km. Furthermore, the Z_{TOR} – **M** data suggest that the applicable range of Z_{TOR} should be narrowing with increasing **M**. We do not recommend using large Z_{TOR} value beyond what was represented in the NGA-West2 database.

The majority of $Z_{1.0}$ data used in our model were obtained from 3D velocity models for southern California, the San Francisco Bay Area, and Japan. When applying our GMPE to these three regions, the same 3D velocity models should be used to obtain site $Z_{1.0}$. Information on accessing these 3D models is provided in Ancheta et al. [2013]. For application to a site not covered by these velocity models and without other information to determine the site $Z_{1.0}$, we recommend using $\Delta Z_{1.0} = 0$, preferably with an increase in aleatory variability too. When applying our GMPE to a site whose $Z_{1.0}$ is much smaller than the average $Z_{1.0}$ (a large negative $\Delta Z_{1.0}$), the predicted motions should be checked to ensure that they are not lower than the predictions for reference condition of V_{S30}=1130 m/sec.

REFERENCES

Ancheta T.D., Darragh R.B., Stewart J.P., Seyhan E., Silva W.J., Chiou B.S.-J., Wooddell K.E., Graves R.W., Kottke A.R., Boore D.M., Kishida T., Donahue J.L (2013). PEER NGA-West2 database, *PEER Report 2013/03*, Pacific Earthquake Engineering Research Center, University of California, Berkeley, CA.

Bozorgnia, Y., Abrahamson N.A., Al Atik, L., Ancheta T.D., Atkinson G.M., Baker J.W., Baltay A., Boore D.M., Campbell K.W., Chiou B.S.-J., Darragh R., Day S. Donahue J., Graves R.W., Gregor N., Hanks T., Idriss, I.M., Kamai R., Kishida T., Kottke A., Mahin S.A., Rezaeian S., Rowshandel B., Seyhan E., Shahi S., Shantz T., Silva W.J., Spudich P., Stewart J.P., Watson-Lamprey J., Wooddell K.E., Youngs R.R. (2014). NGA-West2 research project, *Earthq, Spectra*, submitted..

Campbell K.W. (2003). Prediction of strong ground motion using the hybrid empirical method and its use in the development of ground motion (attenuation) relations in eastern North America, *Bull. Seismol. Soc. Am.* 93, 1012–1033.

Chiou B.S.-J., Youngs R.R. (2012). Updating the Chiou and Youngs NGA model: regionalization of anelastic attenuation, *Proceedings*, *15th World Conference on Earthquake Engineering*, Lisbon, Portugal.

Chiou B.S.-J., Youngs R.R. (2013). Update of the Chiou and Youngs NGA ground motion model for average horizontal component of peak ground motion and response spectra, *PEER Report 2013/07*, Pacific Earthquake Engineering Research Center, University of California, Berkeley, CA.

Donahue J.L., Abrahamson N.A. (2013). Simulation-based hanging wall effects model, *PEER Report 2013/14*, Pacific Earthquake Engineering Research Center, University of California, Berkeley, CA).

Kamai R. (2012). Progress report on nonlinear vertical site amplification model, Pacific Earthquake Engineering Research Center, University of California, Berkeley, CA.

R Development Core Team (2012). R: A language and environment for statistical computing, R Foundation for Statistical Computing, Vienna, Austria. ISBN 3-900051-07-0, URL http://www.R-project.org.

PEER REPORTS

PEER reports are available as a free PDF download from http://peer.berkeley.edu/publications/peer_reports_complete.html. Printed hard copies of PEER reports can be ordered directly from our printer by following the instructions at http://peer.berkeley.edu/publications/peer_reports.html. For other related questions about the PEER Report Series, contact the Pacific Earthquake Engineering Research Center, 325 Davis Hall mail code 1792, Berkeley, CA 94720. Tel.: (510) 642-3437; Fax: (510) 665-1655; Email: peer_editor@berkeley.edu

PEER 2013/24 *NGA-West2 Ground Motion Prediction Equations for Vertical Ground Motions.* September 2013.

PEER 2013/23 *Coordinated Planning and Preparedness for Fire Following Major Earthquakes.* Charles Scawthorn. November 2013.

PEER 2013/22 *GEM-PEER Task 3 Project: Selection of a Global Set of Ground Motion Prediction Equations.* Jonathan P. Stewart, John Douglas, Mohammad B. Javanbarg, Carola Di Alessandro, Yousef Bozorgnia, Norman A. Abrahamson, David M. Boore, Kenneth W. Campbell, Elise Delavaud, Mustafa Erdik and Peter J. Stafford. December 2013.

PEER 2013/21 *Seismic Design and Performance of Bridges with Columns on Rocking Foundations.* Grigorios Antonellis and Marios Panagiotou. September 2013.

PEER 2013/20 *Experimental and Analytical Studies on the Seismic Behavior of Conventional and Hybrid Braced Frames.* Jiun-Wei Lai and Stephen A. Mahin. September 2013.

PEER 2013/19 *Toward Resilient Communities: A Performance-Based Engineering Framework for Design and Evaluation of the Built Environment.* Michael William Mieler, Bozidar Stojadinovic, Robert J. Budnitz, Stephen A. Mahin and Mary C. Comerio. September 2013.

PEER 2013/18 *Identification of Site Parameters that Improve Predictions of Site Amplification.* Ellen M. Rathje and Sara Navidi. July 2013.

PEER 2013/17 *Response Spectrum Analysis of Concrete Gravity Dams Including Dam-Water-Foundation Interaction.* Arnkjell Løkke and Anil K. Chopra. July 2013.

PEER 2013/16 *Effect of hoop reinforcement spacing on the cyclic response of large reinforced concrete special moment frame beams.* Marios Panagiotou, Tea Visnjic, Grigorios Antonellis, Panagiotis Galanis, and Jack P. Moehle. June 2013.

PEER 2013/15 *A Probabilistic Framework to Include the Effects of Near-Fault Directivity in Seismic Hazard Assessment.* Shrey Kumar Shahi, Jack W. Baker. October 2013.

PEER 2013/14 *Hanging-Wall Scaling using Finite-Fault Simulations.* Jennifer L. Donahue and Norman A. Abrahamson. September 2013.

PEER 2013/13 *Semi-Empirical Nonlinear Site Amplification and its Application in NEHRP Site Factors.* Jonathan P. Stewart and Emel Seyhan. November 2013.

PEER 2013/12 *Nonlinear Horizontal Site Response for the NGA-West2 Project.* Ronnie Kamai, Norman A. Abramson, Walter J. Silva. May 2013.

PEER 2013/11 *Epistemic Uncertainty for NGA-West2 Models.* Linda Al Atik and Robert R. Youngs. May 2013.

PEER 2013/10 *NGA-West 2 Models for Ground-Motion Directionality.* Shrey K. Shahi and Jack W. Baker. May 2013.

PEER 2013/09 *Final Report of the NGA-West2 Directivity Working Group.* Paul Spudich, Jeffrey R. Bayless, Jack W. Baker, Brian S.J. Chiou, Badie Rowshandel, Shrey Shahi, and Paul Somerville. May 2013.

PEER 2013/08 *NGA-West2 Model for Estimating Average Horizontal Values of Pseudo-Absolute Spectral Accelerations Generated by Crustal Earthquakes.* I. M. Idriss. May 2013.

PEER 2013/07 *Update of the Chiou and Youngs NGA Ground Motion Model for Average Horizontal Component of Peak Ground Motion and Response Spectra.* Brian Chiou and Robert Youngs. May 2013.

PEER 2013/06 *NGA-West2 Campbell-Bozorgnia Ground Motion Model for the Horizontal Components of PGA, PGV, and 5%-Damped Elastic Pseudo-Acceleration Response Spectra for Periods Ranging from 0.01 to 10 sec.* Kenneth W. Campbell and Yousef Bozorgnia. May 2013.

PEER 2013/05 *NGA-West 2 Equations for Predicting Response Spectral Accelerations for Shallow Crustal Earthquakes.* David M. Boore, Jonathan P. Stewart, Emel Seyhan, Gail M. Atkinson. May 2013.

PEER 2013/04 *Update of the AS08 Ground-Motion Prediction Equations Based on the NGA-West2 Data Set.* Norman Abrahamson, Walter Silva, and Ronnie Kamai. May 2013.

PEER 2013/03 *PEER NGA-West2 Database.* Timothy D. Ancheta, Robert B. Darragh, Jonathan P. Stewart, Emel Seyhan, Walter J. Silva, Brian S.J. Chiou, Katie E. Wooddell, Robert W. Graves, Albert R. Kottke, David M. Boore, Tadahiro Kishida, and Jennifer L. Donahue. May 2013.

PEER 2013/02 *Hybrid Simulation of the Seismic Response of Squat Reinforced Concrete Shear Walls.* Catherine A. Whyte and Bozidar Stojadinovic. May 2013.

PEER 2013/01 *Housing Recovery in Chile: A Qualitative Mid-program Review.* Mary C. Comerio. February 2013.

PEER 2012/08 *Guidelines for Estimation of Shear Wave Velocity.* Bernard R. Wair, Jason T. DeJong, and Thomas Shantz. December 2012.

PEER 2012/07 *Earthquake Engineering for Resilient Communities: 2012 PEER Internship Program Research Report Collection.* Heidi Tremayne (Editor), Stephen A. Mahin (Editor), Collin Anderson, Dustin Cook, Michael Erceg, Carlos Esparza, Jose Jimenez, Dorian Krausz, Andrew Lo, Stephanie Lopez, Nicole McCurdy, Paul Shipman, Alexander Strum, Eduardo Vega. December 2012.

PEER 2012/06 *Fragilities for Precarious Rocks at Yucca Mountain.* Matthew D. Purvance, Rasool Anooshehpoor, and James N. Brune. December 2012.

PEER 2012/05 *Development of Simplified Analysis Procedure for Piles in Laterally Spreading Layered Soils.* Christopher R. McGann, Pedro Arduino, and Peter Mackenzie–Helnwein. December 2012.

PEER 2012/04 *Unbonded Pre-Tensioned Columns for Bridges in Seismic Regions.* Phillip M. Davis, Todd M. Janes, Marc O. Eberhard, and John F. Stanton. December 2012.

PEER 2012/03 *Experimental and Analytical Studies on Reinforced Concrete Buildings with Seismically Vulnerable Beam-Column Joints.* Sangjoon Park and Khalid M. Mosalam. October 2012.

PEER 2012/02 *Seismic Performance of Reinforced Concrete Bridges Allowed to Uplift during Multi-Directional Excitation.* Andres Oscar Espinoza and Stephen A. Mahin. July 2012.

PEER 2012/01 *Spectral Damping Scaling Factors for Shallow Crustal Earthquakes in Active Tectonic Regions.* Sanaz Rezaeian, Yousef Bozorgnia, I. M. Idriss, Kenneth Campbell, Norman Abrahamson, and Walter Silva. July 2012.

PEER 2011/10 *Earthquake Engineering for Resilient Communities: 2011 PEER Internship Program Research Report Collection.* Eds. Heidi Faison and Stephen A. Mahin. December 2011.

PEER 2011/09 *Calibration of Semi-Stochastic Procedure for Simulating High-Frequency Ground Motions.* Jonathan P. Stewart, Emel Seyhan, and Robert W. Graves. December 2011.

PEER 2011/08 *Water Supply in regard to Fire Following Earthquake.* Charles Scawthorn. November 2011.

PEER 2011/07 *Seismic Risk Management in Urban Areas. Proceedings of a U.S.-Iran-Turkey Seismic Workshop.* September 2011.

PEER 2011/06 *The Use of Base Isolation Systems to Achieve Complex Seismic Performance Objectives.* Troy A. Morgan and Stephen A. Mahin. July 2011.

PEER 2011/05 *Case Studies of the Seismic Performance of Tall Buildings Designed by Alternative Means.* Task 12 Report for the Tall Buildings Initiative. Jack Moehle, Yousef Bozorgnia, Nirmal Jayaram, Pierson Jones, Mohsen Rahnama, Nilesh Shome, Zeynep Tuna, John Wallace, Tony Yang, and Farzin Zareian. July 2011.

PEER 2011/04 *Recommended Design Practice for Pile Foundations in Laterally Spreading Ground.* Scott A. Ashford, Ross W. Boulanger, and Scott J. Brandenberg. June 2011.

PEER 2011/03 *New Ground Motion Selection Procedures and Selected Motions for the PEER Transportation Research Program.* Jack W. Baker, Ting Lin, Shrey K. Shahi, and Nirmal Jayaram. March 2011.

PEER 2011/02 *A Bayesian Network Methodology for Infrastructure Seismic Risk Assessment and Decision Support.* Michelle T. Bensi, Armen Der Kiureghian, and Daniel Straub. March 2011.

PEER 2011/01 *Demand Fragility Surfaces for Bridges in Liquefied and Laterally Spreading Ground.* Scott J. Brandenberg, Jian Zhang, Pirooz Kashighandi, Yili Huo, and Minxing Zhao. March 2011.

PEER 2010/05 *Guidelines for Performance-Based Seismic Design of Tall Buildings.* Developed by the Tall Buildings Initiative. November 2010.

PEER 2010/04 *Application Guide for the Design of Flexible and Rigid Bus Connections between Substation Equipment Subjected to Earthquakes.* Jean-Bernard Dastous and Armen Der Kiureghian. September 2010.

PEER 2010/03 *Shear Wave Velocity as a Statistical Function of Standard Penetration Test Resistance and Vertical Effective Stress at Caltrans Bridge Sites.* Scott J. Brandenberg, Naresh Bellana, and Thomas Shantz. June 2010.

PEER 2010/02 *Stochastic Modeling and Simulation of Ground Motions for Performance-Based Earthquake Engineering.* Sanaz Rezaeian and Armen Der Kiureghian. June 2010.

PEER 2010/01 *Structural Response and Cost Characterization of Bridge Construction Using Seismic Performance Enhancement Strategies.* Ady Aviram, Božidar Stojadinović, Gustavo J. Parra-Montesinos, and Kevin R. Mackie. March 2010.

PEER 2009/03 *The Integration of Experimental and Simulation Data in the Study of Reinforced Concrete Bridge Systems Including Soil-Foundation-Structure Interaction.* Matthew Dryden and Gregory L. Fenves. November 2009.

PEER 2009/02 *Improving Earthquake Mitigation through Innovations and Applications in Seismic Science, Engineering, Communication, and Response. Proceedings of a U.S.-Iran Seismic Workshop.* October 2009.

PEER 2009/01 *Evaluation of Ground Motion Selection and Modification Methods: Predicting Median Interstory Drift Response of Buildings.* Curt B. Haselton, Ed. June 2009.

PEER 2008/10 *Technical Manual for Strata.* Albert R. Kottke and Ellen M. Rathje. February 2009.

PEER 2008/09 *NGA Model for Average Horizontal Component of Peak Ground Motion and Response Spectra.* Brian S.-J. Chiou and Robert R. Youngs. November 2008.

PEER 2008/08 *Toward Earthquake-Resistant Design of Concentrically Braced Steel Structures.* Patxi Uriz and Stephen A. Mahin. November 2008.

PEER 2008/07 *Using OpenSees for Performance-Based Evaluation of Bridges on Liquefiable Soils.* Stephen L. Kramer, Pedro Arduino, and HyungSuk Shin. November 2008.

PEER 2008/06 *Shaking Table Tests and Numerical Investigation of Self-Centering Reinforced Concrete Bridge Columns.* Hyung IL Jeong, Junichi Sakai, and Stephen A. Mahin. September 2008.

PEER 2008/05 *Performance-Based Earthquake Engineering Design Evaluation Procedure for Bridge Foundations Undergoing Liquefaction-Induced Lateral Ground Displacement.* Christian A. Ledezma and Jonathan D. Bray. August 2008.

PEER 2008/04 *Benchmarking of Nonlinear Geotechnical Ground Response Analysis Procedures.* Jonathan P. Stewart, Annie On-Lei Kwok, Yousseff M. A. Hashash, Neven Matasovic, Robert Pyke, Zhiliang Wang, and Zhaohui Yang. August 2008.

PEER 2008/03 *Guidelines for Nonlinear Analysis of Bridge Structures in California.* Ady Aviram, Kevin R. Mackie, and Božidar Stojadinović. August 2008.

PEER 2008/02 *Treatment of Uncertainties in Seismic-Risk Analysis of Transportation Systems.* Evangelos Stergiou and Anne S. Kiremidjian. July 2008.

PEER 2008/01 *Seismic Performance Objectives for Tall Buildings.* William T. Holmes, Charles Kircher, William Petak, and Nabih Youssef. August 2008.

PEER 2007/12 *An Assessment to Benchmark the Seismic Performance of a Code-Conforming Reinforced Concrete Moment-Frame Building.* Curt Haselton, Christine A. Goulet, Judith Mitrani-Reiser, James L. Beck, Gregory G. Deierlein, Keith A. Porter, Jonathan P. Stewart, and Ertugrul Taciroglu. August 2008.

PEER 2007/11 *Bar Buckling in Reinforced Concrete Bridge Columns.* Wayne A. Brown, Dawn E. Lehman, and John F. Stanton. February 2008.

PEER 2007/10 *Computational Modeling of Progressive Collapse in Reinforced Concrete Frame Structures.* Mohamed M. Talaat and Khalid M. Mosalam. May 2008.

PEER 2007/09 *Integrated Probabilistic Performance-Based Evaluation of Benchmark Reinforced Concrete Bridges.* Kevin R. Mackie, John-Michael Wong, and Božidar Stojadinović. January 2008.

PEER 2007/08 *Assessing Seismic Collapse Safety of Modern Reinforced Concrete Moment-Frame Buildings.* Curt B. Haselton and Gregory G. Deierlein. February 2008.

PEER 2007/07 *Performance Modeling Strategies for Modern Reinforced Concrete Bridge Columns.* Michael P. Berry and Marc O. Eberhard. April 2008.

PEER 2007/06 *Development of Improved Procedures for Seismic Design of Buried and Partially Buried Structures.* Linda Al Atik and Nicholas Sitar. June 2007.

PEER 2007/05 *Uncertainty and Correlation in Seismic Risk Assessment of Transportation Systems.* Renee G. Lee and Anne S. Kiremidjian. July 2007.

PEER 2007/04 *Numerical Models for Analysis and Performance-Based Design of Shallow Foundations Subjected to Seismic Loading.* Sivapalan Gajan, Tara C. Hutchinson, Bruce L. Kutter, Prishati Raychowdhury, José A. Ugalde, and Jonathan P. Stewart. May 2008.

PEER 2007/03 *Beam-Column Element Model Calibrated for Predicting Flexural Response Leading to Global Collapse of RC Frame Buildings.* Curt B. Haselton, Abbie B. Liel, Sarah Taylor Lange, and Gregory G. Deierlein. May 2008.

PEER 2007/02 *Campbell-Bozorgnia NGA Ground Motion Relations for the Geometric Mean Horizontal Component of Peak and Spectral Ground Motion Parameters.* Kenneth W. Campbell and Yousef Bozorgnia. May 2007.

PEER 2007/01 *Boore-Atkinson NGA Ground Motion Relations for the Geometric Mean Horizontal Component of Peak and Spectral Ground Motion Parameters.* David M. Boore and Gail M. Atkinson. May. May 2007.

PEER 2006/12 *Societal Implications of Performance-Based Earthquake Engineering.* Peter J. May. May 2007.

PEER 2006/11 *Probabilistic Seismic Demand Analysis Using Advanced Ground Motion Intensity Measures, Attenuation Relationships, and Near-Fault Effects.* Polsak Tothong and C. Allin Cornell. March 2007.

PEER 2006/10 *Application of the PEER PBEE Methodology to the I-880 Viaduct.* Sashi Kunnath. February 2007.

PEER 2006/09 *Quantifying Economic Losses from Travel Forgone Following a Large Metropolitan Earthquake.* James Moore, Sungbin Cho, Yue Yue Fan, and Stuart Werner. November 2006.

PEER 2006/08 *Vector-Valued Ground Motion Intensity Measures for Probabilistic Seismic Demand Analysis*. Jack W. Baker and C. Allin Cornell. October 2006.

PEER 2006/07 *Analytical Modeling of Reinforced Concrete Walls for Predicting Flexural and Coupled–Shear-Flexural Responses*. Kutay Orakcal, Leonardo M. Massone, and John W. Wallace. October 2006.

PEER 2006/06 *Nonlinear Analysis of a Soil-Drilled Pier System under Static and Dynamic Axial Loading.* Gang Wang and Nicholas Sitar. November 2006.

PEER 2006/05 *Advanced Seismic Assessment Guidelines.* Paolo Bazzurro, C. Allin Cornell, Charles Menun, Maziar Motahari, and Nicolas Luco. September 2006.

PEER 2006/04 *Probabilistic Seismic Evaluation of Reinforced Concrete Structural Components and Systems.* Tae Hyung Lee and Khalid M. Mosalam. August 2006.

PEER 2006/03 *Performance of Lifelines Subjected to Lateral Spreading.* Scott A. Ashford and Teerawut Juirnarongrit. July 2006.

PEER 2006/02 *Pacific Earthquake Engineering Research Center Highway Demonstration Project.* Anne Kiremidjian, James Moore, Yue Yue Fan, Nesrin Basoz, Ozgur Yazali, and Meredith Williams. April 2006.

PEER 2006/01 *Bracing Berkeley. A Guide to Seismic Safety on the UC Berkeley Campus.* Mary C. Comerio, Stephen Tobriner, and Ariane Fehrenkamp. January 2006.

PEER 2005/16 *Seismic Response and Reliability of Electrical Substation Equipment and Systems.* Junho Song, Armen Der Kiureghian, and Jerome L. Sackman. April 2006.

PEER 2005/15 *CPT-Based Probabilistic Assessment of Seismic Soil Liquefaction Initiation.* R. E. S. Moss, R. B. Seed, R. E. Kayen, J. P. Stewart, and A. Der Kiureghian. April 2006.

PEER 2005/14 *Workshop on Modeling of Nonlinear Cyclic Load-Deformation Behavior of Shallow Foundations.* Bruce L. Kutter, Geoffrey Martin, Tara Hutchinson, Chad Harden, Sivapalan Gajan, and Justin Phalen. March 2006.

PEER 2005/13 *Stochastic Characterization and Decision Bases under Time-Dependent Aftershock Risk in Performance-Based Earthquake Engineering.* Gee Liek Yeo and C. Allin Cornell. July 2005.

PEER 2005/12 *PEER Testbed Study on a Laboratory Building: Exercising Seismic Performance Assessment.* Mary C. Comerio, editor. November 2005.

PEER 2005/11 *Van Nuys Hotel Building Testbed Report: Exercising Seismic Performance Assessment.* Helmut Krawinkler, editor. October 2005.

PEER 2005/10 *First NEES/E-Defense Workshop on Collapse Simulation of Reinforced Concrete Building Structures.* September 2005.

PEER 2005/09 *Test Applications of Advanced Seismic Assessment Guidelines.* Joe Maffei, Karl Telleen, Danya Mohr, William Holmes, and Yuki Nakayama. August 2006.

PEER 2005/08 *Damage Accumulation in Lightly Confined Reinforced Concrete Bridge Columns.* R. Tyler Ranf, Jared M. Nelson, Zach Price, Marc O. Eberhard, and John F. Stanton. April 2006.

PEER 2005/07 *Experimental and Analytical Studies on the Seismic Response of Freestanding and Anchored Laboratory Equipment.* Dimitrios Konstantinidis and Nicos Makris. January 2005.

PEER 2005/06 *Global Collapse of Frame Structures under Seismic Excitations*. Luis F. Ibarra and Helmut Krawinkler. September 2005.

PEER 2005//05 *Performance Characterization of Bench- and Shelf-Mounted Equipment.* Samit Ray Chaudhuri and Tara C. Hutchinson. May 2006.

PEER 2005/04 *Numerical Modeling of the Nonlinear Cyclic Response of Shallow Foundations.* Chad Harden, Tara Hutchinson, Geoffrey R. Martin, and Bruce L. Kutter. August 2005.

PEER 2005/03 *A Taxonomy of Building Components for Performance-Based Earthquake Engineering.* Keith A. Porter. September 2005.

PEER 2005/02 *Fragility Basis for California Highway Overpass Bridge Seismic Decision Making*. Kevin R. Mackie and Božidar Stojadinović. June 2005.

PEER 2005/01 *Empirical Characterization of Site Conditions on Strong Ground Motion.* Jonathan P. Stewart, Yoojoong Choi, and Robert W. Graves. June 2005.

PEER 2004/09 *Electrical Substation Equipment Interaction: Experimental Rigid Conductor Studies.* Christopher Stearns and André Filiatrault. February 2005.

PEER 2004/08 *Seismic Qualification and Fragility Testing of Line Break 550-kV Disconnect Switches.* Shakhzod M. Takhirov, Gregory L. Fenves, and Eric Fujisaki. January 2005.

PEER 2004/07 *Ground Motions for Earthquake Simulator Qualification of Electrical Substation Equipment.* Shakhzod M. Takhirov, Gregory L. Fenves, Eric Fujisaki, and Don Clyde. January 2005.

PEER 2004/06 *Performance-Based Regulation and Regulatory Regimes.* Peter J. May and Chris Koski. September 2004.

PEER 2004/05 *Performance-Based Seismic Design Concepts and Implementation: Proceedings of an International Workshop.* Peter Fajfar and Helmut Krawinkler, editors. September 2004.

PEER 2004/04 *Seismic Performance of an Instrumented Tilt-up Wall Building.* James C. Anderson and Vitelmo V. Bertero. July 2004.

PEER 2004/03 *Evaluation and Application of Concrete Tilt-up Assessment Methodologies.* Timothy Graf and James O. Malley. October 2004.

PEER 2004/02 *Analytical Investigations of New Methods for Reducing Residual Displacements of Reinforced Concrete Bridge Columns.* Junichi Sakai and Stephen A. Mahin. August 2004.

PEER 2004/01 *Seismic Performance of Masonry Buildings and Design Implications.* Kerri Anne Taeko Tokoro, James C. Anderson, and Vitelmo V. Bertero. February 2004.

PEER 2003/18 *Performance Models for Flexural Damage in Reinforced Concrete Columns.* Michael Berry and Marc Eberhard. August 2003.

PEER 2003/17 *Predicting Earthquake Damage in Older Reinforced Concrete Beam-Column Joints.* Catherine Pagni and Laura Lowes. October 2004.

PEER 2003/16 *Seismic Demands for Performance-Based Design of Bridges.* Kevin Mackie and Božidar Stojadinović. August 2003.

PEER 2003/15 *Seismic Demands for Nondeteriorating Frame Structures and Their Dependence on Ground Motions.* Ricardo Antonio Medina and Helmut Krawinkler. May 2004.

PEER 2003/14 *Finite Element Reliability and Sensitivity Methods for Performance-Based Earthquake Engineering.* Terje Haukaas and Armen Der Kiureghian. April 2004.

PEER 2003/13 *Effects of Connection Hysteretic Degradation on the Seismic Behavior of Steel Moment-Resisting Frames.* Janise E. Rodgers and Stephen A. Mahin. March 2004.

PEER 2003/12 *Implementation Manual for the Seismic Protection of Laboratory Contents: Format and Case Studies.* William T. Holmes and Mary C. Comerio. October 2003.

PEER 2003/11 *Fifth U.S.-Japan Workshop on Performance-Based Earthquake Engineering Methodology for Reinforced Concrete Building Structures.* February 2004.

PEER 2003/10 *A Beam-Column Joint Model for Simulating the Earthquake Response of Reinforced Concrete Frames.* Laura N. Lowes, Nilanjan Mitra, and Arash Altoontash. February 2004.

PEER 2003/09 *Sequencing Repairs after an Earthquake: An Economic Approach.* Marco Casari and Simon J. Wilkie. April 2004.

PEER 2003/08 *A Technical Framework for Probability-Based Demand and Capacity Factor Design (DCFD) Seismic Formats*. Fatemeh Jalayer and C. Allin Cornell. November 2003.

PEER 2003/07 *Uncertainty Specification and Propagation for Loss Estimation Using FOSM Methods.* Jack W. Baker and C. Allin Cornell. September 2003.

PEER 2003/06 *Performance of Circular Reinforced Concrete Bridge Columns under Bidirectional Earthquake Loading*. Mahmoud M. Hachem, Stephen A. Mahin, and Jack P. Moehle. February 2003.

PEER 2003/05 *Response Assessment for Building-Specific Loss Estimation.* Eduardo Miranda and Shahram Taghavi. September 2003.

PEER 2003/04 *Experimental Assessment of Columns with Short Lap Splices Subjected to Cyclic Loads*. Murat Melek, John W. Wallace, and Joel Conte. April 2003.

PEER 2003/03 *Probabilistic Response Assessment for Building-Specific Loss Estimation.* Eduardo Miranda and Hesameddin Aslani. September 2003.

PEER 2003/02 *Software Framework for Collaborative Development of Nonlinear Dynamic Analysis Program.* Jun Peng and Kincho H. Law. September 2003.

PEER 2003/01 *Shake Table Tests and Analytical Studies on the Gravity Load Collapse of Reinforced Concrete Frames.* Kenneth John Elwood and Jack P. Moehle. November 2003.

PEER 2002/24 *Performance of Beam to Column Bridge Joints Subjected to a Large Velocity Pulse.* Natalie Gibson, André Filiatrault, and Scott A. Ashford. April 2002.

PEER 2002/23 *Effects of Large Velocity Pulses on Reinforced Concrete Bridge Columns.* Greg L. Orozco and Scott A. Ashford. April 2002.

PEER 2002/22 *Characterization of Large Velocity Pulses for Laboratory Testing.* Kenneth E. Cox and Scott A. Ashford. April 2002.

PEER 2002/21 *Fourth U.S.-Japan Workshop on Performance-Based Earthquake Engineering Methodology for Reinforced Concrete Building Structures*. December 2002.

PEER 2002/20 *Barriers to Adoption and Implementation of PBEE Innovations.* Peter J. May. August 2002.

PEER 2002/19 *Economic-Engineered Integrated Models for Earthquakes: Socioeconomic Impacts.* Peter Gordon, James E. Moore II, and Harry W. Richardson. July 2002.

PEER 2002/18 *Assessment of Reinforced Concrete Building Exterior Joints with Substandard Details.* Chris P. Pantelides, Jon Hansen, Justin Nadauld, and Lawrence D. Reaveley. May 2002.

PEER 2002/17 *Structural Characterization and Seismic Response Analysis of a Highway Overcrossing Equipped with Elastomeric Bearings and Fluid Dampers: A Case Study.* Nicos Makris and Jian Zhang. November 2002.

PEER 2002/16 *Estimation of Uncertainty in Geotechnical Properties for Performance-Based Earthquake Engineering.* Allen L. Jones, Steven L. Kramer, and Pedro Arduino. December 2002.

PEER 2002/15 *Seismic Behavior of Bridge Columns Subjected to Various Loading Patterns.* Asadollah Esmaeily-Gh. and Yan Xiao. December 2002.

PEER 2002/14 *Inelastic Seismic Response of Extended Pile Shaft Supported Bridge Structures.* T.C. Hutchinson, R.W. Boulanger, Y.H. Chai, and I.M. Idriss. December 2002.

PEER 2002/13 *Probabilistic Models and Fragility Estimates for Bridge Components and Systems.* Paolo Gardoni, Armen Der Kiureghian, and Khalid M. Mosalam. June 2002.

PEER 2002/12 *Effects of Fault Dip and Slip Rake on Near-Source Ground Motions: Why Chi-Chi Was a Relatively Mild M7.6 Earthquake.* Brad T. Aagaard, John F. Hall, and Thomas H. Heaton. December 2002.

PEER 2002/11 *Analytical and Experimental Study of Fiber-Reinforced Strip Isolators*. James M. Kelly and Shakhzod M. Takhirov. September 2002.

PEER 2002/10 *Centrifuge Modeling of Settlement and Lateral Spreading with Comparisons to Numerical Analyses***.** Sivapalan Gajan and Bruce L. Kutter. January 2003.

PEER 2002/09 *Documentation and Analysis of Field Case Histories of Seismic Compression during the 1994 Northridge, California, Earthquake.* Jonathan P. Stewart, Patrick M. Smith, Daniel H. Whang, and Jonathan D. Bray. October 2002.

PEER 2002/08 *Component Testing, Stability Analysis and Characterization of Buckling-Restrained Unbonded Braces™.* Cameron Black, Nicos Makris, and Ian Aiken. September 2002.

PEER 2002/07 *Seismic Performance of Pile-Wharf Connections.* Charles W. Roeder, Robert Graff, Jennifer Soderstrom, and Jun Han Yoo. December 2001.

PEER 2002/06 *The Use of Benefit-Cost Analysis for Evaluation of Performance-Based Earthquake Engineering Decisions*. Richard O. Zerbe and Anthony Falit-Baiamonte. September 2001.

PEER 2002/05 *Guidelines, Specifications, and Seismic Performance Characterization of Nonstructural Building Components and Equipment*. André Filiatrault, Constantin Christopoulos, and Christopher Stearns. September 2001.

PEER 2002/04 *Consortium of Organizations for Strong-Motion Observation Systems and the Pacific Earthquake Engineering Research Center Lifelines Program: Invited Workshop on Archiving and Web Dissemination of Geotechnical Data, 4–5 October 2001*. September 2002.

PEER 2002/03 *Investigation of Sensitivity of Building Loss Estimates to Major Uncertain Variables for the Van Nuys Testbed.* Keith A. Porter, James L. Beck, and Rustem V. Shaikhutdinov. August 2002.

PEER 2002/02 *The Third U.S.-Japan Workshop on Performance-Based Earthquake Engineering Methodology for Reinforced Concrete Building Structures*. July 2002.

PEER 2002/01 *Nonstructural Loss Estimation: The UC Berkeley Case Study.* Mary C. Comerio and John C. Stallmeyer. December 2001.

PEER 2001/16 *Statistics of SDF-System Estimate of Roof Displacement for Pushover Analysis of Buildings.* Anil K. Chopra, Rakesh K. Goel, and Chatpan Chintanapakdee. December 2001.

PEER 2001/15 *Damage to Bridges during the 2001 Nisqually Earthquake.* R. Tyler Ranf, Marc O. Eberhard, and Michael P. Berry. November 2001.

PEER 2001/14 *Rocking Response of Equipment Anchored to a Base Foundation.* Nicos Makris and Cameron J. Black. September 2001.

PEER 2001/13 *Modeling Soil Liquefaction Hazards for Performance-Based Earthquake Engineering.* Steven L. Kramer and Ahmed-W. Elgamal. February 2001.

PEER 2001/12 *Development of Geotechnical Capabilities in OpenSees.* Boris Jeremić. September 2001.

PEER 2001/11 *Analytical and Experimental Study of Fiber-Reinforced Elastomeric Isolators*. James M. Kelly and Shakhzod M. Takhirov. September 2001.

PEER 2001/10 *Amplification Factors for Spectral Acceleration in Active Regions.* Jonathan P. Stewart, Andrew H. Liu, Yoojoong Choi, and Mehmet B. Baturay. December 2001.

PEER 2001/09 *Ground Motion Evaluation Procedures for Performance-Based Design.* Jonathan P. Stewart, Shyh-Jeng Chiou, Jonathan D. Bray, Robert W. Graves, Paul G. Somerville, and Norman A. Abrahamson. September 2001.

PEER 2001/08 *Experimental and Computational Evaluation of Reinforced Concrete Bridge Beam-Column Connections for Seismic Performance*. Clay J. Naito, Jack P. Moehle, and Khalid M. Mosalam. November 2001.

PEER 2001/07 *The Rocking Spectrum and the Shortcomings of Design Guidelines.* Nicos Makris and Dimitrios Konstantinidis. August 2001.

PEER 2001/06 *Development of an Electrical Substation Equipment Performance Database for Evaluation of Equipment Fragilities*. Thalia Agnanos. April 1999.

PEER 2001/05 *Stiffness Analysis of Fiber-Reinforced Elastomeric Isolators.* Hsiang-Chuan Tsai and James M. Kelly. May 2001.

PEER 2001/04 *Organizational and Societal Considerations for Performance-Based Earthquake Engineering.* Peter J. May. April 2001.

PEER 2001/03 *A Modal Pushover Analysis Procedure to Estimate Seismic Demands for Buildings: Theory and Preliminary Evaluation.* Anil K. Chopra and Rakesh K. Goel. January 2001.

PEER 2001/02 *Seismic Response Analysis of Highway Overcrossings Including Soil-Structure Interaction.* Jian Zhang and Nicos Makris. March 2001.

PEER 2001/01 *Experimental Study of Large Seismic Steel Beam-to-Column Connections.* Egor P. Popov and Shakhzod M. Takhirov. November 2000.

PEER 2000/10 *The Second U.S.-Japan Workshop on Performance-Based Earthquake Engineering Methodology for Reinforced Concrete Building Structures.* March 2000.

PEER 2000/09 *Structural Engineering Reconnaissance of the August 17, 1999 Earthquake: Kocaeli (Izmit), Turkey.* Halil Sezen, Kenneth J. Elwood, Andrew S. Whittaker, Khalid Mosalam, John J. Wallace, and John F. Stanton. December 2000.

PEER 2000/08 *Behavior of Reinforced Concrete Bridge Columns Having Varying Aspect Ratios and Varying Lengths of Confinement.* Anthony J. Calderone, Dawn E. Lehman, and Jack P. Moehle. January 2001.

PEER 2000/07 *Cover-Plate and Flange-Plate Reinforced Steel Moment-Resisting Connections.* Taejin Kim, Andrew S. Whittaker, Amir S. Gilani, Vitelmo V. Bertero, and Shakhzod M. Takhirov. September 2000.

PEER 2000/06 *Seismic Evaluation and Analysis of 230-kV Disconnect Switches.* Amir S. J. Gilani, Andrew S. Whittaker, Gregory L. Fenves, Chun-Hao Chen, Henry Ho, and Eric Fujisaki. July 2000.

PEER 2000/05 *Performance-Based Evaluation of Exterior Reinforced Concrete Building Joints for Seismic Excitation.* Chandra Clyde, Chris P. Pantelides, and Lawrence D. Reaveley. July 2000.

PEER 2000/04 *An Evaluation of Seismic Energy Demand: An Attenuation Approach.* Chung-Che Chou and Chia-Ming Uang. July 1999.

PEER 2000/03 *Framing Earthquake Retrofitting Decisions: The Case of Hillside Homes in Los Angeles.* Detlof von Winterfeldt, Nels Roselund, and Alicia Kitsuse. March 2000.

PEER 2000/02 *U.S.-Japan Workshop on the Effects of Near-Field Earthquake Shaking.* Andrew Whittaker, ed. July 2000.

PEER 2000/01 *Further Studies on Seismic Interaction in Interconnected Electrical Substation Equipment.* Armen Der Kiureghian, Kee-Jeung Hong, and Jerome L. Sackman. November 1999.

PEER 1999/14 *Seismic Evaluation and Retrofit of 230-kV Porcelain Transformer Bushings*. Amir S. Gilani, Andrew S. Whittaker, Gregory L. Fenves, and Eric Fujisaki. December 1999.

PEER 1999/13 *Building Vulnerability Studies: Modeling and Evaluation of Tilt-up and Steel Reinforced Concrete Buildings.* John W. Wallace, Jonathan P. Stewart, and Andrew S. Whittaker, editors. December 1999.

PEER 1999/12 *Rehabilitation of Nonductile RC Frame Building Using Encasement Plates and Energy-Dissipating Devices.* Mehrdad Sasani, Vitelmo V. Bertero, James C. Anderson. December 1999.

PEER 1999/11 *Performance Evaluation Database for Concrete Bridge Components and Systems under Simulated Seismic Loads.* Yael D. Hose and Frieder Seible. November 1999.

PEER 1999/10 *U.S.-Japan Workshop on Performance-Based Earthquake Engineering Methodology for Reinforced Concrete Building Structures.* December 1999.

PEER 1999/09 *Performance Improvement of Long Period Building Structures Subjected to Severe Pulse-Type Ground Motions*. James C. Anderson, Vitelmo V. Bertero, and Raul Bertero. October 1999.

PEER 1999/08 *Envelopes for Seismic Response Vectors.* Charles Menun and Armen Der Kiureghian. July 1999.

PEER 1999/07 *Documentation of Strengths and Weaknesses of Current Computer Analysis Methods for Seismic Performance of Reinforced Concrete Members.* William F. Cofer. November 1999.

PEER 1999/06 *Rocking Response and Overturning of Anchored Equipment under Seismic Excitations.* Nicos Makris and Jian Zhang. November 1999.

PEER 1999/05 *Seismic Evaluation of 550 kV Porcelain Transformer Bushings.* Amir S. Gilani, Andrew S. Whittaker, Gregory L. Fenves, and Eric Fujisaki. October 1999.

PEER 1999/04 *Adoption and Enforcement of Earthquake Risk-Reduction Measures.* Peter J. May, Raymond J. Burby, T. Jens Feeley, and Robert Wood.

PEER 1999/03 *Task 3 Characterization of Site Response General Site Categories*. Adrian Rodriguez-Marek, Jonathan D. Bray, and Norman Abrahamson. February 1999.

PEER 1999/02 *Capacity-Demand-Diagram Methods for Estimating Seismic Deformation of Inelastic Structures: SDF Systems*. Anil K. Chopra and Rakesh Goel. April 1999.

PEER 1999/01 *Interaction in Interconnected Electrical Substation Equipment Subjected to Earthquake Ground Motions.* Armen Der Kiureghian, Jerome L. Sackman, and Kee-Jeung Hong. February 1999.

PEER 1998/08 *Behavior and Failure Analysis of a Multiple-Frame Highway Bridge in the 1994 Northridge Earthquake.* Gregory L. Fenves and Michael Ellery. December 1998.

PEER 1998/07 *Empirical Evaluation of Inertial Soil-Structure Interaction Effects.* Jonathan P. Stewart, Raymond B. Seed, and Gregory L. Fenves. November 1998.

PEER 1998/06 *Effect of Damping Mechanisms on the Response of Seismic Isolated Structures.* Nicos Makris and Shih-Po Chang. November 1998.

PEER 1998/05 *Rocking Response and Overturning of Equipment under Horizontal Pulse-Type Motions.* Nicos Makris and Yiannis Roussos. October 1998.

PEER 1998/04 *Pacific Earthquake Engineering Research Invitational Workshop Proceedings, May 14–15, 1998: Defining the Links between Planning, Policy Analysis, Economics and Earthquake Engineering.* Mary Comerio and Peter Gordon. September 1998.

PEER 1998/03 *Repair/Upgrade Procedures for Welded Beam to Column Connections.* James C. Anderson and Xiaojing Duan. May 1998.

PEER 1998/02 *Seismic Evaluation of 196 kV Porcelain Transformer Bushings.* Amir S. Gilani, Juan W. Chavez, Gregory L. Fenves, and Andrew S. Whittaker. May 1998.

PEER 1998/01 *Seismic Performance of Well-Confined Concrete Bridge Columns.* Dawn E. Lehman and Jack P. Moehle. December 2000.

ONLINE PEER REPORTS

The following PEER reports are available by Internet only at http://peer.berkeley.edu/publications/peer_reports_complete.html.

PEER 2012/103 *Performance-Based Seismic Demand Assessment of Concentrically Braced Steel Frame Buildings.* Chui-Hsin Chen and Stephen A. Mahin. December 2012.

PEER 2012/102 *Procedure to Restart an Interrupted Hybrid Simulation: Addendum to PEER Report 2010/103.* Vesna Terzic and Bozidar Stojadinovic. October 2012.

PEER 2012/101 *Mechanics of Fiber Reinforced Bearings.* James M. Kelly and Andrea Calabrese. February 2012.

PEER 2011/107 *Nonlinear Site Response and Seismic Compression at Vertical Array Strongly Shaken by 2007 Niigata-ken Chuetsu-oki Earthquake.* Eric Yee, Jonathan P. Stewart, and Kohji Tokimatsu. December 2011.

PEER 2011/106 *Self Compacting Hybrid Fiber Reinforced Concrete Composites for Bridge Columns.* Pardeep Kumar, Gabriel Jen, William Trono, Marios Panagiotou, and Claudia Ostertag. September 2011.

PEER 2011/105 *Stochastic Dynamic Analysis of Bridges Subjected to Spacially Varying Ground Motions.* Katerina Konakli and Armen Der Kiureghian. August 2011.

PEER 2011/104 *Design and Instrumentation of the 2010 E-Defense Four-Story Reinforced Concrete and Post-Tensioned Concrete Buildings.* Takuya Nagae, Kenichi Tahara, Taizo Matsumori, Hitoshi Shiohara, Toshimi Kabeyasawa, Susumu Kono, Minehiro Nishiyama (Japanese Research Team) and John Wallace, Wassim Ghannoum, Jack Moehle, Richard Sause, Wesley Keller, Zeynep Tuna (U.S. Research Team). June 2011.

PEER 2011/103 *In-Situ Monitoring of the Force Output of Fluid Dampers: Experimental Investigation.* Dimitrios Konstantinidis, James M. Kelly, and Nicos Makris. April 2011.

PEER 2011/102 *Ground-motion prediction equations 1964 - 2010.* John Douglas. April 2011.

PEER 2011/101 *Report of the Eighth Planning Meeting of NEES/E-Defense Collaborative Research on Earthquake Engineering.* Convened by the Hyogo Earthquake Engineering Research Center (NIED), NEES Consortium, Inc. February 2011.

PEER 2010/111 *Modeling and Acceptance Criteria for Seismic Design and Analysis of Tall Buildings.* Task 7 Report for the Tall Buildings Initiative - Published jointly by the Applied Technology Council. October 2010.

PEER 2010/110 *Seismic Performance Assessment and Probabilistic Repair Cost Analysis of Precast Concrete Cladding Systems for Multistory Buildlings.* Jeffrey P. Hunt and Božidar Stojadinovic. November 2010.

PEER 2010/109 *Report of the Seventh Joint Planning Meeting of NEES/E-Defense Collaboration on Earthquake Engineering. Held at the E-Defense, Miki, and Shin-Kobe, Japan, September 18–19, 2009.* August 2010.

PEER 2010/108 *Probabilistic Tsunami Hazard in California.* Hong Kie Thio, Paul Somerville, and Jascha Polet, preparers. October 2010.

PEER 2010/107 *Performance and Reliability of Exposed Column Base Plate Connections for Steel Moment-Resisting Frames.* Ady Aviram, Božidar Stojadinovic, and Armen Der Kiureghian. August 2010.

PEER 2010/106 *Verification of Probabilistic Seismic Hazard Analysis Computer Programs.* Patricia Thomas, Ivan Wong, and Norman Abrahamson. May 2010.

PEER 2010/105 *Structural Engineering Reconnaissance of the April 6, 2009, Abruzzo, Italy, Earthquake, and Lessons Learned.* M. Selim Günay and Khalid M. Mosalam. April 2010.

PEER 2010/104 *Simulating the Inelastic Seismic Behavior of Steel Braced Frames, Including the Effects of Low-Cycle Fatigue.* Yuli Huang and Stephen A. Mahin. April 2010.

PEER 2010/103 *Post-Earthquake Traffic Capacity of Modern Bridges in California.* Vesna Terzic and Božidar Stojadinović. March 2010.

PEER 2010/102 *Analysis of Cumulative Absolute Velocity (CAV) and JMA Instrumental Seismic Intensity (I_{JMA}) Using the PEER–NGA Strong Motion Database.* Kenneth W. Campbell and Yousef Bozorgnia. February 2010.

PEER 2010/101 *Rocking Response of Bridges on Shallow Foundations.* Jose A. Ugalde, Bruce L. Kutter, and Boris Jeremic. April 2010.

PEER 2009/109 *Simulation and Performance-Based Earthquake Engineering Assessment of Self-Centering Post-Tensioned Concrete Bridge Systems.* Won K. Lee and Sarah L. Billington. December 2009.

PEER 2009/108 *PEER Lifelines Geotechnical Virtual Data Center.* J. Carl Stepp, Daniel J. Ponti, Loren L. Turner, Jennifer N. Swift, Sean Devlin, Yang Zhu, Jean Benoit, and John Bobbitt. September 2009.

PEER 2009/107 *Experimental and Computational Evaluation of Current and Innovative In-Span Hinge Details in Reinforced Concrete Box-Girder Bridges: Part 2: Post-Test Analysis and Design Recommendations.* Matias A. Hube and Khalid M. Mosalam. December 2009.

PEER 2009/106 *Shear Strength Models of Exterior Beam-Column Joints without Transverse Reinforcement.* Sangjoon Park and Khalid M. Mosalam. November 2009.

PEER 2009/105 *Reduced Uncertainty of Ground Motion Prediction Equations through Bayesian Variance Analysis.* Robb Eric S. Moss. November 2009.

PEER 2009/104 *Advanced Implementation of Hybrid Simulation.* Andreas H. Schellenberg, Stephen A. Mahin, Gregory L. Fenves. November 2009.

PEER 2009/103 *Performance Evaluation of Innovative Steel Braced Frames.* T. Y. Yang, Jack P. Moehle, and Božidar Stojadinovic. August 2009.

PEER 2009/102 *Reinvestigation of Liquefaction and Nonliquefaction Case Histories from the 1976 Tangshan Earthquake.* Robb Eric Moss, Robert E. Kayen, Liyuan Tong, Songyu Liu, Guojun Cai, and Jiaer Wu. August 2009.

PEER 2009/101 *Report of the First Joint Planning Meeting for the Second Phase of NEES/E-Defense Collaborative Research on Earthquake Engineering.* Stephen A. Mahin et al. July 2009.

PEER 2008/104 *Experimental and Analytical Study of the Seismic Performance of Retaining Structures.* Linda Al Atik and Nicholas Sitar. January 2009.

PEER 2008/103 *Experimental and Computational Evaluation of Current and Innovative In-Span Hinge Details in Reinforced Concrete Box-Girder Bridges. Part 1: Experimental Findings and Pre-Test Analysis.* Matias A. Hube and Khalid M. Mosalam. January 2009.

PEER 2008/102 *Modeling of Unreinforced Masonry Infill Walls Considering In-Plane and Out-of-Plane Interaction.* Stephen Kadysiewski and Khalid M. Mosalam. January 2009.

PEER 2008/101 *Seismic Performance Objectives for Tall Buildings.* William T. Holmes, Charles Kircher, William Petak, and Nabih Youssef. August 2008.

PEER 2007/101 *Generalized Hybrid Simulation Framework for Structural Systems Subjected to Seismic Loading.* Tarek Elkhoraibi and Khalid M. Mosalam. July 2007.

PEER 2007/100 *Seismic Evaluation of Reinforced Concrete Buildings Including Effects of Masonry Infill Walls.* Alidad Hashemi and Khalid M. Mosalam. July 2007.

The Pacific Earthquake Engineering Research Center (PEER) is a multi-institutional research and education center with headquarters at the University of California, Berkeley. Investigators from over 20 universities, several consulting companies, and researchers at various state and federal government agencies contribute to research programs focused on performance-based earthquake engineering.

These research programs aim to identify and reduce the risks from major earthquakes to life safety and to the economy by including research in a wide variety of disciplines including structural and geotechnical engineering, geology/seismology, lifelines, transportation, architecture, economics, risk management, and public policy.

PEER is supported by federal, state, local, and regional agencies, together with industry partners.

PEER Core Institutions:
University of California, Berkeley (Lead Institution)
California Institute of Technology
Oregon State University
Stanford University
University of California, Davis
University of California, Irvine
University of California, Los Angeles
University of California, San Diego
University of Southern California
University of Washington

PEER reports can be ordered at http://peer.berkeley.edu/publications/peer_reports.html or by contacting

Pacific Earthquake Engineering Research Center
University of California, Berkeley
325 Davis Hall, mail code 1792
Berkeley, CA 94720-1792
Tel: 510-642-3437
Fax: 510-642-1655
Email: peer_editor@berkeley.edu

ISSN 1547-0587X